NASA/TM—1999-209237

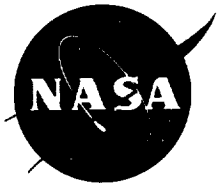

Assessment of the Effects of High-Speed Aircraft in the Stratosphere: 1998

S. Randolph Kawa, Assessment Chair, NASA Goddard Space Flight Center

James G. Anderson, Harvard University
Steven L. Baughcum, Boeing Co.
Charles A. Brock, University of Denver
William H. Brune, Pennsylvania State University
Ronald C. Cohen, University of California, Berkeley
Douglas E. Kinnison, National Center for Atmospheric Research
Paul A. Newman, NASA Goddard Space Flight Center
Jose M. Rodriguez, University of Miami
Richard S. Stolarski, NASA Goddard Space Flight Center
Darryn Waugh, Johns Hopkins University
Steven C. Wofsy, Harvard University

National Aeronautics and
Space Administration

Goddard Space Flight Center
Greenbelt, Maryland 20771

June 1999

Available from:

NASA Center for AeroSpace Information
7121 Standard Drive
Hanover, MD 21076-1320
Price Code: A17

National Technical Information Service
5285 Port Royal Road
Springfield, VA 22161
Price Code: A10

ASSESSMENT OF THE EFFECTS OF HIGH-SPEED AIRCRAFT IN THE STRATOSPHERE: 1998

Table of Contents

EXECUTIVE SUMMARY

INTRODUCTION

This report assesses the potential atmospheric impacts of a proposed hypothetical fleet of high speed civil transport (HSCT) aircraft. Civil supersonic transport aircraft were first developed in the 1970s, but, due to economic and environmental concerns, the number of commercial supersonic aircraft in regular service has been small (fewer than 20 aircraft). Recent developments in aviation technology and passenger demand, however, indicate that a substantially larger fleet of HSCTs may be environmentally and economically feasible in the next few decades. During the 1990s, the National Aeronautics and Space Administration (NASA) and the aerospace industry have embarked on a technology research and development program, the High-Speed Research Program, to facilitate technology development and help make widespread supersonic travel possible. The purpose of this report is to assess the effects of HSCTs on atmospheric composition and climate in order to provide a scientific basis for making technical, commercial, and environmental policy decisions regarding the HSCT fleet.

The work summarized here was carried out as part of NASA's Atmospheric Effects of Aviation Project (AEAP) (a component of the High-Speed Research Program) as well as other NASA, United States, and international research programs. Impacts of supersonic aircraft have been assessed previously in 1975 by the Climate Impact Assessment Program and by NASA in 1993 and 1995. Here we describe progress in understanding atmospheric processes and the current state of understanding of the atmospheric effects of HSCTs. The principal focus is on change in stratospheric ozone concentrations. The impact on climate change is also a concern. We delineate the principal uncertainties in atmospheric predictions and estimate the associated errors in predicted effects of HSCTs. The findings represent a broad consensus of the atmospheric research community, comprising the authors, contributors, and reviewers.

A. What are the emissions of greatest concern for the HSCT aircraft fleet?

The HSCT emissions of primary concern for stratospheric ozone and climate are **oxides of nitrogen** (NO_x), **water** (H_2O), and **aerosol particles and particle precursor gases**.

NO_x

Nitrogen oxides participate in a wide range of chemical processes that affect ozone. (a) The principal loss process for ozone in the middle and upper stratosphere involves NO_x radicals, and thus, exhaust that is transported to these regions will reduce ozone. The transport of NO_x from HSCTs to altitudes above 22 km and accumulation at these altitudes is a critical question for the assessment. (b) In the lower stratosphere, NO_x radicals moderate ozone loss due to other radical species (hydrogen oxides (HO_x), chlorine oxides (ClO_x), bromine oxides (BrO_x)); thus addition of NO_x from HCST exhaust can either increase or decrease ozone in this region depending on the

relative balance among the radicals. (c) In the polar winter stratosphere, nitrogen oxides participate in formation of polar stratospheric clouds (PSCs), which lead to large seasonal ozone loss in these regions, e.g., the Antarctic ozone "hole." The net effect of increasing NO_x depends on interactions between transport, heterogeneous chemistry, homogeneous chemistry, and the composition of the unperturbed atmosphere.

WATER

HSCT emissions could increase lower stratospheric water vapor by about 0.5 parts per million by volume (ppmv) (10 to 15% for a fleet of 500 aircraft) affecting climate, aerosol processes, and rates for chemical reactions. Warming of the lower atmosphere as a result of increased stratospheric water is predicted to be the main climatic effect of HSCTs, although the magnitude of this effect is not well determined at this time. The composition and growth of aerosol particles, including PSCs, is influenced because increased water vapor raises the condensation temperature. Increased water also increases the reactivity of aerosol toward gases, such as hydrogen chloride (HCl) and chlorine nitrate ($ClONO_2$), thus influencing the relative concentrations of radical species. Since water is the source of HO_x radicals, increased water leads directly to higher concentrations of HO_x. Model calculations suggest that the associated increase in HO_x is as important as changing NO_x for enhancing ozone loss.

AEROSOL PARTICLES

Repeated observations since 1994 consistently show that a large number of ultrafine (<20 nm diameter) aerosol particles exist in jet engine exhaust plumes, and that particle production increases as the sulfur content of fuel increases. Emission of small particles and sulfur dioxide (SO_2) can potentially increase aerosol surface area throughout the stratosphere which suppresses NO_x and enhances ozone loss by ClO_x and HO_x. Proposed mechanisms for small particle formation are still controversial, and the effects on particle abundance throughout the stratosphere are uncertain, but atmospheric ozone is definitely sensitive to changing aerosol conditions.

B. What factors determine the impact of HSCTs on stratospheric ozone?

The impacts of HSCTs depend on:

- The quantity of exhaust deposited (water, NO_x, particle mass and surface area) and its location in altitude and latitude;
- Atmospheric transport, especially the eventual accumulation of exhaust products in various parts of the stratosphere. The integration of changes in chemical rates for ozone loss and transport of ozone produces the perturbed ozone distribution;
- Microphysics (formation, growth, coagulation, and settling) of aerosol particles in the atmosphere;
- Chemical reactions of the exhaust products with aerosols, atmospheric radicals, and ozone; and

- The background state (meteorology and composition) of the future atmosphere onto which the HSCT perturbation is superimposed.

The linkage between transport, chemistry, aerosol microphysics, and the atmospheric background makes predicting ozone change due to HSCT emissions challenging.

C. What major progress has been accomplished since the previous HSCT assessment?

Great progress has been made in ozone assessment science since the previous HSCT assessment. Progress is led by new atmospheric observations and numerical model development. Observations pave the way for improved understanding and simulation of transport, chemistry, and emission processes. Models have been developed which are more soundly based in physical principles with fewer restrictive assumptions.

Transport Diagnosis

Observations of chemical tracers, studies using analyzed meteorological fields and idealized models, and advances in theory have improved understanding and quantification of several key components of transport necessary to predicting the distribution of HSCT exhaust. *In situ* measurements of chemical tracers have been obtained within the previously data-sparse tropics. These observations permit quantitative diagnosis of key pathways for dispersal of HSCT exhaust into the upper stratosphere where chemical sensitivity to NO_x is high. Measurements of carbon dioxide (CO_2), sulfur hexafluoride (SF_6), and hydrogen fluoride (HF) over a range of latitude and altitude have enabled mean ages of air in the stratosphere to be determined. Age of air is a directly measured diagnostic related to stratospheric residence time and hence to the potential accumulation of HSCT exhaust in the stratosphere. The quantitative analysis of tropical transport and mean age provide stringent new tests of transport within numerical models. Comparison between observations and models is essential for assessing the uncertainty in the ozone perturbation and in developing more accurate models.

Model Development

Three-dimensional (3-D) atmospheric models have been applied to the HSCT assessment for the first time. Three-dimensional models incorporate a more physically realistic representation of the atmosphere than two-dimensional (2-D) models. The modular design of the Global Modeling Initiative 3-D model has made it possible to test the different components of the model (e.g., the numerical transport algorithm and the source of the wind and temperature fields). Objective criteria for performance with respect to data have been applied. Thus, we discern differences among models in their response to the HSCT perturbation and begin to weigh their results. A major model-measurement comparison and model intercomparison (M&M II) has been conducted, and all models in this assessment have been tested in comparison to a standard set of performance benchmarks. Also, the 2-D models have incorporated more complete process representations including those for aircraft aerosol exhaust, PSCs, heterogeneous reaction rates, and wave-driven mixing. These model developments give us more confidence in our physical representation of the stratospheric system.

CHEMISTRY

Improved confidence in chemistry has come about largely through observational data on chemicals not previously measured and more accurate data over a more comprehensive range of conditions, including the first in summer polar regions. Observations of key species and new laboratory measurements, placed in a diagnostic model framework, show good accuracy in partitioning components of reactive nitrogen, chlorine, and hydrogen in the models. This establishes confidence that we are not missing significant reactions or unknown species that would alter the calculated response of the chemical system to the HSCT perturbation.

EMISSIONS

The most important progress on emissions comes in confirming the importance of near-field production of small sulfate aerosol particles by HSCTs. New direct measurements for existing aircraft show formation of volatile ultra-fine aerosol particles in exhaust plumes from all aircraft sampled. In-flight measurements indicate that the number of particles is dependent on fuel sulfur content, while altitude chamber measurements show that sulfur emissions at the engine exit plane are primarily SO_2. These observations support earlier inferences of a composition of sulfuric acid $(H_2SO_4)/H_2O$ for the volatile particles detected in the plume. Soot emissions from current aircraft engines are roughly two orders of magnitude lower in particle number density than volatile aerosols, and soot from HSCTs is expected to have a negligible effect on ozone and climate. Measurements of gaseous constituents, including HO_x and NO_x, emitted from current aircraft are consistent with expected emissions and plume models of gas-phase chemistry and dispersion. This reduces our uncertainty in applying current knowledge of emissions to the proposed future fleet.

D. What are the predicted impacts of the HSCT fleet on stratospheric ozone and climate?

Predictions of the impact of the future HSCT fleet have been calculated using a set of numerical models of chemistry and transport. Model calculations have been performed for a variety of scenarios to test a range of HSCT design parameters and atmospheric variations.

Based on a combination of model calculations and expert judgement, the estimated column ozone change in the Northern Hemisphere is -0.4% for a fleet of 500 HSCTs flying Mach 2.4 with an NO_x emission index (EI_{NOx}) of 5 g/kg, EI_{SO2} of 0.4 g/kg, and 10% of fuel sulfur converted to particles. Based on the same combination of model calculations and expert judgement for the uncertainty in component processes, the hemispheric ozone response will likely be in the range of -2.5 to +0.5%.

We also note that the maximum seasonal and latitudinal ozone changes will be greater than the hemispheric annual mean. Polar regions are a special concern. All models show their largest amount of column ozone loss at high latitudes and a minimum change in the tropics. The column ozone change is the sum of an ozone increase at lower stratospheric/upper tropospheric altitudes plus a decrease generally at and above the HSCT flight altitude. This balance between net production and loss is different for different models and depends strongly on latitude. The season

of maximum change is not consistent among the models, with most predicting a springtime maximum ozone decrease but others a maximum in the summer or fall. These variations are connected to the models' sensitivity to chemical reactions in cold polar regions and PSC processes.

The climate forcing attributable to an HSCT fleet in the year 2050 is predicted to result in a warming which is small relative to that expected from other anthropogenic sources. The total radiative forcing from 1000 HSCTs is calculated to be +0.1 W m^{-2} in 2050. This HSCT number is a concern because the radiative forcing is disproportionately large for the amount of fuel used and equivalent to about 50% of the forcing from the entire projected subsonic fleet. Climate forcing is sensitive to HSCT emissions because the H_2O accumulation is localized in the lower stratosphere. The uncertainty in the HSCT climate forcing is estimated to be about a factor of 3 due to uncertainty in the exhaust accumulation and uncertainty in the temperature adjustment to a non-uniform perturbation of radiatively active gases in the stratosphere.

Several findings relevant to HSCT design issues come out of the atmospheric assessment. These are considered reliable notwithstanding uncertainties in model results, because they derive from basic understanding of stratospheric processes.

- The HSCT impact on ozone depends directly on total emissions, i.e., fleet size and fuel use.

- Water vapor, which is inherent to jet fuel combustion, accounts for a major part of the calculated stratospheric ozone impact. Increased water vapor in the stratosphere may also contribute to global climate warming.

- NO_x emissions are important. Although current atmospheric models do not show much relative sensitivity to very low (EI_{NO_x} = 5 to 10) emissions, higher NO_x emissions clearly increase the impact, especially for larger fleet sizes.

- Production of sulfate aerosol particles makes a significant contribution to the calculated ozone impact. This implies that low-sulfur fuel options and methods to control production of particle precursors should be explored.

- Flying the HSCT at lower altitudes reduces stratospheric impacts. The atmospheric residence time of the exhaust is decreased and the chemical sensitivity is reduced.

- Special issues are associated with exhaust build-up in polar regions, both winter and summer. Under current HSCT route scenarios, direct emissions into the polar vortex are minimal.

E. What are the major uncertainties in the prediction of HSCT impacts?

In several key areas, comparisons of model simulations and observational data challenge current model predictions.

TRANSPORT

Most exhaust will be emitted in the lower stratosphere in the Northern Hemisphere. Observations and models show that much of this exhaust will be carried downward into the troposphere and lost, but a fraction will be transported into the tropics, where it will be carried upward and mixed back into the mid-latitudes at higher altitudes. This material will increase stratospheric concentrations of total reactive nitrogen (NO_y), water vapor, and small particles globally. Predicting the magnitude of the fraction dispersed globally, and its residence time in the stratosphere, is a critical part of the assessment. There is a large difference among the models in the calculated accumulation of HSCT exhaust. Current models, both 2-D and 3-D, differ from diagnostic observations that test global stratospheric residence times. In particular, models predict a smaller mean age of stratospheric air, by about a factor of two, than inferred from observations. This tendency suggests that models may underestimate stratospheric residence times and the actual accumulation of exhaust that would occur in the atmosphere.

Transport uncertainties are also primarily responsible for models differing in their simulation of key trace species distributions, both from each other and from observations. To the extent that these model distributions do not match reality, the HSCT perturbation is superimposed on an incorrect background atmosphere. In particular, the model background NO_y controls the HSCT ozone response to a large extent, and no solution is known to simultaneously fix model comparisons to mean age and NO_y measurements.

AEROSOL EMISSIONS

The impact of HSCT emissions on stratospheric sulfate aerosol and the resultant effect on chemistry and ozone has emerged as one of the most important effects of aircraft in the stratosphere. Multi-phase reactions on sulfate particles strongly influence the balance among chemical ozone loss pathways in the lower stratosphere globally. More small volatile particles are formed in jet aircraft exhaust than previously expected, and the mechanism and control of this production are currently not well understood. Particle production has been shown to depend on fuel sulfur, but the particle emission yield for the HSCT is still very uncertain. Model calculations testing the atmospheric sensitivity to a range of particle emissions under differing atmospheric aerosol loadings, which are mainly controlled by volcanic eruptions, result in a range of impacts larger than that attributed to nitrogen oxides or water.

POLAR PROCESSES

Processes occurring at cold polar temperatures in winter are important to ozone because they initiate chlorine-catalyzed ozone destruction that is responsible for large seasonal ozone depletions (e.g., the "ozone hole"). Properly predicting the interaction of aircraft water, nitrogen oxides, and particles with cold polar processes is an important component of the HSCT assessment. However, our basic understanding of how polar stratospheric clouds, sulfate aerosol, and gases interact to produce rapid polar ozone loss is not complete and simulation in global models is difficult. Test calculations show that inclusion of these processes does significantly alter the calculated impact of HSCT emissions by increasing polar ozone loss, but the amount of loss varies between models

depending on their method of parameterization. In this assessment we have begun to quantify these previously unquantified effects, but the uncertainty is still significant.

CHEMISTRY

Recent measurements suggest inaccuracies in the chemical kinetic rates used in current model calculations of the partitioning of nitrogen oxides between NO_x radical and non-radical species. In general, models using current rates predict lower concentrations of radicals than observed, a tendency that would underestimate reductions in ozone. Known deficiencies in both transport and chemistry appear to lead to underestimation of ozone reduction due to HSCTs. Also, changes in the total ozone column due to HSCT exhaust result from a balance between ozone increases in the lower, aerosol-rich lower stratosphere and ozone losses in the NO_x-rich middle and upper stratosphere. Models differ in the magnitude of the vertical and latitudinal contributions to this critical balance.

THE FUTURE ATMOSPHERE

HSCTs would operate in a future stratosphere that will likely have different trace constituent mixing ratios and aerosol abundances. Climate change from increasing CO_2 will also change stratospheric temperatures and winds. Future changes in these and related quantities cannot be predicted with high accuracy. Since the effect of HSCT exhaust depends on the composition and meteorology of the background atmosphere, estimates of future changes in ozone are correspondingly uncertain. Changes in polar regions deserve special attention. In addition, the response to HSCT emissions has been tested in models with observations from current and past atmospheric conditions. The applicability to future conditions is less certain.

CLIMATE FORCING

The uncertainty in the HSCT climate forcing is estimated to be about a factor of 3. This is due to uncertainty in the exhaust accumulation and uncertainty in the temperature adjustment to a non-uniform perturbation of radiatively active gases in the stratosphere. This level of uncertainty, combined with the small magnitude of the calculated effect, makes it difficult to assess whether the HSCT climate impact is a serious concern or not.

F. Where do we stand now?

As a result of the progress on numerous aspects of the HSCT prediction problem, we are now able to predict the effects of stratospheric aviation with greater certitude than ever before. In this assessment a central value for the column ozone perturbation has been estimated based on model calculations, our understanding of the fundamental physics and chemistry of the atmosphere, and knowledge of the potential exhaust emissions. Uncertainties have been estimated for the key processes in calculating HSCT ozone impacts and a range of uncertainty about the central value has been estimated. The sensitivity of the ozone change to a set of aircraft design and atmospheric variables has been assessed. Along with the assessment of ozone change, uncertainty, and sensitivity, we have identified the significant issues and reasons for concern about the accuracy and reliability of HSCT predictions. Taken together, these results should provide useful guidance for

informed decisions on environmental policy and technology development for the HSCT aircraft. The status of several specific issues follows.

On stratospheric transport, the new measurement diagnostics and model comparisons allow us to begin to quantitatively evaluate model performance. Rapid model improvement will follow as specific shortcomings are addressed. Although the means to improvement are not all apparent, the new metrics will become part of standard procedure and models will respond. A limited number of 3-D model runs have been made for this assessment. A major emphasis will be diagnosing transport in 3-D models. These models are now on the verge of major advancement, almost certain to follow with further analysis and maturity. Until that time, though, stratospheric transport remains a major uncertainty for HSCT assessment.

Although the formation of particles in HSCT exhaust is not quantitatively predictable, the parametric studies used in this assessment limit the range of uncertainty in the chemical effect from this source. Continued process modeling and measurements should allow a mechanistic understanding of particle formation in current aircraft engine exhaust sufficient to better predict the formation of particles in HSCT plumes, thereby reducing the range used in this assessment. The processes controlling the background stratospheric aerosol distribution also need to be better quantified through systematic analysis of satellite and *in situ* observations.

Gas-phase photochemical mechanisms are generally understood and most are modeled within the combined uncertainties of the measurements and rate coefficients. Recent laboratory measurements are likely to resolve the NO_x/NO_y chemical issue identified for models used in this assessment. The possibility of missing chemical processes, which could invalidate our HSCT assessment, is significantly decreased, but continued observations are needed to minimize the risk.

We continue to be cautious about the potential effects of HSCTs in polar regions because of the demonstrated high sensitivity of ozone to changes there. This assessment does not find unexpectedly large changes near the poles, but we allow the possibility that we have not probed the full possible range of response. An upcoming measurement campaign should help to improve our ability to simulate ozone in polar regions and enhance HSCT assessment confidence. The natural evolution of climate research directed toward international climate assessments will further limit uncertainties in the state of the future atmosphere and the potential climate effects of HSCTs.

In summary, great progress has been made in understanding the potential effects of HSCTs in the atmosphere. However, we are not yet able to establish statistically rigorous error bounds on the effects of supersonic aircraft. We can carefully and critically develop a set of expert opinions on the likely ranges for future effects. To be more quantitative requires improvements in understanding and model capabilities not yet realized. We believe a strong foundation for future advances has been built: the enhanced capability to test models should pave the way for improved models in the future.

G. What can be done to reduce the uncertainties?

Research objectives consistent with the assessed sensitivities and the largest known uncertainties should include improved quantitative understanding of:

- *Transport and dynamics of the stratosphere.* Model differences from tracer observations (especially NO_y), underestimates of mean age, and the relation of residence time with HSCT exhaust accumulation make it a high priority to obtain improved knowledge of the rates for the residual mean circulation and improvements in data in the tropopause region.

- *Production of ultrafine aerosol particles by jet engines.* We need to understand the mechanism for particle production in current engines and the dependence on fuel sulfur well enough to predict HSCT particle production. Progress in understanding this phenomenon will follow from studying the process in the engine components, through the aircraft near field, and out to global scales.

- *Polar studies,* especially the mechanism for polar denitrification and the sensitivity of ozone loss in the Arctic to changes in H_2O, aerosols, and NO_y. These issues are the focus of the upcoming SAGE III Ozone Loss and Validation Experiment (SOLVE) mission.

- *Photochemistry,* laboratory studies, atmospheric observations, and analysis should continue with an emphasis on quantifying uncertainties and evaluating the potential for missing chemistry. Specific discrepancies in NO_x/NO_y partitioning must be resolved.

- *Continued development, evaluation, and refinement of models.* Fundamental processes represented in current models, with particular attention to transport, model resolution, and numerical artifacts require continued scrutiny. Methods for evaluating model performance, uncertainty quantification, and use of 3-D models should be continued.

1. INTRODUCTION AND FRAMEWORK FOR UNCERTAINTY ANALYSIS

1.1 Background

The purpose of this document is to assess the potential atmospheric impacts of a proposed fleet of high speed civil transport (HSCT) aircraft. It reviews work done under the National Aeronautics and Space Administration (NASA) Atmospheric Effects of Aviation Project (AEAP) as well as other NASA, United States, and international research programs. The findings represent a broad consensus of the atmospheric research community comprising the authors, contributors, and reviewers. This report follows a previous NASA assessment in 1995 [Stolarski *et al.*, 1995] and an interim assessment in 1993 [Albritton *et al.*, 1993].

The HSCT is a proposed conceptual aircraft that would carry approximately 300 passengers, similar to current airliners, but at more than twice the speed (Mach 2.4, 1600 mph). Critical new technologies required for such an aircraft are being developed in partnership between NASA and the aerospace industry [Wilhite and Shaw, 1997]. In conceptual configuration, this airplane would cruise at an optimum altitude in the 17- to 20-km range (56,000 to 66,000 ft). A flight altitude of 20 km puts the exhaust emission from the HSCT well into the stratosphere where most of the atmospheric ozone resides (Figure 1-1). Concern about the impact of aircraft exhaust on ozone contributed to the decision not to develop a supersonic transport (SST) in the United States in the 1970s [Johnston, 1971; CIAP, 1975]. Much has changed, however, both in our understanding of ozone perturbations and in the aeronautical technology which controls emissions [Albritton *et al.*, 1993; Stolarski *et al.*, 1995].

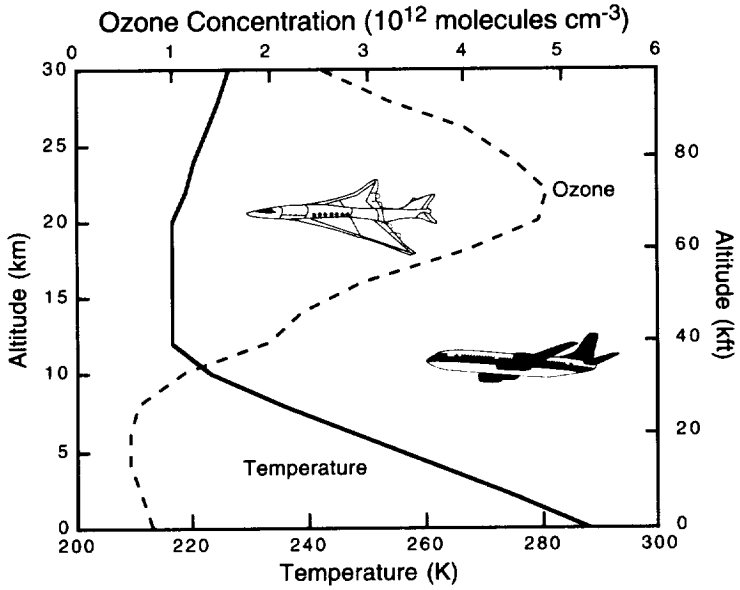

Figure 1-1. Schematic of the atmosphere between the ground and 30 km. Temperature is shown by the solid curve using the bottom scale and concentration of ozone molecules is shown as a dashed curve using the top scale. Both are for mid-latitude conditions from the U.S. Standard Atmosphere [1976]. Typical cruise altitudes for HSCTs and subsonic aircraft are indicated.

A primary environmental concern regarding HSCT emissions is the possibility of stratospheric ozone depletion. Reduction in stratospheric ozone poses risks to human health through increased ultraviolet radiation at the Earth's surface, possible damage to the biota, and changes in atmospheric temperature and climate. Considerable depletion in stratospheric ozone (several percent per decade) has already occurred as a result of the release of chlorofluorocarbons (CFCs) and other gases produced by human activities [McPeters *et al.,* 1996]. Assessment of CFC impacts has led to international treaties to control emissions and stop production of numerous substances [WMO, 1995, 1999]. Changes in stratospheric ozone may also result from changes in stratospheric temperature and dynamics due to increasing amounts of so-called "greenhouse gases," e.g., water (H_2O), and carbon dioxide (CO_2) [WMO, 1999]. The predicted impact of HSCTs on stratospheric ozone is the main focus of the current assessment.

HSCT exhaust may affect ozone in several ways. The exhaust components of interest for ozone impacts are oxides of nitrogen (NO_x (= nitric oxide (NO) + nitrogen dioxide (NO_2))), H_2O, and particulate matter. Engine combustion produces NO_x. NO_x is known to participate in one of the main catalytic chemical cycles destroying ozone in the atmosphere. Adding NO_x will, in much of the stratosphere, increase the chemical removal rate of ozone. The effect of added NO_x in some regions, however, is not so straightforward. NO_x interferes with other chemical loss processes and may even contribute to a net increase of ozone in the lowermost stratosphere.

HSCT engines will also produce H_2O. H_2O in the stratosphere is a source of oxides of hydrogen (HO_x), another chemical destroyer of ozone. In addition, H_2O plays a major role in condensation of cloud particles in the stratosphere, which in turn affect the balance of chemicals destroying ozone [Carslaw *et al.*, 1997]. Jet engine exhaust is also a source of soot and sulfate particles to the stratosphere. These products will interact with the other exhaust products and the components of the background atmosphere in a non-linear fashion to produce an overall impact on ozone.

The net chemical effect of the emissions depends strongly on the transport, dispersion, and residence time of the effluent in the stratosphere. Once transported into the troposphere, the exhaust is largely removed by precipitation, mixing, and deposition to the Earth's surface. Because the loss processes for HSCT exhaust are rapid, unlike CFCs, the lifetime of the HSCT perturbation is relatively short, about 1 to 3 years [Schoeberl *et al.,* 1998].

In addition to their potential effect on ozone, HSCT emissions may affect temperature and climate through emission of the radiatively important gases CO_2 and H_2O, and particles. Changes in ozone will also affect temperature in the stratosphere. These effects were assessed previously [Rind and Lonergan, 1995; Stolarski *et al.*, 1995], and the impact was generally considered to be small. Recently, however, HSCT radiative forcing has been re-examined, and the issue has emerged as a concern, albeit with large uncertainties in the magnitude of the effect. The issues and uncertainties in HSCT climate forcing are reviewed in Chapter 4, but climate impact is not a major focus of this report.

The possible interactions of HSCT exhaust with the atmosphere are complex and uncertain. The fleet does not yet exist, and thus the effect cannot be measured, nor do we have an analogous perturbation to compare it to. Because of this, the potential effects of HSCTs are calculated in numerical models of atmospheric chemistry and transport. Such chemical transport models

(CTMs) are necessarily incomplete representations of the real atmosphere. We have an incomplete fundamental understanding of how the atmosphere works. Furthermore, computers have limited capacity to simulate the atmospheric system at all time and spatial scales. These factors lead to significant uncertainty in calculation of HSCT impacts. In this work we assess the current state of understanding of important processes, our ability to accurately simulate them in models, and the consequent uncertainty in predicted impacts of stratospheric aviation.

Assessment of the impact of aviation on the atmosphere will also be found in the Intergovernmental Panel on Climate Change (IPCC) Special Report on Aviation and the Global Atmosphere scheduled for publication in 1999. The IPCC report is closely related to this NASA report. Many of the HSCT model calculations are the same. The NASA report is written by AEAP researchers, many of whom also participated in the IPCC report. The IPCC report, however, has a major focus on the current and future subsonic aircraft fleet while this NASA report concentrates fully on HSCT-specific issues, including enhanced discussion and further exploration of uncertainties.

1.2 Summary of Previous Assessment

A summary of key findings and recommendations from the previous NASA report [Stolarski *et al.*, 1995] is as follows:

- The impact of HSCT NO_x on ozone was smaller than thought in the 1970s. Understanding of the NO_x chemistry of the stratosphere improved significantly since the original evaluations in the 1970s. We now understand that aerosol reactions play a major role in controlling the abundances of NO_x, HO_x, and reactive chlorine. Aerosol reactions increase HO_x and the amount of catalytically active chlorine while at the same time decreasing the amount of NO_x. The result is a lessening of the predicted effect of NO_x from the earlier results of the 1970s.

- Chemical mechanisms were confirmed by *in situ* data on ozone loss rates. The partitioning of nitrogen into NO_x and its less reactive reservoirs was confirmed by *in situ* measurements in the lower stratosphere. These measurements lend additional credence to the loss rates calculated in models that are used to predict the impact of HSCTs.

- Climate impacts were estimated to be small. Simple calculations showed that the radiative forcing due to changing ozone, water vapor, soot, CO_2, and sulfate particles was expected to be small compared to other changes in greenhouse gases. Model calculations with a low-resolution three-dimensional (3-D) model supported the small impact of changing ozone and water vapor relative to model variability.

- Sulfur conversion to particles was identified as a potential problem not previously considered. A new finding was that sulfur coming from the exhaust might be in the form of tiny new particles rather than gas. This was experimentally observed in the exhaust of a Concorde SST aircraft. It implies that the increase in ambient particle surface area due to a fleet of HSCTs will be greater than previously thought. This increase in particulate leads to an enhancement in active chlorine and ozone loss through the chlorine loss cycle. The effect would diminish somewhat as chlorine decreases in future years. Model calculations showed that this effect is

sensitive to a number of factors, especially the fraction of the sulfur that appears as new particles.

- A crude attempt was made at estimating overall uncertainties. Some were quantitatively estimated, but others required pure guesses. It was not clear how to combine all of the known sources of uncertainty into an overall estimate.

- Several recommendations were made. To deal with transport uncertainties the report recommended an augmentation of chemical tracer measurements which led to a series of aircraft and balloon missions. The report also recommended the development of a 3-D CTM which resulted in formation of the Global Modeling Initiative (GMI). The report recommended an improved modeling of particle formation in exhaust and the inclusion of a standard particle description in two-dimensional (2-D) models. Finally, the report recommended an improved characterization of exhaust aerosols which led to in-flight and altitude-chamber engine tests.

1.3 Overview of 1998 Assessment Report

Major progress has been achieved since the last assessment. Field measurement campaigns have been carried out to obtain data with which to begin quantitatively evaluating model transport processes. Observational data have also augmented our ability to constrain and evaluate modeling of stratospheric chemistry. These data have been used in the Models and Measurements II (M&M II) intercomparison and evaluation exercise [Park *et al.*, 1999]. Assessments have been performed for the first time with 3-D CTMs. The assessment numerical models have been made more complete in their representation of atmospheric processes including sulfate microphysics, heterogeneous reactions, polar stratospheric clouds, and planetary wave parameterizations. And finally, the current assessment includes an extensive test of the impact of sulfate particle production by aircraft.

Along with this progress, new issues have arisen which must be considered in the aircraft assessment. Research into the manifestations of climate change from CO_2 and other greenhouse forcings indicates that the stratosphere in which the HSCT will eventually fly may be very different than today's atmosphere. We have strong indication that the chemical, radiative, and dynamical elements of the system are tightly coupled. The wave-driven transport circulation, which controls the global distribution of stratospheric ozone, may be altered by temperature changes in the lower atmosphere. Stratospheric temperature and the abundance of water and other trace species will change in ways often difficult to predict. Sensitivity to these changes is magnified by non-linearities in the chemical system triggered by a combination of homogeneous catalysis, titration points, and phase transitions in combination with heterogeneous catalysis. These factors caution that the response to a relatively small perturbation like the HSCT has the potential to be significant and that we must accurately describe the background atmosphere onto which the perturbation is projected. Although the future atmosphere in 2015 to 2050 cannot be known, in this assessment we have begun to probe how some of the expected compositional changes may interact with the HSCT emission and what level of uncertainty is engendered.

In this introduction (Chapter 1) to the report we review the background and content of the assessment report. We then proceed to establish a framework for evaluating and compounding

uncertainties in the calculated estimates of the HSCT impact on ozone (below). Several components of the uncertainty and methods for combining them are not yet available. Hence the framework has missing components and the final evaluation is to a large extent qualitative.

In Chapter 2 we assess the current state of understanding of atmospheric processes, specifically transport and chemistry, as related to calculation of HSCT ozone impacts. Transport issues are identified which are critical to reliably predicting HSCT impacts. New measurements have begun to quantify rates of some key transport processes. For others, direct measurements are not available, and large uncertainties remain in the aggregate of transport processes that determine the distribution and lifetime of HSCT exhaust. By comparison, confidence is fairly high in our understanding of gas-phase chemical processes related to HSCT impacts on ozone. Extensive analysis of chemical measurements from aircraft, balloon, and satellite indicates that our description of stratospheric chemistry is generally accurate and appears nearly complete. There are several exceptions, but we see a clear pathway to resolving the problems. Understanding of heterogeneous (gas-particle) chemical and particle microphysical interactions has improved but these processes remain difficult to represent precisely.

We assess the expected emissions from the HSCT and their deposition in the stratosphere in Chapter 3. We establish the emissions scenarios that will be input to the assessment CTMs and review the methodology for estimating the emitted amounts and spatial distribution. Of particular interest are the emissions of CO_2, H_2O, NO_x, and sulfur gases and particles. Unknowns in the ultimate aircraft configuration, number, and date for deployment are treated parametrically. A major uncertainty is identified in the aircraft production of small sulfate particles, which have a major impact on calculated ozone.

Calculated impacts of HSCTs on stratospheric ozone are given in Chapter 4. A number of models, including 3-D CTMs, are used under a variety of different assumptions. The models are used to evaluate engineering outcomes, e.g., NO_x emission index (EI), HSCT flight altitude, etc. They are also used to evaluate sensitivity to atmospheric unknowns like background sulfate surface area, chlorine loading, temperature, and aircraft aerosol production. A major part of this work is assessing our ability to accurately simulate atmospheric processes important to the HSCT calculation in numerical models.

In Chapter 5 we synthesize the effect of HSCTs in the stratosphere with particular emphasis on the uncertainty in the various processes which control the ozone impact. Estimates of the magnitude and uncertainty of ozone change are summarized along with the sensitivity of ozone to various assumptions about HSCT technology development and the state of the future atmosphere. Key processes and the level of confidence associated with their simulation in HSCT calculations are extracted from Chapters 2 to 4. We attempt to combine the uncertainties and roll them up into an integrated estimate of HSCT impact uncertainty. This procedure is far from complete or rigorous, but should provide some guidance for policy and technology decision making. Finally, we summarize the major findings and make recommendations for the future path to improved assessment of potential HSCT impacts.

1.4 Framework for Evaluating Uncertainties

The task of representing uncertainties in predicted ozone column changes, which result from secular trends in chemical, radiative, and dynamical variables, has confronted the atmospheric research community for at least three decades. Through the course of evolving observational methods; laboratory results; developments in modeling strategies; surprises in the Antarctic, Arctic and mid-latitudes; and varying degrees of cooperation among the affected communities (regulatory, agency, scientific, corporate, engineering, etc.) lessons have been learned:

- The fundamentals of the atmospheric system must be described such that the dominant mechanistic links are exposed and clarified for the technically literate reader.

- The boundary must be clear between that which has been tested by observations and that which is hypothesized to be true.

- The coupled nature of the system and the existence of strong non-linearities must be emphasized.

- The state of the atmosphere onto which an external forcing is projected must be accurately prescribed for the period of interest.

We must accomplish each of these tasks in assessing HSCT impacts.

The uncertainty in predictions of the impact of HSCTs is made up of the uncertainty in each step in the chain of processes which leads from the exhaust, through the spread to global atmosphere, to the chemical changes, and eventually to the possible feedbacks on atmospheric transport. Here the focus is on evaluation of the uncertainty in calculation of the HSCT impact on ozone concentrations.

Key issues in evaluating the effects of a fleet of HSCTs are:

1) Emission of exhaust - What is emitted and how is it deposited in the atmosphere? How much fuel will be burned and where? How much NO_x is emitted per kg of fuel? How many particles of what size are emitted or formed in the exhaust plume/wake?

2) Transport of exhaust - Where will exhaust go? How much will accumulate in various regions of the atmosphere?

    a) Will exhaust be primarily confined to mid-latitude lower stratosphere where it is emitted?

    b) How much exhaust will be transported to the equatorial region and then upward where NO_x is more effective at destroying ozone?

    c) How much exhaust will be transported to polar regions where polar stratospheric cloud chemistry is occurring?

d) How rapidly will the exhaust be transported down into the lowermost stratosphere and upper troposphere where it will be removed?

3) Representation of the atmosphere in which the aircraft will fly - How well can we represent the background atmosphere against which the HSCT perturbation is superimposed? This is a question of both how well we simulate the current atmosphere and how well we can forecast future conditions. In forecasting the future, how well can we predict atmospheric winds and temperatures in the face of expected climate change? How well can we forecast future source gas concentrations?

4) Chemical effect of exhaust - How much will exhaust species increase ozone loss rates? How much will they interfere with background loss rates due to other chemicals? How much will added particles affect the balance of the loss cycles? How much different are chemical sensitivities in the model from those in the atmosphere because the model doesn't calculate the correct background atmosphere?

5) Effects in polar regions - How will exhaust species interact chemically with existing polar processes? How much will condensibles (H_2O, nitric acid (HNO_3), sulfuric acid (H_2SO_4)) change the particle and polar stratospheric cloud amounts and hence chlorine-driven ozone loss in the polar regions?

6) Transport of the HSCT perturbation - How will the chemical perturbation be propagated by atmospheric transport? To what extent will the ozone-chemical feedbacks tend to damp out or amplify?

The calculation of the effect of this chain of processes is accomplished by using computer models. The models used are 2- and 3-D CTMs which integrate these effects and interactions, resulting in an estimate of the impact of HSCTs. Models use our knowledge of processes gained from studying the present and past atmospheres to project impacts of changes into the future. Uncertainty in this future projection will result from errors in our theoretical understanding of the basic processes and inaccuracies in the approximations used to incorporate them in the numerical model calculation. Uncertainty also arises from our inability to accurately predict the future state of the atmosphere.

We aspire to a complete statistical description of the uncertainty in each of the processes in the chain which we use to calculate ozone impact. Some parts of this chain are better understood and quantified than others. The description of each step ideally includes a most probable value and probability distribution of outcomes based on known uncertainties in the calculations, e.g., Figure 1-2. It is not yet possible, however, to put defensible numbers on this schematic for many of the processes nor is the shape of the probability distribution known. However, the probability diagram is still useful as a conceptual framework for uncertainty analysis though.

If we had quantitative estimates for the probability distribution of each individual process comprising the total ozone change, these could then be combined to form an uncertainty in the calculated perturbation. The combination of the chemical terms can be thought of in the form of a

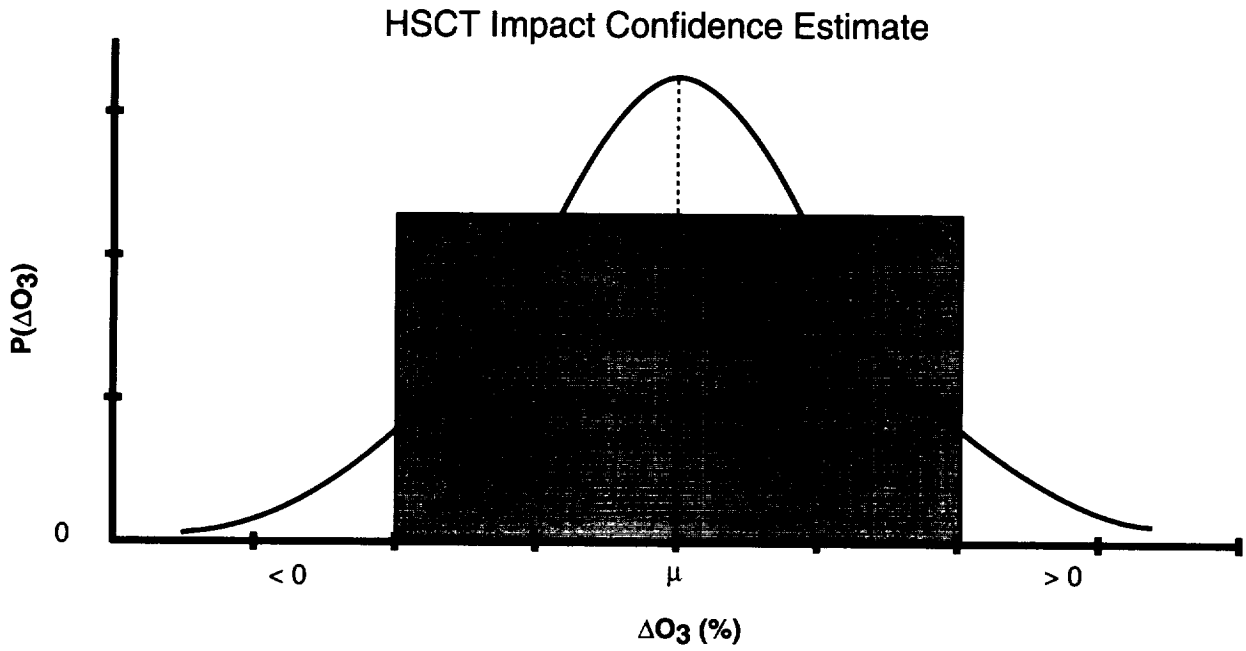

Figure 1-2. Schematic probability density diagram for HSCT impacts: in an ideal situation shown by the curve and for a semi-quantitative range of estimates represented by the shaded box. $\Delta(O_3)$ represents the Northern Hemisphere, annual average column ozone perturbation due to HSCTs. $P(\Delta(O_3))$ is the estimated probability of impact. μ is the most probable value of $\Delta(O_3)$ (which in general is not 0). Note that in reality the probability may not be normally distributed. In this report we attempt to identify the range of likely impact based on model calculations and expert interpretation.

simplified representation of the chemistry. The loss rate for ozone (O_3) is a function of the concentrations of NO_x, HO_x, chlorine oxides (ClO_x), and bromine oxides (BrO_x).

The perturbation of ozone caused by an increase in NO_x is then composed of several terms. The first of these is the increase in the catalytic destruction of ozone due to added NO_x. The second is the interference of the added NO_x in the catalytic destruction by HO_x and the third and fourth are the interference with the catalytic destruction by ClO_x and BrO_x. The uncertainty in each of these terms can be derived from estimates of the uncertainties in input reaction rates or can be estimated from atmospheric measurements of the concentrations of key radical species. Once these uncertainties have been estimated, they can be combined to give an uncertainty in the chemical part of the ozone calculation. Much of the chemical sensitivity described in this way has been tested with observations as discussed in Chapter 2.

Unfortunately this approach can only be partially applied because we lack complete information. We do not have simple representations and relational operators for some terms such as transport of the exhaust (e.g., ΔNO_x), nor quantitative estimates for some errors. Inter-model variability provides a partial estimate of uncertainty, but cannot at present be used to measure the total uncertainty with respect to reality. Transport uncertainty is also responsible to a large extent for

persistent errors in model background tracer abundances, against which the HSCT impact is assessed. The perturbation terms above must be calculated at the right place in the (non-linear) function, but our ability to simulate the current atmosphere is imperfect (Chapter 4). On top of all this, even if we had a complete model, there would be uncertainty in predicting the composition of the future atmosphere, which depends on technology development, population growth, resource consumption, etc. Thus we are forced to give qualitative estimates of uncertainty based on partially quantitative analysis. We follow the approach of Mahlman [1997] in dividing processes into several categories:

a) Well understood and demonstrated by measurements;

b) Highly likely to be correct but not demonstrated by measurements; and

c) Uncertain and difficult to quantify.

For all of the key processes we attempt to estimate uncertainties according to the above categories.

The uncertainties are combined and presented in Chapter 5 in terms of a range. If all values within that range were equally probable, then the distribution would look like the box Figure 1-2. In reality, our best knowledge would indicate that the actual perturbation is more likely to be somewhere near the center of the range. Values of the perturbation outside the given uncertainty limits are less likely to occur. The real answer, however, may still fall outside this range. As one goes farther and farther from the centerline, our best knowledge is that the probability decreases toward, but does not reach, zero.

The uncertainty range represents an estimate of known uncertainties around a most-probable $\Delta(O_3)$ value. This range includes definitely quantified uncertainties such as inter-model variability and kinetics uncertainty in addition to unquantified uncertainty in processes such as transport. In the case of processes with unquantified uncertainty an estimate has been made assuming that there are no major errors in our formulation. The uncertainty estimate does not reflect possible effects of unknown, unmodeled processes (e.g., surprises) on $\Delta(O_3)$ calculations. Limits on this range of impact are imposed by comparisons of model and observations under as many circumstances as possible. We are not able to estimate a $\Delta(O_3)$ range for such unknown processes.

The sensitivity to certain input assumptions is tested in parametric studies, such as aircraft fleet emissions. Within the range of parameters, quantitative sensitivities can be calculated which may be valuable to help guide aircraft technology development or deployment strategies. Establishing confidence in these results introduces still another category of uncertainty, precision in the assessment calculations. Relative to the probability curve, engineering sensitivity tests (e.g., fleet size, EI, altitude of emissions) may shift the most-probable outcome. The uncertainty in the direction of change may be significantly less than the uncertainty in the absolute magnitude of a perturbation. We have limited confidence, however, in estimating how these tests change the shape of the probability curve.

Sensitivity tests of atmospheric variables in the future, e.g., background atmosphere with a different sulfate surface area, Cl, or T, may have a differently shaped probability curve but our

current level of refinement is not adequate to distinguish. At our current level of understanding these tests have similar uncertainty characteristics to the engineering tests, i.e., they may shift the curve but change in shape is unknown.

In summary, this assessment of the effects of high-speed aircraft in the stratosphere contains predictions of the change in ozone resulting from proposed HSCT fleet emissions and our evaluation, or assessment, of confidence in these predictions. The assessment is based on theoretical understanding, comparisons with observations, numerical tests, and expert opinion. We attempt to express our confidence with uncertainty estimates, however, these are not fully quantitative or statistical. The chapters that follow document the scientific information and process of this assessment.

2. THE ATMOSPHERE: OBSERVATIONS AND FUNDAMENTAL PHYSICS AND CHEMISTRY

2.1 Introduction

O_3 is produced in the stratosphere primarily by the photodissociation of molecular oxygen at wavelengths less than 240 nanometers (nm):

$$O_2 + h\nu \rightarrow O + O$$

followed by reaction of the oxygen atoms with O_2:

$$O_2 + O \rightarrow O_3$$

From a starting point in the mesosphere, the ozone concentration increases with decreasing altitude because of the exponential increase in molecular oxygen concentration. The concentration reaches a peak at about 22 km at mid-latitudes and then decreases with decreasing altitude because of the attenuation of ultraviolet photons by molecular oxygen. This production term is balanced by the catalytic removal of ozone due to cycles involving nitrogen, hydrogen, halogen and oxygen radicals, for example,

$$\begin{aligned} & O_3 + h\nu \rightarrow O_2 + O \\ & NO + O_3 \rightarrow NO_2 + O_2 \\ & NO_2 + O \rightarrow NO + O_2 \\ \text{Net: } & O_3 + O_3 \rightarrow 3\,O_2 \end{aligned}$$

$$\begin{aligned} & HO_2 + O_3 \rightarrow OH + O_2 + O_2 \\ & OH + O_3 \rightarrow HO_2 + O_2 \\ \text{Net: } & O_3 + O_3 \rightarrow 3\,O_2 \end{aligned}$$

$$\begin{aligned} & ClO + BrO \rightarrow Cl + Br + O_2 \\ & Cl + O_3 \rightarrow ClO + O_2 \\ & Br + O_3 \rightarrow BrO + O_2 \\ \text{Net: } & O_3 + O_3 \rightarrow 3\,O_2 \end{aligned}$$

Transport distributes ozone between regions where chemical production and loss are not exactly balanced.

The issue we face in this report is to determine the response of the atmosphere to HSCT effluents including nitrogen oxides, aerosol particles, water vapor, and carbon dioxide. The response depends on transport because atmospheric motions redistribute the aircraft effluent, and because of the influence of transport on ozone. The response depends on photochemistry because of the effects of the accumulated aircraft exhaust on the abundance of free radicals that drive catalytic removal of ozone.

We assume that the HSCT perturbation to ozone will not significantly alter the stratospheric circulation and temperature. This assumption is supported by calculations (e.g., Schoeberl and Strobel [1978]). Therefore, we treat the chemical consequences of the HSCT perturbation in detail without explicitly coupling these consequences to changes in atmospheric dynamics and transport. A variety of models and calculations show the exhaust will change the composition of the atmosphere. Important trace species including H_2O, NO_y, and aerosol will be enhanced. In some places the increases will be as much as a factor of 2, although the global average perturbation will be smaller than that. Given this assumption, we estimate that the assessment of aircraft effects on the ozone layer will be accurate enough if we study only the primary chemical consequences of the HSCT exhaust and neglect feedbacks of those consequences on the atmospheric transport. We neglect higher order feedbacks of changes to transport on the chemistry, as well. For the sake of discussion, it is useful to think that the HSCT effect on the atmosphere can be described by the sensitivity of the atmosphere to an infinitesimal amount of each component of the exhaust multiplied by the total amount of the exhaust. The sensitivity term is a property of the atmosphere independent of the number of aircraft or the quantity of emissions from any one aircraft. Historically, this property of the atmosphere has been extremely difficult to calculate. In fact, many of the historical changes in our predictions of the effect of HSCT exhaust derive more from changes in our descriptions of the atmospheric sensitivity than from changes to assessments of the accumulation of aircraft exhaust. In many parts of the atmosphere, as we discuss below, we now have direct measures of the local chemical component of the sensitivity.

Ideally (from the point of view of evaluating the effect of HSCTs accurately), the natural variability of the atmosphere would possess sufficient range about its average state to include conditions similar to those that will be created by the HSCT effluent. We would then try to identify which year or season in the record of atmospheric observations is most like a year in which HSCTs fly. This is not possible. Small regions of the atmosphere do, on occasion, have excursions in composition that are far enough from its mean state to provide an analogy to the HSCT perturbation, but, taken as a whole, the stratosphere does not exhibit conditions represented by the accumulated HSCT exhaust. Nevertheless, measurements of these excursions are extremely important to our understanding. They have been used to construct a set of partial derivatives describing the local chemical response of the present atmosphere to changes in NO_x concentrations and to changes in aerosol (see Section 2.4). These measurements increase our confidence in our understanding of the chemical terms that control ozone and in the expected response of these terms to the NO_x and aerosol perturbations by HSCTs in a future atmosphere. Measurements have also determined the rate of transport of air into and within the stratosphere placing constraints on models describing how transport will distribute aircraft exhaust in the atmosphere and how the atmosphere will act to integrate the effects of local photochemistry over the ~1 year life cycle of ozone (see Section 2.3). Large volcanic eruptions have provided the opportunity to directly measure the integrated chemical-dynamical response of the stratosphere to changes in aerosol. These well-documented observations are some of the most exacting constraints on the potential effects of aircraft. Unfortunately, our estimations of the aerosol EI by HSCT engines are more uncertain than the EI of other exhaust components such as NO_x or H_2O. The trend in emissions of CFCs has provided observations of the atmosphere's response to changes in halogen radicals.

Lacking observations that correspond directly to aircraft exhaust, detailed mechanistic models are the primary tool we use for integrating our knowledge about atmospheric processes and for making

predictions about atmospheric composition and temperature in the future. These detailed models are discussed in Chapter 4. In this chapter, we focus on simpler concepts that provide insight into atmospheric behavior and that have a more direct link to atmospheric and laboratory observations. These measurements and elementary concepts guide our interpretation of the output from complex models and provide a basis for our estimates of the uncertainty in the predicted effects of the HSCT.

We begin by describing the major trace constituents of the stratosphere and the range of their likely evolution over the next century in Section 2.2. This section describes our knowledge about the reference state of the future atmosphere. Our present understanding of atmospheric transport and photochemistry is described in Sections 2.3 and 2.4, in which we highlight some recent advances. These sections identify the mechanisms that provide a basis for evaluating the perturbation. Finally, in Section 2.5, we summarize the main results and highlight issues in evaluating the uncertainty associated with this assessment.

Throughout this chapter we compare our understanding of the atmosphere and our attempts to represent the atmosphere in a numerical model with observations. In some instances, recent interpretations of measurements confirm the correspondence between observations of the atmosphere and numerical representations of it. These analyses increase our confidence in understanding the behavior of the atmosphere and in the model predictions. In other instances, recent analyses point out differences between observations of the atmosphere and the models. These studies point to directions for improvements of the representation of the atmosphere in the numerical models in the future. They identify aspects of models where we must utilize our understanding of the atmosphere to extrapolate from model results to a better estimate of the HSCT perturbation.

2.2 Atmospheric Composition and Trends

2.2.1 Source Gases

Tropospheric source gases define an initial boundary condition for air entering the stratosphere. Relatively few chemical species survive to enter the stratosphere in abundance, as most reactive compounds are destroyed within the troposphere. Some of the compounds that do enter the stratosphere continue to be unreactive there, e.g., CO_2, sulfur hexafluoride (SF_6), and perfluoromethane (CF_4). Many—nitrous oxide (N_2O), methane (CH_4), H_2O, H_2, CFCs, hydrochlorofluorocarbons (HCFCs), methyl chloride (CH_3Cl), halons, methyl bromide (CH_3Br), and carbonyl sulfide (OCS)—react slowly, yet are the primary sources for the free radicals and aerosol that regulate chemical change in the stratosphere.

Predictions of the response of the atmosphere to the HSCT in the mid-21st century require estimates of the distributions of the source gases in the future. We estimate the evolution of distributions in the future from analysis of observations of the source gases at the surface, in the stratosphere, and in historical air preserved in glacial ice cores together with industrial production and projections of economic growth. Many of these compounds are the subject of existing or developing international treaties. Their future distribution will no doubt be affected by the evolution of political and economic decision making that cannot easily be extrapolated on the basis

of current trends. Where possible, we describe changes in atmospheric composition that may result from political and economic options currently being explored.

Once in the stratosphere, the source gas distributions are determined by a combination of chemistry and transport. Measurements and models show that the distribution of the slowly-reacting trace gases depends on processes that occur on time scales of several years. This is in contrast with the time scales controlling ozone column abundances of about 1 year and the time scales controlling free radical concentrations of seconds to as long as weeks (local ozone lifetimes in the stratosphere are shorter in the middle and upper stratosphere and longer in the lower stratosphere, contributing to a global average lifetime of about 1 year). The separation in time scales allows us to focus attention separately on the accuracy of predictions of future source gas distributions, future free radical abundances, and ozone distributions. The separation in time scales also implies that different aspects of the chemistry and transport in models will determine the quality of our predictions of radicals, ozone, and long-lived reservoirs.

The source gas distributions used in the calculations described in Chapter 4 are based on estimates presented in WMO [1995] and IPCC [1996]. The following sections briefly touch on each of the major families of source gases with attention to the uncertainty in these estimates.

2.2.2.1 N_2O

N_2O produced at the Earth's surface is the primary source of NO_x to the stratosphere. Once in the stratosphere, N_2O is removed irreversibly by photolysis and reaction with electronically excited oxygen atoms ($O(^1D)$). These reactions are most rapid in the upper tropical stratosphere. Global N_2O distributions (Figure 2-1a) have been recently measured directly by the Cryogenic Limb Array Etalon Spectrometer (CLAES) instrument aboard the Upper Atmosphere Research Satellite (UARS) [Roche *et al.*, 1996]. Climatologies have been constructed from ER-2 aircraft data [Strahan *et al.*, 1999], and observations from Atmospheric Trace Molecule Spectroscopy (ATMOS) and balloon-borne instruments provide additional information [Chang *et al.*, 1996b; Kondo *et al.*, 1994, 1996].

Surface mixing ratios of N_2O in the early 20th century were ~280 parts per billion by volume (ppbv) [Battle *et al.*, 1996]. Concentrations have been steadily increasing as a result of industrial and agricultural processes. The surface mixing ratio in 1997 was 317 ppbv [Butler *et al.*, 1998]. Models and observations have attempted to characterize individual sources of N_2O and their growth [see IPCC, 1996]. N_2O release depends on plant species, nutrient availability, and numerous other ecological factors that have wide variation on spatial scales of meters. Nevison and Holland [1997] describe the increase of N_2O using a simple model fit to the observations of atmospheric N_2O over the last three decades. It predicts N_2O mixing ratios near 340 ppbv in 2015 and near 400 in 2050. These estimates are higher than 333 ppbv in 2015 and 371 ppbv in 2050 estimated by the IPCC [IPCC, 1996]. The dominant uncertainties in N_2O growth over the next 50 years are the rate of global population and economic growth, the rate of change of per capita fertilizer use in developing countries, technological improvements in the efficiency of fertilizer use, and growth in the use of bio-engineered nitrogen fixing crops. Estimates of the uncertainty in future N_2O are derived from the range of reasonable model parameters described by Nevison and Holland [1997]. This analysis suggests the absolute concentration predicted for N_2O is probably accurate to 10% in

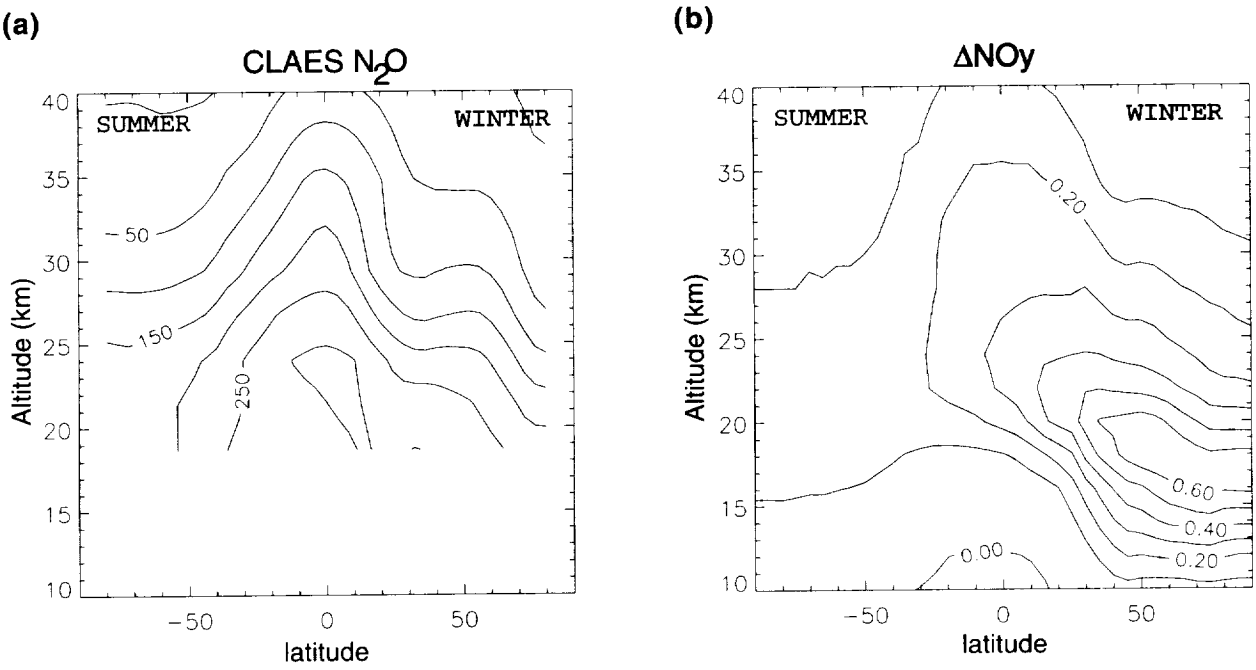

Figure 2-1. Zonal-mean distributions of (a) N2O in ppbv (measurements from CLAES instrument on UARS), and (b) HSCT NOy emissions in ppbv (from GMI 3-D model) for January.

2050. As a result of the increasing concentration of N_2O, in the absence of stratospheric aircraft, we expect the concentration of stratospheric NO_x to be 10 to 25% higher in 2050 than today.

2.2.2.2 Halocarbons

Industrial halocarbons are currently the major sources of chlorine and bromine free radicals in the stratosphere. Much of the remaining chlorine comes from natural sources of methyl chloride (CH_3Cl) and the remaining bromine is derived from natural sources of methyl bromide (CH_3Br). Observations at the surface continue to show that the Montreal Protocol and its amendments have effectively reduced the release of halocarbon molecules to the atmosphere. Montzka *et al.* [1996] report that the mixing ratio of tropospheric halocarbons was decreasing at a rate of 25 ppt of chlorine atoms/year in mid-1995. Decreases in the abundance of chlorinated hydrocarbons near the surface have been dominated by decreases in methyl chloroform. Observations in the stratosphere show very slow growth over the last few years and are consistent with the changes in surface concentration [Engel *et al.*, 1998].

Future halocarbon emissions are regulated by international treaty. Holmes and Ellis [1996] have modeled the political economy of global CFC use taking into account expected world economic and population growth and conclude that atmospheric halocarbon concentrations will decrease until 2050 or so, as long as compliance with international treaties is greater than 90%. After that, compliance rates of 98% or better are required to continue to reduce chlorine mixing ratios. Predicted concentrations in 2015 are 3.3 ppbv and in 2050 range from 2.2 ppbv (100% compliance) to 3.3 ppbv (90% compliance). Uncertainties in these estimates are significant and

increase at longer time horizons. Modeling suggests that reactive chlorine in 2015 will be somewhere between 3.0 and 3.6 ppbv, as long as compliance ranges from 90 to 100%, while in 2050 predictions range from 2.2 to 3.4 ppbv.

Halons deliver 40% and CH_3Br delivers 55% of the 17 parts per trillion by volume (pptv) of bromine observed entering the stratosphere [Schauffler *et al.*, 1998]. Concentrations of halons in the troposphere are changing more slowly than expected and industrial reservoirs are capable of releases that will be important for decades [Butler *et al.*, 1998]. CH_3Br has both natural and man-made sources and its future contribution to stratospheric bromine is more difficult to predict. Total phase-out of industrial CH_3Br production by 2010 should reduce mixing ratios, although perhaps imperceptibly. Analysis of air trapped in firn ice since 1900 suggests a natural CH_3Br abundance of 7 to 8 pptv [Butler *et al.*, 1999]. Current uncertainties in the CH_3Br budget, including the roles of surface and ocean processes, leave open the possibility that CH_3Br inputs to the stratosphere will remain near 10 pptv throughout the next century [Yvon-Lewis and Butler, 1997; Shorter *et al.*, 1995].

2.2.2.3 H_2O, CH_4, and H_2

Water, methane, and hydrogen are the sources for production of hydroxyl radicals (HO_x = OH + HO_2) in the stratosphere. Equally important, and a factor that contributes more prominently to the uncertainty of this assessment, water vapor that condenses as a liquid or solid onto sulfuric acid aerosol is a highly reactive medium (see Section 2.2.2.4).

The concentrations of water vapor entering the stratosphere are controlled by condensation and precipitation/sedimentation at the tropical tropopause, and by the seasonal cycle in temperature at the tropical tropopause which produces a nearly sinusoidal seasonal cycle in H_2O [Mote *et al.*, 1996; Weinstock *et al.*, 1999]. Peak mixing ratios of 6 parts per million by volume (ppmv) enter the stratosphere in the months of June-July-August and minimum mixing ratios of 2 ppmv enter in January-February-March. In addition to direct input from the troposphere, oxidation of CH_4 (which enters the stratosphere with a mixing ratio of approximately 1.8 ppmv) produces an increase in H_2O mixing ratios as the air mass ages. Observations at the surface have established that CH_4 mixing ratios are increasing. Until recently, the rate of increase was thought to be linear at about 0.010 ppm/year (0.6%/year) [IPCC, 1996]. Recently however, Dlugokencky *et al.* [1998] have presented an analysis suggesting that CH_4 concentrations are approaching steady-state with the anthropogenic source. Assuming that anthropogenic inputs remain constant, this analysis implies that atmospheric concentrations will soon settle at a value somewhere between the present day mixing ratio of 1.8 ppmv and 2 ppmv. Measurements of H_2O and CH_4 in the stratosphere show that 2 water molecules are produced for each CH_4 removed, indicating the hydrogen is not increasingly stored in H_2 as the CH_4 oxidation proceeds [Dessler *et al.*, 1994; Le Texier *et al.*, 1988]. This is consistent with observations of H_2, which suggest that the concentration is uniformly 0.5 ppmv throughout most of the stratosphere [Hurst *et al.*, 1999].

Predicting the future stratospheric H_2O is thus dependent on predicting future tropical tropopause temperatures and future CH_4 mixing ratios, in addition to inputs due to HSCTs. If tropopause temperatures cool (warm), then H_2O entering the stratosphere should decrease (increase). Uncertainty in the rate of CH_4 increase affects our estimates of H_2O as well. If the rate of increase

remains constant, CH_4 concentrations will be near 2 ppmv in 2015 and almost 2.5 ppmv in 2050. In 2050, this CH_4 increase would result in a 1.4 ppmv increase in peak H_2O mixing ratios compared to the present. On the other hand, CH_4 may stabilize at present day values. The resulting increases (decreases) in H_2O, should lead to more (less) reactive aerosol and an increase (decrease) in the onset temperature associated with polar stratospheric clouds (see Section 2.4.5). The exponential sensitivity of low temperature chemistry on aerosol surfaces to H_2O make this one of the major uncertainties in our predictions about the background atmosphere in the future. Changes to H_2O and CH_4 may also affect HO_x photochemistry, although to a lesser extent because of the strong buffering of HO_x by HNO_3 and reaction of OH with HO_2 (see Section 2.4.4).

2.2.2.4 OCS, SO_2, and Aerosol

Stratospheric aerosol particles are composed primarily of sulfuric acid and water. Reactions on the surface and in the liquid phase of these particles have a substantial effect on the distribution of catalytically active free radicals and, therefore, ozone. Chemical reactions on particles depress NO_x, and enhance hydrogen, chlorine, and bromine free radical abundances (see Section 2.4.5). Thus, the distribution of aerosol is central to describing the atmospheric base state. In addition, aircraft emit sulfur compounds in some combination of gas-phase molecules or directly as particles. When aerosol surface area densities are low, HSCT-produced aerosol particles could be a significant perturbation to atmospheric aerosol, and consequently NO_x and ozone. In contrast, in a volcanically perturbed atmosphere, aircraft aerosol will likely have a minor incremental effect on NO_x and ozone (see Section 2.4.5 and Chapter 4 below).

Sulfate precursor gases, predominantly OCS and sulfur dioxide (SO_2), are transported into the stratosphere through the tropical tropopause. Subsequent photochemistry leads to the formation of H_2SO_4. Volcanic eruptions also sporadically inject significant quantities of SO_2, which oxidizes with a time scale of ~1 month to form H_2SO_4 [Krueger *et al.*, 1995]. The H_2SO_4 condenses to form new particles or adds to the mass of preexisting particles. Most new aerosol particles are formed by homogeneous nucleation in the upper tropical troposphere and are transported upward across the tropical tropopause [Brock *et al.*, 1995] or by condensation onto meteoritic material in the high latitude-middle stratosphere [Turco *et al.*, 1981]. Stratospheric H_2SO_4 aerosol particles may change composition and size through coagulation and uptake of H_2O, H_2SO_4, and HNO_3 in a manner dependent on the mixing ratios of these gases, pressure, temperature, and the particle size distribution [Del Negro *et al.*, 1997; Carslaw *et al.*, 1994; Steele and Hamill, 1981].

An approximately uniform 500 ppt mixing ratio of OCS is observed in the troposphere. Recent modeling studies indicate that this source alone may be insufficient to supply the sulfur in the stratospheric particles during volcanically quiescent periods (see e.g., Chin and Davis [1995]). Transport of larger than expected SO_2 from the upper troposphere [Chatfield and Crutzen, 1984] has been invoked to explain the mass loading [Chin and Davis, 1995; Weisenstein *et al.*, 1997]. Transport of small sulfate particles formed in the upper troposphere to the stratosphere has a large impact of the surface area density [Weisenstein *et al.*, 1997]. Aerosols are removed from the stratosphere by transport into the troposphere and by gravitational sedimentation. Published analyses of the stratospheric sulfur budget may reflect coupled errors in transport and the chemistry and physics controlling aerosol formation, growth, and sedimentation (see Section 2.3). While there is some indication of an upward trend in the stratospheric aerosol burden [Hofmann, 1990],

the issue is in dispute [Hitchman *et al.*, 1994; Thomason *et al.*, 1997]. Significant uncertainties remain in understanding the budget of the background, or volcanically unperturbed, stratospheric aerosol, and therefore in the relative perturbations predicted due to emissions from the HSCT fleet. As one example, a very recent intercomparison of the Stratospheric Aerosol and Gas Experiment (SAGE) and *in situ* measurements showed similar aerosol extinctions but significantly different (nearly a factor of 2) surface area densities presumably because the measured size distributions are different from those assumed in the analysis of the SAGE data [Reeves *et al.*, 1998].

The record of significant perturbations to the stratospheric aerosol layer from injections of volcanic particles and gases is of high quality since 1881. This record shows periods of volcanic inactivity of ~10 to 30 years interrupted by relatively active episodes [Stothers, 1996]. A particularly long active period occurred from 1960 to 1991, bracketed by the eruptions of Agung and Pinatubo. The H_2SO_4/H_2O aerosol created following the Mt. Pinatubo eruption in June 1991 was extremely well documented by *in situ* [Jonsson *et al.*, 1996] and remote measurements [McCormick *et al.*, 1995] throughout its formation and decay. The aerosol produced from Pinatubo resulted in peak enhancements in the mass (surface area) of the stratospheric aerosol of factors of ~200 (~35), decaying with a time scale of ~1 year. By 1998, these quantities were near or below pre-Pinatubo values. Such large but unpredictable perturbations to the stratospheric sulfate layer clearly dwarf any potential effect due to the proposed HSCT fleet over time scales of a few years.

In addition to the H_2SO_4/H_2O particles described above, particles with more complex compositions are also found in the stratosphere. Particles containing large fractions of HNO_3 have been observed near the poles in winter (e.g., Del Negro *et al.* [1997]); these PSC particles may be composed of solid hydrates of HNO_3 or ternary mixtures of $H_2SO_4/H_2O/HNO_3$ [Carslaw *et al.*, 1994]. These particles have been shown to play an important role in the distribution of nitrogen oxides, water and aerosol. Sheridan *et al.* [1994] observed small but significant fractions of nonsulfate particles in the mid-latitude lower stratosphere, including soot and crustal material. Pueschel *et al.* [1997] and Blake and Kato [1995] report surprisingly large abundances of carbon soot particles in the mid-latitude stratosphere near 18-km altitude. These observations of soot have not been fully explained in terms of potential sources and known transport mechanisms. Very recent observations using a new particle ionization-mass spectroscopy instrument [Murphy and Thomson, 1995; Murphy *et al.*, 1998] show a surprising variety of compounds present in stratospheric aerosol particles in trace quantities. These observations indicate the need for an evaluation of possible catalytic reactions, as well as consideration of the effect of trace compounds on polar stratospheric cloud formation.

2.2.2 Stratospheric Temperature

The temperatures in the stratosphere affect photochemistry; the size, phase, and composition of aerosol; and the input of water vapor from the troposphere (the latter is affected by temperatures at the tropical tropopause rather than the temperatures throughout the stratosphere). Temperatures are determined by a balance between radiative and dynamical processes. To first order, global mean temperatures are determined by radiative processes. However, dynamical processes produce large seasonal and hemispheric variations. In particular, outside the tropics there is a strong annual cycle, with lowest temperatures in the winter. There are higher temperatures (particularly in polar regions) and larger interannual variations in the Northern Hemisphere (NH) because of the

stronger dynamical activity there. There is a local minimum in temperature at the tropical tropopause because of deep convection and dynamical cooling associated with upwelling. This temperature minimum has an annual cycle with coldest temperatures in NH winter and warmest in NH summer. As a result of this temperature cycle at the tropical tropopause, mixing ratios for water vapor entering the stratosphere, which are close to the saturation mixing ratio at the tropopause, are much lower in NH winter than in NH summer.

Satellite and ground-based observations show a cooling trend of approximately 0.6°C/decade in the global annual-mean lower stratospheric temperature since 1980 (~0.75°C/decade for mid-latitudes only), with a larger cooling in polar regions during winter (3°C/decade) [WMO, 1999]. This change is associated with changes in radiative forcing, predominantly because of the depletion of lower stratospheric ozone.

Because stratospheric temperatures affect photochemistry, aerosol characteristics, and water vapor concentrations, consideration of future changes in stratospheric temperatures is vital when assessing the possible impact of aircraft emissions on ozone. However, our ability to predict stratospheric temperatures in the future is especially unsatisfactory. Three-dimensional general circulation models (GCMs) (as well as coupled dynamical-chemical-radiative models) have been used to predict future changes in temperature, and although there is qualitative agreement between models, with the troposphere becoming warmer and the stratosphere colder, the precise magnitude of these changes depends on details of the model formulation. Two factors are of particular importance for this assessment. First, temperature changes at the tropical tropopause, and consequently changes to H_2O mixing ratios entering the stratosphere, are highly uncertain. Second, temperature changes to the wintertime polar vortices, and consequently the frequency of conditions that make extensive springtime polar ozone depletion possible, are highly uncertain.

2.3 Transport Processes

The distribution of stratospheric ozone is determined by a complex balance between photochemical production and destruction, and by transport. In short, transport processes regulate ozone concentrations both by the transport of ozone itself from net source regions to net sink regions on time scales shorter than or comparable to the photochemical lifetime of odd-oxygen; and by the transport of tropospheric source gases, such as N_2O, H_2O, CFCs, and CH_4, that are precursors to the free radicals that participate in catalytic cycles that remove ozone. Injection of HSCT exhaust directly into the stratosphere, primarily at mid-latitudes between 18 and 20 km, will bring transport processes into play in yet another sense: the effect of HSCT emissions on global ozone levels will depend critically on how rapidly the exhaust is dispersed into different regions of the stratosphere and to what extent the pollutants can build up, i.e., what the "steady-state" distribution will be.

In the following sections, we discuss our current knowledge and the key remaining uncertainties of stratospheric transport, derived from a combination of observations, theory, and numerical simulations (with emphasis on progress since the last assessment). An overview of the circulation of air within the stratosphere is given in Section 2.3.1, followed by an examination of each of the primary components of the circulation in Sections 2.3.1 to 2.3.6. The combined effect of these processes on the dispersal and residence time of HSCT emissions is then discussed in Section 2.3.7.

2.3.1 Global View of Stratospheric Transport

When considering the circulation of air in the stratosphere and its influence on trace gas distributions, it is useful to regard the stratosphere as composed of several regions, each with different transport characteristics (Figure 2-2). The region above potential temperatures of ~380 K is known as the "overworld," and may be further divided into four distinct regions: the tropics, the mid-latitude region of extensive wave activity (i.e., the "surf zone"), the high-latitude polar vortex in the winter hemisphere, and the extratropical summer lower stratosphere. Generally, upward, diabatic transport occurs within the tropics, and downward, diabatic transport occurs in the extratropics of both hemispheres (except in the summer upper stratosphere where there is weak upward transport). Rapid quasi-horizontal (i.e., isentropic) transport and mixing occur within the surf zone, with relatively weak quasi-horizontal mixing in the other regions. The boundaries between these regions are often referred to as "transport barriers," but these boundaries are variable in nature, and, as will be discussed below, transport across these boundaries does indeed occur. Below the overworld there is a separate region where isentropes (surfaces of constant potential temperature) cross the tropopause. This region is known as the "middleworld," with the stratospheric part of the middleworld often referred to as the "lowermost stratosphere." Because the isentropes are not confined to the stratosphere, it is possible for rapid transport along isentropes to produce mixing between the stratosphere and troposphere within this region (see Holton *et al.* [1995] and references therein).

The key components of the stratospheric circulation that control the distributions of long-lived gases, such as N_2O, and the dispersal of the aircraft emissions are (see Figure 2-2) (1) quasi-horizontal transport from mid-latitudes into the tropics; (2) the strength of diabatic (i.e., vertical) motions; (3) transport out of the lowermost stratosphere into the troposphere; (4) transport across the polar vortex edge; and (5) generally weak summertime transport. The distributions of long-lived tracers and aircraft emissions depend on an aggregate of all of these transport processes. For example, Figure 2-1 shows (a) the distribution of N_2O from satellite observations and (b) simulation of the HSCT exhaust perturbation during northern winter. The effect of the different transport characteristics within the distinct regions of the stratosphere can be seen in the tracer isopleths. The N_2O isopleths are flat within the mid-latitude surf zone (resulting from rapid quasi-horizontal mixing); bulge up within the tropics (resulting from a combination of ascent and slower horizontal transport into the tropics); and bulge down in northern high latitudes (resulting from descent and slower mixing into the polar vortex). Similarly, a model predicts that the largest concentration of HSCT emissions will occur in the northern extratropics at and below flight altitudes, reflecting the predominance of downward transport in the extratropics and weak transport into the tropical upwelling region. There are also steep tracer gradients near the tropopause, reflecting slow transport across the tropopause and loss in the troposphere.

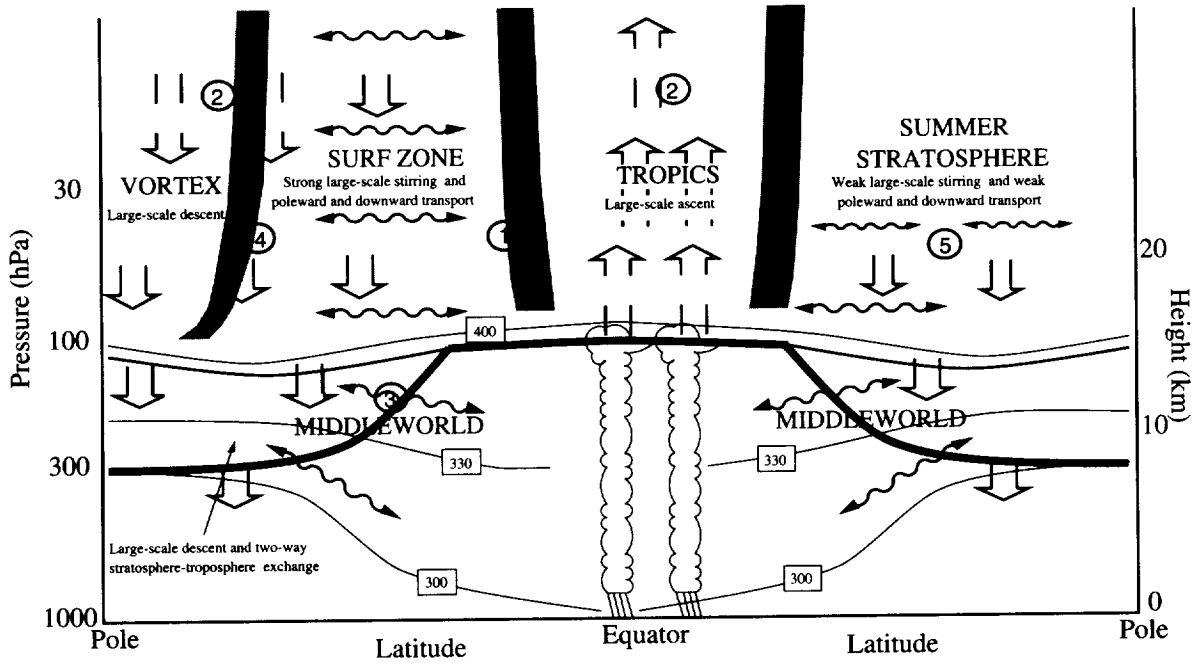

Figure 2-2. Schematic of the principal regions of the lower stratosphere with distinct transport characteristics. Circled numbers correspond to regions/processes discussed in Sections 2.3.2 to 2.3.6 [adapted from WMO, 1999]. The thick solid line represents the tropopause and the thin solid lines are at constant potential temperature.

Reliably predicting the exact distribution of long-lived tracers and aircraft exhaust depends on a quantitative representation in the assessment models of the processes in (1) to (5) above, which can be judged to some degree by how well the models reproduce the effects of stratospheric transport on observed tracers (discussed in detail in Chapter 4). We now discuss, in the following sections, our current understanding of each of these components of stratospheric transport.

2.3.2 Transport in the Tropics and Tropical/Extratropical Exchange

The mean advection of air in the middle latitudes, where the majority of HSCT exhaust will be emitted, is downwards and out of the stratosphere. Exactly how much air is transported from mid-latitudes into the tropics, where the mean advection is upwards into the middle and upper stratosphere, plays a critical role in determining the stratospheric distribution and residence time of the exhaust. Ideally, the amount of mid-latitude air entering the tropical upwelling region could be determined from analyses of tropical winds. However, limitations in meteorological analyses within the tropics (due to lack of *in situ* meteorological data and the breakdown of the geostrophic balance), make this approach unreliable [Waugh, 1996]. Fortunately, significant insight into the exchange across the subtropical "barrier," as well as transport within the tropics, has been gained from recent observations of trace gases measured by instruments aboard aircraft, satellites, and balloons.

Estimates of the amount of transport into the tropics have been obtained using a variety of trace gas measurements (e.g., Avallone and Prather [1996]; Hall and Waugh [1997a]; Herman *et al.* [1998]; Minschwaner *et al.* [1996]; Mote *et al.* [1996]; Schoeberl *et al.* [1997]; Tuck *et al.* [1997]; Volk *et al.* [1996]). These studies have predominantly used simple one-dimensional (1-D) ("tropical leaky pipe") models which parameterize the entrainment of extratropical air into the tropics as simple relaxation to observed extratropical mixing ratios with time constant τ_{in}. All studies conclude that the tropics are not totally isolated from mid-latitudes, and the estimates of τ_{in} in the lower stratosphere are ~11 to 15 months (i.e., about 30 to 60% of air at 20 km in the tropics is of mid-latitude origin). Furthermore, analyses of UARS satellite and balloon data suggest that the entrainment rate varies with altitude, with weaker entrainment in the middle stratosphere [Herman *et al.*, 1998; Mote *et al.*, 1998; Schoeberl *et al.*, 1997]. Satellite and balloon measurements have also been used to identify individual intrusions of extratropical air into the tropics [Dunkerton and O'Sullivan, 1996; Jost *et al.*, 1998].

The entrainment of mid-latitude air into the tropics is also evident from observations of the attenuation of the amplitude of the annual cycles in total hydrogen $H = H_2O + 2CH_4$ and in CO_2 (e.g., Boering *et al.* [1996]; Andrews *et al.* [1999]; Mote [1996, 1998]; Randel *et al.* [1998]) (Figure 2-3a). Both H_2O and CO_2 show periodic seasonal variations in their mixing ratios at the tropical tropopause, and as the air moves upward in the tropics, these seasonal variations are observed to propagate vertically. If there were no mixing of air into the tropics from the mid-latitudes (and no significant vertical diffusion, which as we show below is indeed the case), then the amplitudes would remain constant as the air moves upwards. However, as shown in Figure 2-3a, the amplitudes of these cycles are observed to attenuate with altitude. From these observed attenuations, estimates of the time scale for mixing in of air from mid-latitudes (15 to 18 months) or the proportion of tropical air originating at mid-latitudes (~50%) have been derived [Boering *et al.*, 1996; Mote *et al.*, 1996].

Further observational evidence for the mixing of mid-latitude air into the tropics comes from differences in the "propagation" time scales for tracers with an annual cycle, such as H and CO_2, versus those for tracers that are increasing approximately linearly over time, such as SF_6 and CO_2. This "phase lag time" represents the time it takes seasonal maxima and minima to propagate from the tropical tropopause (~16 km) to a given altitude. The "mean age" of air is defined as the time lag between stratospheric observations and the mixing ratios at the tropical tropopause for a tracer that is increasing linearly with time in the troposphere and represents the average over the ensemble of transit times from the tropical tropopause (e.g., Hall and Plumb [1994]). Quasi-horizontal mixing of older mid-latitude air, with little or no remnant of the annual cycles, into the tropical upwelling region significantly increases the mean age but has little effect on the phase lag time [Hall and Waugh, 1997b]. Phase lag times from tropical observations of H [Mote, 1998] and CO_2 [Boering, 1996; Andrews *et al.*, 1999] are compared with tropical mean ages derived from SF_6 and CO_2 [Boering *et al.*, 1998 (data published in the Photochemistry of Ozone Loss in the Arctic Region in Summer (POLARIS) CD-ROM); Andrews 1999; Park *et al.*, 1999] in Figure 2-3b. Note that the observed phase lag times and mean ages diverge with altitude, as expected as older mid-latitude air mixes into the tropics.

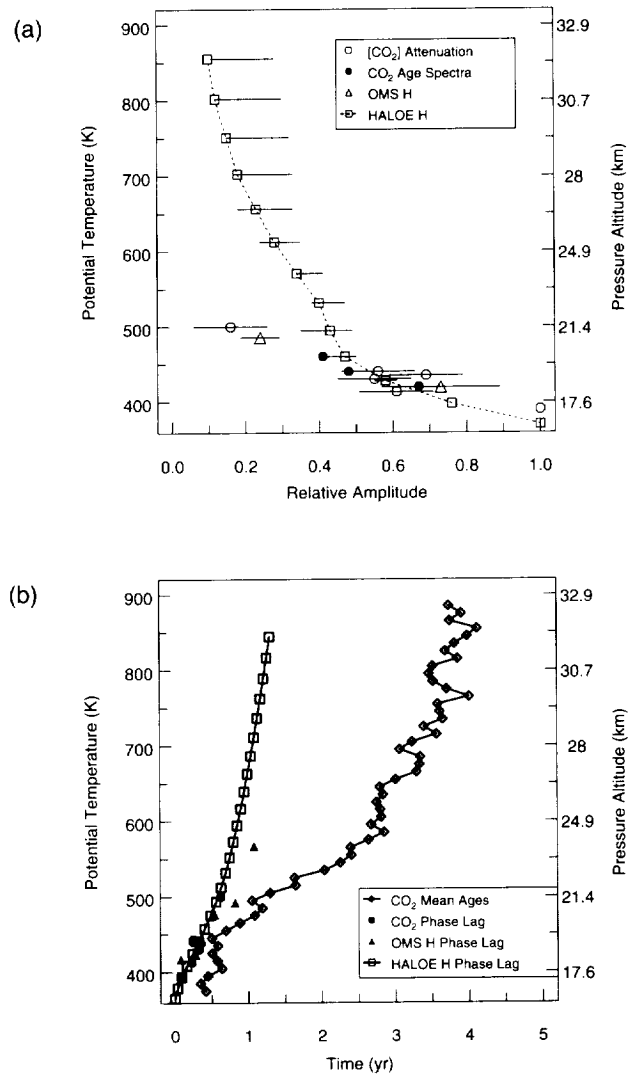

Figure 2-3. Vertical profiles of (a) amplitude (relative to amplitude at 16 km) and (b) phase propagation derived from observations of tracers with annual cycles in the tropics. Amplitude and phase are shown for: H = H_2O + CH_4 from Halogen Occultation Experiment (HALOE) aboard the UARS and from a balloon-borne frost point hygrometer during Observations of the Middle Stratosphere (OMS) campaigns, and CO_2 from instruments aboard the NASA ER-2 aircraft and OMS balloon platforms. Also shown in (b) is mean age derived from OMS measurements of CO_2 [adapted from Park *et al.*, 1999].

Once in the tropics, the rate at which HSCT exhaust will be lofted into the middle stratosphere depends on both the mean ascent rate and vertical diffusion within the tropics. Estimates of tropical ascent rates have been derived from calculations of the residual circulation using satellite measurements (e.g., Eluszkiewicz *et al.* [1996]; Rosenlof [1995]; Yang and Tung [1996]). These

studies indicate a large seasonal variation in the magnitude of the ascent rates, with the value during northern winter (0.4 x 10^{-3} ms^{-1}, 1 km/month) being about 2 to 3 times larger than that in northern summer (0.15–0.2 x 10^{-3} ms^{-1} ~0.4–0.5 km/month). Ascent rates have also been derived from measurements of the vertical propagation (i.e., phase lag times) of seasonally varying tracers (e.g., Boering *et al.* [1996]; Andrews *et al.* [1999]; Mote *et al.* [1995, 1996, 1998]; Weinstock *et al.* [1995]), yielding rates broadly consistent with the calculated values. Trace gas measurements have also been used to estimate the extent of vertical diffusion within the tropics resulting from small-scale processes such as gravity wave-induced turbulence or large-scale diabatic dispersion. Hall and Waugh [1997a] and Mote *et al.* [1998] both estimated the value of vertical diffusion coefficient, Kz, appropriate for the 1-D "tropical leaky pipe" model. Both studies obtained very small values for Kz (less than 0.04 m^2s^{-1}) within the lower tropical stratosphere, indicating that diffusion plays only a small role in the transport of trace gases in this region. For altitudes above 24 km, however, Mote *et al.* [1998] estimated larger values of Kz (~0.1 m^2s^{-1}), suggesting that vertical diffusion may be more important in the middle stratosphere, where there is weaker mixing in of air from mid-latitudes.

As outlined above, substantial progress in quantifying transport processes in the tropics—including mean vertical ascent rates, vertical diffusion, and the extent of transport across the subtropical "barrier"—has been made in recent years from observations and theory. However, significant uncertainties remain with regard to vertical, seasonal, and interannual variations (such as the effect of the Quasi-Biennial Oscillation (QBO)) in these transport rates. The mechanistic and dynamical details of the physical processes causing the transport and mixing also remain unclear. In spite of these uncertainties, the tracer measurements mentioned above provide stringent tests of the parameterization of tropical transport processes within numerical models. For example, observations of the vertical propagation of annual cycles in H_2O and CO_2 (e.g., Figure 2-3) provide tests of the balance of ascent, mixing in of mid-latitude air, and vertical diffusion within models. This is discussed in detail in Chapter 4.

2.3.3 Meridional Circulation

The dispersal of HSCT emissions throughout the atmosphere depends not only on quasi-horizontal transport from the mid-latitude flight corridors to the tropics, but also on the strength of the large-scale meridional diabatic circulation. Within the tropics, this circulation will be the predominant means of transporting emissions to the middle and upper stratosphere, while, at middle and high latitudes, this circulation is responsible for transport of exhaust into the lowermost stratosphere (where air is flushed out of the stratosphere into the troposphere; see below). The strength of the meridional circulation is therefore one of the key factors controlling the time scale for the dispersal of HSCT emissions.

The sensitivity of trace gas distributions to the strength of the meridional circulation has been illustrated in two recent modeling studies. Schoeberl *et al.* [1998] performed 3-D trajectory calculations of the dispersal of inert "particles" released in the lower stratosphere (simulating HSCT exhaust, for example) and examined the sensitivity of the simulations to the different heating rates (and hence different meridional circulations) used in the calculations. They found that the stratospheric lifetimes (i.e., the e-folding decay times) of the particles in their model varied between 1 and 1.6 years for realistic changes in the heating rates. Another illustration is the comparison of the transport simulations using winds from two different versions of the National Center for Atmospheric Research (NCAR) Middle Atmosphere version of the Community Climate Model version 2 (MACCM2, or "Monash1" and "Monash2" in the notation of M&M II [Park *et*

al., 1999]). The residual circulations from the two MACCM2 simulations have different magnitudes because different gravity wave drag parameterization schemes were used in the two simulations. This results in different simulations of the stratospheric mean age as well as different climates (neither of which is realistic). The mean age is older, and the residence time for HSCT emissions is longer for the model with the weaker residual circulation [Park *et al.*, 1999]. These examples demonstrate that a quantitatively realistic meridional circulation is necessary for accurate simulations of distribution and lifetime of HSCT emissions.

2.3.4 MIDDLEWORLD TRANSPORT

HSCT exhaust emitted in the stratosphere above potential temperatures of 380 K (the overworld) will be transported out of the stratosphere by first descending into the lowermost stratosphere, and then into the troposphere via synoptic-scale transport events. The rate at which this stratosphere-to-troposphere transport occurs is another of the key factors that will determine the residence time of HSCT emissions in the stratosphere.

The time-averaged mass flux across the extratropical tropopause into the troposphere is equal to the diabatic descent from the overworld across the upper boundary of the lowermost stratosphere (~380 K), which is driven primarily by wave-breaking processes in the region above (the so-called "downward control" principle, e.g., Haynes *et al.* [1991]; Holton *et al.* [1995]). The same applies to the flux of chemical tracers that are conserved in the lowermost stratosphere. Gettelman *et al.* [1997] have used this fact to estimate the flux of several tracers, including ozone, from the stratosphere into the troposphere. However, there may be seasonal variations between the two mass fluxes. Appenzeller *et al.* [1996b] inferred the time series of mass fluxes across the extratropical tropopause by calculating the mass flux across the upper boundary of the lowermost stratosphere and the change in mass within the lowermost stratosphere. The mass flux across the upper boundary of the lowermost stratosphere in the NH maximizes in midwinter (consistent with the expected variation of the wave driving) but the flux across the extratropical tropopause maximizes five months or so later. Thus, there is a strong seasonal dependence in tropopause height and the volume of the middleworld.

Although the time-averaged, large-scale, cross-tropopause flux is controlled by wave driving within the stratosphere and mesosphere, the flux over shorter time scales, or at smaller spatial scales, will depend on the details of synoptic-scale events. Therefore, consideration of exchange at these scales is required when considering constituents with sources or sinks within the middleworld.

Transport from the lowermost stratosphere into the troposphere occurs in synoptic-scale events, such as "tropopause folds" and cut-off cyclones. During such events, there can be rapid adiabatic advection along isentropes as well as diabatic advection across isentropes. The isentropic transport may be viewed as resulting from filamentation of the tropopause, in much the same way that exchange in the winter stratosphere between polar vortex and surf zone results from filamentation of the vortex edge [Appenzeller *et al.*, 1996a], and ultimate transport occurs when these filamentary structures are mixed into the background by small-scale (diabatic) mixing processes.

Potential vorticity analyses and transport calculations show that there is two-way transport across the extra-tropical tropopause, with transport both into (e.g., Lamarque and Hess [1994]; Holton *et al.* [1995]; Appenzeller *et al.* [1996a] and out of [Chen, 1995; Peters and Waugh, 1996; Vaughan and Timmis, 1998] the troposphere. Transport across the extra-tropical tropopause into the

lowermost stratosphere can also be inferred from observations of trace gases (e.g., water vapor) [Dessler *et al.*, 1995; Hintsa *et al.*, 1998; Pan *et al.*, 1997; Tuck *et al.*, 1997]. This transport occurs predominantly across the subtropical tropopause rather than up through the mid-latitude tropopause. Although occasional upward transport across the mid-latitude tropopause is implied by observations, this air remains very close to the tropopause [Hintsa *et al.*, 1998].

Several modeling studies have estimated the time scale for transport out of the lowermost stratosphere. Schoeberl *et al.* [1998] used a 3-D trajectory model to examine the stratospheric lifetime for particles released at several different altitudes (between 11 and 19 km), while Gettelman [1998] used a 3-D chemical transport model to calculate a similar quantity for subsonic aircraft emissions in the lowermost stratosphere. Both studies indicate that material is flushed rapidly out of the lowermost stratosphere, with e-folding lifetimes of less than a few months. As mentioned above, this transport occurs primarily through isentropic transport followed by small-scale diffusive mixing. This isentropic transport in the middleworld is represented differently in 2-D and 3-D models. High-resolution 3-D models can resolve (at least partially) this filamentary process, and there is rapid transport out of the lowermost stratosphere. On the other hand, 2-D models must rely on parameterized diffusive mixing. The model results reported in Shia *et al.* [1993] showed that the removal of bomb ^{14}C out of the stratosphere is dominated by the horizontal eddy flux across the boundary between the upper tropical troposphere and the middle world. Comparisons of 2-D and 3-D simulations of aircraft emissions show more vigorous transport into the troposphere and smaller stratospheric concentrations with 3-D models [Rasch *et al.*, 1994; Schoeberl *et al.*, 1998], see Figure 2-4. Taken at face value, this suggests that the removal rate parameterized by horizontal mixing in 2-D models is too small compared to 3-D models.

In summary, for realistic transport of tracers (or emissions) out of the stratosphere it is necessary to realistically simulate the large-scale stratospheric circulation (which controls the time-averaged, large-scale flux) and synoptic-scale mixing events in upper troposphere / lower stratosphere (which control the flux over shorter times and smaller spatial scales). Accurately representing the latter processes in models is challenging (particularly for 2-D models that must rely on parameterized diffusive mixing). Furthermore, observations that can quantitatively constrain these processes are lacking, making it difficult to bound the uncertainties of these processes on models of the aircraft perturbation.

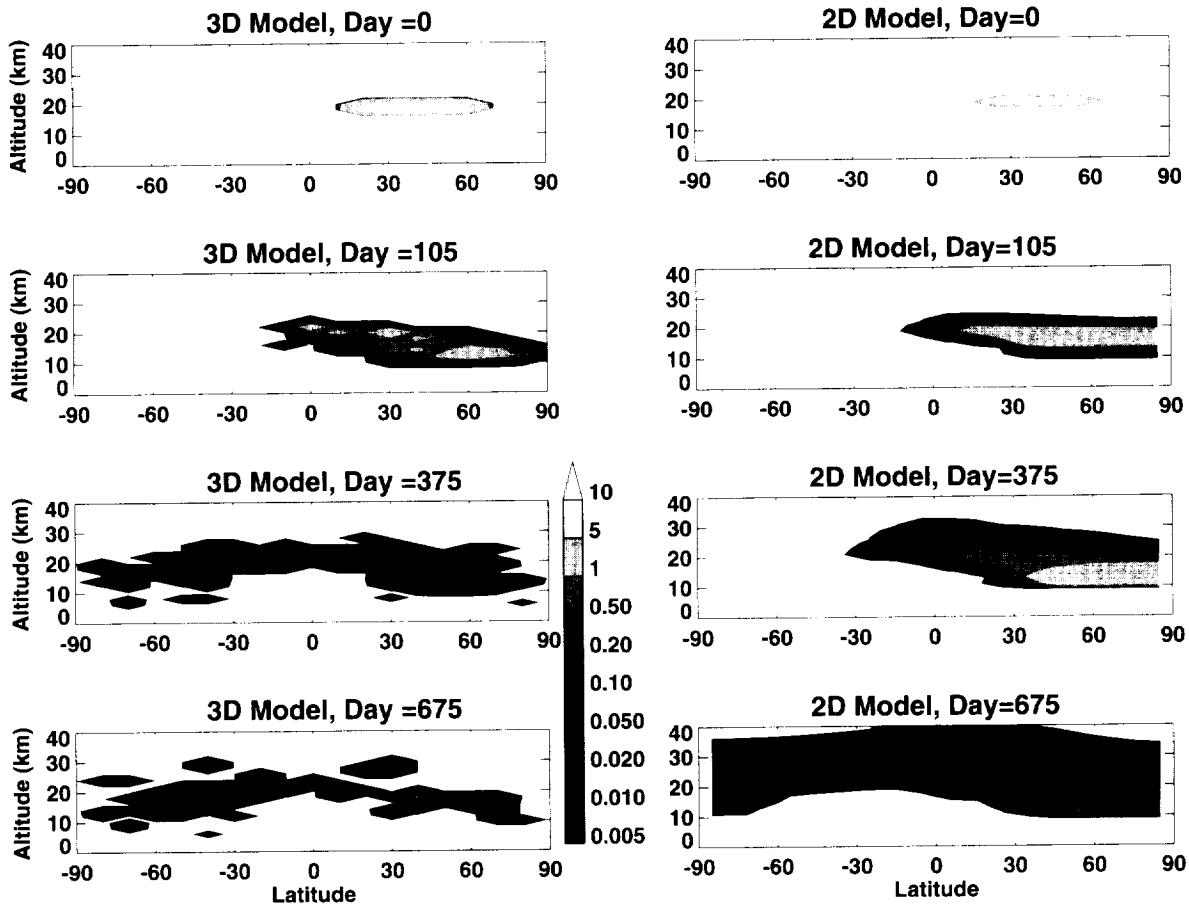

Figure 2-4. Evolution of the mixing ratio distribution of an instantaneous tracer release at 19 km, analogous to aircraft emissions, from simulations using 3-D trajectory model and the Goddard Space Flight Center (GSFC) 2-D model [adapted from Schoeberl *et al.*, 1998].

2.3.5 Polar Vortex

The influence of HSCT emissions on the chemical and microphysical processes that occur within the polar vortices will depend on the magnitudes of the perturbations caused by deposition directly in the winter vortices, by quasi-horizontal transport from mid-latitude flight corridors across the vortex edge, and by multi-year accumulation of exhaust in the middle and upper stratosphere (Figure 2-2).

Analysis of aircraft flight corridors and the Arctic vortex edge shows that the flight corridors are seldom inside the vortices, with only a small percentage (1 to 3%) of global emissions occurring inside the Arctic vortex [Baughcum, 1996; Sparling *et al.*, 1995]. On a typical day there are unlikely to be more than a few flights into the vortex. While there are brief periods when the vortex is displaced off the pole over the North Atlantic, and during these periods there could be significant emissions within the vortex (10 to 20% of global emissions over the duration of the displacement [Baughcum, 1996]), a "regional" accumulation of exhaust in the vortex from this magnitude of direct deposition is expected to have a minimal impact on regional ozone levels.

There is an extensive body of research on the rate of quasi-horizontal transport into and out of the polar vortices. A difficulty when comparing these studies is the different definitions of vortex edge that have been used (such as the wind maxima, maximum gradients in potential vorticity (PV) or tracers, or minima in stretching rates). However, high-resolution trace constituent observations and numerical simulations frequently show multiple fine-scale (filamentary) structures near the polar jet (e.g., Tuck *et al.* [1992]; Waugh *et al.* [1994]), indicating that it is sometimes more appropriate to consider a finite-width "vortex edge region" rather than defining a single, sharp vortex edge, (e.g., Nash *et al.* [1996]). This vortex edge region encloses the above definitions of the vortex edge, and surrounds the so-called "inner vortex." Notwithstanding the different "edge" definitions, the overwhelming majority of observational, modeling, and theoretical studies indicate that during winter the inner vortex region of both vortices is substantially isolated from mid-latitudes above about 16 km (or potential temperatures of 400 K); see WMO [1995] and the more recent studies of Dahlberg and Bowman [1994]; Rosenlof *et al.* [1997]; Sparling *et al.* [1995]; Wauben *et al.* [1997]; and Waugh *et al.* [1997]. Thus, an exhaust perturbation due to direct quasi-horizontal transport from mid-latitude flight corridors into the inner vortex region is expected to be negligible.

Given the small expected perturbations of direct deposition or transport into the polar vortices during any given winter, changes in H_2O, NO_y, and aerosol in the vortices due to HSCTs are likely to result mainly from global changes in these species as a result of emissions over years. Furthermore, since high latitude lower stratospheric air descends into the middle world during vortex formation, air incorporated into the lower stratospheric vortex comes primarily from higher altitudes. The magnitude of these changes will depend on the extent to which exhaust is transported into the middle and upper stratosphere and, therefore, on the exhaust's residence time.

2.3.6 Summer Stratosphere

During the summer (June to August in the NH), there are easterly winds in the mid-latitudes of the stratosphere. This results in reduced planetary wave activity, as the upward propagation of waves from the troposphere is reduced in the presence of easterlies. There is then reduced transport/mixing in the stratosphere: the time scale for dispersion of a locally released tracer in the summer is greater than four months compared to about two months during winter [Sparling and Schoeberl, 1995]. This slow mixing means that tracer features may be "frozen in" over summer [Andrews *et al.*, 1987; Hess and Holton, 1985], which is supported by tracer observations in northern mid- and high latitudes in late June 1997 showing unmixed ex-vortex air masses [Herman *et al.*, 1998]. Thus, there is a possibility that emissions may build up in the flight corridors during summer months [Sparling *et al.*, 1995]. There is also weaker descent during summer [Holton *et al.*, 1995 and references therein], which will further increase the build up of emissions in the lower stratosphere during summer.

Consistent with this, most models that participated in the M&M II experiment have peak stratospheric emission loading in the fall [Park *et al.*, 1999]. However, the magnitude of the seasonal variation in the stratospheric loading varied considerably between models, with differences between maximum and minimum loading ranging from a few percent to over 30% of the annual-mean. It is not known which estimates are more realistic. Note that the majority of the flight paths in these simulations are confined to northern mid- and low latitudes (see Section 3.7.2). If however, there were more flights over high latitudes, there would likely be a greater build up of emissions over summer.

2.3.7 The Aggregate: Mean Age and Residence Time

The distribution of long-lived tracers and HSCT emissions depends on an aggregate of all the transport processes discussed above. Thus, to determine the accumulation of the emissions and their potential to alter global ozone levels, it is necessary to understand how all these processes couple together.

Information on the integrated effect of these transport processes on tracer distributions can be obtained from time scales derived from measurements of trace gases whose spatial gradients are due to temporal increases in their concentrations. In particular, conserved tracers with linearly increasing tropospheric trends can be used to derive the mean transit time from the troposphere to a stratospheric location (also referred to as the mean age of air in the stratosphere). The mean age is an important diagnostic of transport since it is independent of chemical processes and depends on the strengths of, and balance between, the residual circulation and quasi-horizontal mixing. Mean ages in the stratosphere have been derived from measurements of several different tracers which have approximately linear trends (e.g., SF_6 [Elkins *et al.*, 1996; Harnisch *et al.*, 1996; Patra *et al.*, 1997; Waugh *et al.*, 1997], CO_2 [Bischof *et al.*, 1985; Andrews *et al.*, 1999; Boering *et al.*, 1996; Nakazawa *et al.*, 1995; Schmidt and Khedim, 1991], CFC-115 [Daniel *et al.*, 1996; Pollock *et al.*, 1992], and hydrofluoric acid (HF) [Russell *et al.*, 1996]). Results from these studies show that the mean age (relative to the tropical tropopause) at 20 km varies from ~1 year in the tropics to ~5.5 years at high latitudes, while at 30 km it varies from 4 years in the tropics to 5 to 8 years at high latitudes. Mean ages derived from 5 years of extensive *in situ* aircraft observations and from balloon measurements are shown in Figure 2-5 and compared with a number of model results, which will be discussed in Section 4.3.3.

In addition to being an important diagnostic of the stratospheric circulation, we expect the residence time of HSCT exhaust to be related to mean age. Both time scales depend on the strength of the residual circulation and on the quasi-horizontal mixing within the stratosphere, particularly extratropical-tropical exchange. Furthermore, in a simple 2-box atmosphere, mean age and residence time are equivalent: if the stratosphere were a well-mixed reservoir (a box) in contact with the troposphere (the other box), then the lag time in the stratosphere from the time of entry from the troposphere (i.e., the mean age) is equivalent to the decay time of material in the stratosphere with the troposphere held at zero concentration (the residence time) [Boering *et al.*, 1996]. This equivalence breaks down in the real atmosphere because the stratosphere is not well-mixed and HSCT emissions will be highly localized at mid-latitudes. However, mean age and residence time likely still scale with one another, although the proportionality is unknown. Indeed, a correlation between mean age and HSCT emission tracers has been seen in the lower mid-latitude stratosphere across a wide range of models (see Section 4.4.3.2 and Figure 4-14).

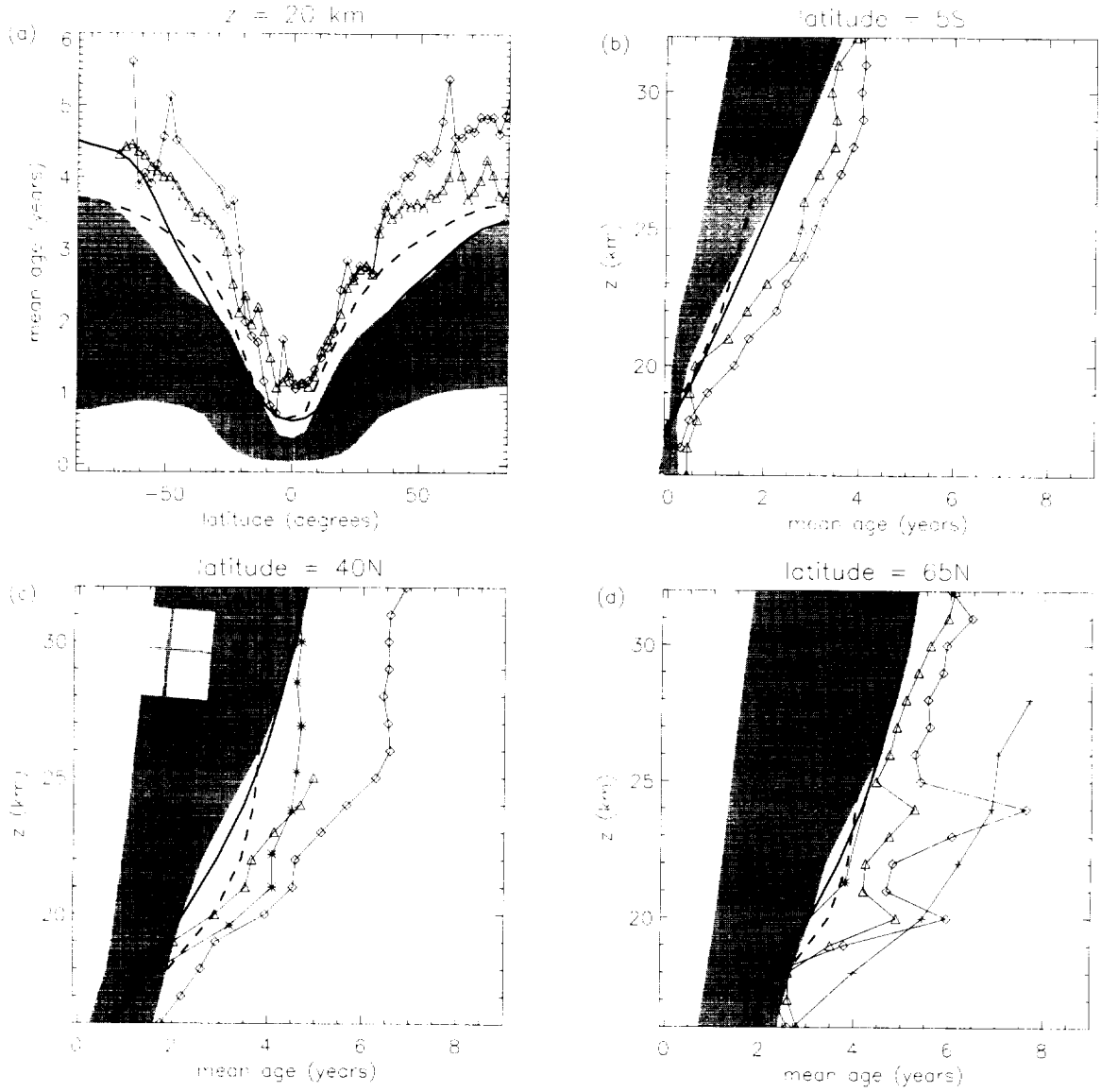

Figure 2-5. Comparison of mean ages from observations and models for (a) latitudinal profile at 20 km, and vertical profiles in (b) tropics, (c) mid-latitudes, and (d) high latitudes. The shaded region indicates the range of mean ages from a majority of models in the M&M II intercomparison [Park *et al.*, 1999] while the curves (without symbols) correspond to mean age profiles from the GSFC (dashed) and Monash1 (solid) models. The symbols correspond to mean age inferred from observations: *in situ* CO_2 (triangles), *in situ* SF_6 (diamonds), and whole-air samples of SF_6 (asterisk, pluses). (a) Latitudinal profile of *in situ* aircraft measurements from SPADE, ASHOE/MAESA, STRAT, and POLARIS for CO_2; and from ASHOE/MAESA (spring only), STRAT and POLARIS for SF_6 (diamonds). (b) Vertical OMS balloon profiles at 7S averaged in 1 km altitude bins over three flights for *in situ* CO_2 (one February, two November 1997) and over two flights for *in situ* SF_6 (February, November 1997). (c) *In situ* SF_6 and CO_2 mean ages from a single OMS balloon flight of September 1996, at 35N, and from SF_6 whole air samples, September 1993, at 44°N. (d) *In situ* CO_2 and SF_6 mean age from the OMS balloon flight of June 1997, 65°N, and whole air samples at 68°N inside (asterisk; average of four flights) and outside (pluses; single flight) the winter polar vortex [from Hall *et al.*, 1999].

To gain further insight into the combined effect of these transport processes on HSCT emissions, it would be useful to have extensive measurements of chemical species with sources and sinks in the atmosphere that are similar to those of the emissions (e.g., a tracer with a lower stratospheric source and tropospheric sink). Appropriate species include ^{14}C from atmospheric nuclear bomb testing in the 1960s [Johnston, 1989] and ^{7}Be and ^{10}Be (and the ratio $^{10}Be/^{7}Be$) [Raisbeck 1981; Dibb 1994]. While these measurements have served as tests of model transport (e.g., Koch and Rind [1998]; Shia *et al.* [1993]; Kinnison *et al.* [1994]; Rasch *et al.* [1994]; Prather and Remsberg *et al.* [1993]) uncertainties as to initial conditions and/or a sparsity of observations currently limit their application for extracting detailed information about model transport.

In addition to its role in determining exhaust accumulation, the integrated stratospheric transport also plays a role in determining the concentrations of free radical precursors and aerosol in the background atmosphere. Observations show a high correlation between mean age and long-lived tracers affected by photochemical processes in the stratosphere, such as N_2O, NO_y, Cl_y, and H_2O (see Figure 2-6). Recognizing these correlations allows an important logical division of the problem of describing the base state of the atmosphere against which we superimpose the HSCT perturbation. Accurate simulations of radical precursors can be judged first by how well the models reproduce mean age (i.e., the integrated effects of transport, independent of photochemistry) followed by how well they reproduce the correlations of mean age with long-lived species affected by photochemistry. As discussed in Chapter 4, each of the models used for this assessment differs from the observations with respect to these two criteria. The conceptual framework provided by the observations of age and the correlation of tracers with age allows a primitive, but logical, extrapolation from predictions made using these models to predictions that are more likely to represent the behavior of the real atmosphere.

2.3.8 Impact of Climate Change

Climate change will affect future temperatures and circulation within the stratosphere. The distribution of HSCT emissions and of long-lived tracers, such as NO_y and Cl_y, in future atmospheres will be dependent on any changes in the stratospheric transport. For example, if there is a slower meridional circulation because of, say, reduced wave driving then, following the arguments in previous sections, we would expect the mean age and HSCT lifetime to be older and for NO_y and Cl_y to be increased.

There is interannual variability in stratospheric transport, and some indications that the stratospheric circulation has changed over the last two decades. During the 1990s there has been reduced wave activity, weaker diabatic descent in the extratropics and a colder more persistent polar vortex during northern winter and spring (e.g., Coy *et al.* [1997]). Also, recent observed changes in some trace constituents have been linked to changes in dynamics: Hood *et al.* [1997] and Fusco and Salby [1999] have shown statistical links between decadal changes in total ozone and changes in lower stratospheric circulation and wave driving, while Nedoluha *et al.* [1998] have linked decreases in upper stratosphere CH_4 between 1991 and 1997 to changes in the circulation, in particular to reduced tropical upwelling. However, it is not clear that these changes in constituent concentrations are driven solely by dynamical changes. Furthermore, it is not known whether the changes in circulation will continue over a longer time scale or whether they are part of natural decadal variability.

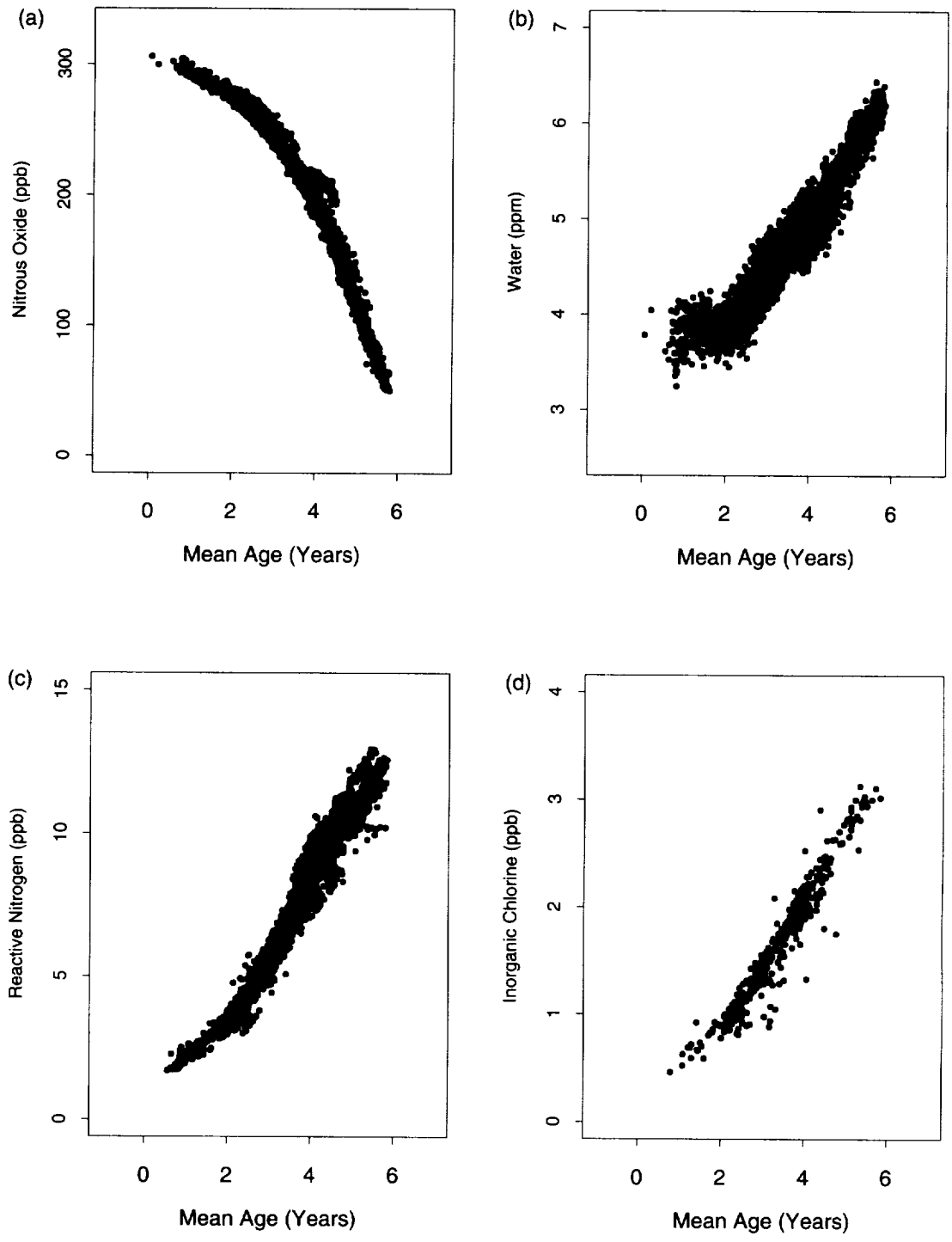

Figure 2-6. Scatter plots of (a) nitrous oxide (N_2O), (b) water (H_2O), (c) reactive nitrogen (NO_y), and (d) inorganic chlorine (Cl_y), vs. mean age (derived from CO_2) from ER-2 observations in northern mid- and high latitudes.

Unfortunately, current GCMs have limited ability to predict stratospheric circulation over interannual timescales, and provide little guidance on the details of future stratospheric climate. Recent modeling studies suggest that a cooling of the polar lower stratosphere and enhanced polar ozone loss may result from greenhouse gas warming (e.g., Shindell *et al.* [1998]; Dameris *et al.* [1998]). However, such model results are very uncertain. Hence possible climatic changes in the stratospheric circulation is a major uncertainty in predicting the distribution and impact of HSCT emissions.

2.4 Chemistry and Microphysics

Assuming that a model accurately describes transport and the input of source gases from the troposphere, then the specification of three elements are required to accurately compute ozone loss:

- The efficiency of conversion of the source gases to chemically active species;
- The partitioning of chemically active species between catalytically active radicals and less reactive species, known as reservoirs; and
- The rates of ozone catalytic loss cycles and the null cycles that interfere with them.

We discuss the qualitative features of the rates of the catalytic cycles in Section 2.4.1 and in Section 2.1 above. We show how the effect of aircraft NO_x in the lower stratosphere is primarily through null catalytic cycles that modulate the efficiency of the HO_x and halogen cycles. The aircraft effect in the middle and upper stratosphere is less complex, determined primarily by the amount of exhaust that is transported to high altitudes. In Sections 2.4.2 to 2.4.4, we discuss our knowledge of these three fundamental elements for the major chemical families.

2.4.1 Catalytic O_3 Loss

In an idealized sense, the HSCT exhaust will perturb the stratosphere in two places. In the middle and upper stratosphere, the response of the local ozone removal rate to changes in NO_x and HO_x radicals is proportional to changes in the concentration of these radicals. In the lower stratosphere, NO_x buffers the catalysis of hydrogen and halogen radicals. In this region, the response of the local ozone removal rate can be either positive or negative depending on the abundance of NO_x at atmospherically relevant concentrations. When NO_x concentrations in the lower stratosphere are diminished (during winter and following major volcanic eruptions), the rate of catalytic removal of ozone by HO_x and halogens (Section 2.1) in this region of the atmosphere is enhanced. When NO_x is at a maximum (in summer and during volcanically quiescent periods) the rate of catalytic removal of ozone by HO_x and halogen radicals in the lower stratosphere is suppressed. In the present atmosphere, NO_x seldom reaches levels where it is the dominant sink of O_3 in the lower stratosphere.

Figure 2-7 represents the lower stratospheric ozone removal rate schematically. The total ozone removal rate follows the top of the shaded area, and the different shades of gray reflect the portion of the total due to NO_x, HO_x and halogen catalysis, respectively. The left side of the figure (low NO_x) describes a NO_x poor region of the stratosphere. In this region, ozone catalysis is rapid and

it is dominated by HO_x and halogens. The ozone removal rates have a steep dependence on NO_x, increasing rapidly when NO_x decreases. If the curve were extended to the left, it would describe the chemistry of springtime polar ozone depletion. As NO_x levels approach zero, halogen catalysis increases 100-fold above that shown in the figure. At intermediate NO_x concentrations, ozone removal rates are insensitive to changes in NO_x. Increases in NO_x (and therefore in NO_x catalysis of ozone) are almost exactly balanced by decreases in the rate of ozone catalysis by HO_x and halogens. The width of this intermediate region is approximately a factor of 2 in NO_x concentration. At still higher concentrations of NO_x, NO_x catalysis dominates over all other reactions and ozone removal rates increase linearly in proportion to NO_x.

Much of the chemical impact of HSCTs (or any other perturbation to the lower stratosphere) can be qualitatively understood using this schematic and an estimate of what fraction (in space or time) of the lower stratosphere is characterized by each of the three regions coupled with estimates of the rate of transport between them and from higher altitudes where the HSCT exhaust will clearly reduce ozone. Perturbations to NO_x in the middle and upper stratosphere will cause changes to ozone in proportion to the fractional change in NO_x but of opposite sign. The lower stratosphere oscillates between intermediate NO_x and NO_x-poor regimes seasonally, latitudinally, and as a function of aerosol loading. On average, at 20 km, it is NO_x poor, even at the lowest aerosol loadings observed in the last decade. Small perturbations to NO_x in this region of the atmosphere

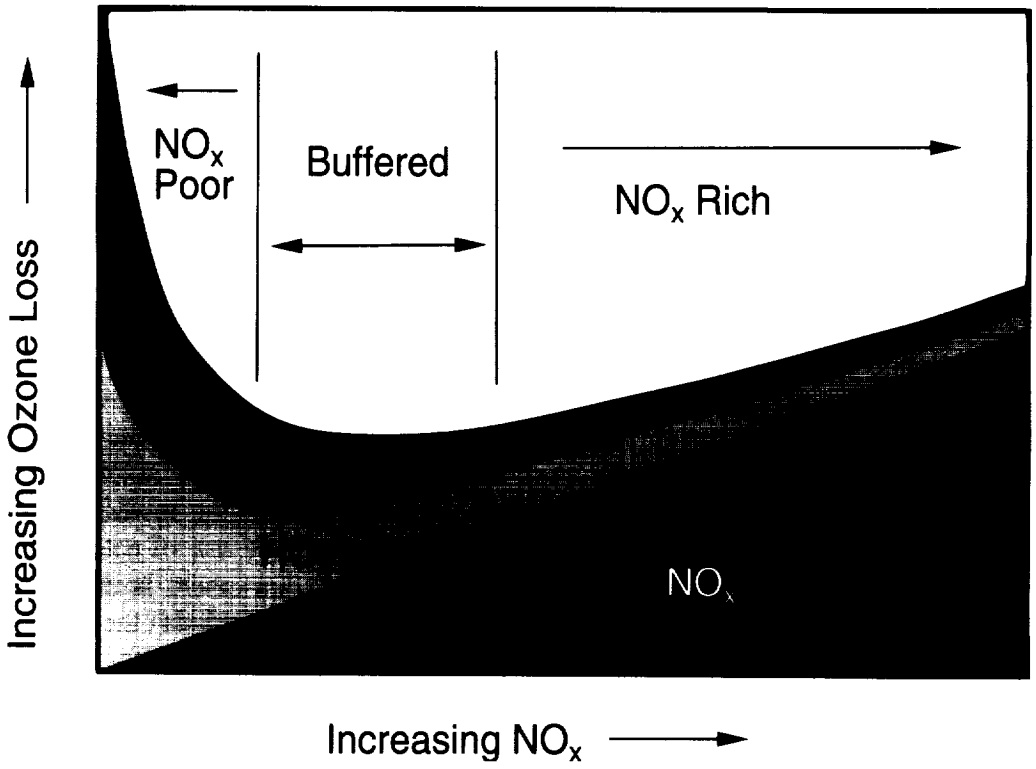

Figure 2-7. Schematic representation of the response of the stratosphere to changing NO_x levels. The schematic assumes fixed values for Br_y, Cl_y and OH (adapted from Wennberg *et al.* [1994]).

will cause changes in ozone of the same sign. Large increases in NO_x will however, push an increasing fraction of the lower stratosphere toward NO_x-rich chemistry and ozone loss. HSCT exhaust will increase stratospheric H_2O. This change will enhance HO_x catalytic ozone loss and simultaneously shift the balance between hydrogen and nitrogen catalysis, making the region more NO_x poor. Depending on the balance between H_2O, NO_x, and aerosol emissions, HSCT exhaust may either increase or decrease NO_x in the lower stratosphere. This qualitative picture emerges quantitatively in the calculations presented in Chapter 4. In the upper stratosphere, models all predict ozone decreases in response to the HSCT perturbation. In the lower stratosphere, where the chemistry of ozone is slower than at higher altitudes, transport and photochemistry both have direct effects on ozone. Here, the models tend to be NO_x poor (but not necessarily to the same degree as the atmosphere), and the NO_x change due to aircraft outweighs the H_2O change. For the most part, the models used in this assessment predict ozone increases in the lower stratosphere in response to the NO_x/H_2O perturbation (Figures 4-11, 4-12).

Historically (although our conceptual understanding was less clear than it is today), changes to predictions of the effects of stratospheric aircraft have come about because of changes in the fraction of the model atmosphere that was NO_x poor, NO_x buffered, or NO_x rich. In the early 1970s, most of the lower stratosphere was thought to be NO_x rich, and SST NO_x emissions were predicted to cause significant ozone depletion. We now have direct, simultaneous observations of NO_x, HO_x and halogen radicals [Wennberg *et al.*, 1994; Jucks *et al.*, 1996] and extensive observations of the interdependence of these radical concentrations [Cohen *et al.*, 1994; Stimpfle *et al.*, 1994]. These observations provide unequivocal evidence for the relative roles of these radicals throughout the lower, middle, and upper stratosphere. Measurements from the ER-2 aircraft beginning in 1993 provide observational constraints on the distribution of all three radical catalysts as function of latitude (70°S–90°N), altitude (12 to 21 km), and season [Gao *et al.*, 1997; Keim *et al.*, 1997] (see also Stratospheric Photochemistry, Aerosols, and Dynamics Expedition (SPADE) CD-ROM [Hathaway *et al.*, 1994]; Airborne Southern Hemisphere Ozone Expedition/ Measurements for Assessing the Effects of Stratospheric Aircraft (ASHOE/MAESA) CD-ROM [Gaines, 1995]; Stratospheric Tracers of Atmospheric Transport (STRAT) CD-ROM [Gaines and Hipskind, 1997]; and POLARIS CD-ROM [Gaines, 1998]). Measurements of radicals from a variety of remote-sensing platforms provide data measures in the middle and upper stratosphere (e.g., Jucks *et al.* [1996]; Newchurch *et al.* [1996]). The chemical reaction rates used in present models are considerably more accurate than the rates used in the 1970s. Laboratory techniques for measuring these rates have dramatically improved and atmospheric observations have provided direct tests to evaluate the models that use these rates. The observations show the lower stratosphere is almost always NO_x-poor, although the summer polar regions of the lower stratosphere are characterized by NO_x that is intermediate.

NO_x control is a dominant feature of stratospheric chemistry, but it is not the only important one. Other aspects of the photochemistry determine the abundance of hydrogen and halogen radicals. For example, the last 30 years of halocarbon releases at the surface is reflected in high concentrations of inorganic chlorine and bromine radicals in the stratosphere and in decreasing ozone levels. The effect of these radicals on ozone is clearly seen at 40 km where Molina and Rowland [1974] predicted, in their classic paper, it would be observed as well as in the large depletions that occur at polar sunrise and in the steady decline at mid-latitudes [WMO, 1995].

2.4.2 Nitrogen Species

2.4.2.1 The Distribution of the NO_y Reservoir

N_2O is chemically converted to active nitrogen molecules (denoted NO_y where $NO_y = HNO_3 + ClONO_2 + NO_2 + NO + 2 \times N_2O_5 + HO_2NO_2 + BrONO_2 + NO_3 + \ldots$). NO_y is removed from the stratosphere by photochemical reactions (N + NO) and transport out of the stratosphere both in gas-phase form or as solid HNO_3 incorporated in PSC particles. The ratio of $[NO_y]/[N_2O]$ in the lower stratosphere has a global annually averaged value of about 0.07 reflecting the globally integrated stratospheric production and loss for each species [Fahey *et al.*, 1993; Keim *et al.*, 1997; Nevison *et al.*, 1997]. Data described by Keim *et al.* [1997] show that the seasonal variance in the ratio is much larger in the SH than in the NH (30% vs. 5%). Gravitational sedimentation of HNO_3-containing aerosol in the polar regions during winter, followed by transport of air with higher NO_y/N_2O ratios from upper to lower stratosphere during the remainder of the year, is consistent with a seasonal cycle in the ratio. The weaker seasonal amplitude in the NH follows since aerosol sedimentation is less frequent in the NH. The mechanisms that control particle sedimentation in the polar regions and the subsequent influence on mid-latitude distributions of NO_y and water vapor are the subjects of active research. They are also the source of significant uncertainty in this assessment. The sharp thresholds in the formation temperatures of polar stratospheric clouds that remove nitric acid and water are strongly influenced by the partial pressure of water. For a given temperature, an increase in water vapor will enhance condensation, which may result in additional sedimentation that can irreversibly remove more nitric acid (enhanced denitrification). Alternatively, with no change in the sedimentation, NO_y would be increased by HSCT operations. Without a mechanistic understanding of polar stratospheric cloud formation, sedimentation, and evaporation processes, it is difficult to assess the impact of polar processes on global water and NO_y abundances. The immediate result of an increase in sedimentation of NO_y due to increases in H_2O would be more severe ozone depletion during Arctic spring. However, there is also a subtle feedback that operates on time scales longer than a single season: the global rate of removal of NO_y, H_2O and other HSCT effluent from the stratosphere might be enhanced by an increase in the sedimentation rate, thus reducing the magnitude of the HSCT perturbation or modifying the distribution of the perturbation within the stratosphere.

2.4.2.2 Partitioning of NO_y

NO_y is predominantly composed of HNO_3, $ClONO_2$, NO_2, and NO. The partitioning of NO_y among the various species occurs via reactions that usually reach a steady state in a few days (although from late fall through early spring and in the lower tropical stratosphere, time scales slow down to the point where weeks are required to reach steady state). Because of these rapid time scales, transport generally has only a minor effect on the partitioning of NO_y species. The balance between radicals (NO and NO_2) and reservoirs (HNO_3, $ClONO_2$, ...) is determined by reactions that interconvert short-lived NO_y species and the long-lived reservoir HNO_3. The important reactions fall into two classes: homogeneous gas-phase reactions mediated by NO_2, and heterogeneous reactions at the gas-particle interface and/or in the aerosol liquid phase mediated by the short-lived reservoir species (dinitrogen pentoxide (N_2O_5), $ClONO_2$, and bromine nitrate ($BrONO_2$)).

Laboratory measurements have provided the rates of these processes, especially the heterogeneous reactions and the low temperature photolysis cross-sections [DeMore *et al.*, 1997]. In particular, we note an improved understanding of the rates and mechanisms of hydrolysis of $ClONO_2$ on liquid sulfate aerosol [Robinson *et al.*, 1997; Hanson and Lovejoy, 1995], the reactions of $BrONO_2$ on aerosol [Hanson *et al.*, 1996], and the photolysis rates of several key species [Barnes *et al.*, 1996; Rattigan *et al.*, 1996; Yokelson *et al.*, 1997; Burkholder *et al.*, 1995].

Atmospheric observations during the 1990s demonstrated that heterogeneous processes are fast enough to reduce NO_x concentrations by factors of 2 or more relative to model calculations of NO_x in a hypothetical atmosphere where these reactions do not take place. Observations demonstrating the importance of hydrolysis of N_2O_5 are abundant, partly as a result of the natural experiment initiated by the eruption of Mt. Pinatubo and the subsequent evolution of stratospheric aerosol [Fahey *et al.*, 1993; Koike *et al.*, 1993]. The effects of heterogeneous reactions involving $ClONO_2$ and hydrogen chloride (HCl) on the chemistry of polar winter are well documented [WMO, 1995]. Observations show that the same chemistry can occur at mid-latitudes if the temperatures are low and H_2O concentrations high [Keim *et al.*, 1996]. Atmospheric observations that unambiguously demonstrate the importance of $BrONO_2$ hydrolysis as a sink of NO_x have been more difficult to obtain. Slusser *et al.* [1997] report that inclusion of $BrONO_2$ hydrolysis improves agreement with their observations of column NO_2 at 65°S during summer. Lary *et al.* [1996] report that inclusion of this reaction improves the agreement with observations of HO_x at sunrise by Wennberg *et al.* [1994].

Analyses of atmospheric observations, especially those following soon after the eruption of Mt. Pinatubo, argued for good agreement of models and observations of NO_y partitioning [Gao *et al.*, 1997; Koike *et al.*, 1993; Mills *et al.*, 1993; Fahey *et al.*, 1993]. Nearly all of these papers also identified exceptions to the "good agreement." Recent observations and analyses are making a stronger point about the deficiencies in our understanding of the partitioning of NO_y. Measurements of NO_x/NO_y obtained by infrared (IR) remote sensing [Sen *et al.*, 1998; Slusser *et al.*, 1997, 1998] and from *in situ* measurements during POLARIS [Gao *et al.*, 1999] exhibit higher concentrations of NO_x than models constrained by the measured NO_y. Taken together, the measurements show that models using currently accepted photochemistry are more NO_x poor than the atmosphere by about 30%, even when constrained with observed OH and NO_y.

Interpretation of these observations is still incomplete. However, measurements suggest the presence of more than one error in the set of rate constants as currently recommended [DeMore *et al.*, 1997]. The gas-phase processes controlling NO_2/HNO_3 ratios favor HNO_3 too much, implying that the rate of $OH + NO_2 \rightarrow HNO_3$ is slower than in models and/or the rate of NO_2 production via HNO_3 photolysis or reaction with OH is faster than in models. Donahue *et al.* [1997] have addressed the first possibility, showing that the NO_2 + OH room temperature reaction rate measured by some 15 different research groups was poorly described by the Jet Propulsion Laboratory (JPL)-94 compendium [DeMore *et al.*, 1994]. The JPL-97 compendium, which is used as the basis for the model calculations in Chapter 4, recommended a new formulation of this rate constant [DeMore *et al.*, 1997]. The new formulation does a better job of describing the observations at room temperature, but it does not pass through the mean of the laboratory measurements at stratospheric temperatures. Both Dransfield *et al.* [1999] and Brown *et al.* [1999] have revisited this rate constant in the laboratory. Their measurements are nearly identical to each

other and to those that were previously obtained; however, the new measurements expand the data base for the form of the rate expression at stratospheric temperature and pressures. Use of a rate constant that is consistent with the laboratory observations over a range of temperatures and pressures will improve agreement of measurements with highly-constrained photochemical box models. Brown *et al.* [1999] also remeasured the rate of OH + HNO_3 and suggest that this rate is considerably faster at low temperature than is recommended by JPL-97. Models using both new rate constants are in better agreement with observations of NO_x/NO_y ratios during polar summer, about 10% when constrained by observed NO_y and OH [Gao *et al.*, 1999].

2.4.3 Halogen Species

2.4.3.1 The Distribution of Cl_y and Br_y

Decomposition of halocarbons results in each chlorine and bromine atom being converted to the reactive species, inorganic chlorine (Cl_y) and inorganic bromine (Br_y). Cl_y and Br_y production occurs by ultraviolet (UV) photolysis of organic halocarbons while loss occurs by transport to the troposphere. These chemicals are only slightly soluble in stratospheric sulfate aerosol and thus are not affected by sedimentation processes. The spatial distributions of stratospheric Cl_y and Br_y are reasonably well known on the basis of measurements. Throughout the stratosphere Cl_y and Br_y exhibit tight correlations with other long-lived tracers, as well as stratospheric mean age.

HCl and $ClONO_2$ are typically the dominant components of Cl_y in the lower stratosphere. Observations of $ClONO_2$ and HCl add to about 95% of the Cl_y inferred from measurements of CFCs [Bonne *et al.*, 1999; Zander *et al.*, 1996]. Wamsley *et al.* [1998] have discussed measurements of the correlation of organic bromine with N_2O in the stratosphere. These measurements combined with assumptions about the growth of organic bromine compounds in the stratosphere (supported by measurements of the growth of organic bromine at the surface) can be used to infer the distribution of Br_y in the stratosphere. Increases in stratospheric halogen abundances are thought to be responsible for observed decreases in stratospheric ozone since 1980 [Jackman *et al.*, 1996; Solomon *et al.*, 1998].

2.4.3.2 The Partitioning of Cl_y and Br_y

Prior to 1997, when *in situ* measurements of $ClONO_2$ first became available, Cl_y partitioning was checked by taking the sum of the measured concentrations of HCl, ClO, and the derived concentration of $ClONO_2$ and comparing that with the total inorganic chlorine concentration derived from measurements of the organic chlorine species. $ClONO_2$ was derived from measured ClO, NO_2 derived from observations of NO and O_3, and the rates of $ClONO_2$ formation and photolysis. The agreement is relatively poor for AASE-II and SPADE data taken between 1991 and 1993 [Bonne *et al.*, 1999; Salawitch *et al.*, 1994a; Wennberg *et al.*, 1994]. The sum of the measured HCl, measured ClO and derived $ClONO_2$ was smaller than the derived Cl_y by up to 40% [Webster *et al.*, 1994]. The agreement improved from 1993 to 1997 in subsequent campaigns. The reason can be traced to an increasing trend in the measured HCl between 1993 and 1998 from the ALIAS instrument [Webster *et al.*, 1998]. Dessler *et al.* [1997] also found a trend in HCl in the same period in UARS observations, but the magnitude is much smaller.

With the availability of *in situ* and remote sensing $ClONO_2$ measurements, analyses confirm the accuracy of the rates of $ClONO_2$ formation and photolysis [Chang *et al.*, 1996a; Dessler *et al.*, 1996a; Stimpfle *et al.*, 1994; Zander *et al.*, 1996]. These analyses lend support to techniques used to reconstruct $ClONO_2$ from measurements of ClO and NO_2 [Stimpfle *et al.*, 1994]. There are several ways to reconcile the data taken prior to 1993:

- There is a yet-to-be-identified mechanism that was effective prior to 1993 that would decrease HCl, without affecting ClO or NO and presumably not affecting derived $ClONO_2$;

- or the data (measured HCl, ClO, or derived Cl_y, or some combination) are wrong.

No mechanism has been identified that is capable of simultaneously explaining both the *in situ* ClO and HCl data between 1991 and 1993 (Jaeglé *et al.* [1996]; Abbatt [1995]). Models using the rates from JPL-97 produce results that are consistent with the measured ClO and inconsistent with the measured HCl. Other measurements during the same time period [Chang, 1996a; Dessler *et al.*, 1996a; Zander *et al.*, 1996] did not observe such low values of HCl. We consider the possibility small that the discrepancy implies a missing mechanism in the models.

In the upper stratosphere, there is now remarkable agreement between models of the partitioning of Cl_y and measurements of HCl, $ClONO_2$, and ClO [Michelsen *et al.*, 1996]. Use of a minor channel producing HCl and O_2 in the reaction OH + ClO, as shown in the laboratory virtually eliminates a persistent discrepancy between models and measurements [Lipson *et al.*, 1997]. Observations of O_3 and chlorine species in the upper stratosphere have long been in conflict with models that did not include this channel or its chemical equivalent [McElroy and Salawitch, 1989]. In the lower stratosphere, a conservative estimate based on propagation of errors in rate constants and measurements suggests an uncertainty as large as 30 to 40% in the ratio of $ClONO_2$/HCl.

Bromine compounds contribute to halogen-catalyzed ozone loss in the lower stratosphere with remarkable potency relative to more abundant chlorine compounds on a per atom basis. This increased efficiency arises because bromine is more rapidly converted into forms capable of destroying ozone than chlorine. During daylight about half of inorganic bromine is present in radical forms (bromide monoxide (BrO), Br) capable of efficient O_3 removal, whereas only a few percent of chlorine is present as radicals. In addition, the rates for two limiting reactions for catalytic O_3 loss involving bromine, BrO + HO_2 and BrO + ClO, are rapid compared to rates for analogous reactions involving chlorine, ClO + HO_2 and ClO + ClO. In the mid-latitude lower stratosphere, bromine is typically 55 to 65% of the total halogen-induced loss rate. In the upper stratosphere and in the polar spring, bromine is considerably less important. Halogen-controlled ozone loss in the lower stratosphere is comparable to HO_x catalysis and typically larger than that due to NO_x.

Recent laboratory work suggests important revisions in key photochemical processes that govern production and loss of $BrONO_2$ and hypobromous acid (HOBr). The rate of the BrO + HO_2 reaction (the main production channel for HOBr) has been measured to proceed at approximately half the value that was used in the 1995 assessment [Elrod *et al.*, 1996; Larichev *et al.*, 1995; Li *et al.*, 1997]. A consensus of new cross-section measurements for HOBr photolysis, for which estimates had previously been based on aqueous phase spectra, leads to a value for the photolysis

rate that is much more rapid than previously thought [Rattigan *et al.*, 1996; Barnes *et al.*, 1996]. New cross-section measurements of $BrONO_2$ photolysis lead to a 16% increase in its recommended J value [Burkholder *et al.*, 1995]. Each of these changes tends to increase the relative abundance of BrO within the Br_y family. All of these changes are recommended by JPL 1997 [DeMore *et al.*, 1997] and are therefore included in the models used in this assessment. Models that also incorporate changes in NO_x chemistry discussed above will increase $BrONO_2$ and decrease BrO by about 25%.

There is broad agreement within the stated errors between a) estimates of inorganic bromine based on BrO measurements and photochemical models, and b) estimates of inorganic bromine using measurements of organic bromine source gases. This agreement indicates that there are no large (30%) missing sources of bromine in the stratosphere [Wamsley *et al.*, 1998; Stimpfle *et al.*, 1999; Avallone *et al.*, 1995; Harder *et al.*, 1998; Fish *et al.*, 1997].

From the point of view of this assessment, these conclusions make three crucial points. First, it is important that models reproduce observations of Cl_y and Br_y, and their variations with altitude and latitude. Second, the characterizations of the partitioning of chlorine and bromine reservoirs from observations and the agreement with improved photochemical parameterizations improve confidence in our understanding of the underlying fundamental chemistry. Finally, observations of the response of halogens to NO_x confirm that modeled halogen chemistry will vary with NO_x abundances in a manner that is nearly identical to that of the present atmosphere.

2.4.4 Hydrogen Species: OH and HO_2

Hydrogen radical photochemistry is more complex than that of nitrogen and halogen radicals, because more processes (typically about a dozen) contribute to production and destruction of HO_x while half that number are important to halogen and nitrogen radical chemistry. In general, reactions that break the OH bond in water or other bonds to a hydrogen atom are the net sources of OH, although at any instant intermediate reservoirs such as HNO_3, HNO_4, or H_2CO are also important sources. The primary production mechanism of OH is the photolysis of O_3 yielding $O(^1D)$ which subsequently reacts with hydrogen-containing molecules, mainly H_2O, CH_4, and H_2, to produce OH. The hydrogen radicals are removed via reactions that reform water bonds, mainly $OH + HNO_3 \rightarrow H_2O + NO_3$ and $OH + HO_2 \rightarrow H_2O + O_2$, and by reactions that reform reservoirs, such as $OH+NO_2 \rightarrow HNO_3$.

Measurements of OH and HO_2 in the lower stratosphere have now been obtained at latitudes from 70°S to 90°N. As shown in Figure 2-8a, these measurements show remarkably constant concentrations of OH over this region, despite the variation in O_3, NO_x and other atmospheric constituents [Wennberg *et al.*, 1994]. The observed OH concentrations have little or no dependence on O_3 and HNO_3 concentrations, but show the expected dependence on UV flux, which is shown by the model curve in Figure 2-8a. Photochemical steady-state model calculations constrained by simultaneous measurements of O_3, H_2O, CH_4, H_2, NO, NO_2, NO_y and the solar radiation field reproduce observed OH concentrations well (±25%) over this wide range of observations, including most of the variability and fine details shown in Figure 2-8a. The strong buffering of OH exists because of the correlation of NO_2, HNO_3 and other sinks of OH with O_3 and other sources of OH in the lower stratosphere.

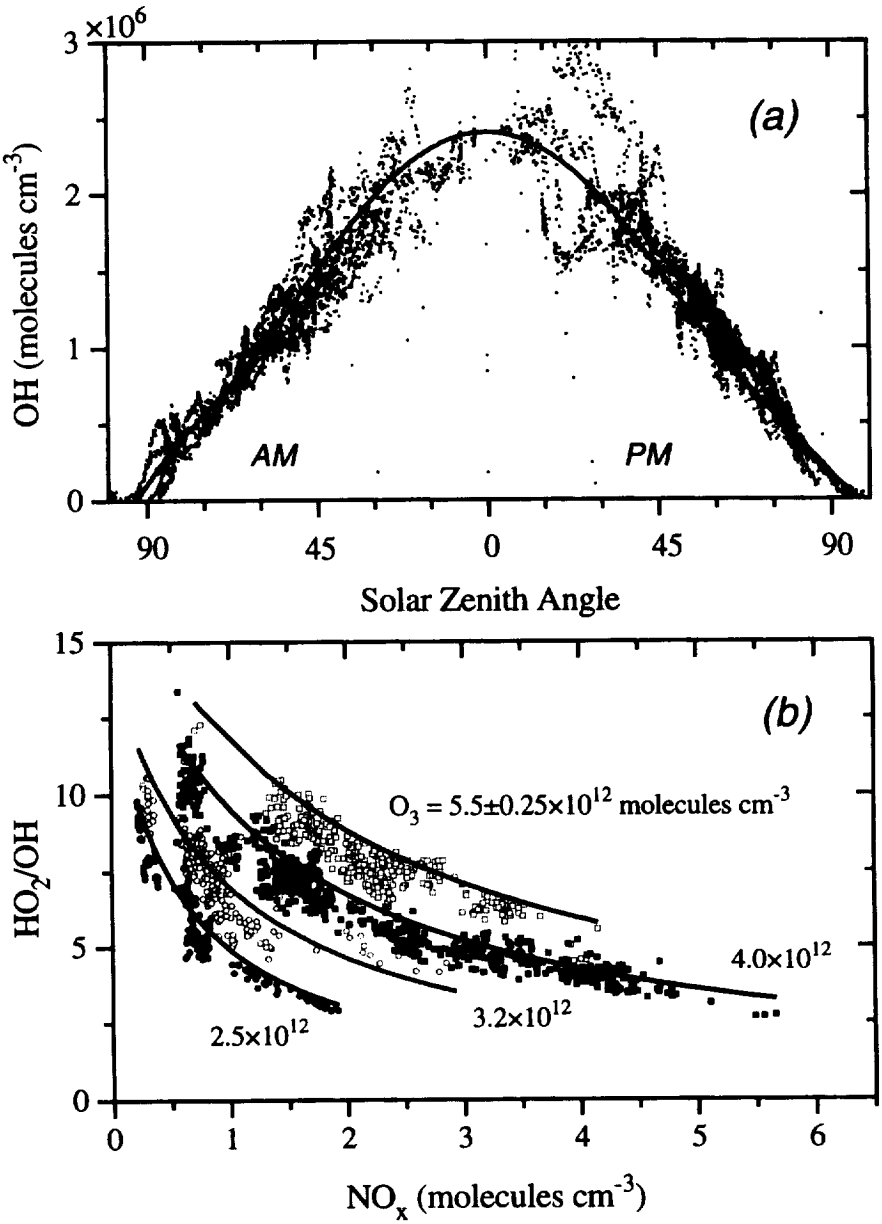

Figure 2-8. Observations of OH and HO_2/OH. The data was obtained over several years, on flights of the ER-2 at latitudes from 70°S to the North Pole. Observations of OH vs. solar zenith angle (a) show that OH is nearly invariant to other parameters including O_3, HNO_3, and H_2O within the range these quantities vary in the lower stratosphere. In contrast, HO_2, normalized b y coincident measurements of OH, is a strong function of NO shown as NO_x (10^9 molecules cm^{-3}) in (b). Both observations are consistent with current models (solid curves).

At large solar zenith angles, high aerosol loading, and low NO_x, the agreement between modeled and the observed OH concentration improves with the inclusion of the heterogeneous hydrolysis reactions of bromine and chlorine nitrate and the subsequent photolysis of the products: $XONO_2$ +

$H_2O \rightarrow HOX + HNO_3$, $HOX + h\nu \rightarrow OH + X$, X = Cl, Br. These sources are small compared to the $O(^1D)$ sources in general, but can account for most of the OH source at high solar zenith angles [Jaeglé *et al.*, 1997; Lary *et al.*, 1996]. As a result, measurements of OH and HO_2 have proven useful in evaluating our understanding of the heterogeneous reactions described in the next section. These reactions are included in the models described in Chapter 4. Wennberg *et al.* [1999] note that $BrONO_2$ hydrolysis is not rapid enough to completely explain the high values of OH observed near sunset under low aerosol/high NO_x conditions. They propose a source in addition to those described above with a strong photolysis cross-section at wavelengths near 1 μm.

While OH concentrations are strongly buffered, HO_2 concentrations in the lower stratosphere and the upper troposphere show substantial variation with NO_x and O_3. The changes in HO_2 can be described accurately (±10%) by an analysis using measured concentrations and laboratory rates for an extremely wide range of atmospheric conditions [Cohen *et al.*, 1994]. This analysis has two-fold significance: first, it shows that the reactions that interconvert OH and HO_2, which include the rate-limiting step ($HO_2 + O_3 \rightarrow OH + 2O_2$) for catalytic removal of O_3 by HO_x, are accurately described by mechanisms used in current models. Second, as shown in Figure 2-8b, it shows directly the response of the catalytically active HO_2 to changes in NO_x. The suppression of HO_2 concentrations by NO explains, in part, why the O_3 response to the sum of NO_x and H_2O perturbations is not simply the sum of the individual perturbations to catalytic cycles of ozone.

2.4.5 Aerosol

Chemical transformations on aerosol surfaces affect the partitioning of nitrogen and halogen reservoirs. The reactions:

$$N_2O_5 + H_2O \rightarrow 2HNO_3 \quad \text{(R1)}$$
$$ClONO_2 + H_2O \rightarrow HNO_3 + HOCl \quad \text{(R2)}$$
$$BrONO_2 + H_2O \rightarrow HNO_3 + HOBr \quad \text{(R3)}$$
$$ClONO_2 + HCl \rightarrow HNO_3 + Cl_2 \quad \text{(R4)}$$
$$HCl + HOCl \rightarrow H_2O + Cl_2 \quad \text{(R5)}$$

have been characterized in the laboratory. Observational evidence exists that all of these reactions occur in the atmosphere.

The reaction with the most pervasive effect on stratospheric photochemistry is the hydrolysis of N_2O_5, R1. Numerous laboratory measurements (see Hanson [1997]; Robinson *et al.* [1997]; Hu and Abbatt [1997] for recent results) demonstrate this reaction occurs frequently, about once in 10 collisions of N_2O_5 with an aerosol particle. When the sulfate layer is not volcanically enhanced, this reaction reduces NO_x concentrations in the lower stratosphere by almost a factor of 2 compared to gas-phase chemistry alone. At high aerosol loadings NO_x is reduced by a factor of 3. These effects were extensively documented from aircraft, balloon, satellite and ground-based instrumentation following the massive eruption of Mt. Pinatubo in 1991 [WMO, 1995]. The effect of N_2O_5 hydrolysis on NO_x depends on temperature because N_2O_5 is formed more rapidly at higher temperatures. It also depends on season because N_2O_5 is formed almost exclusively at night.

Short summer nights provide little time for N_2O_5 formation even though the rate is enhanced by the warm temperatures. Long winter nights result in significant N_2O_5 formation. In addition, N_2O_5 is photolyzed during the day. At a given aerosol loading, photolysis competes more effectively with hydrolysis and may dominate during the summer when the long days give the sun more opportunity. The aerosol layer thins significantly with increasing altitude so all of the reactions discussed in this section are less important in the middle and upper stratosphere.

At the poles, the direct cause of springtime ozone loss is the high concentration of chlorine radicals. To enable this catalysis, NO_x must first be driven almost entirely from the system via aerosol reactions. With the exception of HCl + HOCl all of the reactions listed above denoxify, that is convert short-term reservoirs of NO_x to HNO_3, and all but N_2O_5 + H_2O activate halogen radicals as well. The HNO_3 produced in these reactions is then sequestered on aerosol. If temperatures remain cold enough to sustain these heterogeneous reactions, any HNO_3 that evaporates and is converted to NO_x is rapidly reconverted back to HNO_3. When this situation persists until and beyond polar sunrise, ensuing ozone loss rates approach a few percent per day [WMO, 1995]. In a matter of weeks nearly all of the ozone within the polar vortex can be destroyed. In the Antarctic, it frequently remains cold enough for complete loss of ozone, while in the Arctic the temperatures are more variable and ozone loss in recent years has ranged from minimal to nearly 40% [WMO, 1995].

Aerosol particles grow to large sizes (>10 μm) in the cold temperatures of the lower stratospheric polar winter. At large sizes, these aerosols are often referred to as polar stratospheric clouds. The details of the number of large particles that form, exactly how large they become, and what they are composed of are not well-understood (see review in Peter [1997]). If the HNO_3 in particles sediments to lower altitudes, a process known as denitrification, low NO_x chemical conditions can be sustained until the air mixes with higher-NO_x. Sedimentation rates are determined by air density and particle size, shape, and density. The chemistry and microphysics that govern particle size, shape, and density are difficult to model accurately. Consequently the mechanistic models of stratospheric aerosol needed to make accurate predictions of the interaction of HSCT exhaust with aerosol, and the subsequent effects on stratospheric NO_y and H_2O concentrations are not available.

The rates of Reactions 1-5 and hence their effect on springtime ozone loss depends on the phase and water content of the aerosol. These processes are better understood than those that control aerosol size and that lead to sedimentation and evaporation. The chlorine reactions are particularly sensitive to the water activity of sulfuric acid aerosol. As a result, at low temperatures, there is nearly complete conversion of inorganic chlorine to free radical form [Kawa *et al.*, 1997]. This effect has also been observed under mid-latitude conditions of low temperature and unusually high water abundance [Keim *et al.*, 1996]. The temperature-water vapor dependence of aerosol surface area used in the models of this assessment is taken from the thermodynamic model of Carslaw *et al.* [1997] and the reactivity per unit area from Hanson *et al.* [1994] and Robinson *et al.* [1997]. Direct verification of the temperature dependence of the ClO mixing ratio that results from these reactions was obtained from *in situ* observations that relied on the ER-2 to sample inside the Antarctic vortex (Figure 2-9).

These laboratory and field observations demonstrate the impact of changes in the water vapor mixing ratio on the threshold temperature for increases in ClO concentration. At H_2O mixing ratios

of 5 to 10 ppmv, the threshold temperature for near complete conversion of Cl_y to ClO shifts to ~1 K higher temperature for a 20% increase in water. A critical question for the HSCT assessment is then: what will be the temperature *and* the water vapor mixing ratio in three decades as the proposed use of HSCTs emerges? Aircraft NO_x and H_2O will likely raise the temperature at

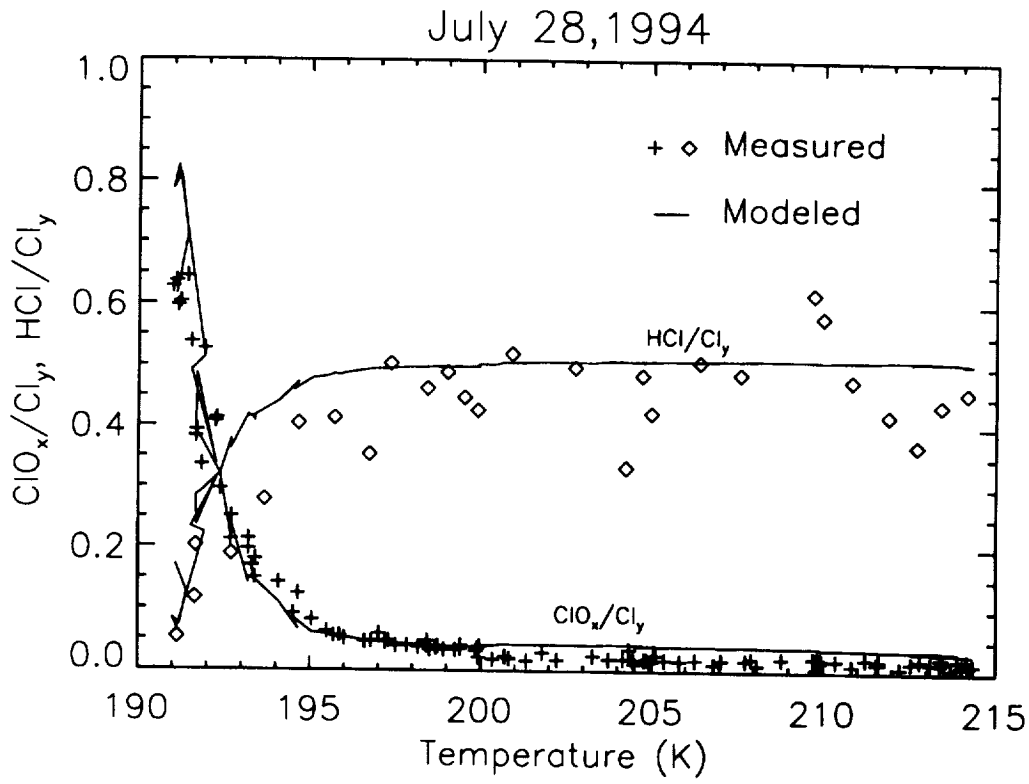

Figure 2-9. Observations and a model analysis of the temperature dependence of inorganic chlorine partitioning (adapted from Kawa *et al.* [1997]).

which denoxification can happen, increasing the likelihood of severe polar ozone loss. However, the combined uncertainties of climate and trace gases in the future atmosphere, as well as the nonlinearity of these reaction rates, makes it extremely difficult to estimate the response of the future atmosphere.

While the majority of stratospheric aerosol particles are sulfate and water, there are few measurements of the trace composition of stratospheric aerosol. Observations of carbon aerosol in the lower stratosphere have provoked considerable debate about the source of the particles and the mechanism for their transport into and/or within the stratosphere. Laboratory measurements show that initial rates of reaction of O_3 and HNO_3 on clean carbon aerosol are rapid, although the rates often slow with time indicating some mechanism for deactivating the surface [Fendel *et al.*, 1995; Rogaski *et al.*, 1997]. Model studies have investigated whether reactions on these particles might

be important to recent ozone trends [Bekki, 1997] or to explaining the relative concentrations of HNO_3 and NO_2 [Lary *et al.*, 1997]. Both these studies maximize the possible effect of carbon particles by assuming the reactions are catalytic with respect to carbon or that a source of carbon soot exists that is large enough to sustain a steady-state concentration at present values. Laboratory evidence suggests that the reaction of O_3 + soot yields is 15 to 35% CO or CO_2 [Stephens *et al.*, 1986]. CO and CO_2 are also observed as products of HNO_3 + soot [Thlibi and Petit, 1994]. In other words, the reactions are not catalytic, which suggests they cannot be occurring rapidly in the atmosphere. The lifetime of soot in the atmosphere would be a few hours if the O_3 and HNO_3 reactions were proceeding at rates observed in the laboratory. To sustain the observed soot concentrations against this rapid loss would require an enormous unidentified source and would produce concentrations of CO and CO_2 that would be easily detectable (and have not been) against the background of other sources of CO and CO_2.

2.5 Summary

Since the last HSCT assessment in 1995, new observations, theoretical work, and modeling have 1) reinforced our understanding of some of the fundamental features of stratospheric chemistry and transport, and 2) led to significant advances in our ability to interpret the differences between models and observations. Improved understanding and quantification of atmospheric transport and photochemical processes leads directly to a more accurate prediction of the effects of HSCTs on the atmosphere and to significantly improvements in our ability to estimate the uncertainty in these predictions. We summarize here some of the key areas of observational and conceptual progress, along with remaining uncertainties in our understanding of the factors that determine the likely effects of HSCT exhaust on the atmosphere. These include the physics responsible for atmospheric transport as it determines the distribution and accumulation of aircraft exhaust, the combined effects of chemistry and transport on the composition of the background atmosphere (especially, the distribution of ozone, NO_y, H_2O and aerosol), and the effects of changes to the rate of free radical catalysis that result from enhancement and suppression of chemical pathways for ozone change by the HSCT exhaust.

- The local response of ozone to changes in NO_x, H_2O, and aerosol is becoming increasingly well understood and the chance for surprise is diminishing. Through a combination of laboratory experiments, observations of atmospheric radicals and reservoir species, and improved approaches to interpreting these observations, uncertainties in chemistry have been reduced.

  - Kinetic parameters controlling radical abundances have been constrained from simultaneous observations of radicals from all three major chemical families. As a result, we expect that models incorporating the most recent kinetic rate parameters will reproduce the distribution of atmospheric free radicals to within 50%. Moreover, we expect that these models correctly predict the sensitivity of ozone loss to changes in atmospheric composition from aircraft. For current atmospheric conditions, increases in NO_x will decrease local ozone. However, due to the buffering effect of competing catalytic chemical cycles, the ozone response is only weakly coupled to NO_x over the narrow (factor of 2) range of NO_x concentrations present in today's lower stratosphere.

- Our understanding of the rates of reactions controlling NO_x and HO_x has been significantly improved by recent atmospheric observations, photochemical process modeling, and laboratory measurements. About 30% more NO_x is observed in the lower stratosphere than predicted by photochemical models using currently recommended rate constants, and constrained by simultaneous measurements of NO_y and OH. There also tends to be less HO_x in models than is observed. Specific errors in the reaction rates that control NO_x and HO_x have been recognized based on analysis of these observations and laboratory experiments. The models used in Chapter 4 were developed before these revisions to the kinetic parameters. They are expected to underestimate NO_x by approximately 30% and, depending on time of day, HO_x as well. The transition to NO_x rich conditions in these models will likely occur at larger values of emission index or exhaust accumulation than it will in these same models once the changes to HO_x and NO_x photochemistry are incorporated.

- Improved laboratory information on several important reactions—such as ozone photolysis to produce $O(^1D)$, OH + ClO to produce HCl, hydrolysis of $BrONO_2$, and the low temperature chemistry of ternary solutions of H_2SO_4, HNO_3, and H_2O—produces much better agreement between photochemical models and atmospheric observations. The comparisons increase our confidence in the accuracy of descriptions of photochemistry and reduce concerns that we might be missing an essential aspect of the photochemistry.

- The effect of HSCT exhaust depends strongly on the background atmosphere in which the aircraft fly. Variations in the background stratospheric aerosol, NO_x, HO_x, halocarbons, and temperature resulting from natural processes (e.g., volcanic eruptions), changes in industrial activity (e.g., N_2O emissions from fertilizer use, halocarbon emissions), and from changes to climate (possibly affecting stratospheric temperature, and water) will affect predicted changes to ozone due to HSCT exhaust. Predictions of the effects of HSCT exhaust are particularly sensitive to the abundance of NO_x in the lower stratosphere. Representing the initial state properly is especially crucial for assessing the relative effects of large and small perturbations (e.g., EI 5 vs. 15; fleet sizes of 500 vs. 1000).

  - Descriptions of the amounts of chlorine, bromine, water, CH_4, and N_2O entering the stratosphere based on measurements at the surface and tropopause temperatures compare with stratospheric observations to better than 10%. Thus an important boundary condition for today's atmosphere is accurate. Futhermore, the processes which control halogen and nitrogen radical source gases, CFCs and N_2O, are sufficiently well known that uncertainties in their concentrations in 2050 are small compared to other uncertainties in this assessment.

  - The interplay of chemistry and transport with respect to the chemical composition of the background atmosphere has been better defined through theory and observations. The relationships among free radical source gases and the distribution of these gases as a function of mean age, altitude, and latitude have been observed and characterized through measurements from aircraft, space, balloons and ground-based sensors.

- Major questions remain about the microphysics of aerosols, including polar stratospheric clouds. We do not understand the factors that control sedimentation rates, and, hence, the representation of the aerosol sinks of NO_y and H_2O in the lower stratosphere is highly uncertain. The effect of aircraft emissions on the aerosol surface area and reactivity is poorly known.

- There is uncertainty attached to the temperature of the future atmosphere, because of possible climate change. Even small changes in temperature may significantly alter stratospheric water vapor concentrations. Uncertainties in future CH_4 abundances are also limit our ability to accurately predict future stratospheric water. Such changes may affect the effects of HSCTs on polar ozone loss.

- The effect of HSCT exhaust depends strongly on its accumulation and dispersion within the stratosphere. The exhaust distribution depends on the aggregate over many different transport processes; in particular, transport from mid-latitude flight corridors into the tropics, strength of meridional circulation, and transport out of the stratosphere into the troposphere. These same processes also determine the distribution of source gases in the background atmosphere.

  - Observations of a suite of chemical tracers within the tropical stratosphere has led to an improved understanding and quantification of key transport processes within the tropics; in particular, the time scale for quasi-horizontal transport from mid-latitudes into the tropical region, and vertical diffusion and ascent rates within the tropics. These processes are believed to determine the extent to which HSCT exhaust will be transported to the middle and upper stratosphere and, consequently, the degree to which it accumulates in the stratosphere. Although there remain uncertainties in the vertical and temporal (i.e., interannual) variations in these processes, the measurements provide stringent tests of tropical transport processes within numerical models.

  - A key component of the dispersal of HSCT emissions is the transport out of the stratosphere into the troposphere. This depends on both the large-scale stratospheric circulation (which controls the time-averaged, large-scale flux) and synoptic-scale mixing events in upper troposphere / lower stratosphere (which control the flux over shorter times and smaller spatial scales). Accurately representing the latter processes in models is challenging, and is currently not well-constrained by observations.

  - Changes in H_2O, NO_y, and aerosol from HSCT exhaust will occur in the polar vortices primarily by multi-year accumulation in the stratosphere rather than by direct deposition of aircraft emissions during a particular winter season. Because air in the vortex comes primarily from higher altitudes, the magnitude of these changes will depend on the extent to which exhaust is transported into the middle and upper stratosphere.

  - Extensive observations of CO_2, SF_6, and HF have enabled the distribution of mean age in the stratosphere to be determined. The mean age contains valuable information on stratospheric transport, independent of chemical processes, and depends on the integrated effect of the different stratospheric transport processes. Because the residence time of HSCT emissions also depends on the integrated effect of these transport processes, the

residence time of emissions in the stratosphere is expected to be related to the mean age. These and other arguments suggest that models, which calculate a stratosphere that is too young, may underestimate the increase of H_2O, NO_y, and aerosol from HSCT exhaust.

3. EMISSIONS

An HSCT fleet would emit gases and introduce particles directly into the stratosphere in the 17- to 20-km altitude range. The NASA High Speed Research (HSR) Program has set an aggressive goal for the NO_x emission levels of the HSCT at supersonic cruise. Linking the concentrations of NO_x, HO_x, SO_x and particles emitted from the HSCT engines, and formed in subsequent plume processes, to the 2- and 3-D global CTMs requires understanding the fluid dynamics, chemistry, and particle microphysics both within individual aircraft plumes and as the plumes mix to larger scales. For incorporation in assessment models, these emissions must then be distributed geographically based on the expected usage of such an aircraft for different assumed fleet sizes. Because many HSCT technologies are not yet proven and the economically viable fleet sizes are not well known, this assessment is based on a series of parametric studies of fleet size, NO_x emission levels, flight altitudes, and sulfate production.

In this chapter, we review the HSCT concept, the likely combustor technologies, and the anticipated engine emissions of NO_x, H_2O, SO_x, and CO_2. The processes leading to the dispersion of these gases in the atmosphere are then discussed, followed by a summary of gas-phase reactions known to take place in the wakes of existing subsonic and supersonic aircraft. Direct particle emissions and in-plume formation from current aircraft are then examined and related to potential production by the HSCT fleet. Finally, the fleet size, geographical and vertical location of the flights, and fuel use and emissions of the HSCT and subsonic fleet for future scenarios are discussed.

3.1 HSCT Overview

The NASA HSR Program is developing the enabling technologies for a second-generation supersonic transport (HSCT) that would be both environmentally acceptable and economically viable. The first generation of supersonic commercial transports, the Concorde, was a technological success but not a great financial success. The major environmental goals of the NASA program are that the HSCT must be acceptable both in terms of noise and emissions.

The current HSCT under consideration would fly at Mach 2.4 with supersonic cruise altitudes of 17 to 20 km. It would have a maximum range of 5000 nautical miles and carry approximately 300 passengers. Because of concerns about the effects of the emissions on stratospheric ozone, a major thrust of the program has been the development of low-NO_x combustors. The program goal has been for NO_x emissions of 5 grams of NO_x (as NO_2 gram equivalent) per kilogram of fuel burned at supersonic cruise conditions [Wilhite and Shaw, 1997].

It is anticipated that the HSCT will fly supersonically only over water, due to the need to mitigate sonic booms over populated land masses. Thus, its major use would be on long intercontinental routes such as the North Atlantic and North Pacific. The potential market for the HSCT is limited by both economic and environmental considerations.

The date for entry into service for the HSCT is still unknown but optimistically could not be expected to begin before around 2020. The growth to fleet sizes of 500 and 1000 as evaluated in this assessment would depend on the economic viability of the HSCT and the world economy at

the time but would be expected to occur over a 10- to 25-year period. The HSCT fleet development depends on the development of new technologies. Technological challenges include lightweight materials/structures development, high-temperature engine materials development, affordability of manufacture and operating, durability, high/low speed aerodynamic performance, variable engine cycle development, and low noise nozzle and inlet design.

3.2 Combustor Concepts

NO_x is produced in combustors by high-temperature reactions between nitrogen and oxygen. The production of NO_x is very sensitive to temperature, residence time, and fuel-air ratio, peaking near stoichiometric conditions (fuel-air equivalence ratio = 1) as illustrated in Figure 3-1. Low-NO_x combustor concepts focus on reducing the residence time and operation at non-stoichiometric conditions.

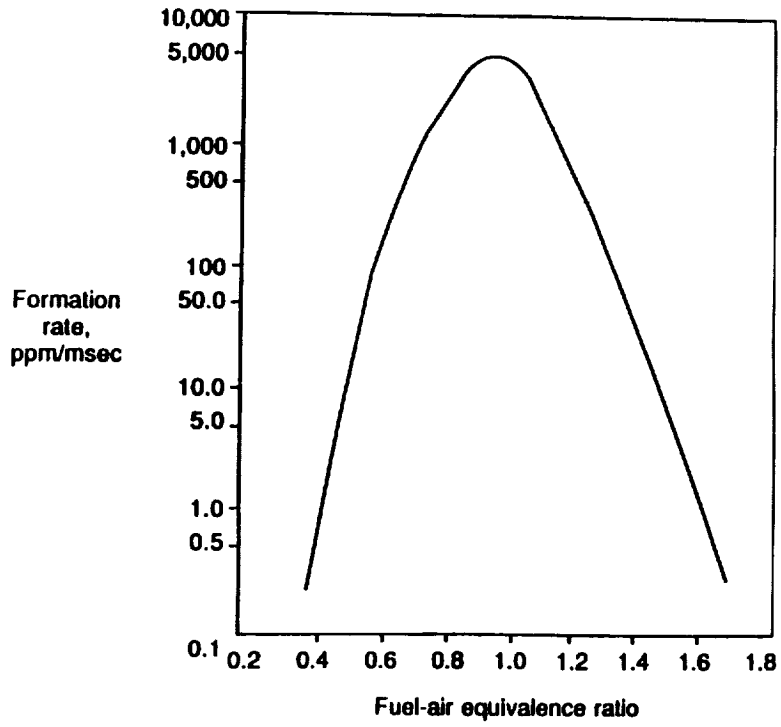

Figure 3-1. Schematic of NO_x formation as a function of fuel-air equivalence ratio.

Two concepts for low-NO_x combustors have been pursued by the NASA HSR Program with the goal of producing a practical combustor with an EI of 5 grams of NO_x/kg fuel burned or better at supersonic cruise. For both concepts, combustion efficiency of greater than 99.9% is a program requirement. In the lean premixed prevaporized (LPP) approach, fuel is vaporized, uniformly mixed with air, and then burned under lean (equivalence ratio <1) conditions (Figure 3-1). The other concept is the rich burn, quick quench, lean burn (RQL) combustor. In this approach, fuel is

evaporated, partly burned in a fuel rich zone, quenched by the rapid introduction of air, and then burning is completed in a fuel lean zone. The NASA HSR Program made the decision in 1998 to pursue the LPP approach in more depth with significantly less effort on the RQL concept.

Both concepts have been demonstrated in combustor rig tests with encouraging results and both have numerous technological challenges associated with them [National Research Council, 1997]. For the LPP, these challenges include the complexity of numerous fuel injection points and combustion stages, and the potential for autoignition, flashback, fuel line coking, and combustion instability. For the RQL, issues include the difficulty of reaching the NO_x emission goal while simultaneously demonstrating acceptable performance and operability using fuel-shifting technology. For both concepts, major issues include the need for high-temperature combustor liner materials to eliminate the need for cooling air and the need for maintainability, safety, inspection, and long-operational life. Because of these challenges, we evaluate the sensitivity of ozone impact over a range of assumed NO_x emission levels.

3.3 Engine Emissions

The primary products of combustion from an aircraft engine are water vapor and carbon dioxide. Their emission rates depend on the chemical composition of the fuel and the fuel burn rate. Typical emission indices are summarized in Table 3-1. Emissions of sulfur oxides (SO_x) are similarly determined by the sulfur content of the jet fuel. Future levels of sulfur in jet fuel will depend on the future specifications and regulations for refined distillates and consequently on the refinery technology implemented. Projections have been made that the level of sulfur in jet fuel will decrease from the current levels of around 0.04% [Hadaller and Momenthy, 1989] to around 0.02% by 2015 [Hadaller and Momenthy, 1993]. Since the future fuel sulfur content is uncertain, a range of apparent sulfate aerosol emission levels are included in the modeling discussion in Chapter 4.

Table 3-1. Recommended emission indices in units of grams emission/kilogram fuel for 1990 and 2015.

Emission	Emission Index	
	1990	2015
Carbon Dioxide (CO_2)	3155	3155
Water (H_2O)	1237	1237
Sulfur oxides (as SO_2)	0.8	0.4

Sulfur oxides emitted from modern aircraft engines are primarily in the form of SO_2 at the combustor exit. Measurements made at the exit plane of a modern military engine (F100) show that 92 +/- 20% of the fuel S was emitted as SO_2; upper limits from attempts to directly measure SO_3 indicate that SO_3 accounted for <11% of the fuel S [Wey *et al.*, 1998]. One-dimensional

models of the hot zone of the German Advanced Technology Testing Aircraft System (ATTAS) and Concorde [Brown *et al.*, 1996b] engines predict that 2 to 10% of the oxidized fuel sulfur is in the form of SO_3 at the engine exit plane. Recent 1- and 2-D modeling studies [Lukachko *et al.*, 1998] predict that some additional SO_2 is oxidized to SO_3 in the turbine by reaction with atomic oxygen. These modeling studies indicate the oxidation process may be sensitive to the interaction of cooling air and main flow near the surface of the turbine blades. These processes are not yet well enough characterized to extrapolate quantitatively to the HSCT, although some $SO_2 \rightarrow SO_3$ conversion is expected in both the combustor and the turbine. Conversion of SO_2 to SO_3 is a limiting step in the conversion of fuel S to particulate S in the exhaust.

Nitrogen oxides, carbon monoxide, and hydrocarbon emissions are produced within the combustors and depend on combustor efficiency and design. Multiple test-stand measurements of NO and NO_x EI at the exit plane of several different engines indicate typical cruise values of NO/NO_x from ~0.85 to ~0.9 (e.g., Howard *et al.* [1996]; Wey *et al.* [1998]; Spicer *et al.* [1992, 1994]). In-flight measurements of the NO/NO_x ratio have been extrapolated to the engine exit plane [Fahey *et al.*, 1995a; Schulte *et al.*, 1997] and give similar values. Although NO/NO_x is specific to the engine technology, the expected high power setting for the HSCT implies similar values for the future engine.

The HSR Program goals include an overall combustor efficiency greater than 99.9% at supersonic cruise conditions. Carbon monoxide and hydrocarbon emission levels are direct measures of combustor efficiency. The HSR combustor team has provided estimates of $EI_{\text{total hydrocarbons}} = 0.3$ and $EI_{CO} = 2.9$ grams/kg fuel burned, corresponding to a projected combustor efficiency of 99.95% at supersonic cruise. This combustor efficiency is similar to current production jet engines.

Soot is emitted as a consequence of combustion processes. In aircraft engines, soot is formed in the combustor from the incomplete combustion of fuel hydrocarbons. Chemically, soot encompasses a range of compositions dominated by polyaromatic hydrocarbons and oxygenated polyaromatic hydrocarbons joined in a graphite-like structure [Smith and Chughtai, 1993]. The chemical reactivity of the soot is in large measure determined by its surface chemistry, which may vary significantly. Soot produced from the combustion of n-hexane can partially hydrate [Chughtai *et al.*, 1996] and oxidize SO_2; such reactions may be enhanced by the presence of trace metal oxides incorporated into the soot during combustion and changed by exposure to NO_x or O_3 [Chughtai *et al.*, 1993]. The soot surface area available for heterogeneous chemical reactions, which depends on the mass, size, and morphology of the particles, is poorly known and may vary significantly. Recent studies [Hagen *et al.*, 1996; Petzold and Schröder, 1998] indicate that most aircraft-produced soot particles have sizes <0.08 μm, although there are unresolved issues associated with the sizing of non-spherical particles.

Soot measurements from combustors designed to test both the LPP and RQL concepts indicate that the RQL soot levels would be comparable to current technology engines while the LPP soot number EIs would be orders of magnitude lower.

Metallic material, including zinc, aluminum, and titanium, has been reported in the residue of evaporated contrail particles [Twohy and Gandrud, 1998; Chen *et al.*, 1998]. Sources for these

metals may be abrasion of engine components, trace metal impurities in the fuel, and ingestion of particles in ambient air into the combustor. The consequences of metallic emissions for the stratosphere are not known, but are probably small relative to the much more abundant soot and sulfate particles likely to be produced by HSCTs. Minor amounts of silicon have been reported in soot collected behind F-16 and C-130 aircraft, and may serve as a marker for aircraft soot emissions in the atmosphere [Wilson *et al.*, 1998].

3.4 Dispersion Processes

Exhaust leaves the aircraft engine at high speed and at high temperatures. The concentrated exhaust gases mix with ambient air to reduce the emissions concentrations, the temperature, and the relative speed in the exhaust flow. Eventually, the exhaust becomes mixed to global scales and ends up contributing to the anthropogenic perturbations of the natural atmosphere.

The evolution of the exhaust fluid dynamics can be broken into three regimes [CIAP 2, 1975; Miake-Lye *et al.*, 1993]:

a) The plume, where the jet of exhaust is primarily influenced by interactions due to its velocity relative to the ambient air;

b) The vortex wake, in which the flows induced by the lift needed to keep the airplane aloft dominate the mixing and transport of the individual engine jet flows; and

c) The wake dispersion regime, where wake instabilities and atmospheric processes overcome the influence of aircraft induced flows in determining the mixing and transport of the exhaust.

From a practical point of view, when considering measurements or computational modeling approaches, these three regimes can be segregated into two stages by those processes happening close to the airplane, the near field, where airplane induced flows contribute to the dispersion (plume, wake, and initial wake breakup), and the far field, which is dominated by atmospheric processes. The far field still represents the exhaust of a single airplane, but is no longer being affected by the airplane's flow and possibly beginning to merge with other diluted exhaust wakes. Thus, a third and ultimate stage is represented by the processes that make the far field indistinguishable from the ambient. These three stages of exhaust dilution, (1) the near field, (2) the far field, and (3) dispersion to global scales are discussed below.

3.4.1 Near Field

The engine exhaust flow behind a supersonic engine moves at speeds that are supersonic with respect to both the engine and even the ambient air [Miake-Lye *et al.*, 1993]. Thus the flow field is that of a supersonic co-flowing jet. Since the engine nozzle is optimized for supersonic cruise, the diverging section will be very close to that required for a perfectly expanded supersonic exit flow and there will be minimal shocks. The shock structure that does occur will be primarily due to the supersonic mixing layer between the exhaust flow and the ambient. The mixing layers will grow, merge, and decelerate the flow, eventually resulting in a subsonic co-flowing jet, not unlike that of a subsonic engine.

Further plume development is affected by the vortical flow shed from the lifting surfaces of the airplane. For a supersonic airplane in cruise, the wing is the primary contributor to this vortical wake flow field. A counter-rotating vortex pair develops as the vorticity distribution from each wing rolls up into a vortex representing downward flow near the fuselage and upward flow near the wing tip. Each vortex engulfs the exhaust from the engines on the same side of airplane from which that vorticity was shed [Anderson *et al.*, 1996a, b]. For supersonic aircraft, a delta wing (or variations on that configuration such as double delta or cranked delta) has a different lift distribution (and thus vortex strength) than that of elliptically loaded wings representative of subsonic flight. This delta wing lift distribution results in somewhat different initial vortex roll-up, taking a little longer distance to achieve tightly rolled vortices; this difference is unlikely to have a major impact on plume capture or the final vortex wake structure. The counter rotating vortex pair shears the co-flowing jets and causes additional mixing initially, but then confines the exhaust in the descending vortex structure and suppresses further mixing [Miake-Lye *et al.*, 1993; Lewellen and Lewellen, 1996; Garnier *et al.*, 1997]. Due to small-scale turbulence and wind shear, the vortex pair structure eventually breaks up, on a time scale of several tens of seconds for a supersonic airplane.

The unstable wake of a subsonic airplane often forms 3-D ring-like structures when the two linear vortices pinch together and then reconnect one with the other. These rings, in the presence of atmospheric non-uniformities, break up further and the aircraft induced flow dissipates. As the aircraft-induced flows dissipate, the mixing of the exhaust is enhanced and atmospheric processes, including turbulence, shear, and buoyancy—due to the vertical displacement of the air entrained in the airplane's downward moving vortex wake—all contribute to additional mixing. For subsonic flight, agreement between theoretical and model predictions of exhaust mixing and flow field structure and that discerned from measured data is reasonable [Baumgardner *et al.*, 1998]. Lidar measurements of the vortical structure behind a 737 in flight show excellent agreement with large eddy simulations [Lewellen and Lewellen, 1996].

3.4.2 Far Field

The atmospherically driven mixing of the exhaust from a single airplane represents the far-field wake. Exhaust spikes from airplanes have been encountered in a number of atmospheric measurement campaigns, and recently dedicated missions have been designed to study the emissions and their dilution [Schumann *et al.*, 1995]. Many measurements of subsonic airplanes have been made in the far field and models have been developed to empirically quantify the mixing processes [Schumann *et al.*, 1995; Lewellen and Lewellen, 1996; Dürbeck and Gerz, 1996; Sykes and Henn, 1995]. Because of the structure of the atmosphere and the vertical stratification, horizontal and vertical mixing are different. Vertical mixing in the far field is essentially negligible [Schumann *et al.*, 1995; Dürbeck and Gerz, 1996]. For subsonic flight in the upper troposphere and lower stratosphere (i.e., usually not far from the tropopause) mixing is complicated by the effects of weather, through turbulence and varying wind shear, and of stratosphere/troposphere exchange.

In the stable stratosphere, where supersonic flight is most efficient and future fleets are likely to fly, the primary transport and mixing is due to stratospheric winds and the wind shear that they produce. Thus, vertical mixing is likely to be significantly reduced for supersonic flight.

However, far-field data for stratospheric flights is currently limited to one encounter of the Concorde [Fahey *et al.*, 1995a] and the self-sampling of the ER-2 exhaust [Fahey *et al.*, 1995b].

3.4.3 Dispersion to Global Scale

Global transport and wind fields have been a subject of study for global modeling since the field's inception, but the essentially continual source represented by a fleet of scheduled commercial aircraft in the stratosphere has been considered only fairly recently [Sparling *et al.*, 1995; Weaver *et al.*, 1995; Sparling and Schoeberl, 1995]. By modeling the trajectory of individual flight tracks or through the use of 3-D transport models, the dispersion of the emissions on global scales can be determined. Seasonal effects are noted with a greater build up of emissions in flight corridors in summer months. Peak levels increase more rapidly in flight corridors [Sparling *et al.*, 1995] but their maximum levels do not exceed the zonal mean by more than a factor of 2 [Weaver *et al.*, 1995]. Mixing times range from 2 months in NH winter to 4 months in summer. In the absence of a supersonic fleet, experimental verification of these modeling studies is not possible.

3.5 Gas-Phase Plume Chemistry

Gas-phase plume chemistry is centered on the reactions involving the HO_x (H, OH, and HO_2), NO_x (NO and NO_2) and SO_x (SO_2 and SO_3) families. Reactions with OH control the gas-phase oxidation rates of NO_x and SO_x species in the plume. These processes take place on a fast time scale in the early stages of the plume (near field) and more slowly as the plume ages (far field). There are numerous modeling studies and *in situ* measurements of aircraft exhaust that address gas-phase chemistry in the plume. There is general agreement between model results and the *in situ* measurements for the gas-phase chemistry discussed below.

3.5.1 Near-Field Chemistry

The exhaust of an engine contains a very large number of reactive species in various abundances. Modeling studies provide highly detailed descriptions of the chemistry of species thought to be emitted from the engine [Brown *et al.*, 1996a; Kärcher *et al.*, 1996]. HO_x is predominantly in the form of OH, NO_x is predominantly NO and NO_2, and SO_x is predominantly SO_2, though SO_3 may be present at the exit plane as well. The most significant reactions are:

$$OH + NO + M \rightarrow HONO \quad (R1)$$
$$OH + NO_2 + M \rightarrow HNO_3 \quad (R2)$$
$$OH + SO_2 + M \rightarrow HSO_3 \quad (R3)$$

Sulfuric acid is generated from subsequent reactions that do not depend on OH:

$$HSO_3 + O_2 \rightarrow SO_3 + HO_2 \quad (R4)$$
$$SO_3 + 2H_2O \rightarrow H_2SO_4 + H_2O \quad (R5)$$

Reaction 3 is the rate-limiting step in the formation of H_2SO_4 from SO_2. Reactions 4 and 5 proceed rapidly because of the high concentrations of O_2 and H_2O. Reactions 1 and 2 together determine the lifetime of OH in the nascent plume. R3 is not a loss process of OH because of the production

of HO_2 in R4 and the fast conversion of HO_2 to OH by NO. Because of the high levels of NO in the exhaust (about 100 ppmv) the lifetime of OH is short, about 5 ms.

The most significant uncertainty of near-field chemistry is centered around the formation mechanism of H_2SO_4 in the exhaust. *In situ* observations of OH in the Concorde exhaust indicate that R3 converts only ~1% of the fuel sulfur assuming it is emitted entirely as SO_2 [Hanisco *et al.*, 1997]. It is not known how much SO_x is emitted as SO_3 and converted to H_2SO_4 via R5. If more than 1% of the fuel sulfur is emitted directly as SO_3, R3 is not the limiting step and R5 determines the formation rate of sulfuric acid in the near field. Model results suggest that 2 to 10% of fuel sulfur might be emitted from the Concorde engine as SO_3 [Brown *et al.*, 1996b], although these quantities are still insufficient to explain the large number of particles thought to be composed of sulfuric acid observed in the exhaust [Kärcher and Fahey, 1997]. The significance of emission of SO_3 followed by R5 is highly uncertain since no direct observations of SO_3 emissions have been made from commercial aircraft engines. Neither model results nor *in situ* measurements can preclude the existence of another mechanism for the generation of H_2SO_4 in the plume.

The effect of wake dynamics on near-field plume chemistry has been specifically addressed in models [Brown *et al.*, 1996a; Kärcher *et al.*, 1996; Anderson *et al.*, 1996a, b]. Model results show that wake dynamics are expected to have some effect on the details of plume chemistry, but do not present a major uncertainty for the reactions described above. The primary effect of the entrainment of ambient air into the exhaust plume is to dilute the concentrations of exhaust gases and to reduce the temperature of the plume. Reactions of entrained species with OH are small and do not compete with emitted reactants in R1 and R2. NO is converted to NO_2 by reaction with O_3 on a slow time scale (about 1 min.), long after OH is removed from the plume via R1. The rates of R1-3 have different temperature dependencies and will have slightly different relative rates depending on the actual entrainment rate.

3.5.2 Far-Field Chemistry

The chemistry in the far field occurs on a much longer time scale than in the near field of the plume. Far-field chemistry is regulated by the lifetime of nitrous acid (HONO) in the plume. Although some HONO is directly emitted from the engine, most is believed to be formed in the near field *via* R1. During daylight HONO is photolyzed to OH and NO, enabling oxidation *via* R2 and R3 as the plume ages. The concentration of HONO is limited by availability of OH to react with NO and reform HONO after photolysis. Since the concentration of OH is controlled by R2 in the far field, the decay time constant of HONO is proportional to the formation rate of nitric acid. The concentration of HONO will decrease faster if other processes remove HONO from the plume. HONO is known to react on sulfuric acid aerosols that may be present in high concentrations in the plume [Zhang, *et al.*, 1995; Fenter and Rossi, 1996]. The number of sulfur atoms in the fuel used by the Concorde in the flight analyzed by Hanisco *et al.* [1997] (0.023 weight %) is at least a factor of three smaller than the number of HONO molecules in the exhaust, indicating that the loss of HONO on sulfuric acid aerosols is small if this process occurs at all. However, for larger amounts of sulfate particle formation the heterogeneous loss of HONO on sulfuric acid aerosols might be significant [Kärcher, 1996].

In situ measurements in the lower stratosphere show that the decay time constant for HONO is about 10 minutes for typical daylight conditions [Hanisco *et al.*, 1997]. Essentially all of the HONO formed in the near field and any that is directly emitted from the engine is converted to HNO_3 via photolysis and R2. The fraction of NO_x converted to HNO_3 in the plume is roughly equal to the fraction of (OH + HONO)/NO_x at the exit plane. The fraction of SO_2 oxidized by OH is determined by this ratio and the relative rates of R1-3. Analysis of far-field measurements of the Concorde exhaust implies that 5% of NO_x and 1% of SO_2 were oxidized by OH at the time of observation. Table 3-2 summarizes the calculated fractional oxidation of NO_x and SO_x by reactions with OH inferred from ER-2 measurements in the lower stratosphere.

Table 3-2. Plume oxidation via R1-5 calculated from OH measurements for ER-2 observations of aircraft in stratospheric flight. The uncertainty of the NO_y EI is ±20%. The uncertainty of the HO_x EI and fractional plume oxidation is ±50%.

Encounter	EI_{NO_y} (gNO_2/kg fuel)	EI_{HO_x} (gOH/kg fuel)	NO_x Oxidized (via R2)	SO_2 Oxidized (via R3-5)
Concorde Mach 2	23	0.35	0.045	0.015
Concorde Mach 1.7[a]	<12	0.2	0.051	0.015
ER-2[b]	4	0.06	0.035	0.01

a) Average of two encounters.
b) Average of seven encounters.

3.5.3 Chemistry During Dispersion to Global Scale

Chemical and physical processes acting during the atmospherically forced mixing of individual and merged aircraft plumes to the large-scale environment may further alter the calculated effects of the aircraft emissions. Potential effects include chemical perturbations due to radiative disequilibria, gas-phase and heterogeneous chemistry, and particle microphysics and chemistry, although most of these effects are expected to be small. Rodriguez *et al.* [1994] calculated the chemical consequences of vertical transport due to radiative cooling of HSCT exhaust for time periods up to 5 days after emissions. The effect of this process on calculated mid-latitude ozone change was found to be negligible. Likewise, the partitioning between NO_x and NO_y during plume dispersion is not expected to significantly alter calculated ozone changes, as the chemical time scales of this partitioning is fast relative to the time scales of transport within the global assessment models. The activation of reactive chlorine due to heterogeneous reactions on the enhanced surface area within dispersing plumes has not been fully considered [Kärcher and Meilinger, 1998], but is likely to be small except for rare cases where local temperatures are below 200 K [Hanson *et al.*, 1994].

The microphysical evolution of HSCT-produced soot and sulfate particles during dispersion to the global scale has been investigated by Danilin *et al.* [1997] and Kärcher and Meilinger [1998]. These findings are discussed in 3.6 below. Because very few HSCT flights are expected to occur in polar vortices or near the tropical tropopause (where temperatures are sufficiently cold for the

significant condensation of nitric acid compounds), the formation of stratospheric clouds in dispersing plumes is not considered.

3.5.4 Extrapolating to HSCT Exhaust

The description of plume chemistry in 3.5.2 is generally consistent with *in situ* observations in the stratosphere for different engine operating conditions and different aircraft engines [Fahey *et al.*, 1995a, b; Hanisco *et al.*, 1997]. The range of emission indices (3.5–25 g NO_x (as NO_2)/kg fuel burned) determined from these observations encompasses the expected range of HSCT emission indices, suggesting that this qualitative picture is applicable to the proposed HSCT scenario. However, the quantitative details of the chemistry depend on the relative abundances of the NO_x, HO_x, and SO_x species in the exhaust of the HSCT engine.

We do not have good estimates of (OH + HONO)/NO_x and SO_3/SO_2 for the HSCT engine exit plane that are necessary to determine plume oxidation rates. Model predictions can give some insight into the problem, especially for the (OH + HONO)/NO_x ratio, which compares well with direct observations [Brown *et al.*, 1996a; Lukachko *et al.*, 1998]. Results show that the (OH + HONO)/NO_x expected from an HSCT-like engine are a factor of two higher than those observed in the Concorde exhaust [Brown *et al.*, 1996a]. For this scenario, oxidation via gas-phase reactions with OH (R2 and R3) will be small, roughly twice the Concorde example. The time scale of NO_x/NO_y partitioning in global assessment models is short relative to the time scale of atmospheric transport. Thus, putting the emitted NO_y into the global assessment models in the form of NO and NO_2 appears to be a good approximation.

In contrast with odd-hydrogen and odd-nitrogen compounds, there are no direct observational data of SO_3/SO_2 in aircraft engine exhaust that can be used to validate engine sulfur chemistry mechanisms, although SO_2 is clearly dominant at the exit plane [Wey *et al.*, 1998]. As a consequence, there is little experimental justification for using model results to predict SO_3/SO_2 in the proposed HSCT engine.

3.6 Particle Emissions and New Particle Formation

Aircraft engines directly emit soot particles and gas-phase aerosol precursors including H_2O, SO_2, SO_3, H_2SO_4, nitrogen and organic compounds, and charged molecules (chemi-ions). In the near- and far-field environment, these compounds dilute, react, and may condense to form solution droplets or surface coatings on preexisting particles. Contrail particles, composed mostly of condensed water ice, may form under appropriate atmospheric thermodynamic conditions [Appleman, 1953]. In the stratosphere at altitudes where supersonic aircraft are likely to cruise, water vapor mixing ratios are generally very low, the criteria for contrail formation are rarely met, and the likelihood of a significant stratospheric perturbation due to contrails is small [Miake-Lye *et al.*, 1993].

Aerosol particles found in aircraft exhaust plumes are believed to be composed of: (1) neutral H_2SO_4/H_2O droplets produced from the oxidation of SO_2 originating from fuel sulfur and subsequent binary nucleation of sulfuric acid and water vapor (see Section 3.5); (2) charged particles, also composed of H_2SO_4/H_2O, derived from growth on chemi-ions [Yu and Turco,

1997, 1998; Kärcher *et al.*, 1998a]; and (3) soot particles resulting from the incomplete combustion of fuel hydrocarbons in low-oxygen regions of the combustor [Smith and Chughtai, 1993; Fabian and Kärcher, 1997]. A schematic diagram illustrates the production and modification of these aerosol types in aircraft exhaust plumes in the absence of contrails (Figure 3-2). In addition, organic compounds, including alkenes and aldehdydes, have been postulated to condense to form particles in the absence of significant fuel S [Kärcher *et al.*, 1998a], and HNO_3 may condense at temperatures <200 K to form ternary solution droplets with H_2SO_4 and H_2O [Carslaw *et al.*, 1994; Kärcher, 1996].

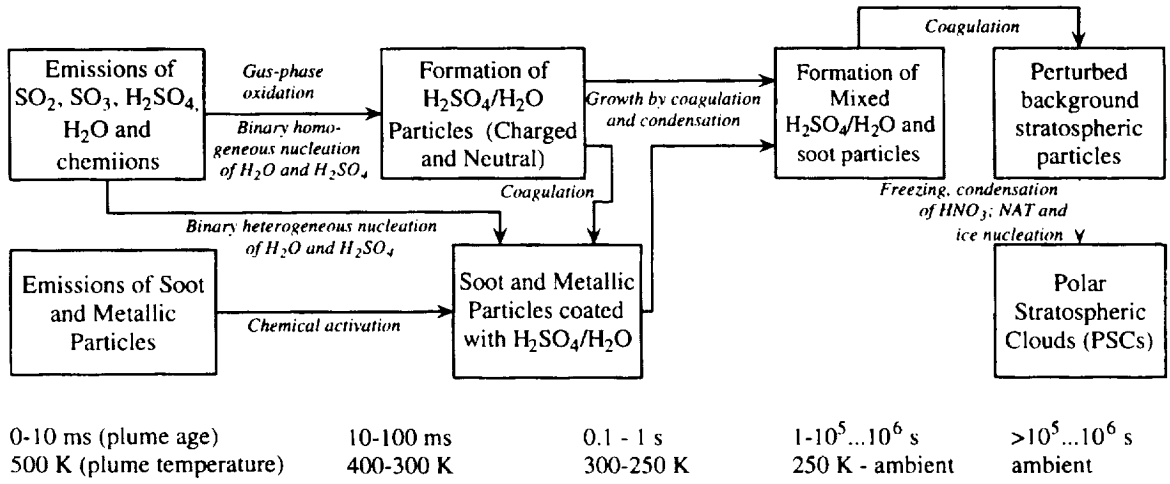

Figure 3-2. Schematic diagram showing the evolution of aerosols in an aircraft exhaust plume and wake in the absence of a visible ice contrail [adapted from Fabian and Kärcher, 1997].

3.6.1 Soot Particles

Aircraft-produced particles that are nonvolatile at temperatures exceeding 150°C are often presumed to be soot. Current understanding based on laboratory studies of soot and soot analogues suggests that heterogeneous reactions on soot particles are unlikely to significantly affect stratospheric gas-phase chemistry (Section 2.4.5). Soot particles behind aircraft in flight have been measured using a number of techniques (e.g., Pueschel *et al.* [1998]; Hagen *et al.* [1998]; Petzold and Schröder [1998]; Anderson *et al.* [1998a, b]; Pitchford *et al.* [1991]; Kärcher *et al.* [1998b]). For all techniques, estimates of the mass EI are complicated by the chain aggregate nature of many soot particles. Measurements of soot particle number and mass EIs vary widely, but generally fall in the range of 10^{13}–10^{16} kg_{fuel}^{-1} and 10^{-4}–10^{0} $g_{soot}kg_{fuel}^{-1}$, respectively. Soot EIs do not appear to vary with fuel sulfur content (FSC).

3.6.2 Sulfate Particles

Sulfur in the exhaust of a future fleet of supersonic aircraft will increase the surface area of the aerosol in the lower stratosphere. This increase is greater when sulfate particles are produced in

the plume than if the fuel S were emitted as SO_2 and allowed to slowly oxidize and condense on the background aerosol [Fahey *et al.*, 1995a; Weisenstein *et al.*, 1996; Danilin *et al.*, 1997; Kärcher and Meilinger, 1998]. For example, for efficiencies of in-plume conversion of fuel S to particulate S (H_2SO_4) of 0%, 10%, 50%, and 100%, the modeled increase in background stratospheric surface area concentration is 30%, 40%, 80%, and 110%, respectively (Section 4.4.3.5). Because of coagulation, this surface area enhancement due to small sulfate particles is relatively insensitive to the number of particles produced in the plume per kg of fuel burned (that is, to the particle number EI) or to the rate of plume dilution [Turco and Yu, 1997; Danilin *et al.*, 1997; Kärcher and Meilinger, 1998]. Thus, the most important factors in considering the effects of the future HSCT fleet on the stratospheric sulfate aerosol are the average fleet fuel S content and the value of η, here defined as the efficiency of conversion, in the engine and near and far field, of fuel S to S in the form of $SO_{3(g)}$ and $H_2SO_{4(g,l)}$. SO_3 is believed to react quickly via R5 to produce H_2SO_4.

The value of η is believed to be determined largely by S oxidation mechanisms within the combustor, turbine, and exhaust nozzle. Models of chemistry and flow with aircraft engine turbines suggest that the fraction of total SO_2 oxidized to SO_3 is limited by the availability of atomic oxygen [Brown *et al.*, 1996b; Lukachko *et al.*, 1998], and should decrease with increasing FSC. Because the in-plume oxidation of SO_2 by OH is small and there is no other known significant oxidation pathway for H_2SO_4 formation, η should decrease with increasing FSC.

Observations taken during SUbsonic aircraft: Contrail and Cloud Effects Special Study (SUCCESS) in subsonic aircraft plumes do not show a systematic decrease in η with increasing FSC as predicted by Brown *et al.* [1996b] and reported in a laboratory study [Durlak, 1997]. Instead, the SUCCESS data show a statistically significant *increase* in η as FSC increased from 72 parts per million by mass (ppmm) to 676 ppmm [Miake-Lye *et al.*, 1998] in measurements taken following the evaporation of transient contrails. Other, simultaneous particle measurements from SUCCESS produce values of η that do not vary consistently with FSC (Table 3-3), although any such trends would be within the stated measurement precision. These estimates of η are likely lower limits due to the presence of contrails during the measurement period. (Contrails reduce the concentration of sub-20 nm aerosol particles [Kärcher *et al.*, 1998a].) In direct contrast, measurements of particle emissions from the ATTAS research aircraft during the SULFUR series of airborne experiments, coordinated by the German agency, the Deutsches Zentrum für Luft- und Raumfahrt (DLR), focused on understanding the influence of fuel sulfur content on subsonic aircraft emissions (SULFUR-5), coupled with detailed modeling of particle nucleation and growth processes [Kärcher *et al.*, 1998a; Schröder *et al.*, 1998], indicate *decreasing* η with increasing FSC, and values of η near 2% for high levels of FSC.

Some of the above variability in experimentally derived estimations of η is likely due to the differences in the engine type and operating parameters, the actual sulfur content of the fuel, size ranges measured, sampling frequency, the accuracy of the techniques and the presence or absence of contrails. Additionally, sampling losses and other uncertainties associated with particle size distribution measurements from aircraft, which often are not evaluated or reported, may contribute to the observed variability. Despite these experimental variabilities, there is clear evidence from SUCCESS- and the SULFUR-5-related flights that the emissions of volatile particles larger than about 3 nm diameter are strongly linked to FSC (Figure 3-3; Anderson *et al.* [1998a, b]; Kärcher *et al.* [1998b]). It should be noted that, despite this evident correlation between FSC and volatile

particle number EI, the complete composition of these particles has not yet been determined by direct measurement. While H_2SO_4 has been detected in both the gas and condensed phase [Miake Lye *et al.*, 1998; Arnold *et al.*, 1998; Curtius *et al.*, 1998], a significant organic component to the particles cannot be excluded [Kärcher *et al.*, 1998b].

Table 3-3. Measurements of volatile particle number EI and fraction of fuel S converted to S(VI), η, measured in the exhaust of aircraft in flight in the absence of contrails. Volatile particles are presumed to be H_2SO_4/H_2O. Arranged by increasing FSC, if known.

Number EI(/kg_{fuel})	η, fraction of fuel S converted to S(VI)	Technique	Aircraft	Engines	Flight Conditions	Fuel S Content (ppmm)	Reference
$8(\pm3)\times10^{16}$		CNC	MD80-2		cruise	unknown	Anderson *et al.* [1998]
$1.6\pm0.2\times10^{15}$			ATTAS			unknown	Petzold and Schröder [1998]
$5\text{-}20\times10^{15}$	0.55	CNC/ Model	ATTAS		varied	20	Schröder *et al.* [1998] Kärcher *et al.* [1998b]
$\sim2\times10^{15}$	>0.08 (±0.03)	CNC	NASA 757	RB211	varied	72	Miake-Lye *et al.* [1998]
	0.06 (0.0-0.34)	CIMS	NASA 757	RB211	varied	72	Miake-Lye *et al.* [1998]
	0.37	impactor/ electron microscopy	NASA 757	RB211	varied	72	Pueschel *et al.* [1998]
$2.1(\pm0.3)\times10^{14}$	.11	DMA	NASA 757	RB211	varied	72	Hagen *et al.* [1998]
$1.7\text{-}6.5\times10^{17}$	>0.12	CNC	Concorde	Olympus 593	supersonic cruise	230	Fahey *et al.* [1995a]
$\sim8\times10^{16}$	>0.15 (±0.07)	CNC	NASA 757	RB211	varied	676	Miake-Lye *et al.* [1998]
	0.31(0.16-0.52)	CIMS	NASA 757	RB211	varied	676	Miake-Lye *et al.* [1998]
$2.5(\pm0.4)\times10^{15}$	.022	DMA	NASA 757	RB211	varied	676	Hagen *et al.* [1998]
	0.10-0.26	impactor/ electron microscopy	NASA 757	RB211	varied	676	Pueschel *et al.* [1998]
$1.0(\pm0.3)\times10^{17}$		CNC	NASA DC-8	CFM56-2-C1	slow cruise	700	Anderson *et al.* [1998]
$1.3(\pm0.4)\times10^{17}$		CNC	NASA 737			800	Anderson *et al.* [1998]
$\sim1\text{-}2\times10^{17}$	0.018	CNC	ATTAS		varied	2700	Schröder *et al.* [1998] Kärcher *et al.* [1998a]

It is difficult to reconcile the observations of high concentrations newly formed, volatile particles with diameters >3 nm within 50 m of the exhaust plane of an aircraft in flight with classical binary homogeneous nucleation theory without resorting to large values of η [Yu and Turco, 1997; Kärcher and Fahey, 1997] that conflict with understanding of engine chemistry and with ground-based measurements of SO_x emissions [Wey *et al.*, 1998]. Recently, Yu and Turco [1997, 1998] investigated the role of ions produced by chemi-ionization during combustion in aircraft engines. The chemi-ions are believed to preferentially agglomerate, leading to charged particle embryos. Subsequent coagulation and condensational growth is enhanced by the electric charge. Incorporating these chemi-ion interactions in numerical models of particle nucleation and growth in

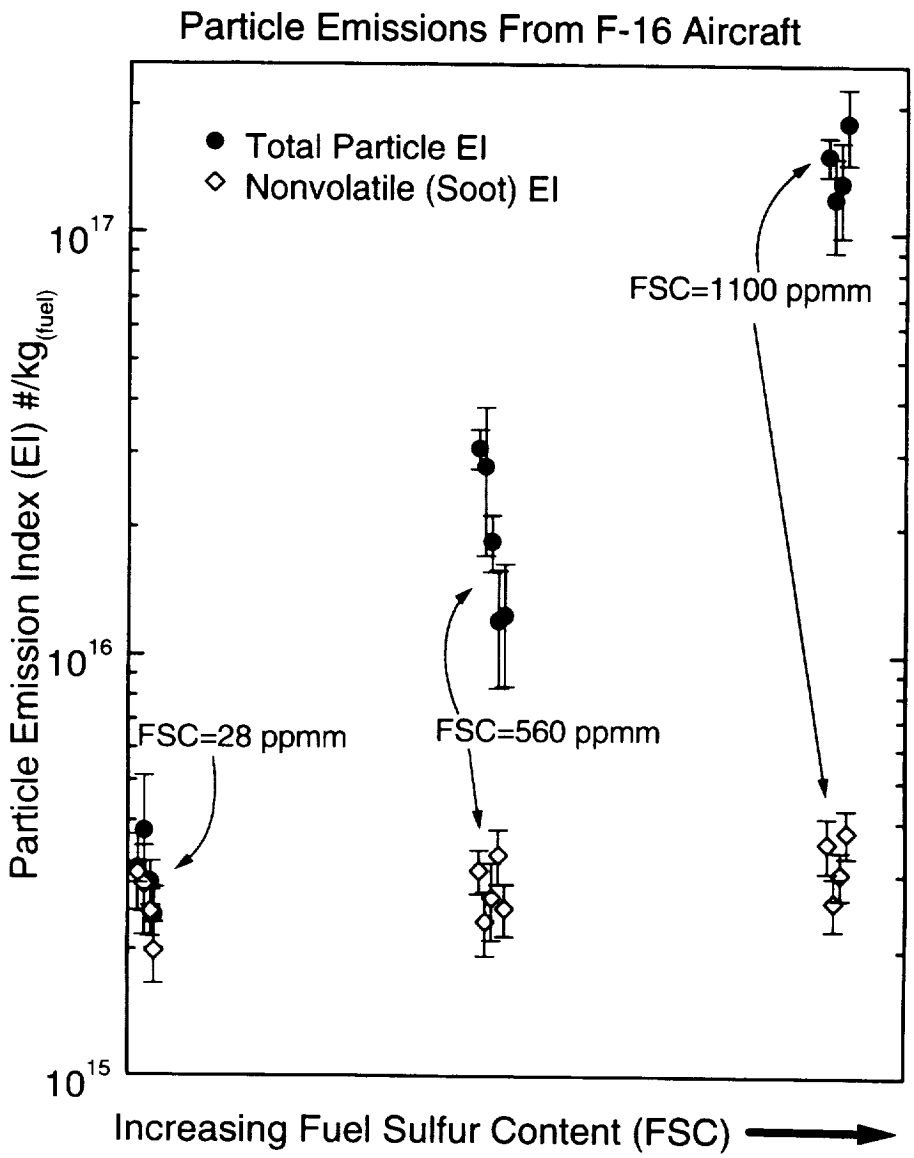

Figure 3-3. Emission indices for all particles (solid symbols) and nonvolatile particles (open symbols) larger than about 3 nm measured behind F-16 aircraft using differing fuel sulfur contents. The error bars indicate the 1-σ variability in the data. The EI of nonvolatile (presumably soot) particles did not change significantly with varying FSC, while the volatile particle EI was clearly linked to FSC. Figure courtesy of B. Anderson [1999].

aircraft plumes, produced substantially better agreement with observations of particle concentration and size than when such interactions were ignored [Kärcher *et al.*, 1998a, b; Yu *et al.*, 1998].

Experimental studies [Arnold *et al.*, 1998; Frenzel and Arnold, 1994] confirm that sulfuric acid and nitric acid-based chemi-ions occur in aircraft engine exhaust and provide lower limits for their concentrations. Higher chemi-ion concentrations than reported, however, are required to

successfully simulate particle observations behind flying aircraft [Yu and Turco, 1998]. Kärcher *et al.* [1998a] suggest that, even in the complete absence of fuel S compounds or soot formation, some small particles would likely form from chemi-ion agglomeration and subsequent condensation of nitrogen-containing and organic compounds.

The inclusion of chemi-ion processes significantly improves the comparison between model calculations and observations of particle size distribution and growth in the wake of the ATTAS aircraft. However, a mechanistic understanding of the factors controlling the formation and partitioning of SO_x that fully accounts for observations behind various aircraft engines—from modern high-bypass turbofans and military engines to the older technology ATTAS engines and the unique Olympus engines on the Concorde—has not been reached. Measurements of chemi-ion, H_2SO_4, and SO_3 emissions provide only lower concentration limits, and are very sparse. The mass EI of particles directly produced by aircraft and formed in the plume has not been determined with adequate accuracy and precision to constrain the sulfur budget, and the bulk composition of the formed particles has not been quantitatively determined. As a consequence of these unknowns, significant uncertainties exist in extrapolating particle and SO_x emissions to the future aircraft fleet.

3.6.3 Assessing Particle Emissions from HSCTs

A major uncertainty in predicting the effect of the proposed HSCT fleet on stratosphere chemistry is the lack of understanding of particle emissions and in-plume production from future engines. As noted above, the conversion of fuel S to H_2SO_4 and subsequent formation of small, volatile particles in the plume is not fully understood, even for current aircraft. Coupled flow-chemistry models of S oxidation in aircraft turbines indicate that this process is highly dependent on the details of the flow, thermodynamics, and chemistry over very small scales. While chemi-ions appear to be important for the nucleation and growth of volatile particles in aircraft engine exhaust, there are very few measurements of chemi-ion concentrations and speciation, and their presence is not incorporated into current engine chemistry models. Modification of particle properties over the time scales of mixing of the plume to the global environment has not been investigated thoroughly. Finally, soot emissions for the HSCT are not known, leading to uncertainties in the assessment of heterogeneous chemistry on stratospheric soot. In the absence of a fundamental understanding of the processes leading to aerosol formation for the HSCT fleet, particle emissions are considered parametrically in this assessment (Section 4.4.3.5). The value of η is parameterized to be 0%, 10%, 50%, and 100% in the assessment models. Of these values, 10% is most consistent with the best characterized estimates of η from current aircraft.

3.7 Scenarios

3.7.1 Overview

To evaluate the effects of supersonic aircraft, it is necessary to project where and how the aircraft will fly. This calculation consists of several parts:

- Projection of total air traffic demand for different city-pairs;
- For a given HSCT fleet size, calculation of the market capture by the HSCT for each city-pair;

- Projection of the HSCT performance and emission characteristics;

- Calculation of the fuel use and emissions onto a 3-D (latitude x longitude x altitude) grid for the projected HSCT fleet size; and

- Projection of the fuel use and emissions by the subsonic fleet both with and without the HSCT fleet.

Since detailed industry forecasts do not extend more than about 20 years into the future, the year 2015 has been used for the detailed projections of air traffic in order to explicitly account for changes in subsonic technology and displacement of subsonic air traffic by the HSCTs. Although 2015 is too early to see fleets of 500 and 1000 HSCTs, earlier 2-D model calculations have shown that the calculated HSCT ozone impact is not very sensitive to the underlying subsonic fleet emissions.

The methodology for calculating both the subsonic and HSCT emission scenarios has been described in detail elsewhere. Detailed calculations for both scheduled (listed in the Official Airline Guide) [Baughcum *et al.*, 1996] and unscheduled air traffic (including military, charter, general aviation, and former USSR/China) [Metwally, 1995; Mortlock and Van Alstyne, 1998] have been made for 1992. Projections of scheduled subsonic air traffic (projected from traffic currently listed in the Official Airline Guide) have been reported and updated several times [Baughcum *et al.*, 1994; Baughcum and Henderson, 1995; Baughcum *et al.*, 1998]. Projections of emissions from unscheduled air traffic are also available [Landau *et al.*, 1994; Mortlock and Van Alstyne, 1998].

Projected scenarios for HSCTs have been updated as more sophisticated market projections were made and as the baseline technology airplane changed over time. [Baughcum *et al.*, 1994; Baughcum and Henderson, 1995; Metwally, 1996; Baughcum and Henderson, 1998].

The base HSCT scenario for this assessment is described in Baughcum and Henderson [1998] and is based on the NASA Technology Concept Airplane (TCA) HSCT which is envisioned to be a Mach 2.4 300-passenger 5000 nautical mile range aircraft. The updated scenarios for scheduled air traffic in 2015, both with [Baughcum and Henderson, 1998] and without HSCTs [Baughcum, *et al.*, 1998], have been used in conjunction with the most recent updates for unscheduled air traffic [Mortlock and Van Alstyne, 1998]. These scenarios are provided on a 1° latitude by 1° longitude by 1 km pressure altitude grid and are then interpolated onto the computational grids of the different assessment models.

The total global fuel use and emissions from these scenarios are summarized in Table 3-4 for fleets of 500 and 1000 high utilization HSCTs. The fleet sizes described here refer to the number of aircraft flying. The number of HSCTs produced would be larger because of the need for maintenance time, spares, and less than optimum utilization of the network. The introduction of HSCTs leads to a net increase in fuel use since HSCTs are not as efficient as modern subsonic aircraft.

Table 3-4. Total global fuel use and emissions projected for 2015 from all aviation sources.

	Fuel (Tg/year)	NO_x (Tg/year)	HC (Tg/year)	CO (Tg/year)
2015 All Subsonic Fleet	305.4	4.08	0.33	2.26
2015 Fleet with 500 HSCTs	338.1	3.86	0.34	2.36
2015 Fleet with 1000 HSCTs	377.5	3.82	0.35	2.49

3.7.2 Geographical Distribution

The geographical distribution of fuel use in the 13- to 20-km altitude band is shown in Figure 3-4 for a fleet of 500 HSCTs. Because of its speed advantage over subsonic aircraft, the HSCT is expected to be used primarily on long intercontinental routes where that advantage can best be utilized. Due to the sonic boom, which trails below the aircraft, the prime HSCT routes have a large portion of the flight path over water with all supersonic flight expected to be over water.

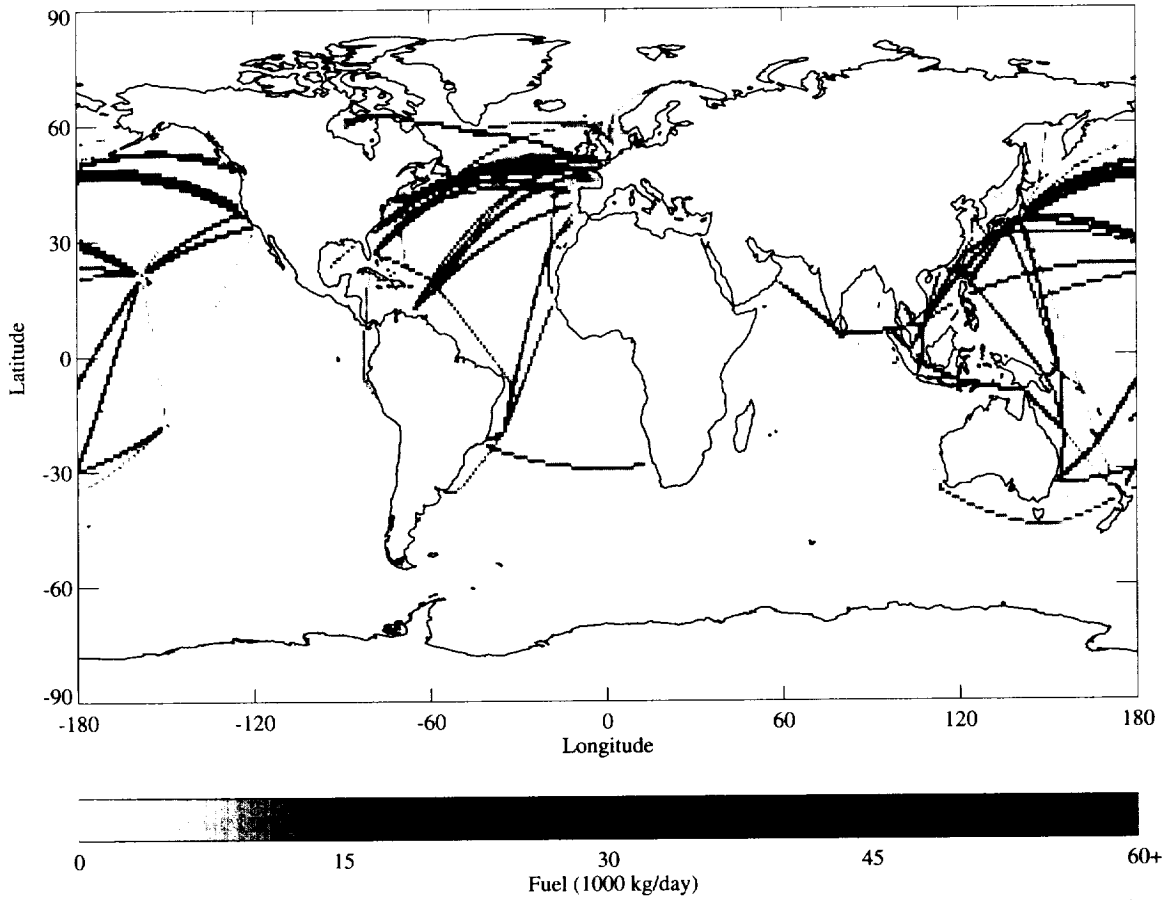

Figure 3-4. Projected HSCT fuel use distribution in the 13- to 20-km altitude band for a fleet of 500 HSCTs.

These conditions combine to put the majority of HSCT routes at northern mid-latitudes over the North Atlantic and North Pacific. Figure 3-5 shows the distribution of NO_x emissions above 13 km as a function of latitude band for a fleet of 500 HSCTs. The majority of stratospheric emissions are expected to occur at northern mid-latitudes. Only a small fraction of the emissions are expected to occur north of 60°N latitude. The range limitations (5000 nautical miles) of the proposed aircraft and the expectation that it will only be allowed to operate supersonically over water result in very few flights in polar regions. Approximately 20% of the emissions are projected to occur in the tropics between 20°S and 20°N latitude. Approximately 15% of the NO_x emissions above 13 km are predicted to occur in the SH.

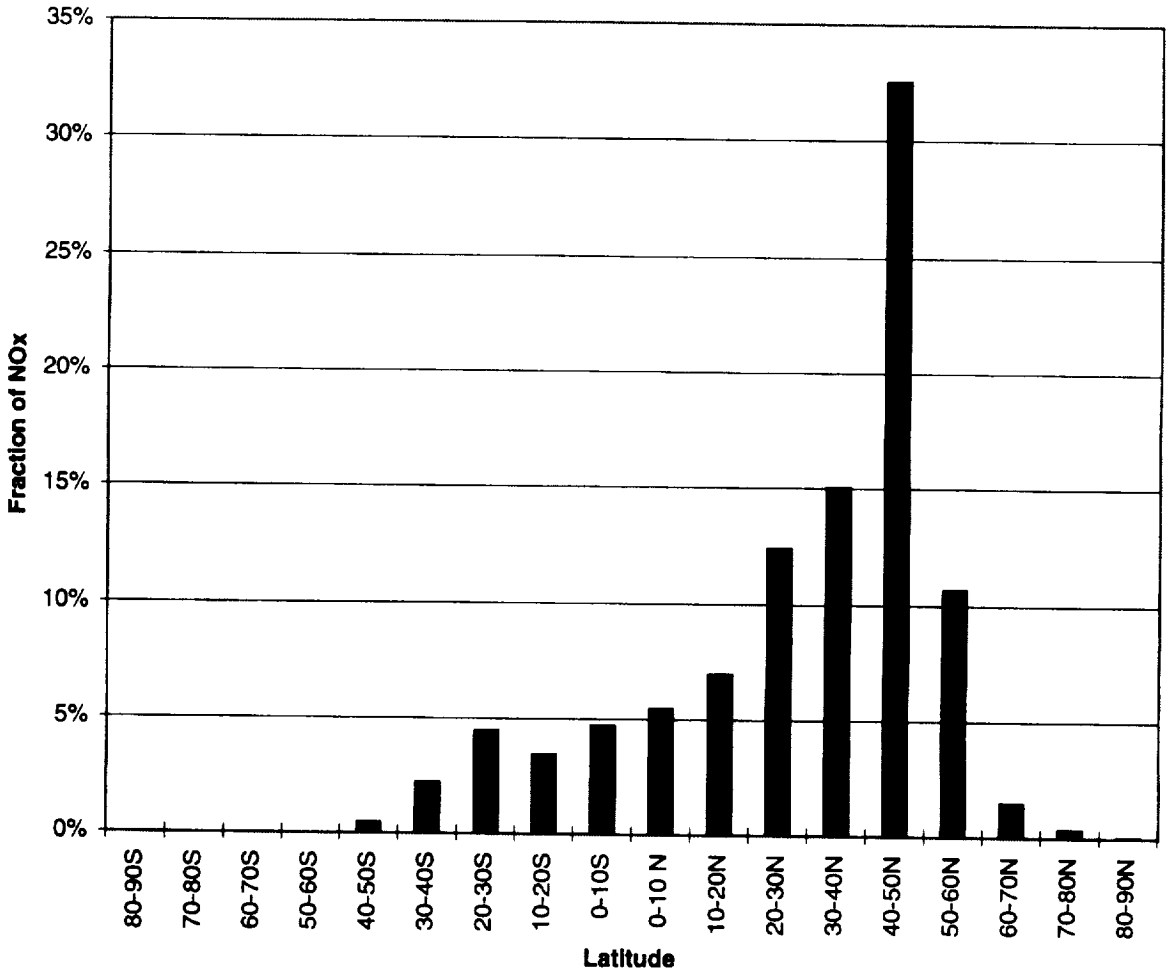

Figure 3-5. Fraction of NO_x emitted above 13 km as a function of latitude.

3.7.3 Altitude Distribution

The NASA TCA is calculated to cruise supersonically in the 17- to 20-km altitude range. Figure 3-6 shows a comparison of the altitude distribution for the TCA aircraft and the HSCT model (Reference H) used in the 1995 AESA assessment. The TCA cruises ~1 km lower than the older model because of changes in the aircraft design and weight. The supersonic cruise altitude is a sensitive function of the planform, speed, weight, and design of the aircraft and is expected to continue to change as the design matures.

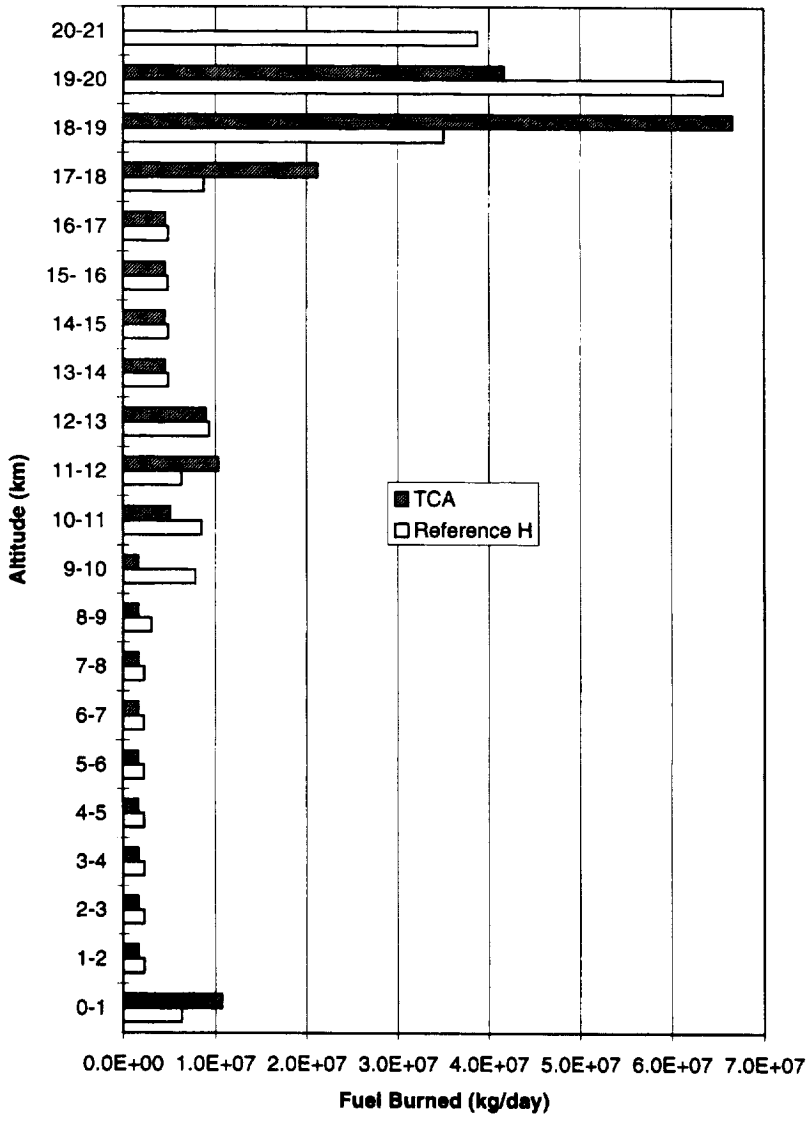

Figure 3-6. Fuel use by an HSCT fleet as a function of altitude, comparing the current scenarios using the NASA TCA aircraft with the HSCT design (Reference H) used in the 1995 AESA assessment.

The altitude distribution of NO_x emissions from the 2015 fleet, with and without the HSCT, is illustrated in Figure 3-7. The HSCT displaces some subsonic air traffic resulting in a net decrease of NO_x emissions in the 9- to 12-km altitude band and an increase in NO_x at 17- to 20-km altitude.

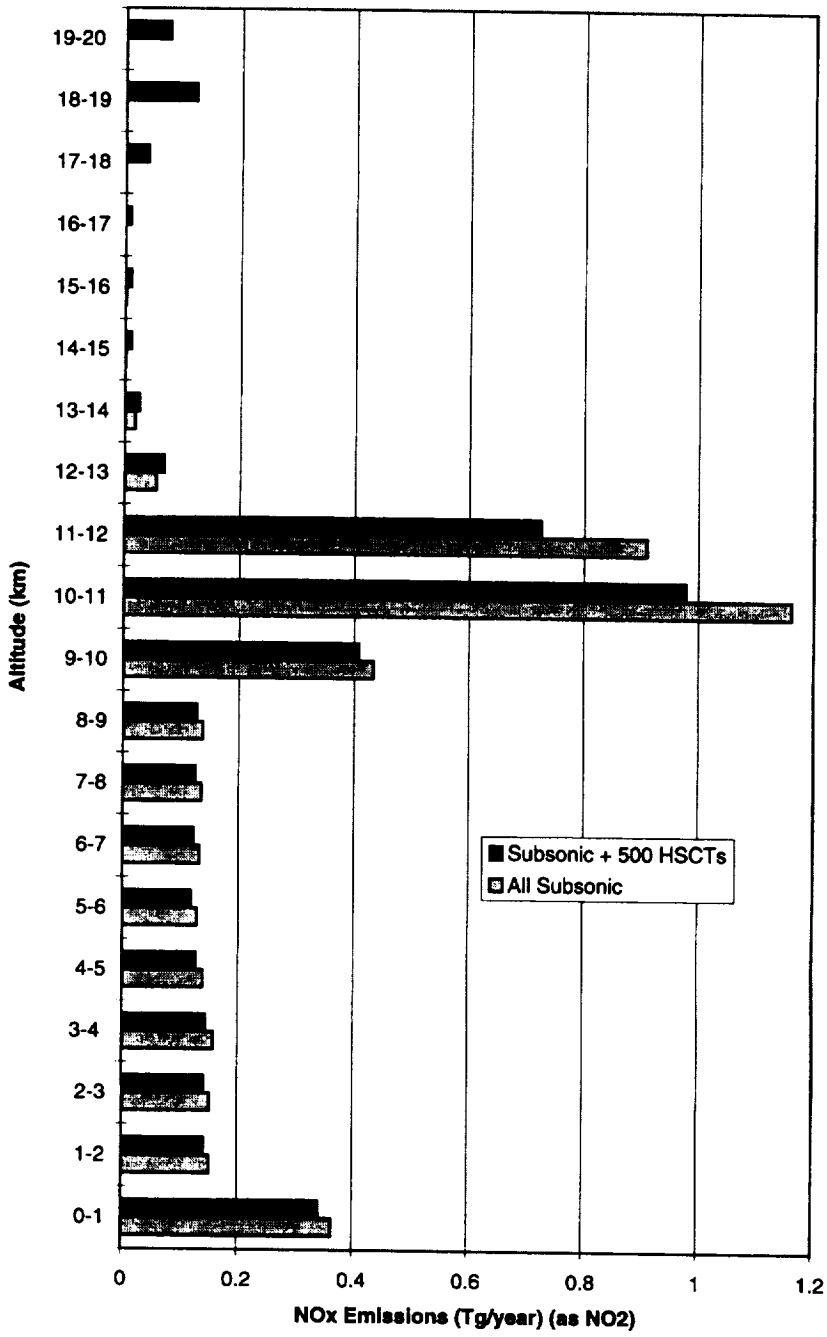

Figure 3-7. NO_x emissions as a function of altitude for fleets of HSCTs.

3.7.4 Emission Parametrics

Since the HSCT is still a conceptual airplane, the assessment can not simply evaluate a single point design, particularly since the results of the assessment may help guide the design to reduce its environmental impact. In addition, the design is evolving. It is not clear when the HSCT technology will be mature enough for viable commercial service and so the fleet sizes and technology levels are treated parametrically. This assessment has used the NASA TCA with $EI_{NO_x} = 5$ as the baseline case and then explored the design parameter space of EI_{NO_x}, flight altitude, fleet size, and sulfate aerosol production. In addition, parametric studies have been done to evaluate the effect of changes in the future atmosphere (chlorine loading, background sulfate aerosol level, stratospheric temperature) on the calculated HSCT ozone impact. The detailed summary of the parametric cases is shown in Table 4-2 to 4-4 along with the results from the model calculations.

3.8 Summary Points

- For current subsonic and supersonic aircraft, there is reasonable agreement between plume models and observations of gas-phase chemical and dispersion processes. The HO_x and NO_x chemistry in these models is generally consistent with the limited observations available. Major uncertainties include lack of understanding of gas-phase sulfur oxidation mechanisms and difficulty in extrapolating current understanding of gas-phase processes to the HSCT engines.

- The magnitudes and mechanisms of particle emissions from the future supersonic fleet are poorly understood.

  - Current supersonic and subsonic aircraft produce large numbers of sub-20 nm diameter, volatile (presumably H_2SO_4) particles. If the proposed future HSCT fleet emits similar quantities of particles, the stratospheric particle surface area is predicted to increase as much as 40% above background levels, assuming 10% conversion to SO_3 in the engine. The fraction η of fuel S converted to SO_3 in the engine and subsequently to sulfate particles in the wake environment controls, in part, the predicted surface area increase for the HSCT.

  - The determination of η from measurements in the wakes of existing aircraft is difficult and results are disparate. Recent estimates of η from engine test stand measurements and from coupled in-flight measurements and models give values on the order of 5 to 10%. Because we do not have a mechanistic understanding of the factors controlling η, we cannot predict its value for HSCTs, and it has been treated parametrically in this assessment.

  - Chemi-ions have been measured in aircraft exhaust and are believed to be important in particle nucleation and growth. Numerical models of particle formation and growth in aircraft plumes require the presence of chemi-ions to successfully simulate observations of particle properties. Measurements of chemi-ions from current aircraft engines are very limited. We have no estimates of chemi-ion production by HSCTs.

  - Soot emissions from current aircraft engines are highly variable, but are roughly two orders of magnitude lower in number EI than are volatile particles. Based on combustor rig

measurements, soot emissions from the LPP combustor concept for the HSCT are expected to be significantly lower than current engines.

- Emission scenarios of future HSCT fleets have been developed using the NASA TCA and are used as the baseline for modeling calculations of ozone impact. A significant change from the baseline aircraft concept used in the 1995 Assessment is a reduction in expected flight altitude the TCA of ~1 km. To guide technology decisions and to evaluate uncertainties, the modeling studies have evaluated the effect of fleet size, NO_x emission index at supersonic cruise, flight altitude, and η on the predicted ozone impact.

4. MODELING

4.1 Background and Introduction

The atmospheric processes and aeronautical emissions described in Chapters 2 and 3 are incorporated into numerical models that predict the impact of HSCTs for different operational scenarios. This chapter presents a description of the models utilized in this assessment, their performance in comparison to observations, and the results of HSCT perturbation calculations.

The 1995 Scientific Assessment of Atmospheric Effects of Stratospheric Aircraft [Stolarski *et al.*, 1995] utilized 2-D models exclusively in arriving at predictions of HSCT impact. A major step forward in that assessment was the development of a benchmark for photolysis calculations, which led to improvements in the models' calculations of photolysis and a dramatic reduction in the spread of calculated rates. Similarly, the chemical solvers utilized in the assessment models were also tested, albeit only from the point of view of their performance in a box model. These tests were carried out by establishing both photolysis and chemical benchmarks to which all participating models were required to compare their results and document discrepancies. The photolysis benchmark was described in Stolarski *et al.* [1995]; the chemical benchmark is described in Appendix E. We have required again that participating models perform these benchmarks if they did not do so in 1995. Participating models agreed with benchmark results to within 10-20% at the worst (see Appendix E). Although the M&M II [Park *et al.*, 1999] exercise has examined a series of tests of model transport, no transport benchmarks have been developed for this assessment.

Several potentially important processes were recognized in 1995, such as accounting for aircraft perturbations of the sulfate aerosol layer and the potential importance of including PSC parameterizations in the assessment models. At the same time, preliminary comparisons of model results with available stratospheric measurements indicated deficiencies in the models' representation of basic processes important for assessment of HSCT impacts. The following recommendations were highlighted: (a) expansion and utilization of available atmospheric observations to reduce uncertainties; (b) systematic development of 3-D models to test transport formulations and limitations of 2-D models; (c) inclusion of aircraft particle exhaust and interaction with background particles; and (d) characterization of the composition and evolution of aircraft exhaust aerosols, and composition and microphysics of PSCs.

The assessment effort summarized here has addressed these concerns and other issues that have arisen since the last assessment. As in previous efforts, a multi-model approach has been adopted to indicate the variability in predictions expected from different assumptions about the chemical and dynamical processes discussed in Chapter 2, as well as the approximations adopted in the specific numerical algorithms. Five 2-D models and three 3-D models have participated in this assessment. A list of participating models, institutions, and scientists is given in Table 4-1. All of these models have complied satisfactorily with the photolysis and photochemistry benchmark requirements. These models are briefly discussed in Section 4.2, and further details given in Appendices F and G. The performance of these models against several atmospheric measurements and other criteria is described in Section 4.3. Calculations have been carried out for a number of different scenarios, summarized in Section 4.4. These scenarios are chosen to reflect existing uncertainties in

operational scenarios, emission characteristics, atmospheric processes, and the state of the future atmosphere. The potential HSCT impact on climate is discussed in Section 4.5. Efforts at arriving at a "best estimate" of the impact of HSCTs, and discussion on future directions are given in Sections 4.6 and 4.7, respectively.

4.2 Description of Participating Models: Progress Since the NASA 1995 Stratospheric Assessment

This assessment effort has incorporated numerous model improvements that lead to a better representation of the atmosphere and reduce uncertainties in the results. These improvements include: (a) utilization of 3-D models in conjunction with 2-D models; (b) incorporation of sulfate particle production in the aircraft exhaust; (c) better representation of heterogeneous chemistry on cold sulfate aerosol and formation of polar stratospheric clouds (PSCs); and (d) parameterizations of planetary wave breaking, which result in better representation of the subtropical and polar barriers to transport. Finally, there has been a concerted effort, discussed in the next section, to systematically evaluate the model results with a broad set of observational data.

4.2.1 Utilization of Three-Dimensional Models

HSCT exhaust will be injected into a 3-D atmosphere. The models used in most stratospheric assessments are 2-D: they average over longitude. These models approximate effects that are inherently 3-D. An example is the use of a probability distribution for temperature at a given altitude, latitude, and time of year. The influence of longitudinal temperature variations on chemical reaction rates and particle formation is thus calculated via an approximation in 2-D. These and other processes can be explicitly represented in 3-D including:

a) A better representation of the wave-mean flow interaction. We would expect 3-D models to better represent mixing due to planetary wave breaking in the "surf zone" as well as across the subtropical and polar jets.

b) A better representation of chlorine activation by PSCs. Representation of air parcel motion between polar night and sunlight, and longitudinal variations in temperature, PSC concentrations and constituent densities are explicitly simulated.

c) A more realistic representation of isentropic stratosphere-troposphere exchange. Three-dimensional models can represent filamentary structures created by breaking Rossby waves and non-diffusive, asymmetric transport across subtropical barriers.

Three-dimensional models using assimilated winds provide a more physically based treatment of the longitudinal and daily circulation changes, and their results are more directly comparable to observations.

Thus, 3-D models should provide a better representation of tracer distribution in the lower stratosphere. Preliminary comparisons indicate that some 3-D models do indeed have a fairly realistic representation of lower stratospheric processes. For example, the MACCM2 [Boville, 1995] model provides realistic simulations of many features of long-lived tracer distributions in the

lower stratosphere [Waugh *et al.*, 1997]. On the other hand, the MACCM2 SH temperatures are too low, a discrepancy corrected in the version of MACCM2 used by GMI by incorporating a larger gravity-wave breaking. Thus, there are still limitations in 3-D models that preclude us from establishing that the tracer distributions from a 3-D model are necessarily more realistic than from a 2-D model. These limitations include, for example, insufficient resolution in the horizontal or vertical, or parameterization of unresolved gravity waves in GCMs. Three-dimensional models are not, at this point, guaranteed to have realistic residual circulations (see discussion in Section 2.3.3). As discussed below, this is particularly evident when we compare tracer distributions calculated from 3-D circulations to observations.

Three-dimensional assessment models at present derive their circulation from GCMs. GCMs must solve the additional problem of generating a representative climate (which is specified from observations in most 2-D models). This presents additional problems for 3-D assessment models, some of which have not yet been solved, but will eventually provide a more accurate assessment of HSCT perturbations including possible chemical-dynamical feedbacks.

Efforts at improving 3-D dynamics have been mostly guided by comparisons to climate variables. We anticipate further improvements in 3-D models from continued comparisons of tracer distribution. We subject the 3-D models to the same tests as the 2-D models. As discussed below, some of the 3-D models utilized in this assessment do give better results than 2-D models, for example, in lower-stratospheric ozone, but are still in poor agreement with observations of other crucial lower-stratospheric constituents, such as NO_y. Incorporation of 3-D model results in this assessment has started to answer an outstanding question from previous assessments; whether a better representation of zonally asymmetric processes would significantly change the conclusions of 2-D assessments.

This assessment includes results from three 3-D models. The model from the NASA/Langley Research Center (LaRC 3-D) and University of Cambridge (SLIMCAT 3-D) are described in Appendix F. Model results from the GMI 3-D model, described in Appendix G, are also given.

The goal of GMI has been to build an assessment-quality model that can both perform multi-year calculations and compare results from different dynamical and chemical formulations. The basic philosophy of the GMI has been discussed in Friedl *et al.* [1997]. In summary, an assessment-quality 3-D model has been integrated, incorporating three different sets of winds into a "core" model. The "core" model includes: (a) a common advection algorithm and transport shell; (b) efficient and accurate chemical solvers; and (c) a PSC parameterization. The winds have been provided from the NCAR MACCM2, the Goddard Institute for Space Studies (GISS) GCM, and the NASA/Goddard Data Assimilation Office (DAO). The integration has allowed an estimate of model variability induced by the choice of advection algorithms and by the choice of winds (see Figure 4-1). Examination of this figure indicates that differences in horizontal resolution (e.g., compare GMI/DAO with GSFC-3D) can introduce variations of order 15% in the calculated peak exhaust accumulation. Results using a Second-Order Moments (SOM) advection algorithm are also consistent with those using the GMI Lin and Rood [1996] scheme. On the other hand, there is a discrepancy of almost a factor of two between the accumulations calculated using a semi-Lagrangian formulation and those using Lin and Rood. This comparison indicates that the semi-

Lagrangian scheme is not appropriate for the assessment of the impact of localized aircraft emissions.

The GMI has evaluated not only the sensitivity to model-model differences, but also the performance of different model components when compared to observations. The GMI team has devised a methodology for grading the different wind fields on their performance in reproducing meteorological parameters and measured distribution of trace species. This effort was in parallel to the M&M II effort, and some of the tests overlapped. A preliminary grading was used to choose the wind fields that agreed best with the measurements. The perturbation calculations used these winds. It must be stressed, however, that no set of winds was able to reproduce all the characteristics of the above quantities observed in the measurements. Details of this grading are described in Appendix G. Based on these tests, the MACCM2 winds were the primary set used by GMI for this assessment report.

The GMI model includes a computationally efficient parameterization of PSCs which, although not incorporating a complete microphysical representation, responds to changes in HNO_3 and H_2O. A realistic evaluation of the impact of PSCs in this model, however, is precluded by the fact that the NH temperatures in the adopted meteorological field are too warm (see Appendix G). Fast chemical solvers have also been incorporated which allow multi-year calculations in a parallel super-computer. These chemical mechanisms perform well when compared to a benchmark calculation. Incorporation of these chemical solvers and comparison to the benchmark has thus allowed an expansion of previous chemical solver evaluations [Stolarski *et al.*, 1995, Appendix A], insofar as the comparison has been carried for all latitudes, altitudes, and seasons in the stratosphere. Incorporation of these efficient numerical solvers and polar chemistry approximations in a parallel computer architecture allowed carrying out the necessary multi-year simulations for both baseline and HSCT-perturbed atmospheres in 3-D.

4.2.2 Inclusion of Sulfate Microphysics

A very significant change in the HSCT scenario calculations in this report relative to the 1995 assessment is the inclusion of sulfur emission by aircraft (Section 3.6). Sulfur emission was recognized as an issue following the 1994 ER-2 campaign in which large numbers of volatile particles were observed in the wake of a Concorde aircraft in supersonic flight [Fahey *et al.*, 1995a]. A sensitivity study with the Atmospheric and Environmental Research, Inc. (AER) 2-D sulfate aerosol model showed that large (factor of two) perturbations to the background aerosol surface area would be expected for an HSCT fleet with emission index of sulfur dioxide (EI_{SO_2}) = 0.4 if most of the emitted sulfur were converted to particles in the aircraft plume [Weisenstein *et al.*, 1996]. A further study provided similar results from three additional 2-D microphysical models [Weisenstein *et al.*, 1998].

Because a majority of the models participating in this assessment do not include sulfate microphysics and thus are not able to calculate changes in sulfate aerosol surface area density (SAD), this parameter has been specified as a model input for all participating models. Details are discussed in Section 4.4.1.

4.2.3 Improved Parameterization for Heterogeneous Rates, Polar Stratospheric Clouds, and Cold Sulfate Aerosols

The 1995 assessment report addressed the potential effects of heterogeneous reactions on PSCs by discussing the three published modeling studies of aircraft emission effects which included PSCs [Pitari *et al.*, 1993; Considine *et al.*, 1994; Tie, 1994]. These studies suggested that heterogeneous reactions on PSCs could be important, but also indicated that there were large uncertainties in the model parameterizations and hence results. This fact remains true today.

A large body of observations have pointed the way towards better parameterizations of heterogeneous reactions on PSCs, in particular, those involving supercooled sulfate aerosols at cold temperatures, when uptake of nitric acid and water leads to ternary solutions. The latest NASA/JPL [DeMore *et al.*, 1997] recommendations include detailed data for accommodation coefficients, reaction probabilities and solubilities of reactants. All participating models have incorporated these heterogeneous representations, although details of the specific treatment may vary from model to model (see Appendix F). Sufficient laboratory work has been carried out on the rates of these heterogeneous reactions that the major modeling uncertainties should be in the model's adopted temperature and aerosol composition, rather than on details of the surface reaction kinetics.

The impact of processes on cold sulfate aerosols and PSCs will also depend on the model's treatment of transport between the polar vortices and mid-latitudes. Model treatment of these processes has not been rigorously evaluated, particularly for the NH. Details of the transport processes involved are discussed in Section 2.3.5. We note that 3-D models explicitly calculate many of the above processes. This points to the need of continued development and utilization of 3-D models to provide a more realistic simulation of the atmosphere and to check the 2-D model approximations.

4.2.4 Incorporation of Planetary Wave Breaking Parameterization, and Simulation of Subtropical Barriers

Improvement in 2-D model spatial and temporal representation of wave-mean flow interactions has been substantial since the 1995 assessment. Planetary wave breaking provides an important mechanism for transport of chemical species. Two-dimensional models attempt to mimic this motion through a combination of wave-induced meridional circulation and horizontal diffusion. Establishing the diffusion coefficients to represent these planetary wave motions is an important component of 2-D models that can strongly influence their ability to accurately model profiles of long lived species and age of air in the stratosphere (Section 2.3). Most important, the 2-D circulations and diffusion coefficients aim at representing the subtropical and polar barriers to transport, which affect a model's ability to correctly simulate the transport of aircraft effluent into the tropical upwelling region and into the polar vortices. This has been accomplished to various degrees of success by a combination of ad-hoc prescription of eddy coefficients and adoption of first-principle parameterizations based on planetary wave breaking theory and observations (see Table F-3, Appendix F).

In each case, 2-D models simulate the large-scale mixing in the mid-latitude stratosphere (the so-called "surf zone") induced by wave breaking. Many of these models also simulate the observed barriers to transport in the tropics and polar region by minimizing the horizontal mixing across the polar vortex and between the mid-latitudes and the tropics (Section 2.3). By using these improved parameterizations, the present assessment models have an improved representation of atmospheric gradients and mixing across the subtropics and polar vortices.

4.3 Model Evaluation

A centerpiece of this assessment is the evaluation of model predictions in comparison to existing measurements. This has been done primarily in conjunction with the M&M II exercise, whose details are given in a separate report [Park *et al.*, 1999]. The approach here is to: (a) identify a subset of the M&M II comparisons, as well as other model characteristics especially relevant to the HSCT assessment; (b) evaluate the performance of models in comparison with observations in a qualitative manner; (c) identify model(s) which deviate consistently relative to several of the criteria; and (d) utilize this information to constrain the probable range of predictions.

In contrast to the internal GMI exercise, no grades have been assigned in M&M II. It is difficult to ascertain exactly which are the most important parameters, and how to weigh the agreement or disagreement of specific models towards a final score. However, this exercise has identified specific comparisons that tend to better discriminate the model results. A prime example is the background NO_y concentrations in the lower stratosphere, as discussed below. We also use this comparison as a way to understand differences between models and point to future directions of model improvement.

4.3.1 Models and Measurement II Approach

Previously, ozone was the only chemical trace species for which there was long-term global coverage to derive a climatology. Given the interest in predicting perturbations to the column ozone, models concentrated on simulating the observed temporal and spatial distributions of ozone column abundance. However, using column ozone by itself as a guide to choose the best representations in a model is problematic since it is never clear whether a good ozone simulation in a particular model is achieved by having the correct combination of transport and chemistry. This makes it impossible to use the agreement between observed and calculated column ozone as the only criteria for having the correct transport.

The current approach in M&M II identifies a number of independent tests for chemistry and transport to be applied to each model. The model-simulated ozone is also compared to observed ozone. Having the independent tests provides a theoretical framework in which further adjustments could be made.

4.3.2 New Data Used for M&M II

Almost all the data sets that were used for M&M I [Prather and Remsberg, 1993] have been revised or replaced with better and more complete compilations. UARS data sets are the primary ones being used for the middle and upper stratosphere. We chose to use the 1992 data as the basis

for our comparison because it is the only full year for which there are UARS/CLAES data available. The CLAES data provide unique global coverage of N_2O, CH_4, HNO_3, and chlorine nitrate ($ClONO_2$). At the same time, the fact that the CLAES measurements were taken shortly after the Mount Pinatubo eruption complicates the analysis.

The M&M II exercise has also benefited from additional data from various ER-2 aircraft and OMS balloon campaigns. New data on SF_6 and CO_2 provide the necessary diagnostics for transport and mean age. In addition, the enhanced payload of the ER-2 has enabled simultaneous measurements of NO_x and NO_y allowing direct determination of the NO_x/NO_y ratio which is critical to accurately evaluating the chemical impact of HSCTs.

A climatology for ozone, consisting of monthly zonal mean column ozone and ozone profiles as a function of latitude were put together for M&M II. The column ozone climatology is based on ozone column data from 1988 to 1996 using Total Ozone Mapping Spectrometer (TOMS) on Nimbus-7, Meteor 3, and Earth Probe satellites. The ozone profile is based on ozone sonde data between 0 and 28 km and SAGE II data between 20 and 60 km. In the region where the two data sets overlap (20 to 30 km), a weighted average is used with a heavier weighting for the sonde data at lower altitudes and a heavier weighting for the SAGE II data at higher altitudes.

4.3.3 Requirements and Tests of Models

In this section, we identify characteristics of models that will determine their abilities to simulate a realistic response of ozone to perturbations in the lower stratosphere. Some of these characteristics, such as vertical resolution in the model and photochemical mechanisms included in the model, are easily identifiable as part of the model formulation. In other cases, the identification and testing of these characteristics are less direct. The spatial and seasonal distributions of certain tracers are affected by the chemistry and transport in the atmosphere. The observed distributions of these species can be used for comparison with model results. Although these tests are discussed in this section as separate tests according to the type of observations used, we stress that they are interrelated through common mechanisms in the models. Thus, changes in model treatment will affect the outcome of several tests in a related way. For this same reason, a quantitative weighing of these parameters is not possible because they are not independent and their interdependence is not fully understood.

4.3.3.1 Model Vertical Resolution in the Lower Stratosphere

The vertical resolution of assessment models is an important parameter for the evaluation of HSCT impact on ozone, both because of the limited vertical extent of HSCT emissions and because of the proximity of the emission region to the tropopause. The vertical resolution of the models used in this assessment is 1.2 km (AER 2-D); 1.5 km (Lawrence Livermore National Laboratory (LLNL) 2-D, GMI 3-D); 2 km (GSFC 2-D, State University of New York, Stony Brook (SUNY-SPB) 2-D, and Commonwealth Scientific and Industrial Research Organization (CSIRO) 2-D, (SLIMCAT 3-D); and 3 km (LaRC 3-D). A finer vertical resolution means that the model can define the tropopause more accurately (to the nearest 1.5 km rather than the nearest 3 km, for example). In addition, a coarser vertical resolution accelerates the effective vertical transport and mixing in the models, leading to a shorter residence time for HSCT exhaust. Experiments by the

AER 2-D model indicate that the calculated ozone depletion can be reduced by up to factors of 2 if the vertical resolution changes from 1.2 to 3.5 km, depending on the adopted numerical scheme for transport. It should also be noted that, in mapping emission scenarios (see Chapter 3) to a particular model grid, the profile of emissions being used by the model will be affected by both the vertical resolution and by the location of the grid centers. Models with low vertical resolution near the tropopause (i.e., greater than 2.0 km) are not used in this assessment to test the sensitivity to HSCT emissions at a cruise altitude lowered by 2 km (Section 4.4.3.6 below).

4.3.3.2 Tests of Chemistry

In situ observations of atmospheric trace species provide data for process studies of the partitioning of radical species over a range of conditions with different sulfate loading and solar illumination. A series of studies demonstrated that a box model run to diurnal steady-state, and constrained by observed values of sulfate surface area, temperature, NO_y, Cl_y, total odd bromine (Br_y), H_2O, ozone, overhead column ozone, and CH_4 can reproduce the observed partitioning of the radical species in a large number of cases [Park *et al.*, 1999]. This method has been used to provide confidence in model chemical mechanisms in the lower stratosphere using the data from Airborne Arctic Stratospheric Expedition II (AASE II), ASHOE/MAESA, SPADE, and POLARIS aircraft campaigns, and in the mid- to upper stratosphere using balloon data.

In the current test, reservoir gas concentrations are taken from the output of the assessment models to constrain the diurnal steady-state model. The radical concentrations calculated by the constrained box model are compared to the radical concentrations calculated in the assessment models. The calculations from the assessment models are in general within 10 to 15% of those produced by the constrained photostationary model. The largest discrepancies reflect approximations in the diurnal treatment of certain species, or poor representation of the troposphere. These are not considered, however, to be first-order uncertainties in the HSCT predictions, when compared to the larger issues surrounding dynamical processes (see below).

This consistency indicates the following: (a) the models are using accurate numerical solvers for the chemistry, and (b) insofar as the photochemical mechanisms used by the photostationary state approach reproduce the observed chemical partitioning (see Section 2.4), the chemical mechanisms in the models are appropriate to simulate atmospheric radical chemistry.

In interpreting the chemistry test, one should be aware of the following caveats. First, results of the photostationary model depend on the reaction rate constants used. With the current JPL-97 recommendation, some discrepancies between calculated results and observed results still exist. Most notable of these are the model ozone deficit above 40 km [Clancy *et al.*, 1987 and reference cited; Natarajan and Callis, 1991; Eluszkiewicz and Allen, 1993; Crutzen *et al.*, 1995; Dessler *et al.*, 1996b; Osterman *et al.*, 1997; Summers *et al.*, 1997] and the model underestimation of the NO_x/NO_y ratio in the summer lower extra-tropical stratosphere [Sen *et al.*, 1998, Gao *et al.*, 1999]. Second, the above procedure provides a valid test only for situations where the photostationary test is a valid assumption. In PSC regions, for example, it is well known that behavior of the radicals depends on the air-parcel trajectory in regions when the temperature is cold enough to trigger PSC formation. In those cases, results from the photostationary model are unrealistic. The chemistry

describing chlorine activation in PSCs has been tested by numerous process studies, particularly in the Antarctic region, but not in the context of a global model.

The chemical mechanisms and numerics in the adopted models yield results which in general agree with those of the chemical benchmarks, and are consistent with radical partitioning derived from measurements. The impact of the exceptions noted above, in particular the recently-noted disagreement in NO_x/NO_y partitioning, will have to be evaluated after appropriate kinetic data are incorporated into the models. In addition, although models have all incorporated some kind of PSC and cold aerosol treatment, the testing of these mechanisms is at this point incomplete. Thus, results at high winter and spring northern latitudes should be viewed with less confidence than for mid-latitudes.

4.3.3.3 N_2O, NO_y and Ozone Gradients in the Lower Stratosphere

The correlation of NO_y with N_2O in the lower stratosphere has been established by numerous aircraft and remote-sensing campaigns (see, for example, Fahey *et al.* [1989]). As described by Plumb and Ko [1992], a compact relationship between these two measurements indicates that the mixing time in the region of interest is faster than the local photochemical lifetimes so that the mixing ratios of both species are constant on the same shared mixing surface. All models yield compact curves, thus qualitatively verifying this condition in the models. For species at steady state, the local slope of these curves is equal to the ratio of their integrated production minus loss above the shared mixing surface. How the local slope changes from one mixing surface to the next is an indication of how the local lifetime of each species changes from surface to surface. This places a further constraint on the combined effects of chemistry and vertical transport in the model. Although models reproduce the general features of the curves, the slopes of the N_2O-NO_y correlations for some models deviate substantially from observations in different regions (Figure 4-2). The AER, GMI, and SUNY-SPB models give the most satisfactory (although still not perfect) agreement with the observed correlations. As discussed below, this comparison is in itself not sufficient to evaluate the assessment quality.

Larger differences among models are observed, however, when we compare the actual vertical profiles against observations of N_2O (Figure 4-3), NO_y (Figure 4-4), and O_3 (Figure 4-5). The primary data set for these comparisons has been recently derived by analysis of N_2O and NO_y data from all ER-2 campaigns [Strahan *et al.*, 1999]. The ozone climatology is as derived by Logan [personal communication] for M&M II. We note that, for some models, agreement with the vertical profiles in one of the above species is accompanied by disagreement in another, thus indicating a disagreement in the correlations. In other cases, models disagree in both the N_2O and NO_y vertical profiles in a manner that keeps the correlations consistent with observations.

Vertical profiles of N_2O in the tropical region test a combination the strength of the upwelling velocity, as well as the degree of mixing between mid-latitudes and tropics (see Section 2.3.2) on a yearly average. At mid-latitudes, the N_2O, NO_y and ozone vertical profiles are determined by a combination of the downwelling residual circulation, the mixing in the model, the model's rate of lower-stratospheric flushing and, finally, the chemistry in the model (see Sections 2.2.2 and 2.3). Thus, it is difficult to isolate an individual process, which is tested by these profiles.

Examination of Figures 4-3 through 4-5 indicates that models exhibit large differences in their calculated N_2O and NO_y profiles at mid-latitudes. The GSFC 2-D model has the largest NO_y concentrations, larger than the data. Both AER 2-D and LLNL 2-D also exhibit high NO_y concentrations. On the other hand, two 3-D models (GMI and LaRC) show concentrations of NO_y lower than data. The SUNY-SPB 2-D model, which derives its 2-D transport from the MACCM2 winds used by GMI, also shows low values of NO_y. This behavior is in general consistent with the N_2O profiles, however, the ordering of the calculated N_2O profiles (from smallest to largest concentrations) does not correspond exactly to what is expected from the NO_y profiles, indicating differences in the NO_y-N_2O correlations in this altitude range. In general, model agreement with N_2O and NO_y profiles are better in the tropics (not shown) than at mid-latitudes. Two-dimensional models overall show only fair to poor comparison to the ozone profiles in the lower stratosphere, although areas of agreement and disagreement occur at different places for different models. Three-dimensional models, on the other hand, seem to do a better job in reproducing the ozone profiles, although future improvements in the NO_y simulation could also affect the ozone calculations. Concentrations of O_3 in the lower stratosphere which are higher/lower than data will in turn induce higher/lower ClO/Cl_y ratios and lower/higher NO_x/NO_y ratios than calculated with a model with correct ozone. Thus, the generally high concentrations of ozone calculated in 2-D models suggest that these models may underestimate the impact of NO_x perturbations if only chemistry was considered. The actual impact needs to be convoluted with transport effects and differences in background Cl_y and NO_y.

The profile comparisons point out a crucial problem with current assessment models: no model has a good enough circulation/chemistry to reproduce all relevant profiles in the lower stratosphere. Although no climatologies for Cl_y and Br_y are available, we expect that similar problems in reproducing correlations and/or profiles would be found. Thus, the question arises as to which profiles are most important to reproduce. The analysis of Wennberg *et al.* [1994] suggests that the amount of NO_y in the lower stratosphere is a major discriminating factor as to the response of the ozone chemistry to a NO_x perturbation. As discussed below, the perturbation results do seem to bear out a strong correlation between ozone impact and NO_y abundances.

4.3.3.4 Age of Air

The concept of age of air, and its derivation from measurements of SF_6 and CO_2 has been discussed in Section 2.3.7. Compared to the mean age derived from the observed SF_6 and CO_2, all 2-D models calculate mean ages that are too young, both in the tropics around 30 km and at the mid-latitude lower stratosphere (see Figure 2-5). Among the 2-D models, the GSFC 2-D model calculates an age distribution that is closest to the observed values. The age of air calculated by the GMI 3-D model using MACCM2 winds also shows age of air smaller than observations. On the other hand, the Monash1 (MACCM2 with older gravity wave parameterization) 3-D yields age of air in reasonable agreement with data while SLIMCAT 3-D has age that is too old.

The formal relation between the age and residence time for materials injected into an idealized well-mixed stratosphere [Boering *et al.*, 1996] implies that mean age and stratospheric residence time are correlated. This suggests that models which calculate younger mean age may underestimate the accumulation of aircraft exhaust injected into the lower stratosphere. As discussed in Section 2.3.7, however, it is not yet possible to quantitatively relate the residence time of aircraft exhaust

injected at a particular location to the mean age (either spatial/seasonal average or at a particular location). Further discussion of this relationship as simulated by different models is given below.

4.3.3.5 Propagation of Annual Cycle

The vertical propagation of an annual cycle in tracer mixing ratio forced by variations at the tropopause, stringently tests model transport in the tropical region (see discussion in Section 2.3.2). Evaluation of model performance in the cycle propagation has two components, phase and amplitude. Details of this comparison are given in Park *et al.* [1999] and Douglass *et al.* [1999].

The GSFC 2-D model performed very well in this comparison. All other 2-D models and the GMI 3-D model performed less satisfactorily. The test was not available from the LaRC or SLIMCAT models. Further model intercomparisons indicate that one reason for the disagreements in the AER model is its adoption of rather large vertical diffusion coefficients in this region. Adoption of smaller coefficients (as in the GSFC 2-D model) leads to better agreement, and also improves the agreement in the ozone vertical profiles. Thus, as in the age of air experiment, most models are inaccurate in simulating this characteristic.

4.3.3.6 Tests of Subtropical and Polar Barriers

As discussed in Chapter 2, there exists a partial barrier to transport between the tropics and extratropics in the lower stratosphere. This subtropical barrier is clearly seen in the measured NO_y/O_3 ratios in the subtropics [Murphy *et al.*, 1993; Fahey *et al.*, 1996]. However, this test does not completely isolate a model's performance in reproducing subtropical barriers, since the chemistry of both NO_y and O_3 must be adequately represented. Fortunately other tests are available; for example, (a) mid-latitude to tropical exchange rates as diagnosed from correlations of trace species [Volk *et al.*, 1996]; (b) attenuation of seasonal cycles of H_2O and CO_2, (above); and (c) horizontal gradients of long-lived tracers (e.g., N_2O from the CLAES instrument).

The exchange time constants derived by Volk *et al.* [1996] (see also Minschwaner *et al.* [1996]; Grecu *et al.* [1996], and Schoeberl *et al.* [1997]) are more independent of chemistry than the NO_y/O_3 ratio, although less altitude specific. The AER results in this assessment come from a model tuned to reproduce these exchange time constants, but other models have not been adjusted for this test. The CSIRO model [Vohralik *et al.*, 1998] yields results in good agreement with both the NO_y/O_3 latitudinal profiles and the exchange time constants, without any specific tuning of the mixing coefficients.

The magnitude of the meridional gradients of N_2O, or other long-lived tracers, in the subtropics provides an indicator of strength of the subtropical barrier. Successful simulation of the correct gradients implies realistic exchange rates. Comparison with N_2O subtropical horizontal gradients from CLAES at 32 hPa indicates good agreement for the AER 2-D, GSFC 2-D, LLNL 2-D, CSIRO 2-D, and GMI 3-D models. At this point we can say that, most models incorporate some sort of subtropical barrier, but have varying degrees of success in reproducing details of the spatial distribution of the observations.

Partial barriers to transport also exist across the edge of the polar vortices (see Chapter 2). Accurately simulating these barriers is important because they limit the amount of emissions that are transported into cold polar regions (where heterogeneous chemical reactions occur). The gradients of N_2O across the vortex edge have also been used to test the realism of the transport within the models. Whereas there is good agreement with CLAES data for subtropical gradients, only the LLNL 2-D model gives good agreement in the magnitude of the gradients across the polar vortices, and even in this case the location of the steep gradients within this model is unrealistic. Since none of the 2-D models has a realistic polar vortex barrier, they are likely to over predict both the transport of HSCT emissions into the polar vortices, and the transport of vortex-processed air into mid-latitudes.

4.3.3.7 Model Temperatures

All 2-D models specify a temperature climatology from either the National Centers for Environmental Protection (NCEP) stratospheric analysis or reanalysis. There are mean temperature differences between the two analyses, with temperature differences as high as 1 to 2 K in the mid- and high-latitude lower stratosphere. The impact of this temperature difference for assessments has not been tested.

The temperatures from the version of the GMI 3-D model used in this assessment have been obtained from a version of MACCM2 which includes a parameterization of gravity waves that induces heat transport to the poles and remedies too-cold temperatures in the SH vortex. At the same time, the NH polar vortex temperatures are too warm (by 2 to 3 K) when compared with existing climatologies. Thus, although the GMI 3-D model includes a complete chemistry on cold sulfate aerosols and PSC formation, the high temperatures in the MACCM2 result in unrealistically negligible PSC formation. Thus we do not consider the GMI 3-D results to estimate the impact of HSCT emissions on PSCs in the NH. To better assess the PSC impact, future work must combine the more realistic 3-D representation of atmospheric motions (such as in the GMI 3-D model) with a better temperature distribution.

4.3.3.8 Ozone Seasonal Distributions and Trends

Examination of ozone seasonal distributions and trends was carried out in conjunction with WMO [1999]. The seasonal behavior of ozone was compared to updated ozone climatology derived from the TOMS instrument. The important features in the TOMS measurements which models are expected to capture include:

1) Tropical low values,
2) Tropical seasonal variations,
3) On-the-pole maximum in the northern late winter - early spring,
4) Off-the-pole maximum in the southern late winter - spring at ~60°S,
5) Very low ozone at high southern polar latitudes in spring,
6) Moderate ozone gradient in 30-60°N latitude band in winter and spring.

The 2-D models (AER, CSIRO, GSFC, LLNL, and SUNY-SPB) used realistic boundary conditions of the source gases and measured sulfate aerosols to predict the total ozone over the 1979 to 1997 time period. This assessment compared 1990 TOMS data with the above mentioned

assessment models. Most models did a reasonable job representing these features. Both GSFC 2-D and SUNY-SPB 2-D represent features 2, 3, 5, and 6 very well.

To help evaluate the ability of the models to predict the effects of aircraft on the stratosphere, it is also useful to examine how the models perform in predicting the past measured changes in total ozone. Using the boundary conditions as described above and including the accelerated loss of ozone after the eruption of Mt. Pinatubo in 1992, the models predicted ozone trends over the 1979 to 1997 period. In general, all models reproduce the general downward trends over this time period, however, the seasonal distributions in the trends are less well simulated.

It is important to emphasize that there does not seem to be a relationship between model performance in tests described in subsections 1-6 and their performance in reproducing the ozone behavior. Predicted ozone concentrations are the result of different transport and chemical processes; models can get the right answer with the wrong balance. Good model performance in reproducing background ozone and chlorine ozone perturbations is not a sufficient criterion for good performance in the HSCT assessment. The HSCT perturbations have a different spatial distribution and a different chemistry, and could depend more on the correct representation by models of lower stratospheric processes to which chlorine perturbations are less sensitive. It is thus important to continue model testing against more "basic" parameters than those provided by total ozone column.

4.3.3.9 Summary of Model Tests

The above exercises point to some general characteristics of current models. No model is perfect, and some models perform better in some tests than others. However, the following can be stated:

a) Models participating in this assessment have a satisfactory representation of gas-phase chemistry, both in their numerics, and in the adoption of a suitable chemical mechanism.

b) Several models have sufficient vertical resolution to provide reasonable assessments. However, care should be taken in models with resolutions greater than 2 km.

c) Most models reproduce some kind of subtropical barrier. CSIRO 2-D does best in this regard; the AER model has been tuned to give the right exchange rate. Two-dimensional models do poorly in reproducing barriers across the polar vortex, whereas the GMI 3-D model yields a fairly isolated vortex (See 4.4.3.1 below). The lack of sufficient testing and development of polar processes is still a problem with assessment models in general.

d) Largest discrepancies occur in comparison of results with measurements primarily determined by stratospheric dynamics. These include the age of air, propagation of seasonal cycles, and concentrations of NO_y in the lower stratosphere. The GSFC 2-D model performs very well in reproducing age of air and propagation of seasonal cycles, but their calculated NO_y concentrations are too large when compared with measurements. On the other hand, the GMI and LaRC 3-D models yield NO_y concentrations that are too low when compared to observations.

4.4 Calculations and Sensitivity

Eight modeling groups participated in this HSCT assessment (Table 4-1). Included within this list are five 2-D and three 3-D CTMs. Detailed descriptions of the dynamics, chemistry, and other processes are described in Appendix F. All eight of these models participated in both the photolysis benchmark [Stolarski *et al.*, 1995] and the chemistry solver benchmark (see Appendix E). In addition, these eight assessment models have also participated in the 1998 NASA Model and Measurements II intercomparison [Park *et al.*, 1999]. These models incorporated the improvements from 1995 as detailed in Section 4.2.

4.4.1 Description of Boundary Conditions and Input

Each assessment model used the HSCT emissions of NO_x, H_2O, hydrocarbons (as CH_4), and CO described in detail in Sections 3.3 and 3.7. The surface source gas boundary conditions and sulfate surface area density distributions are described below.

Boundary conditions for both the 2015 and 2050 background atmospheres are shown in Table 4-2a. The halogen source gases for 2015 and 2050 are taken from Stolarski *et al.* [1995]. Source gases CH_4 and N_2O are taken from the IS92a scenario given in Tables 2.5a and 2.5b of IPCC [1996]. Source gas CO_2 is taken from the IS92a scenario given in Figure 5, p. 23, of IPCC [1996]. Source gas CH_3Br is taken from the IS92a scenario given in Table 2.2 of IPCC [1996].

The SAD for the background atmosphere has been specified according to WMO [1992], Table 8-8, which represents the 1979 SAD as determined by SAGE. This sulfate SAD is representative of a volcanically clean atmosphere. For scenarios including emission of sulfur by HSCT aircraft, the perturbation in SAD was calculated by the AER microphysical model [Weisenstein *et al.*, 1997]. The SAD provided to modeling groups for the scenarios is the AER HSCT scenario SAD minus the AER background calculated SAD added to the World Meteorological Organization (WMO) background SAD. Each scenario specified the fraction of emitted sulfur that was assumed converted to particles in the aircraft plume, ranging from 0 to 100%, with the most likely scenario represented by 10% conversion. The EI of SO_2 was assumed to be 0.4 (or 0.2 for S), which is half of the current average sulfur content of jet fuel. The far-field particle size input to the global model, following nucleation and coagulation in the aircraft plume, was taken to be 10 nm (0.01 μm). In Figure 4-6, an example of the sulfate SAD increase is shown for a 10% SO_2 gas-to-particle plume conversion. Here, an increase in SAD of up to 50% is derived in the NH, lower stratosphere. Note that since this field was specified and was derived from a single model, the transport rates of the AER model influence the results in all the models for scenarios with sulfur emissions, probably decreasing the model-to-model variability of the ozone response. All SAD distributions used in this assessment are described in Table 4-2b and listed in the HSR Program scenario descriptions in Tables 4-3 through 4-6.

4.4.2 Motivation for Scenarios

Scenarios were developed to investigate the model-derived sensitivities to the uncertainty in future atmospheric composition and climate, HSCT operational characteristics, and model engineering assumptions. To examine the future impacts of HSCTs on stratospheric ozone, the periods of

2015 and 2050 were specified. For example, the atmospheric abundance of inorganic chlorine is 3.0 and 2.0 for the 2015 and 2050 atmospheres, respectively. For one set of scenarios, a prescribed temperature change representative of a future 2050 climatic state was imposed on the model chemistry. Numerous sensitivity scenarios were conducted for both the 2015 and 2050 atmospheres, examining the operational impacts of different EI_{NOx} (g NO_2 / kg fuel), sulfate particle production, fleet size (500 and 1000 HSCTs), and cruise altitude (-2 km, normal, and +2 km). The sensitivity of including a polar cold aerosol representation (i.e., nitric acid trihydrate (NAT) or supercooled ternary sulfate (STS), ice, dehydration and denitrification processes) was also examined. In addition, special sensitivity scenarios were designed to examine the model response under the limit where no HSCT emissions of either NO_x or H_2O were specified. Results of these scenarios are shown in Tables 4-3 through 4-6 and discussed in the following sections.

4.4.3 RESULTS

The effect of HSCT emissions of NO_x, H_2O, and to a minor extent hydrocarbons and CO, are discussed below. In all cases the model-derived "delta" impact of NO_y, H_2O, and ozone is relative to an atmosphere that includes a subsonic fleet. The HSCT scenarios also include a subsonic fleet, although slightly reduced to account for expected replacement of some subsonic flights by supersonics (Chapter 3); therefore, the model-derived "delta" is primarily a result of the HSCT fleet emission scenario.

4.4.3.1 HSCT Induced Delta NO_y and Delta H_2O

In Figures 4-7 and 4-8, the ΔNO_y and ΔH_2O are shown respectively for a fleet of 500 HSCTs with $EI_{NOx} = 5$. For the models participating in this assessment, the range of NH maximum ΔNO_y is between 0.4 and 1.0 ppbv. The SH maximum ΔNO_y range is between 0.1 and 0.4 ppbv. This result implies that the eight assessment models used in this assessment have significantly different transport fields. This is also the conclusion derived from the recent NASA Models and Measurement Workshop II Report [Park *et al.*, 1999]. The discussion in Chapter 2 noted that several transport mechanisms, such as mid-latitude stratosphere-troposphere exchange, mixing rates of extratropical air into the tropics, and strength of residual circulation, combine to determine the amount of aircraft exhaust tracer in the atmosphere.

The AER and CSIRO models show less transport of ΔH_2O and ΔNO_y to the SH than most other 2-D models. This can be compared with the model evaluation (Section 4.3.3, test 6), which notes that these models both accurately represent the mid-latitude to tropical exchange rates as diagnosed from observations [Volk *et al.*, 1996]. The AER 2-D model specifically imposes this exchange rate via diffusion coefficients while the CSIRO 2-D model obtains good agreement without any specific modification of transport coefficients. There is also similarity in the global distribution of HSCT ΔH_2O and ΔNOy between the GMI 3-D and SUNY 2-D models. This similarity is not surprising since the SUNY 2-D model residual circulation is derived from the same 3-D meteorological fields that are used in the GMI 3-D model, i.e., MACCM2. Figure 4-9 shows a polar projection of ΔNO_y at 18 km in winter taken from the GMI 3-D model. The perturbation is smaller within the polar vortex, showing that the model maintains a winter barrier to transport at high latitude. This contrasts with the 2-D models, which generally show a constant perturbation between 60°N and 90°N at this altitude.

4.4.3.2 Model-Derived Delta Ozone, Relationship to Ambient Species Distributions

The latitudinal and seasonal variations in the perturbation to column ozone in the NH are highly model-dependent. In Figure 4-10a the impact on column ozone is shown from a 2015 fleet of 500 HSCTs, with an $EI_{NOx} = 5$, under volcanically clean conditions (SAD = SA0). This scenario (4 in Table 4-3) is consistent with the ΔNO_y and ΔH_2O changes shown in Figures 4-7 and 4-8. The AER 2-D model-derived column ozone change show the most negative values, with a -1% reduction at high latitudes in March. Other models (e.g., LLNL 2-D and CSIRO 2-D) derived a maximum NH column ozone depletion of about -0.4%, peaking at high latitudes in September. The GSFC 2-D model does not show a strong NH seasonal variation in HSCT induced column ozone change, peaking broadly at -0.4%. The LaRC 3-D model calculates a positive perturbation at most NH latitudes. The GMI 3-D model predicts a positive column ozone perturbation at most latitudes. SLIMCAT results for total column ozone change are not included in the comparison because this model treats tropospheric ozone differently than the others (Appendix F). Note that the GMI model does not include representation of tropospheric chemical and physical processes, therefore the tropospheric ozone change has been removed from the figures (Appendix G).

The model-derived SH HSCT-induced change in column ozone is also highly model-dependent. Here, the AER 2-D model-derived SH change in column ozone is small, which is correlated with the relatively small interhemispheric exchange of aircraft H_2O and NO_y. The opposite impact is observed in the GSFC 2-D model. As shown in Figures 4-7 and 4-8, the GSFC 2-D model-derived HSCT H_2O and NO_y abundance is relatively large in the SH. This ΔH_2O and ΔNO_y, coupled with the GSFC 2-D cold aerosol representations, significantly worsens the ozone hole in the GSFC 2-D model (also see Section 4.4.3.4). All models, except one (CSIRO 2-D, which does not include PSCs) show enhanced springtime HSCT column ozone depletion in the SH.

Figure 4-10b shows the impact on column ozone similar to 4-10a, except that it is assumed that 10% of the emitted sulfur is converted to particles in the wake (scenario 9). Only 2-D models carried out this calculation. Except for the SUNY-SPB 2-D model, the impact of including gas-to-particle conversion in the plume is substantial; even a 10% conversion essentially doubles the calculated ozone depletion at mid- to high latitudes.

In Figure 4-11, the vertical distribution of zonal mean HSCT-induced change in ozone (ΔO_3 ppbv) for June is shown. In general, all the models calculate ozone reductions of 20 to 80 ppbv above 25 km. Below this altitude level, several models derive significantly positive changes in local ozone (SUNY-SPB 2-D, LaRC 3-D, and GMI 3-D). All models except AER 2-D have a region of ozone increase extending out to at least ~60°N. The AER 2-D model ozone increase extends from the equatorial region to ~30°N, thus inducing larger negative ozone changes in the AER model at high latitudes.

The difference in sensitivity of local ozone concentration, as it impacts the column, can be clearly seen in Figure 4-12. Here, the change in ozone concentration is shown for three latitudes and twice a year, in both hemispheres. Calculations are shown for cases without engine particle production (panels a and b) and 10% fuel sulfur gas-to-particle conversion (panels c and d). At

30°N without particle emissions, all the models derive a similar delta ozone concentration profile, with a positive lobe peaking below 20 km and a negative lobe peaking above 25 km. This illustrates the change between the chemistry of a NO_x-dominated region above 25 km, and a region at lower altitudes where the main impact of added NO_x is to sequester HO_x and halogen radicals thus reducing the total rate of ozone destruction as discussed in Chapter 2. The effect of increasing aerosol through HSCT emissions (Figures 12c and d) is to increase the net ozone loss in the lower stratosphere by enhancing HO_x and halogen loss and decreasing the NO_x buffering effect.

At higher latitudes in the NH, the agreement among models becomes less consistent. The AER 2-D model switches sign and calculates a relatively large decrease in local ozone below 20 km. This negative lobe reflects the large impact of HSCTs on PSCs in the AER formulation. The negative lobe slowly migrates to lower latitudes, and is still noticeable in June both at 45° and 65°N. The slow disappearance of this lobe reflects the "sluggish" circulation of the AER model during winter/spring. By September (not shown), the negative lobe has disappeared. On the other side, the GMI 3-D, LaRC 3-D, and SLIMCAT 3-D models all derive a relatively large positive local ozone concentration change in this region.

In the SH, there is general agreement among models in the local ozone concentration change at 30° and 45°S. The exceptions are the GSFC 2-D model and the SLIMCAT 3-D model. The GSFC model shows relatively large reductions in ozone below 20 km, due to the large transport of HSCT exhaust to the SH (Figures 4-7 and 4-8). SLIMCAT 3-D also shows a negative ozone region, but at altitudes near 30 km. This probably reflects their transport of exhaust to the SH at higher altitudes than other models. The SH ozone change including engine particle emissions is constrained by the fact that the particle perturbation is specified using the AER model transport.

To first order, the differences in the HSCT induced sensitivities between the eight assessment models used in this report can be explained in terms of their ambient reactive trace species distributions. The different models are shown in Figure 4-13 for the same scenario as in Figures 4-7 to 4-12. Panel (a) shows the background NO_y concentrations calculated by the assessment models, which were compared to ER-2 data in Figure 4-4. Panel (b) shows profiles of the sensitivity of the O_3 change to the change in NO_y due to HSCTs calculated by each model. This behavior is consistent with our understanding of the response to NO_x changes as outlined in Section 2.4.1. All the models produce larger ozone loss per unit NO_y change at the higher altitudes where background NO_y is greater, as expected in a NO_x-controlled region. The sensitivity of O_3 to delta NO_y is near zero in the lower stratosphere. Moreover, normalized delta O_3 in the lower stratosphere is ordered with background NO_y differences among the models. This behavior (positive delta O_3/delta NO_y at low NO_y background and negative delta O_3/delta NO_y at high NO_y background) is expected for the ozone response in a HO_x-controlled region of the atmosphere (see Figure 2-7).

Figures 4-11 and 4-12 show that the ozone column response is a sum of the negative response near 30 km and a positive response near cruise altitude, and that there is a large variation in the response among the different models. The question arises as to what observations best constrain a model in the regions of negative and positive ozone response. Because the ozone response depends on the accumulation of exhaust, and we expect that accumulation is related to stratospheric age of air through the residence time (Section 2.3.7), we examine correlations with age of air. Figure 4-14

shows the correlation of NO_y, delta NO_y, and delta O_3 calculated by different models against the respective model-calculated age of air at 18 and 26 km, 45°N. Figure 4-14a shows age is well correlated, among models, with background NO_y especially in the lower stratosphere. This is consistent with the transport and chemistry processes discussed in Chapter 2 indicating that models with more active transport circulations have shorter residence time, lower mean age, and less production of NO_y from N_2O-the tropospheric source gas. Age also correlates well with Cl_y (not shown) among models in the lower stratosphere consistent with N_2O-NO_y-Cl_y observations (Section 2.4). The observations (filled symbols) show that several models produce an age similar to measurements in the lower stratosphere (18 km) at this latitude, but their corresponding NO_y is greater than measured. At higher altitude (26 km) almost all models underestimate age, and most by a large factor. Low age and high-to-accurate NO_y exemplifies a serious dilemma for the models: changing circulation characteristics to improve age comparisons often worsens comparisons with other tracer observations.

Figure 4-14b shows that, consistent with theory, age is correlated, among models, with the accumulation of aircraft NO_y in the lower stratosphere (18 km). Less dependence of delta NO_y on model age is seen in the middle stratosphere (26 km). Comparison with measured age suggests that the models with higher age and delta NO_y in the lower stratosphere are more likely to be correct. However, the source regions for aircraft exhaust and age tracers are very different and the degree to which age comparison is an indicator of the accuracy of model transport and dispersion of HSCT exhaust is not clear. In fact, examination of all models participating in M&M II indicates that the correlation between 3-D model age and exhaust tracer accumulation (Figure 4-15) is different from that shown in Figure 4-14b. Thus, the best choice of model for HSCT transport is difficult to identify. Figure 4-14c shows that the O_3 perturbation among models is not well-correlated with age at either altitude, which is understandable in view of the low correlation between delta NO_y and age at 26 km and the lack of sensitivity of delta O_3 to delta NO_y at 18 km (Figure 4-13).

4.4.3.3 Ozone Sensitivity to HSCT NO_x and H_2O Emission

The sensitivity of ozone column response to the EI of NO_x from HSCT aircraft varies from model-to-model and from a volcanically clean background atmosphere to a volcanically perturbed background atmosphere. The percent change in NH ozone column is plotted as a function of EI_{NOx} in Figure 4-16a for the clean background atmosphere (SA0) and for the volcanically perturbed background atmosphere (4 x SA0) in Figure 4-16b. Both calculations assume no sulfur emission in the aircraft plumes. In the volcanically clean atmosphere, the GSFC 2-D, LLNL 2-D, and CSIRO 2-D models calculate slightly higher ozone depletion with increasing EI_{NOx}. The AER 2-D and SUNY-SPB models calculates less ozone depletion between $EI_{NOx} = 0$ and $EI_{NOx} = 5$ and little change between $EI_{NOx} = 5$ and $EI_{NOx} = 15$. In the volcanically perturbed atmosphere, all models calculate less ozone depletion with increasing EI_{NOx}.

It is also evident from Figure 4-16 that at $EI_{NOx} = 0$ (HSCT H_2O only emissions) has the dominant negative impact on the NH column ozone change. In fact, under both clean (in some models) and volcanically enhanced conditions, the additional NO_x tends to lessen model-derived ozone depletion by H_2O. This indicates that, in all the models considered, the lower stratosphere is HO_x-dominated, and increases in NO_x in the lower stratosphere lead to an increase in ozone that more

than compensates for the decrease at higher altitudes. In an atmosphere with volcanically perturbed aerosol loading, the lower stratospheric ozone loss becomes more halogen and HO_x-dominated. Increasing NO_y in this environment reduces the active radical loading of the lower stratosphere by forming $ClONO_2$ and HNO_3. This effect dominates the ozone column change in all the models for an atmosphere with four times the background aerosol loading.

4.4.3.4 Sensitivity to Model Polar Cold Aerosol Representation

There are several physical and chemical processes which take place in the lower stratosphere winter and involve cold aerosol particles and PSCs (see Section 2.4.5). These include formation, growth, and evaporation of STS and/or NAT particles; heterogeneous reactions which take place on the particle surfaces; and permanent denitrification and dehydration as a result of sedimentation of large ice and/or NAT particles. Since aerosols and PSCs are composed of H_2O, HNO_3 and H_2SO_4, HSCT emissions impact the evolution of ozone during the winter in at least two ways. Aircraft emissions might increase the size of the particles, particularly STS, thus increasing the available surface for heterogeneous reactions and leading to additional denitrification. Also the enhanced levels of water, HNO_3, and sulfuric acid could increase the chemical reactivity of the particles at a given temperature.

Based on observations of NO_y and aerosol particles as part of ASHOE/MAESA, Del Negro *et al.* [1997] estimate that the STS aerosol volume would increase by more than a factor of 2 below 192 K for a 20% increase in NO_y and a 7% increase in H_2O. Since the heterogeneous chemical reactions are generally rapid, the resulting ozone decrease is more sensitive to the temperature for chlorine activation, rather than the available surface area. Del Negro *et al.* [1997] estimate a change of 0.7 K for the above increases in NO_y and H_2O. The microphysical mechanism by which H_2O and NO_y are removed permanently from the lower stratosphere through sedimentation is not known, but is apparently related to the threshold temperature for formation of water ice.

The sensitivity of HSCT NO_x only, H_2O only, and combined emissions are examined in a model framework with (Table 4-3) and without (Table 4-5) polar cold aerosol processes (i.e., STS or NAT, ice, dehydration and denitrification processes). For a description of how these five participating assessment models represent these heterogeneous processes, see Appendix F. In the NH, only the AER 2-D model shows any significant difference in HSCT-induced ozone column change when including a cold aerosol representation (compare scenario 4 and scenario 31). In the SH, only the GSFC 2-D model derives a significant HSCT-induced sensitivity from the inclusion of cold aerosol processes. In fact, when the GSFC 2-D model cold aerosol parameterization is included, the SH average ozone depletion is significantly greater than the NH average depletion.

This model sensitivity to cold aerosol processes highlights the need to better understand the accuracy and uncertainties of including these processes in multi-dimensional assessment models. This includes not only their PSC and cold aerosol representation, but also the transport of exhaust into the polar vortices and to the SH. As noted in Section 4.3.3.6, the 2-D models do not provide a realistic representation of the winter vortex transport barrier, and calculate larger perturbations to H_2O and NO_x for high latitude winter than the 3-D models: GMI, LaRC, or SLIMCAT. The transport into the SH is presumably most dependent on the degree of isolation of the tropics from mid-latitudes. The AER model has been tuned to get the right mid-latitude to tropical bulk

exchange, and this model calculates less transport from the Northern to the Southern Hemisphere than the GSFC model, for example. As we saw in Section 4.3, however, the test provided by latitudinal gradients of CLAES N_2O did not conclusively favor either of these 2-D models. Thus, further analysis and diagnostics must be developed to test the model's interhemispheric transport rate in the stratosphere.

4.4.3.5 Sensitivity to HSCT Plume Gas-to-Particle Conversion

The sensitivity of ozone response to particle production from HSCT aircraft is shown in Figure 4-17 for the 2015 atmosphere for both volcanically clean and perturbed conditions. The x-axis of these plots is the surface area increase in the 14 to 21 km, 33°N to 90°N region as a percentage of the background SAD. The percentage SAD increase under volcanically clean conditions for the 0%, 10%, 50%, and 100% particle conversion cases is 30%, 40%, 80%, and 110%, respectively (top panel). For a volcanically active period the SAD increase is divided by four (bottom panel). The case with 0% change in SAD is taken from a scenario with no sulfur emissions and could represent future desulfurization of aviation fuel. All models show a significant negative trend in ozone perturbation with increasing particle emission from aircraft. Northern Hemisphere trends are greater than SH trends, because the AER model, from which the changes in SAD were taken, transports little emitted material to the SH (see Figure 4-6). Under volcanic aerosol conditions, the increase in ozone perturbation with increasing particle emissions is reduced relative to clean aerosol conditions.

The mechanism for ozone perturbation by enhanced particle surface area density depends on the relative importance of the NO_x catalytic cycle to ozone removal. Where NO_x losses dominate, in the 25- to 35-km region, increased SAD leads to less ozone removal because a larger fraction of the active NO_x is converted to inactive HNO_3 by heterogeneous reactions. Below 20 km, where HO_x loss dominates ozone removal, increased SAD leads to more HO_x and halogens in active form and thus more ozone loss. The latter effect dominates the ozone column response. In general, even when assuming only a 10% gas-to-particle conversion in the plume, the subsequent SAD increase has one of the largest predicted impacts on ozone change in this assessment.

4.4.3.6 Sensitivity to HSCT Cruise Altitude

The effect of raising or lowering the HSCT cruise altitude is shown in Figure 4-18. Here results from five of the participating assessment models are shown. Reducing the cruise altitude by 2 km significantly reduces the negative impact on Northern Hemispherical column ozone. Increasing the cruise altitude significantly increases the amount of ozone depletion relative to the normal cruise altitude case. This conclusion is in agreement with the previous NASA 1995 assessment [Stolarski *et al.*, 1995].

For cases where SO_2 gas-to-particle conversion was considered (e.g., Table 4-6, scenarios 40 and 41), reducing the cruise altitude by 2 km again significantly lessened the hemispheric depletion by ~50% in most participating assessment models.

4.4.3.7 Sensitivity to HSCT Fleet Size

In this assessment, the sensitivity of the HSCT fleet size from 500 to 1000 aircraft was examined for EI_{NO_X} values of 5 and 10. When the HSCT fleet is doubled not only does the HSCT NO_x increase, but more importantly, the amount of HSCT H_2O is doubled. In addition, the mature fleet in not just a doubling of flights in the same flight corridor but includes a higher proportion of flights in the tropics (see Chapter 3). For $EI_{NO_X} = 5$, the doubling of the fleet increased the NH average column ozone reduction in approximately a linear manner (compare Table 4-3, scenarios 4 and 6). For the $EI_{NO_X} = 10$ case, all the participating assessment models derived an increased NH average column ozone reduction by more than a factor of two (compare scenarios 5 and 7). These results are consistent with the previous NASA HSCT assessment [Stolarski *et al.*, 1995].

4.4.3.8 Sensitivity to 2050 Conditions

In this assessment, inorganic chlorine abundances between 1.0 ppbv and 4.0 ppbv were tested. Scenarios with 2.0 ppbv and 3.0 ppbv corresponded to 2050 and 2015 conditions, respectively. The 2050 scenarios also assumed a fleet of 1000 HSCTs. Extreme scenarios with 1.0 and 4.0 ppbv were also considered. Results from this assessment, with no change to sulfate aerosol background from aircraft, suggest that there is little sensitivity to background inorganic chlorine abundances (see Table 4-3, scenarios 4, 19, and 22). However, this assessment did find sensitivity to chlorine levels when sulfate particle production in the plume is included (see Table 4-3, scenarios 10, 20, and 23). Here, as the Cl_y abundance increased from 1.0 ppbv to 4.0 ppbv, the model-derived column ozone depletion increased, maximizing and leveling off between 3.0 and 4.0 ppbv.

Several participating models examined the temperature uncertainty in future climate. The possible temperature impact on the model-derived ambient and HSCT perturbed chemistry was investigated. There was no attempt to simulate the impact that climate/temperature feedback may have on model-derived circulation. The delta temperature change supplied to the participating assessment models was taken from a time-dependent integration (present day to 2050) using the GISS 3-D GCM [Shindell *et al.*, 1998]. The temperature was averaged zonally and annually, and changes in temperatures (delta temperatures) were calculated from similar zonal and annual averages for the decade of the 1990s. The resulting delta temperatures were a few degrees colder throughout most of the lower stratosphere. These delta temperatures were then added to the model mean temperature fields. In general, the participating 2-D models (AER, GSFC, SUNY-SPB, LLNL, and CSIRO) did not derive any large excursions from the reference perturbation (compare Table 4-6, scenarios 36 and 43).

It should be noted that the above study used annual average delta temperatures, and that there may be months where the future climate in the lower stratosphere is significantly colder than the annual average difference of about -2 K. In addition, climate changes could also affect the tropopause temperature, leading to increases/decreases in the amount of water delivered to the tropical lower stratosphere, depending on whether the tropical tropopause temperature increases or decreases. Both of these factors are important, given the non-linear behavior of heterogeneous processes and PSC formation. To investigate the additional sensitivity to these changes, the AER 2-D model conducted a series of studies described below.

The AER 2-D model was used in a time-dependent fashion to explore the impact of year-to-year variability in temperature on the ozone response to HSCT. Temperatures from the NCEP reanalysis were used, starting with 1988 and calculating the ozone response for eight consecutive years, until the end of 1995. Ozone concentrations were calculated for the subsonic-only scenario (scenario 1) and for an HSCT scenarios with EI_{NO_x} = 5, 500 aircraft and SA1 (scenario 10) with 2015 boundary conditions. Figure 4-19 shows the calculated annual average column ozone perturbations for the individual years (dashed lines). The spread in ozone column response at high northern latitudes is 0.5%, with 1991 (a warm year) showing the smallest ozone perturbation and 1995 (a cold year) the largest. Also shown in Figure 4-19 is the ozone column response calculated with a climatological temperature. The thick black line represents the 1979 to 1995 average temperature from the NCEP reanalysis, while the thick gray line represents the 1979 to 1985 average temperature from the older NMC analysis. All calculations adopt year-by-year temperature distribution to account for deviations of temperature from the zonal monthly mean. However, it should be noted that these calculations do not include the interannual variability in circulation for these years, and, as such, only represent partially the expected variability in HSCT response. Furthermore, the large spread in the ozone impact at high latitudes is dependent on the large sensitivity of the AER results to incorporation of PSCs.

Climatic changes could also impact the tropical tropopause temperature, and thus the amounts of water entering the stratosphere through the tropical cold trap (Section 2.2.2.3). The AER model was used to test the sensitivity to water at the tropopause by imposing tropopause mixing ratios ranging from 2 ppmv smaller to 4 ppmv larger than its usual climatological values. The largest impact occurs at high northern latitudes during winter/spring, where the maximum calculated ozone depletion ranges from -0.4% to -1.3%, for the lowest and highest values of tropopause water adopted (cf., Figure 4-10a).

4.4.3.9 Sensitivity to Uncertainties in Kinetic Rates

The uncertainty in prediction of the HSCT ozone impact due to the kinetic reaction rate uncertainties can be quantified. As shown in the 1995 Assessment, the estimated uncertainty in the kinetic rates propagates through a 2-D model calculation to yield an uncertainty of about +/-1% at northern mid-latitudes. The uncertainty is slightly larger for northern high latitudes and about half as large for the SH. This uncertainty estimate includes some of the uncertainties already discussed in this chapter and in Chapter 2. For instance, the uncertainty in the NO_x/NO_y ratio is included in the overall estimate. The comparisons to data have indicated that the uncertainty estimates used (JPL-94) in these calculations may actually be overestimates of the real uncertainty (e.g., Cohen *et al.* [1994]).

In another study, box model calculations were conducted to better quantify kinetic rate parameter uncertainties in HSCT induced changes in ozone [Dubey *et al.*, 1997]. Guided by the box model sensitivities, 2-D model runs were repeated with nine targeted input rate parameters altered to 1/3 of their 1-sigma uncertainties to put error bounds on the predicted O_3 change. Results indicate that these kinetic errors can cause predicted local O_3 loss of 1.5% to be uncertain by up to 3% absolute in regions of large aircraft NO_x injection. Overall the derived column ozone change was consistent with the above-mentioned Monte Carlo analysis.

4.5 HSCT Impact on Climate

The impact of HSCTs on climate is estimated to be small in absolute sense relative to total anthropogenic climate forcing. This result is expected since the amount of fossil fuel burned by a fleet of 1000 HSCTs is about 1% of the total fossil fuel consumption projected for 2050 under the assumptions of IPCC scenario IS92a [IPCC, 1996]. Yet, the contribution of an HSCT fleet to global climate change will be more than just its fuel use, with changes from stratospheric ozone and water vapor likely larger than that from CO_2. Various uncertainties remain in the scale of the projected HSCT perturbation, as noted in previous sections, and in the nature of the climate response to a predominantly stratospheric perturbation.

This section first identifies and quantifies the different components of the Radiative Forcing (RF) from HSCTs. Next we discuss the GCM experiments which attempt to translate these RFs into a response in surface air temperature. Results of absolute climate change are then compared with those expected from increased CO_2 and other anthropogenic influences. Finally, we highlight the major areas of scientific uncertainty where progress can be made.

4.5.1 Radiative Forcing as a Measure of Climate Change

The potential climate impact of HSCTs flying in the stratosphere is associated with their release of CO_2, H_2O, NO_x, SO_2, and soot. The H_2O and NO_x both perturb stratospheric O_3; the SO_2 becomes stratospheric sulfate particles; and the CO_2 mixes globally becoming no different from any other fossil fuel source. The added CO_2 and stratospheric H_2O, being greenhouse gases, will warm the surface while cooling the stratosphere. The chemically induced ozone decrease in the stratosphere will cool both the surface and the stratosphere. Stratospheric sulfate (scatterers) and soot (absorbers) intercept solar radiation cooling the surface while warming the stratosphere.

The Earth's climate system is powered by the sun, intercepting 340 W m^{-2} of solar radiation averaged over the surface of the globe. About 100 W m^{-2} is reflected to space, and the remainder, about 240 W m^{-2} heats the planet. On a global average, the Earth maintains a radiative balance between this solar heating and the cooling from terrestrial infrared radiation that escapes to space. When a particular human activity changes greenhouse gas amounts, particles, or land albedo, this results in a radiative imbalance. Such an imbalance cannot be maintained for long, and the climate system, primarily the temperature of the lower atmosphere, adjusts to bring back radiative balance. We calculate the global, annual average of the radiative imbalance (W m^{-2}) to the atmosphere-land-ocean system caused by anthropogenic perturbations and designate that change RF. Thus by definition, the RF of the pre-industrial atmosphere is taken to be zero.

As an example, burning fossil fuel adds the greenhouse gas CO_2 to the atmosphere, and it is responsible for the increase of atmospheric CO_2 from ~280 ppmv in the pre-industrial atmosphere to ~360 ppmv in 1995. Added CO_2 increases the infrared opaqueness of the atmosphere, thereby reducing the terrestrial cooling with little impact on the solar heating. Thus, the radiative imbalance created by adding a greenhouse gas is a positive RF. A positive RF leads to a warming of the lower atmosphere in order to increase the terrestrial radiation and restore radiative balance. Radiative imbalances can also occur naturally, such as the massive perturbation to stratospheric

aerosols caused by Mt. Pinatubo [Hansen *et al.*, 1996]; however, following IPCC convention we reserve the term RF for anthropogenic change.

Because most of the troposphere is coupled to the surface through convection, climate models typically predict that land surface, ocean mixed layer, and troposphere together respond to positive RF in general with a uniform increase in temperature. The global mean surface temperature is a first-order measure of what we consider to be "climate," and its change is roughly proportional to RF. The increase in mean surface temperature per unit RF is termed climate sensitivity and includes feedbacks within the climate system, such as the changes in tropospheric water vapor and clouds in a warmer climate. The RF that is the best metric of climate change is the radiative imbalance of this land-ocean-troposphere climate system, i.e., the RF integrated at the tropopause.

When the radiative perturbation occurs above the tropopause in the stratosphere as for most HSCT impacts, this heating/cooling is not rapidly transported into the troposphere, and the imbalance leads mostly to change in local temperatures that restores the radiative balance within the stratosphere. Such changes in stratospheric temperature, however, alter the tropospheric cooling, e.g., warmer stratospheric temperatures lead to a warmer troposphere and climate system. This adjustment of stratospheric temperatures can be an important factor in calculating RF and is denoted "stratosphere-adjusted."

All RF values used in this report refer to the "stratosphere-adjusted, tropopause RF." For primarily tropospheric perturbations (e.g., additional CO_2 from HSCTs) this quantity can be calculated with reasonable agreement (better than 25%) across the models. For specifically stratospheric perturbations (e.g., H_2O and O_3 perturbations from HSCTs) the definition of tropopause and the calculation of stratospheric adjustment introduce a significant source of error, of order 50%, in the calculated RF.

In mapping RF to climate change, the complexities of regional and even hemispheric climate change have been compressed into a single quantity, global mean surface temperature. It is clear from climate studies that the climate does not change uniformly; some regions warm or cool more than others. Further, the mean temperature does not tell us about aspects of climate change such as floods, droughts, and severe storms that cause the most damage. In the case of aviation, the radiative imbalance driven by perturbations to O_3 and stratospheric H_2O is predominantly in the northern mid-latitudes and not globally distributed as is that driven by increases in CO_2. Does this large north-south gradient in the radiative imbalance lead to climate change of a different nature than for well-mixed gases? The IPCC [Kattenberg *et al.*, 1996] considered this issue of whether the negative RF from fossil-fuel sulfate aerosols (concentrated in industrial regions) would partly cancel the positive RF from increases in CO_2 (global). Studies generally confirmed that the global mean surface warming from both perturbations was additive, i.e., it could be estimated from the summed RF. The local RF from sulfate in northern industrial regions was felt globally. Nevertheless, the regional patterns in both cases were significantly different, and obvious cooling (in a globally warming climate) occurred near the regions of large sulfur emissions. Such differences in climate change patterns are critical to the detection of anthropogenic climate change as reported in IPCC [Santer *et al.*, 1996]. As a further complication to this assessment, the HSCT perturbation occurs primarily in the stratosphere and may alter the vertical profile of tropospheric warming in the future. Thus the patterns of climate change from the HSCT-induced CO_2,

stratospheric H_2O, and O_3 changes individually would likely differ, but we take their summed RF as a first-order measure of the global mean climate change.

4.5.2 The HSCT Scenario and RFs

For continuous HSCT perturbations to H_2O, O_3, sulfate, and soot, the atmospheric response would reach a steady state in less than a decade, and thus the climate impacts can be evaluated based on the instantaneous fleet size. For CO_2, however, the atmosphere accumulates the emissions over a century, and we need to specify the history of the HSCT fleet. The evaluations here assume that HSCTs begin operations in the year 2015 and grow at the rate of 40 aircraft per year, topping out at a fleet of 1000 by the year 2040, which continues operation to 2050. The RF from different perturbations is evaluated for the year 2050. The ozone perturbation is based on a fleet of 1000 with EI_{NOx} of 5 (g NO_2 per kg fuel) and a 10% conversion of fuel sulfur (EI(S) = 0.4) to aerosol particles in the wake.

The additional atmospheric CO_2 attributable to the HSCTs reaches 0.8 ppmv by 2050, with a RF of +0.01 W m^{-2}. Water vapor change in the stratosphere, about a 10% increase in northern mid-latitudes and less elsewhere, gives a RF of about +0.1 W m^{-2}. The ozone depletion gives a net RF of about -0.01 W m^{-2}. The impacts of sulfate aerosols and soot are negligible in comparison. This total RF of about +0.1 W m^{-2} can be compared with the total RF from all human activities which projects a growth in RF from 1.4 W m^{-2} in 1990 to 3.8 W m^{-2} in 2050, using consistent economic growth scenarios from the IPCC IS92a scenario [Prather, Sausen, Grossman, Haywood, Rind, and Subbaraya, personal communication, 1998]. The HSCT is responsible for less than 5% of this change in total RF, but this is still larger than its 1% share of its fossil fuel use by 2050. The cause of this disproportional climate impact is due to the increases in stratospheric H_2O, a radiative forcing calculation with significant, factor of three, uncertainty.

The HSCT fleet needs to be compared with the subsonic fleet that it would displace assuming fixed air traffic demand. In this case the fleet of 1000 HSCTs would displace about 10% of the subsonic fleet. That portion of the subsonic fleet is responsible for about 0.3 ppmv CO_2 by the year 2050, and a total RF of +0.02 W m^{-2} [Prather, Sausen, Grossman, Haywood, Rind, and Subbaraya, personal communication, 1998]. Thus the HSCT fleet would be expected to produce a small additional global warming, larger than the subsonic fleet that it replaces.

Uncertainty in the prediction of potential climate impacts of HSCTs is large. The RF associated with a given stratospheric water vapor or ozone change varies by a factor of two in radiative calculations made by different groups; this is the result of differences in radiative schemes and the lack of a uniform approach in calculating radiative forcing in the 3-D models for the heterogeneously located aircraft impacts. Hence, the RF from HSCT perturbations to ozone is given a range from -0.05 to +0.01 W m^{-2} and to H_2O a range from 0.03 to 0.3 W m^{-2}, based primarily on the extremes from participating models. For aircraft-induced climate perturbations which are not uniform (e.g., ozone, aerosols, stratospheric water vapor), the addition of individual RFs to produce a total climate impact is accurate only to first order at best. An additional uncertainty concerns the relationship between the global-mean RF and the impact on surface air temperature and regional climate as discussed above. For stratospheric changes in some climate models, the resulting "tropopause" RF does not translate to surface air temperature response in the

same manner as for changes in well mixed gases (e.g., CO_2) or in solar forcing. The radiative imbalance at altitudes away from the surface often produces different feedbacks in the tropospheric water vapor and clouds, an important component of the climate response to a given RF. This assessment can only be considered a preliminary evaluation of the climate change induced by HSCTs relative to that of overall human activities.

4.5.3 Direct Climate Modeling of Aviation Perturbations

Several GCM experiments have been run to assess the absolute climate change from HSCT perturbations. Using the NASA GISS 3-D climate/middle atmosphere model, Rind and Lonergan [1995] studied the impact of the combined effect of stratospheric ozone decrease and tropospheric ozone increase due to an assumed subsonic and HSCT fleet. This equilibrium climate simulation leads to a general stratospheric cooling of a few tenths of a degree, combined with a warming of the lower stratosphere in northern polar regions due to altered atmospheric circulation. The globally averaged surface temperature change was not significant, due to compensating effects of stratospheric ozone reduction and tropospheric ozone increase.

Rind and Lonergan [1995] also investigated the surface temperature response to altered stratospheric water vapor from HSCTs. The surface temperature response was on the order of +0.04°C for an increase in stratospheric water vapor of 7%. Scaling this result to the current estimate for a fleet of 1000 HSCTs (a peak increase of 10%), would provide for an equilibrium warming of about 0.06°C, which is only slightly larger than the model's year-to-year variability. It is also only about half of that expected from the RF given above, since the GCM normally displays a sensitivity of 1°C per W m^{-2} sensitivity. The reduced sensitivity was the result of a reduction in high level cloud cover, as the stratospheric emissions provided radiative warming of the upper troposphere, reducing the relative humidity. This is an example of how the climate response to a specific RF may differ according to the latitudinal and vertical structure of the radiative imbalance. Such results tend to vary from model to model and represent an important uncertainty in the assessment.

4.5.4 The Uncertainty of Background Climate in 2050

Human activities appear to be increasing greenhouse-gas climate warming faster than cooling effects from aerosols [IPCC, 1996]. For a typical scenario for economic growth and emissions of greenhouse gases (IS92a), the global mean surface temperature is expected to increase 0.9°C by the year 2050; and sea level, to rise by 21 cm. Such anthropogenic forcing is likely also to produce a stratosphere different from that in which the current assessment calculations are based.

Current research is addressing this issue. To first order, the increase in CO_2 will lead to cooler temperatures over much of the stratosphere (e.g., Rind *et al.* [1990]), but no clear consensus exists as to potentially more important changes in the circulation and the exchange with the troposphere. For example, one proposal would alter the water vapor cold trap at the tropical tropopause with consequent increases/decreases in stratospheric water vapor. An evaluation of this impact on the HSCT ozone change has been discussed above in the context of the AER model. Another model predicts that the polar lower stratosphere is likely to be several degrees colder. This increase in latitudinal temperature gradient would strengthen the zonal winds in the low-to-mid stratosphere,

potentially affecting wave propagation and NH stratospheric warmings [Shindell *et al.*, 1997] as well as altering the residual circulation by up to 50% in the lower stratosphere [Rind *et al.*, 1998]. These changes could affect the accumulation of HSCT exhaust and the response of ozone in polar regions.

Without an accurate forecast of the future climate, this assessment of HSCT perturbations to the stratosphere acquires some additional uncertainty that is, in most part, beyond the scope of such an environmental assessment. The changes in atmospheric chlorine loading (e.g., our sensitivity studies with 2 and 3 ppbv stratospheric chlorine) impact the HSCT ozone perturbation and are only predictable insofar as nations follow the Montreal Protocol. The volcanic loading of stratospheric sulfur throughout the next century is likewise not predictable and may considered as natural variability. The anthropogenic forcing of a warmer climate can only be treated here as a sensitivity, a parameter of future global economic, technological, and social growth. The response to such scenarios is a major focus of assessments of the physical climate system (e.g., IPCC [1996]). Ideally, here we could adopt the IS92a scenario as given and describe the future climate, including the stratosphere; but this problem is not yet solved and is well beyond this assessment.

In perspective, we note that these external changes lead to background shifts in ozone and climate that are in most cases much larger than the parametric uncertainty in the HSCT assessment. For example, the modeled ozone change between volcanic background aerosols and four times the background is greater than the difference between the HSCT ozone change between these two states. Likewise the possibility of a colder, more isolated Arctic winter vortex in the future would enhance chlorine-catalyzed ozone depletion much more than the differential expected between with and without HSCTs.

4.6 Estimate of HSCT Impact

Tables 4-3 to 4-6 and Figures 4-7 to 4-18 once again illustrate a fact born out by previous assessment efforts: the predicted HSCT impact for different scenarios shows a spread of results, corresponding to the different formulations of assessment models. For decision-making considerations, it is desirable to estimate what is the most likely predicted ozone impact and what are the uncertainties associated with the prediction. These estimates are guided by the range of model results, their behavior in data comparisons, and our knowledge of basic processes.

4.6.1 Criteria for Picking the Central Values

The method we have used to arrive at a "central" value for the HSCT perturbation follows. In the course of our model evaluation, we identified two model characteristics which determine the magnitude and sign of the ozone perturbation: these are the accumulated aircraft NO_y and water (which are primarily controlled by transport), and the concentration of NO_x relative to H_2O and Cl_y, (which indicates whether additions of NO_x will increase or decrease the net chemical ozone tendency). Since H_2O and Cl_y are correlated with NO_y both in models and the atmosphere, we take background NO_y in the lower stratosphere as the best measure of a model's fidelity in calculating the chemical impact of HSCT perturbations.

No measurements of NO_y accumulation exist. Since age of air and accumulation are both related to stratospheric residence time, we use age measurements to estimate the more likely range of accumulation in models. The calculated accumulations correlate positively across models with calculated age of air, however the relationships are different between 2-D and 3-D models (see Figures 4-14 and 4-15). In general, 2-D models' accumulations are better correlated to their calculated age of air and exhibit a larger spread (about a factor of two), while 3-D models exhibit a smaller spread and accumulation is less sensitive to their corresponding age of air. Thus, we assume that the accumulation will lie somewhere between that calculated by 2-D models and 3-D models which best calculate age of air in agreement with observations, GSFC and Monash1.

A central value can then be estimated from model predictions which have two characteristics: a) the NO_y profiles in the lower stratosphere are in good agreement with measurements (Figures 4-2 to 4-4), and b) the calculated accumulation is in the range spanned by 2-D and 3-D model results. Since most models satisfy the second criteria, we use the lower stratospheric NO_y concentrations as the primary discriminator to arrive at a central value. As discussed in Chapter 5, this value is chosen from the CSIRO 2-D model. We expect that refinement of 3-D models will be able to further constrain these estimates.

4.7 Future Directions

This assessment has illustrated a concerted modeling effort in three areas: (a) continued use of 2-D models, with improved parameterization of processes such as PSCs, sulfate aerosol perturbations, and mixing across subtropical and polar barriers; (b) implementation of 3-D assessment models; and (c) incorporation of atmospheric observations which aid in discriminating among model results and point towards more precise prioritization of model-measurement comparison.

The results of these studies suggest future strategies, which could further reduce the current uncertainty in model predictions. These include: (1) 2-D models will continue to play an important role in exploring the parameter space of HSCT perturbations which, due to computational limitations, cannot be carried out by current 3-D assessment models. (2) 2-D models would also play an important role in exploring the impact of dynamical and chemical parameterizations, which can be reduced, to first order, to a 2-D approximation. (3) 3-D models provide the best representation of lower stratospheric/upper tropospheric processes, in a manner that is qualitatively different from 2-D models. However, future reliance on 3-D models will rest upon the accuracy of their chemical and dynamical representations. In particular, it is important to achieve consistency in 3-D predictions of temperature, age-of-air, propagation of seasonal cycles, and calculated NO_y and ozone concentrations in the lower stratosphere. (4) Model improvements to reduce the discrepancy with atmospheric observations will reduce the uncertainty in HSCT predictions. We have utilized the comparison of model performance for age of air and lower stratospheric NO_y to guide our assessment of the predictions and thus reduce the subjectivity involved in estimating the ozone impact and uncertainties. However, model performance against other parameters remains unexplored, and should be addressed in future assessments. These include: profiles of Cl_y and H_2O; and development and application of appropriate diagnostics for polar processes.

4.8 Summary

General Conclusions

- A set of global atmospheric chemistry and transport models has been used to calculate the impacts of a proposed fleet of HSCT aircraft for a variety of possible future scenarios. This report expands on previous assessments with the inclusion of a number of 3-D models in addition to the 2-D models that have been the backbone of previous assessments. In addition to individual research 3-D models, we introduce the GMI that for the first time provides 3-D assessment calculations within a framework allowing direct comparison of critical model components (e.g., tracer transport, photochemical modules).

- In most cases the models have incorporated a number of improvements guided by recent observations, analysis of model results, and recommendations of previous assessments. These improvements are: (1) inclusion of exhaust sulfur particle production; (2) updated parameterization for heterogeneous reaction rates; and (3) the effect of PSCs and/or cold sulfate aerosols with parameterized temperature variability.

- For a projected fleet of 500 HSCTs the models calculate a decrease in ozone in the middle and upper stratosphere. In the lower stratosphere, most models calculate an increase in ozone, particularly if the sulfur particle production in the exhaust is assumed to be negligible. The extent of the region of calculated increase in ozone is variable from model to model due to differences in their transport formulation and their interaction with chemistry (see Figure 4-12). The response of the total column ozone is thus often a cancellation between the decreases in the middle-upper stratosphere and the increases in the lower stratosphere.

- The calculated column ozone perturbation for volcanically clean conditions does not change significantly over the range of EI_{NO_X} from 0 to 10, for a fleet of 500 HSCTs. In this case, the dominant perturbation to ozone is driven by HO_x from H_2O emissions. For EI_{NO_X} of order 10 or larger, or with a fleet size of 1000, the ozone depletion increases with increasing EI_{NO_X}.

- Fuel sulfur has a potentially important impact on the calculated ozone perturbation. The HSCTs act similar to a volcanic injection of sulfur in increasing the surface area of stratospheric sulfate particles available for heterogeneous reactions and increasing the HO_x and halogen-catalyzed destruction of ozone in the lower stratosphere. Note that the potential increase in sulfate area and the consequent decrease in column ozone that are possible for HSCTs are dwarfed by that which occurred for the two recent volcanic eruptions of El Chichon and Mount Pinatubo.

- All models calculate a significantly smaller perturbation in column ozone when the flight altitude is decreased by 2 km.

Model Tests

- For the first time we have quantitative tests of both the dynamics and chemistry in the stratospheric models. These tests are still incomplete but provide a guide for discriminating a

subset of models that can better simulate certain atmospheric processes, and thus guide us in estimating the likely value for the ozone change due to HSCTs.

- The age of air calculated by models was compared to values derived from CO_2 and SF_6 observations. For most models, the calculated age of air is too young. HSCT exhaust accumulation in models is expected to be related to the model's age of air through the stratospheric residence time. Results from different 2-D models show accumulations which span a range of over a factor of three. The exhaust amounts exhibit a clear correlation with each model's calculated age of air. On the other hand, 3-D models participating in the M&M II exercise yield a narrower range of accumulations (ranging by a factor of about 1.5) and less correlation with age of air. For a given age of air, the accumulations calculated by 2-D models are larger than those calculated by 3-D models. Thus, we choose that the best estimate for accumulation as that between the values calculated by 2-D and 3-D models with the most realistic age of air.

- Models were also evaluated on their calculated profiles of ambient NO_y and ozone in the lower stratosphere. The range of model-calculated NO_y showed a large scatter about the observations, spanning a range of a factor of 2 larger and smaller than the measurements. Three-dimensional models generally calculate NO_y smaller than observations. On the other hand, agreement with ozone profiles is better for 3-D models than for most 2-D models. Since the ozone perturbation in the lower stratosphere is also very sensitive to the relative abundance of NO_y, water, and Cl_y, we consider the NO_y test crucial. The relative importance of agreement with ozone, Cl_y and water needs to be evaluated.

Specific Results

- For an HSCT fleet of 500 aircraft with an EI_{NO_x} of 5, volcanically-clean 2015 atmospheric conditions and no sulfur emissions, the models in this assessment calculate a mean Northern Hemispheric total ozone change of -0.4% to +0.2 (see Table 4-3). The extreme positive and negative perturbations correspond to models with the lowest and highest NO_y concentrations in the lower stratosphere (i.e., GMI and GSFC 2-D, respectively).

- When 10% of the sulfur in the fuel is assumed to be converted into small particles, the models (only a subset of those used above) calculate a mean Northern Hemispheric total ozone change of -0.8 to -0.2% (in the absence of volcanic aerosols). At the extreme of assuming that 100% of the sulfur is converted to small particles, the model calculations for mean Northern Hemispheric total ozone change range from -1.3 to -0.3%. These sulfur calculations are subject to uncertainty because the change in surface area was done by only one 2-D model.

- Adopting as most likely the case where 10% of the sulfur is converted into fine particles, our best estimate for the HSCT-induced ozone change is -0.4% for mean Northern Hemispheric ozone loss. This is the value obtained by the model (2-D model from CSIRO) which most closely reproduces the observed NO_y in the lower stratosphere. This model's calculated accumulation also lies between the bounds provided by those 2-D and 3-D models with calculated age of air closest to observations.

- For an atmosphere with volcanically perturbed aerosol surface area densities at four times the background, the models (only a subset of those used above) calculate a mean Northern Hemispheric total ozone change of -0.2% to 0%. This volcanically perturbed atmosphere typically has less ozone even in the absence of HSCTs, because of the increase in surface area density of aerosols.

- The models calculate smaller HSCT-induced perturbations at the equator than at mid-latitudes and polar regions. Some models found significantly increased perturbations in the polar winter and spring (as much as -1.0 to -1.5% for the basic scenario with a fleet of 500 aircraft with an EI_{NO_X} of 5 g/kg of fuel and no conversion of sulfur to particles). The 2-D models do not have good representations of transport processes across the polar vortex, and overestimate the transport of exhaust and ozone into and out of the vortex. Thus these results must be viewed with caution, but they do highlight an important potential sensitivity of the stratosphere to aircraft exhaust.

- A notable uncertainty in these assessments of future HSCT-induced ozone change is the future atmosphere. Depending on scenarios for changes in key source gases and the climate itself (particularly the polar temperatures) the models can become more or less sensitive to HSCT perturbations to NO_y, H_2O and particles. This uncertainty cannot be quantified at this time.

- The forcing of climate attributable to an HSCT fleet has been calculated. The most prominent climate-related perturbations are to stratospheric H_2O, global CO_2, and stratospheric O_3. The net result is a surface warming by 2050, which is small relative to that expected from other anthropogenic forcings.

- The accumulation of HSCT water vapor in the stratosphere is the dominant climate forcing, although the ability to predict this accumulation and its climate impact is uncertain to a factor of three or more. Flying 2 km lower would reduce the accumulation of stratospheric H_2O.

Table 4-1. List of models that contributed results to this report.

Model Names	Institution	Model Team	Contact Person for Model	Contact Person for Results in this Report
2-D Models				
AER	Atmospheric and Environmental Research, Inc., USA	Malcolm Ko, Debra Weisenstein, Courtney Scott, Jose Rodriguez, Run-Lie Shia, N. D. Sze	Malcolm Ko	Debra Weisenstein
CSIRO	Commonwealth Scientific and Industrial Research Organization (CSIRO) Telecommunications and Industrial Physics, Australia	Keith Ryan, Ian Plumb, Peter Vohralik, Lakshman Randeniya	Keith Ryan	Peter Vohralik
GSFC	NASA Goddard Space Flight Center, USA	Charles Jackman, David Considine, Eric Fleming	Charles Jackman	Charles Jackman
LLNL	Lawrence Livermore National Laboratory USA	Peter Connell, Keith Grant, Douglas Kinnison, Douglas Rotman	Douglas Kinnison	Douglas Kinnison
SUNY-SPB	State University of New York at Stony Brook, USA, and Russian State Hydrometeorological Institute, St. Petersberg, Russia	Sergei Smyshlyaev, Marvin Geller, Victor Dvortsov, Valery Yudin	Sergei Smyshlyaev	Sergei Smyshlyaev
3-D Models				
GMI	NASA AESA	Douglas Rotman, Jose Rodriguez, GMI Science Team	Jose Rodriguez	Douglas Rotman
SLIMCAT	University of Cambridge, UK	Helen Rogers, Martyn Chipperfield, John Pyle	Martyn Chipperfield	Helen Rogers
LaRC	NASA Langley Research Center, USA	William Grose Richard Eckman	William Grose	William Grose

Table 4-2. A) Source gas boundary conditions for the 2015 and 2050 atmospheres. B) SAD distributions used in this assessment. These SAD distributions consider volcanically clean conditions, average conditions over a volcanically active period, and assumptions on additional SAD from proposed aircraft plume produced SO_2 gas-to-particle conversions.

A)

Species	Units	Year 2015	Year 2050
CFC-11	pptv	220	120
CFC-12	pptv	470	350
CFC-113	pptv	80	60
CCl_4	pptv	70	35
HCFC-22	pptv	250	15
CH_3CCl_3	pptv	3	0
HCFC-141b	pptv	12	0
Halon-1301	pptv	1.4	0.9
Halon-1211	pptv	1.1	0.2
CH_3Cl	pptv	600	600
CH_3Br	pptv	10	10
CH_4	ppbv	2052	2793
N_2O	ppbv	333	371
CO_2	ppmv	405	509

B)

Sulfate Surface Area Density Name	Fleet Size	SO_2 Gas-to-Particle Conversion in Plume	Additional Comments
SA0**	0	None	Volcanically Clean
4xSA0	0	None	Volcanically Active Period
SA1	500	50%	-
SA2	1000	50%	-
SA2-2km	1000	50%	HSCT Cruise Altitude Lowered by 2km
SA3	500	100%	-
SA5	500	10%	-
SA6	1000	10%	-
SA6-2km	1000	10%	HSCT Cruise Altitude Lowered by 2km
SA7	500	0%	-

**SAO is taken from Table 8.8, WMO [1992].

Table 4-3. Percentage changes in total column ozone for each assessment model. All total column ozone changes are relative to a reference atmosphere that includes a subsonic fleet and a sulfate surface area density that is representative of a volcanically clean atmosphere. The top value is for the NH average, the bottom value is for the SH average. Source gas boundary conditions are for the year 2015. The HSCT cruise altitude is representative of a TCA. The model results have been rounded off to one significant figure for clarity.

HSR Scenario	Cl_y ppbv	Fleet Size	EI NO_x	Alt. km	SAD Desc.	Ref. Atm	AER 2-D	GSFC 2-D	LLNL 2-D	CSIRO 2-D	SUNY 2-D	GMI 3-D	LaRC 3-D
1	3.0	Sub	-	-	SA0	-	-	-	-	-	-	-	-
							-	-	-	-	-	-	-
2 No H_2O	3.0	500	5	TCA	SA0	1	-0.07	-0.1	-0.01	-0.09	-0.002	-	-
							-0.03	+0.03	+0.1	-0.07	+0.03	-	-
3 H_2O only	3.0	500	0	TCA	SA0	1	-0.6	-0.4	-0.3	-0.2	-0.2	-	-
							-0.3	-0.8	-0.3	-0.07	-0.1	-	-
4	3.0	500	5	TCA	SA0	1	-0.3	-0.4	-0.2	-0.2	-0.2	+0.2	-0.05
							-0.1	-0.8	-0.2	-0.1	-0.1	+0.05	-0.1
5	3.0	500	10	TCA	SA0	1	-0.3	-0.6	-0.3	-0.3	-0.2	-	+0.07
							-0.1	-0.7	-0.1	-0.2	-0.06	-	-0.03
6	3.0	1000	5	TCA	SA0	1	-0.7	-0.9	-0.5	-0.5	-0.3	-	-
							-0.3	-1.4	-0.3	-0.2	-0.2	-	-
7	3.0	1000	10	TCA	SA0	1	-0.7	-1.4	-0.7	-0.7	-0.4	-	-
							-0.2	-1.4	-0.2	-0.3	-0.1	-	-
8	3.0	500	15	TCA	SA0	1	-0.3	-0.8	-0.4	-0.5	-	-	-
							-0.05	-0.7	-0.01	-0.3	-	-	-
9	3.0	500	5	TCA	SA5	1	-0.8	-0.7	-0.5	-0.4	-0.3	-	-
							-0.3	-0.9	-0.3	-0.1	-0.1	-	-
10	3.0	500	5	TCA	SA1	1	-1.0	-1.1	-0.7	-0.5	-0.3	-	-0.4
							-0.4	-1.1	-0.5	-0.1	-0.2	-	-0.3
11	3.0	500	10	TCA	SA1	1	-0.8	-1.1	-0.7	-0.5	-0.3	-	-
							-0.3	-1.0	-0.4	-0.2	-0.1	-	-
12	3.0	500	5	TCA	SA3	1	-1.1	-1.3	-0.8	-0.5	-0.4	-	-
							-0.4	-1.2	-0.6	-0.1	-0.2	-	-
13	3.0	500	5	TCA	SA7	1	-0.6	-	-	-	-	-	-
							-0.3	-	-	-	-	-	-
14	3.0	500	5	-2 km	SA0	1	-0.1	-0.09	-0.05	-0.05	-0.07	-	-
							-0.04	-0.2	-0.01	-0.03	-0.04	-	-
15	3.0	500	10	-2 km	SA0	1	-0.2	+0.1	-0.03	-0.003	-0.02	-	-
							-0.1	-0.06	+0.07	-0.03	-0.006	-	-
16	3.0	1000	5	-2 km	SA0	1	-0.3	-0.2	-0.1	-0.09	-0.1	-	-
							-0.2	-0.4	-0.02	-0.05	-0.08	-	-
17	3.0	500	5	+2km	SA0	1	-0.7	-1.0	-0.6	-0.6	-	-	-
							-0.2	-1.2	-0.3	-0.2	-	-	-
18	1.0	Sub	-	-	SA0	-	-	-	-	-	-	-	-
							-	-	-	-	-	-	-
19	1.0	500	5	TCA	SA0	18	-0.3	-0.5	-	-	-	-	-
							-0.1	-0.5	-	-	-	-	-
20	1.0	500	5	TCA	SA1	18	-0.5	-0.7	-	-	-	-	-
							-0.2	-0.7	-	-	-	-	-
21	4.0	Sub	-	-	SA0	-	-	-	-	-	-	-	-
							-	-	-	-	-	-	-
22	4.0	500	5	TCA	SA0	21	-0.4	-0.4	-	-	-	-	-
							-0.1	-0.8	-	-	-	-	-
23	4.0	500	5	TCA	SA1	21	-1.0	-1.1	-	-	-	-	-
							-0.4	-1.0	-	-	-	-	-

Table 4-4. Percentage changes in total column ozone for each assessment model. All total column ozone changes are relative to a reference atmosphere that includes a subsonic fleet and a sulfate surface area density that is representative of a volcanically active atmosphere. The top value is for the NH average, the bottom value is for the SH average. Source gas boundary conditions are for the year 2015. The HSCT cruise altitude is representative of a TCA. The model results have been rounded off to one significant figure for clarity.

HSR Scenario	Cl_y ppbv	Fleet Size	EI NO_x	Alt. km	SAD Desc.	Ref. Atm	AER 2-D	GSFC 2-D	LLNL 2-D	CSIRO 2-D	SUNY 2-D
24	3.0	Sub	-	-	4xSA0	-	- -	- -	- -	- -	- -
25 H_2O only	3.0	500	0	TCA	4xSA0	24	-0.5 -0.2	-0.5 -0.7	-0.4 -0.3	-0.3 -0.1	-0.3 -0.2
26	3.0	500	5	TCA	4xSA0	24	-0.2 -0.09	-0.04 -0.5	-0.2 -0.2	-0.09 -0.09	-0.1 -0.1
27	3.0	500	10	TCA	4xSA0	24	+0.04 +0.02	+0.2 -0.4	+0.001 -0.04	+0.03 -0.08	-0.03 -0.01
28	3.0	500	15	TCA	4xSA0	24	+0.2 +0.1	+0.4 -0.3	+0.09 +0.07	+0.09 -0.07	+0.04 +0.04
29	3.0	500	5	TCA	4xSA0+ SA1-SA0	24	-0.5 -0.2	-0.4 -0.6	-0.3 -0.3	-0.2 -0.1	-0.2 -0.1
30	3.0	500	5	TCA	4xSA0+ SA3-SA0	24	-0.6 -0.2	-0.5 -0.7	-0.4 -0.3	-0.3 -0.1	-0.2 -0.1

Table 4-5. Percentage changes in total column ozone for each assessment model. All total column ozone changes are relative to a reference atmosphere that includes a subsonic fleet and a sulfate surface area density that is representative of a volcanically clean atmosphere. The top value is for the NH average, the bottom value is for the SH average. Source gas boundary conditions are for the year 2015. In all the scenarios listed in this table the heterogeneous chemistry processes on cold aerosols were removed. The HSCT cruise altitude is representative of a TCA. The model results have been rounded off to one significant figure for clarity.

HSR Scenario	Cl_y ppbv	Fleet Size	EI NO_x	Alt. km	SAD Desc.	Ref. Atm	AER 2-D	GSFC 2-D	LLNL 2-D	CSIRO 2-D	SUNY 2-D
29 No PSCs	3.0	Sub	-	-	SA0	-	- -	- -	- -	- -	- -
30 No PSCs	3.0	500	0	TCA	SA0	29	-0.5 -0.3	-0.4 -0.3	-0.3 -0.2	-0.2 -0.07	-0.2 -0.1
31 No PSCs	3.0	500	5	TCA	SA0	29	-0.2 -0.1	-0.4 -0.3	-0.3 -0.1	-0.2 -0.1	-0.2 -0.09
32 No H_2O, PSCs	3.0	500	5	TCA	SA0	29	-0.1 -0.1	-0.2 -0.02	-0.06 +0.07	-0.09 -0.07	-0.01 +0.02

Table 4-6. Percentage changes in total column ozone for each assessment model. All total column ozone changes are relative to a reference atmosphere that includes a subsonic fleet and a sulfate surface area density that is representative of a volcanically clean atmosphere. The top value is for the NH average, the bottom value is for the SH average. Source gas boundary conditions are for the year 2050. The HSCT cruise altitude is representative of a TCA. The model results have been rounded off to one significant figure for clarity.

HSR Scenario	Cl_y ppbv	Fleet Size	EI NO_x	Alt. km	SAD Desc.	Ref. Atm	AER 2-D	GSFC 2-D	LLNL 2-D	CSIRO 2-D	SUNY 2-D
33	2.0	Sub	--	TCA	SA0	--	--	--	--	--	--
34	2.0	1000	5	TCA	SA0	33	-0.6	-1.0	-0.5	-0.5	-0.3
							-0.2	-1.4	-0.3	-0.2	-0.2
35	2.0	1000	10	TCA	SA0	33	-0.7	-1.6	-0.8	-0.9	-0.4
							-0.2	-1.5	-0.2	-0.4	-0.2
36	2.0	1000	5	TCA	SA6	33	-0.8	-1.1	-0.6	-0.6	-0.4
							-0.3	-1.5	-0.4	-0.2	-0.2
37	2.0	1000	5	TCA	SA2	33	-0.8	-1.3	-0.8	-0.6	-
							-0.3	-1.7	-0.6	-0.09	-
38	2.0	1000	5	-2 km	SA0	33	-0.2	-0.3	-0.1	-0.1	-0.1
							-0.05	-0.5	-0.02	-0.05	-0.08
39	2.0	1000	10	-2 km	SA0	33	-0.2	-0.6	-0.2	-0.09	-0.08
							+0.01	-0.5	+0.04	-0.05	-0.05
40	2.0	1000	5	-2 km	SA6-2km	33	-0.4	-0.5	-0.3	-0.2	-0.2
							-0.1	-0.6	-0.2	-0.04	-0.1
41	2.0	1000	5	-2 km	SA2-2km	33	-0.5	-0.6	-0.4	-0.2	-0.2
							-0.1	-0.6	-0.2	-0.03	-0.1
42*	2.0	Sub	--	TCA	SA0	--	--	--	--	--	--
43*	2.0	1000	5	TCA	SA6	42	-0.8	-1.0	-0.7	-0.6	-0.4
							-0.2	-1.3	-0.4	-0.2	-0.2

*Climate study (see text).

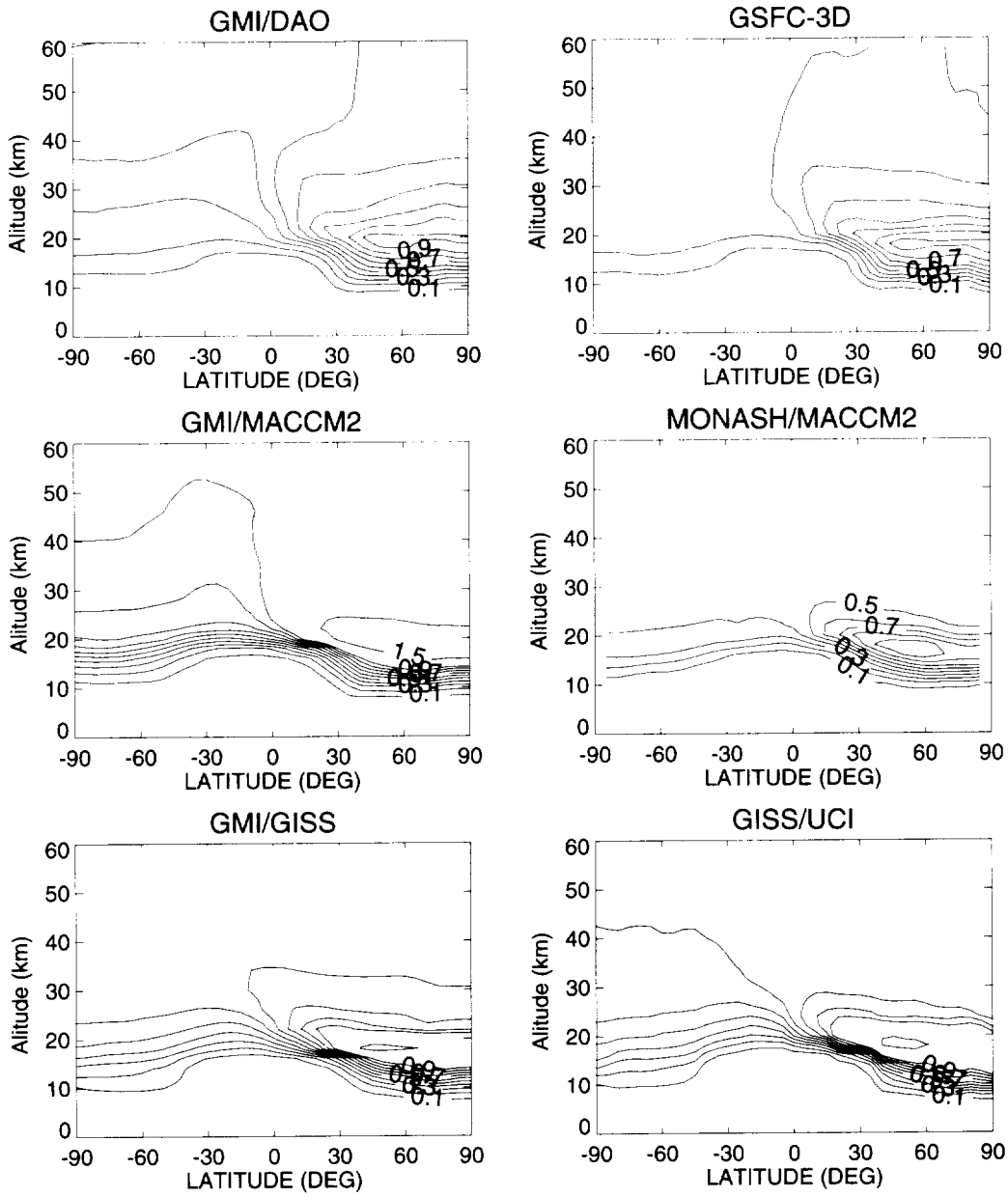

Figure 4-1. Aircraft NO_y tracer accumulation from selected 3-D models participating in the NASA M&M II exercise. Results are plotted in contours of 0.1 ppbv, except for GMI/MACCM2, where an extra contour of 1.5 ppbv has been added. The left column shows results from the GMI model as run with the 3 sets of meteorological input data: NASA/DAO-STRAT assimilated data, the NCAR/MACCM2, and the GISS II' climate model. The right column shows results of simulations using advection schemes from the institutions providing the wind data. Differences between GMI runs and parent institution runs can be attributed to GISS: advection schemes, NASA/DAO: resolution (GSFC ran at finer resolution), and NCAR: combination of advection scheme and impact of the NCAR mass fixer (needed for NCAR's SLT transport). Differences within the 3 GMI simulations show differences in residence time and circulation patterns of the meteorological data.

(a)

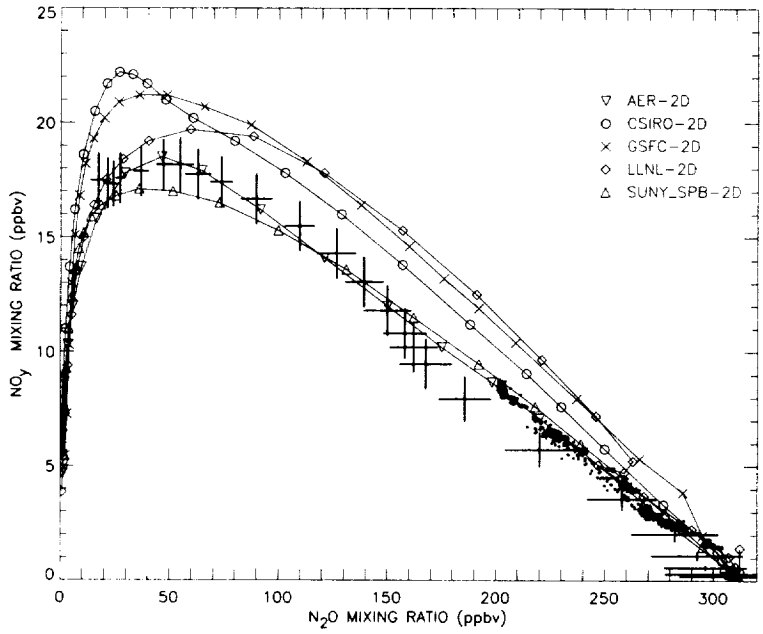

(b)

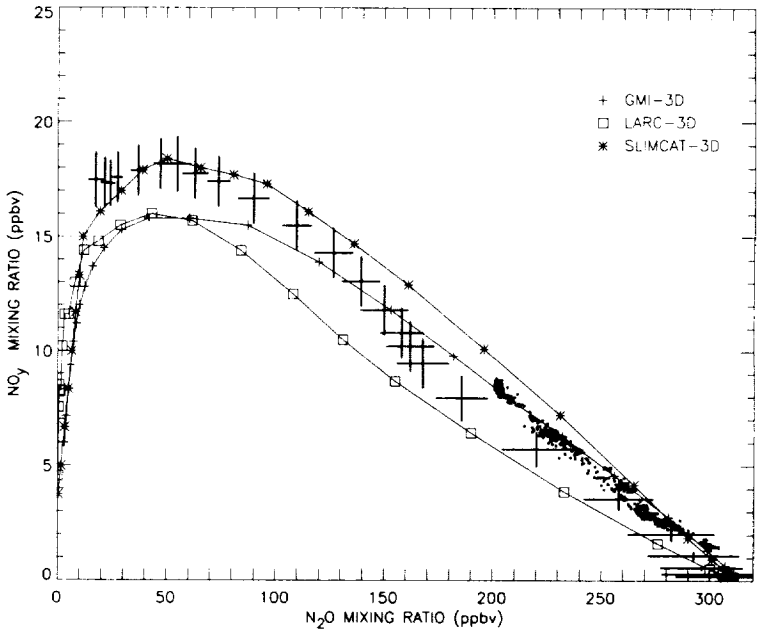

Figure 4-2. NO_y vs. N_2O correlations as derived from data and participating models. Panels a and b compare measured correlations with those calculated by 2-D and 3-D models, respectively. Data are from MkIV measurements at 35°N September 1993 (crosses) and ER-2 data at 25°N-35°N February 1992 (dots). Model calculations are shown for 35°N September. Model output for February is essentially the same as September in the range of the ER-2 data.

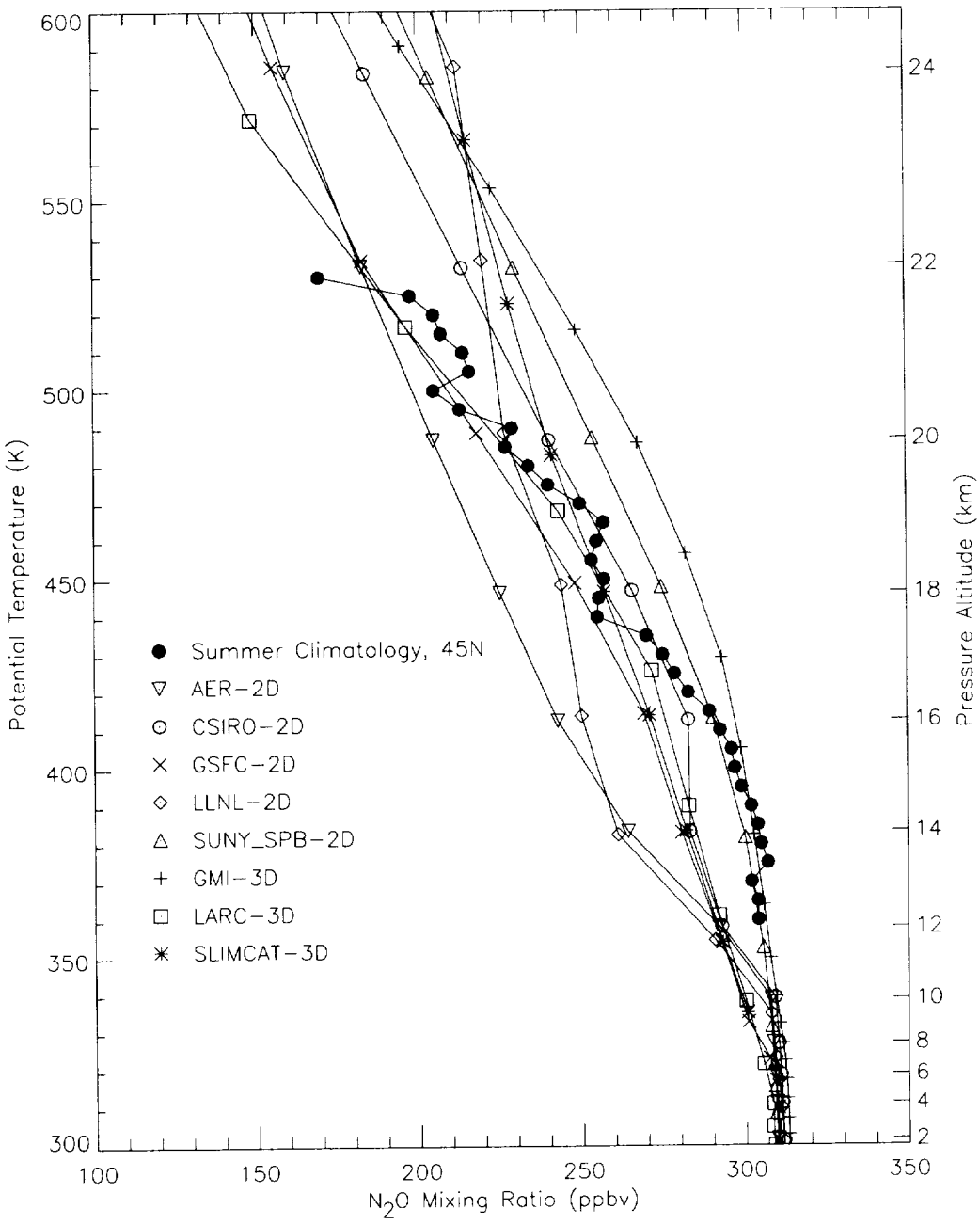

Figure 4-3. Comparison of calculated N_2O profiles (vs. potential temperature) for 1992 model conditions and climatological N_2O profiles derived from all ER-2 flights [Strahan *et al.*, 1999] at 45°N, summer season. The pressure altitude scale assumes a typical mid-latitude model atmosphere.

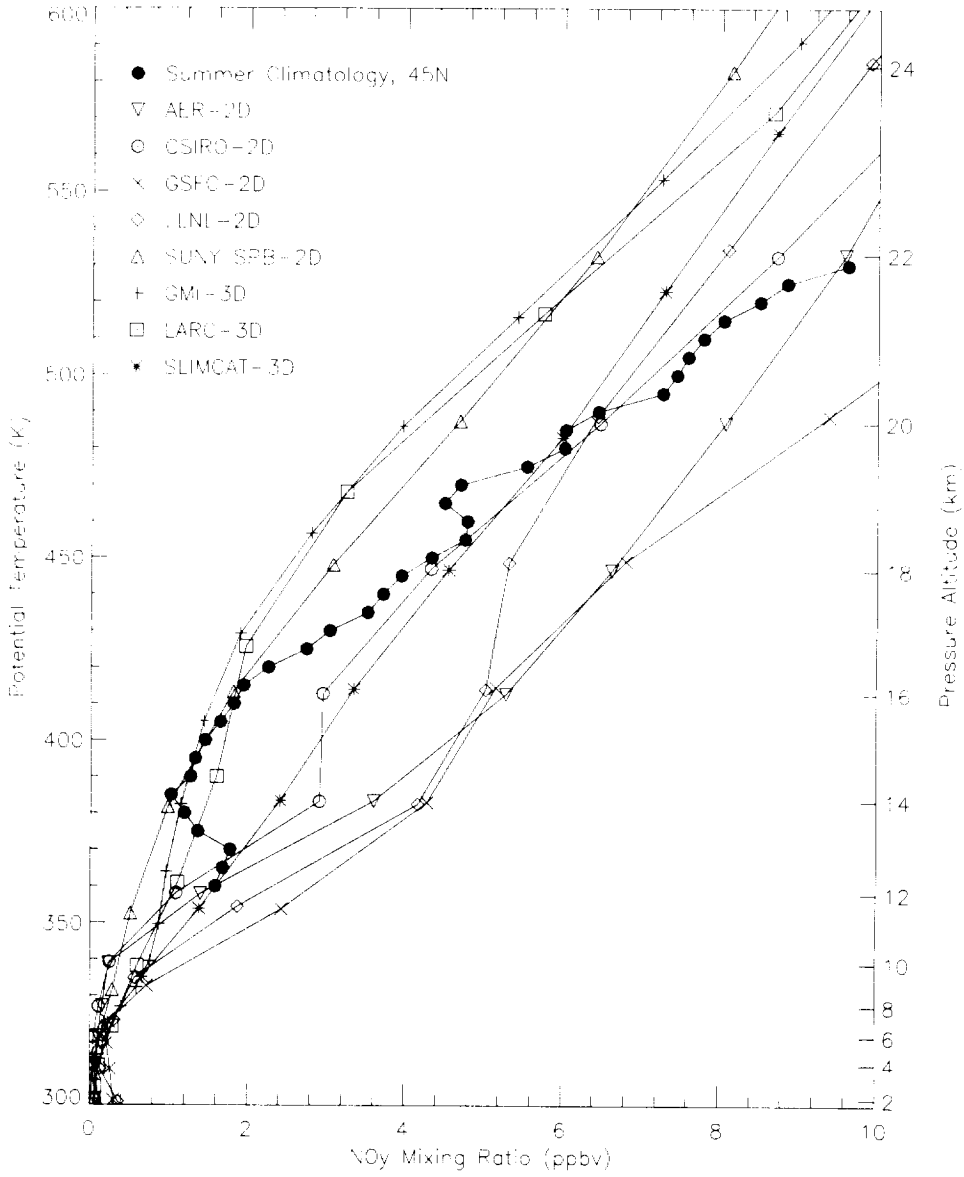

Figure 4-4. Comparison of 1992 model profiles for NO_y and climatological NO_y derived from ER-2 measurements [Strahan, personal communication] at 45°N, summer season. Pressure altitude scale is the same as for Figure 4.3.

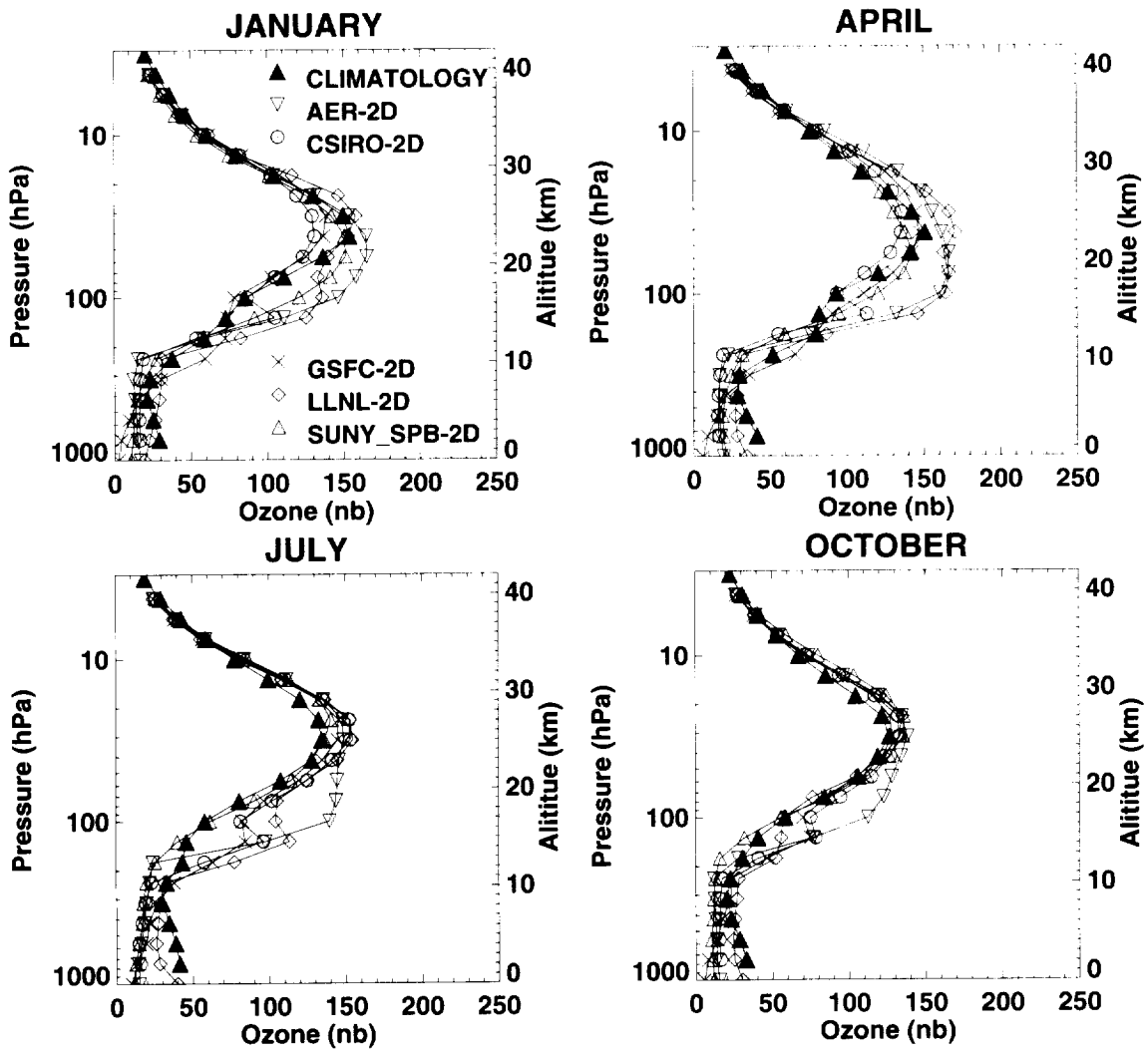

Figure 4-5a. Comparison of 1992 model results and climatological O_3 partial pressures derived from ozone sonde measurements between 40-50°N for January, April, July, and October [Logan, personal communication]. Model results are taken from the 1998 NASA M&M II intercomparison [Park *et al.*, 1999].

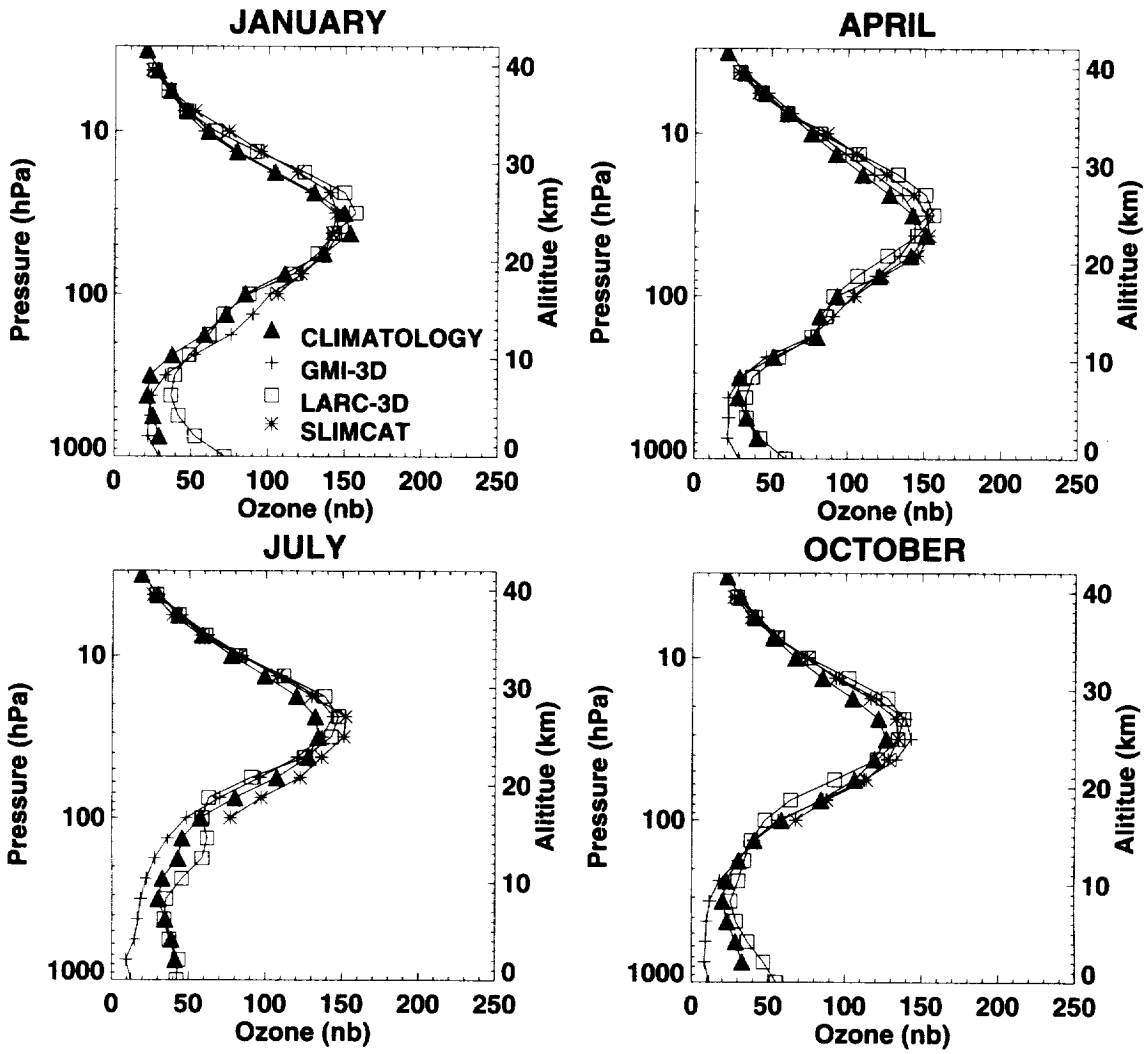

Figure 4-5b. Same as Figure 4-5a, except for model results for participating 3-D models.

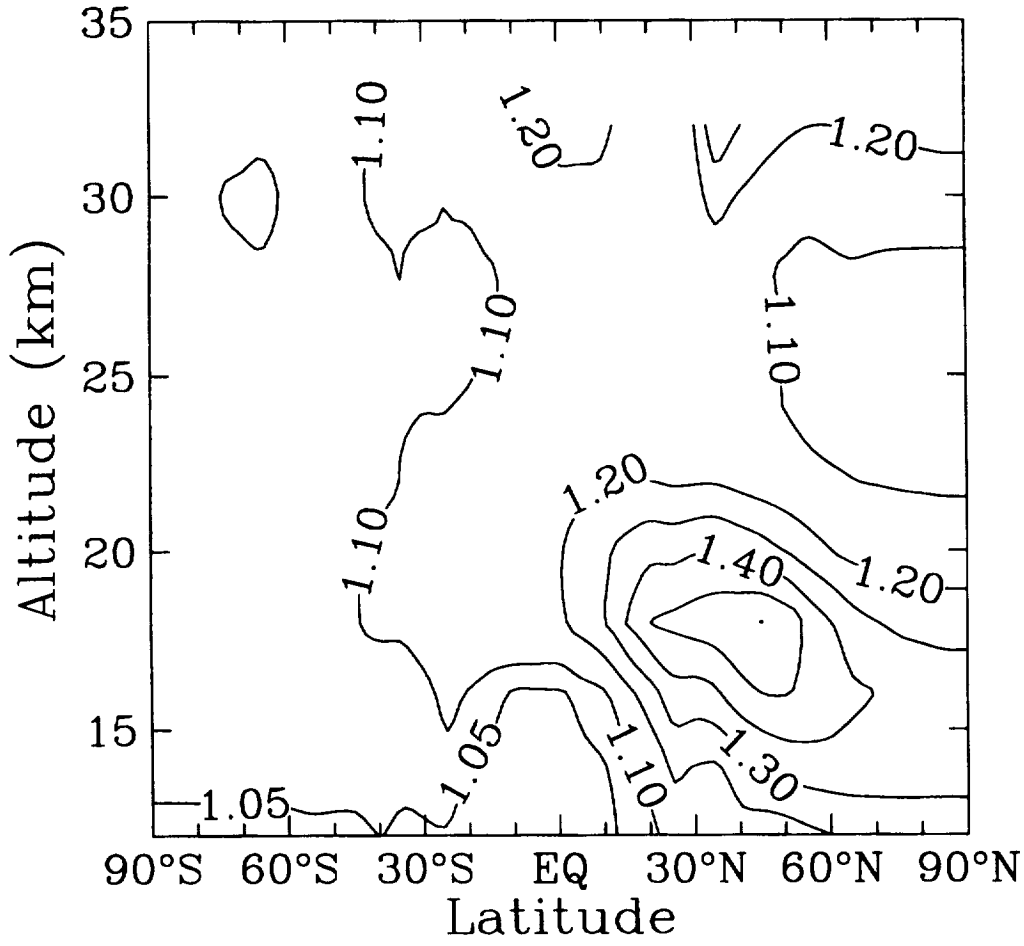

Figure 4-6. Calculated ratio of the HSCT-enhanced sulfate aerosol surface area density to that of clean volcanic conditions. The surface area enhancements were calculated by the AER 2-D model with interactive microphysics, assuming a 10% gas-to-particle conversion of fuel sulfur in the aircraft plume. These enhancements were used by all other participating models.

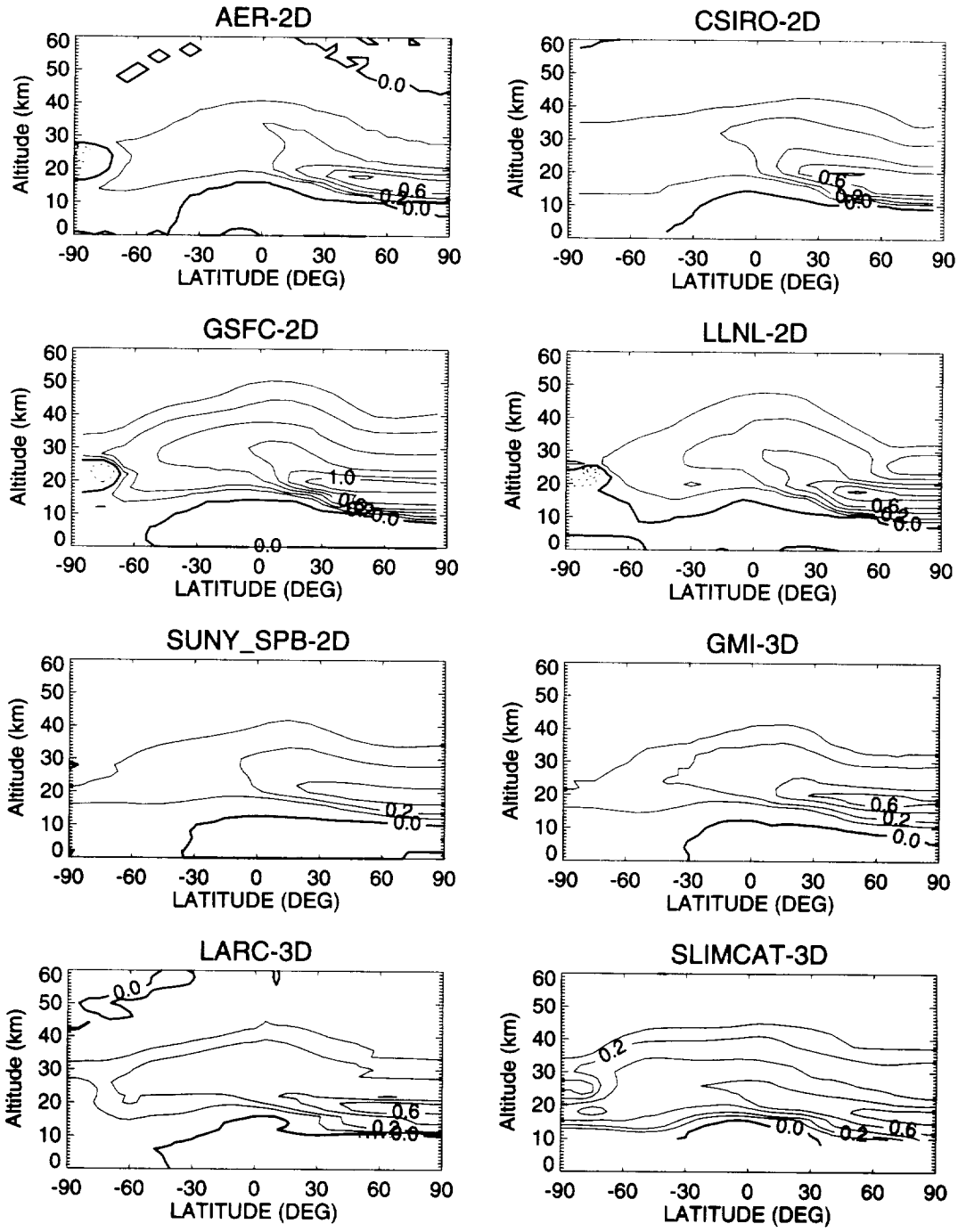

Figure 4-7. Calculated HSCT-induced change in NO_y (ppbv) during June. Results are shown for scenario 4 (EI_{NO_x} = 5 g NO_2/kg fuel, 500 aircraft; see Table 4-3) relative to scenario 1 (subsonic only condition). Contours are drawn for 0.0, 0.1, and 0.2 ppbv, and in increments of 0.2 ppbv thereafter.

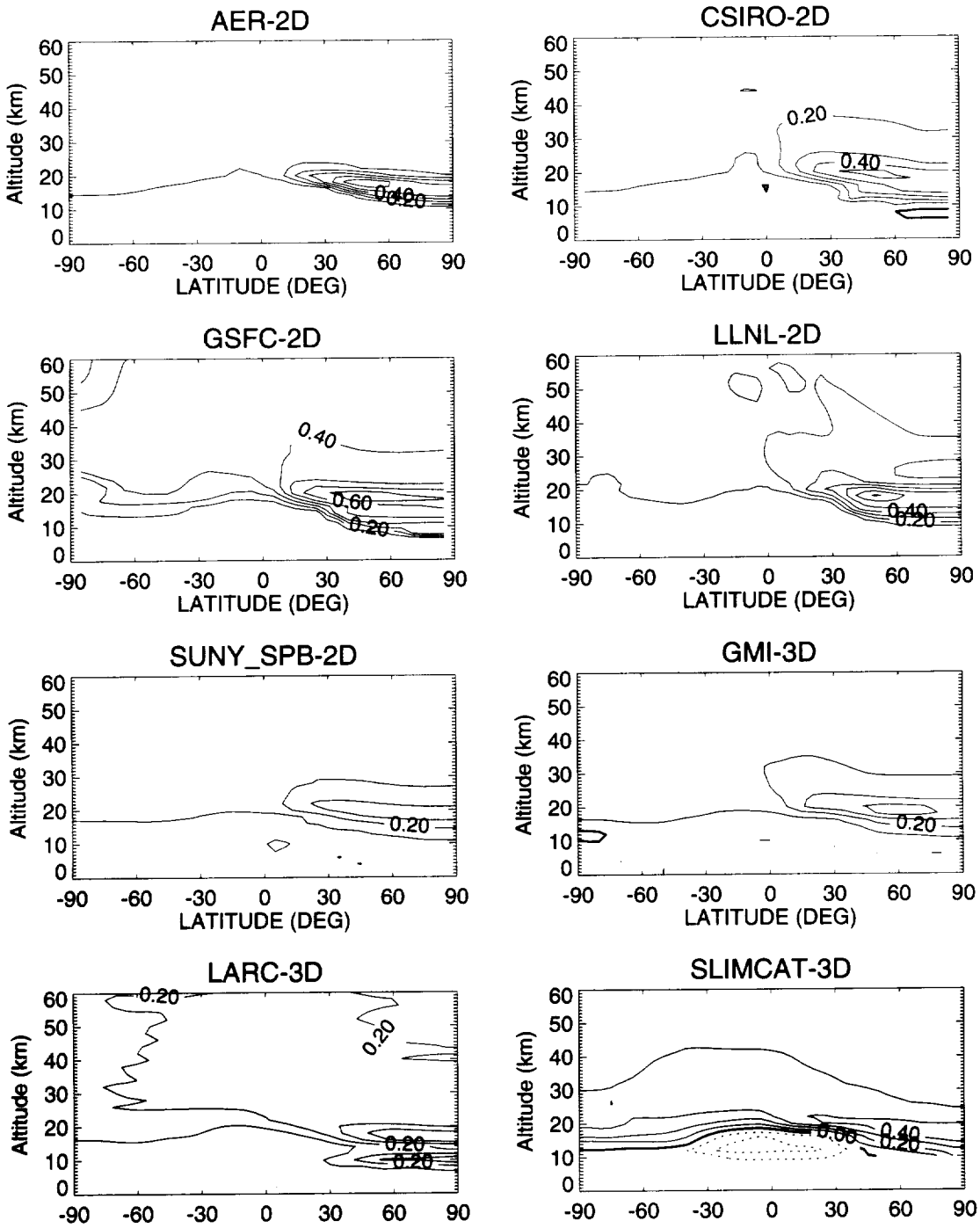

Figure 4-8. Calculated HSCT induced change in H_2O (ppmv) during June. Results are shown for scenario 4 (500 aircraft) relative to scenario 1 (subsonic only condition). Contours are in units of 0.1 ppmv.

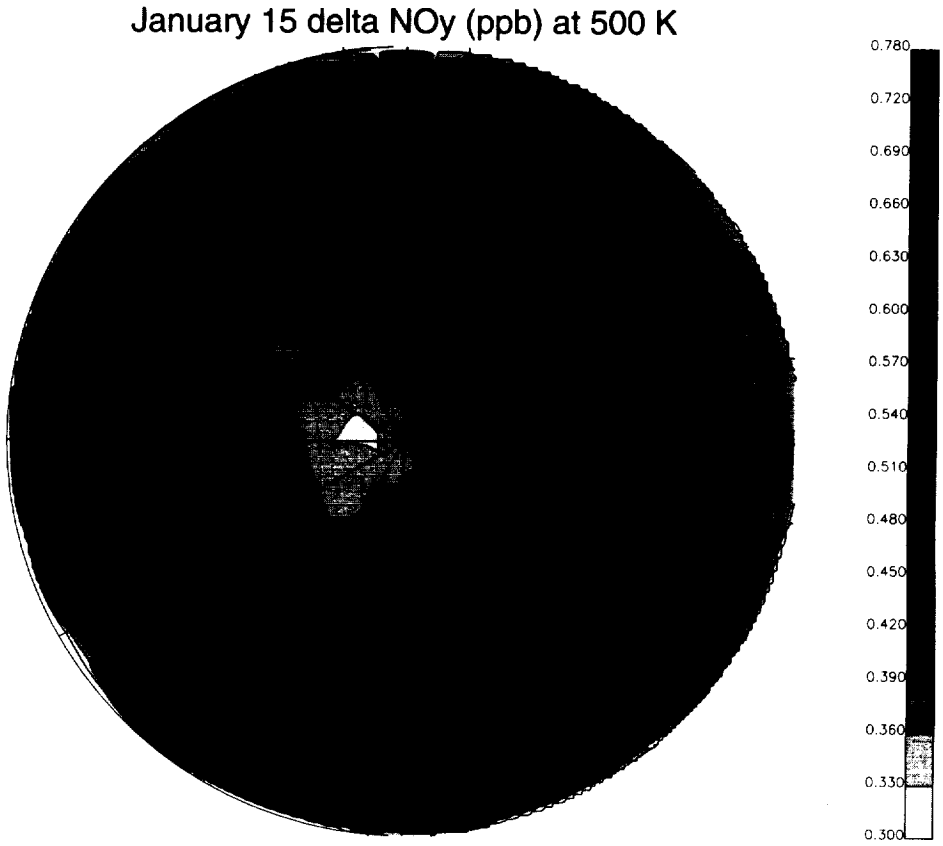

Figure 4-9. Accumulation of NO_y (in ppbv) in the NH at a potential temperature surface of 500 K (around 20 km), as calculated by the GMI model for January 15 conditions, for the standard fleet of 500 HSCTs (scenario 4 – scenario 1). Results are shown in a polar orthographic projection centered at the North Pole.

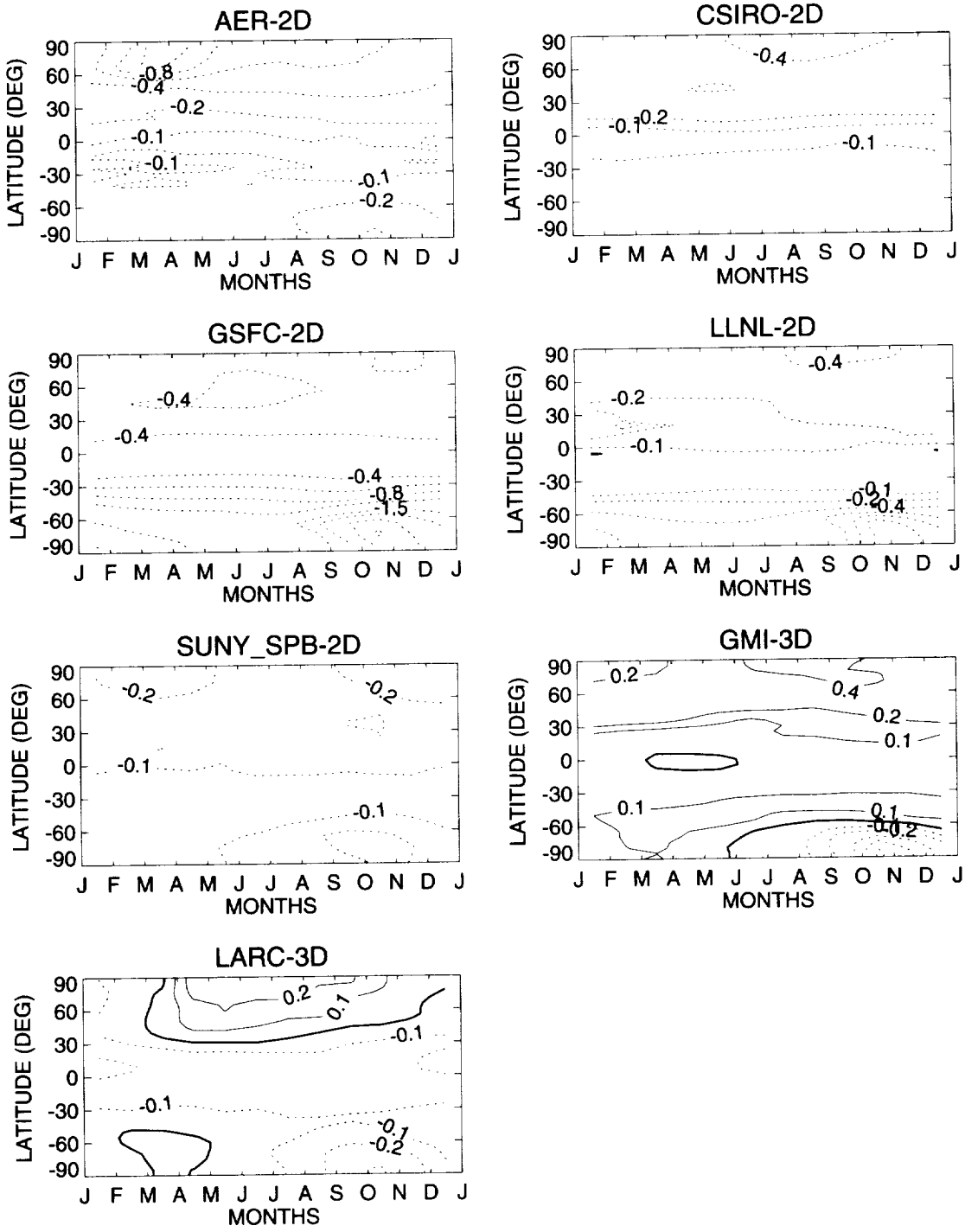

Figure 4-10a. Seasonal dependence of calculated HSCT-induced change in column O_3 (%). Results are shown for scenario 4 (EI_{NO_x} = 5 g NO_2/kg fuel, 500 aircraft) relative to scenario 1 (subsonic only condition). This scenario assumes no sulfur emission in the aircraft exhaust.

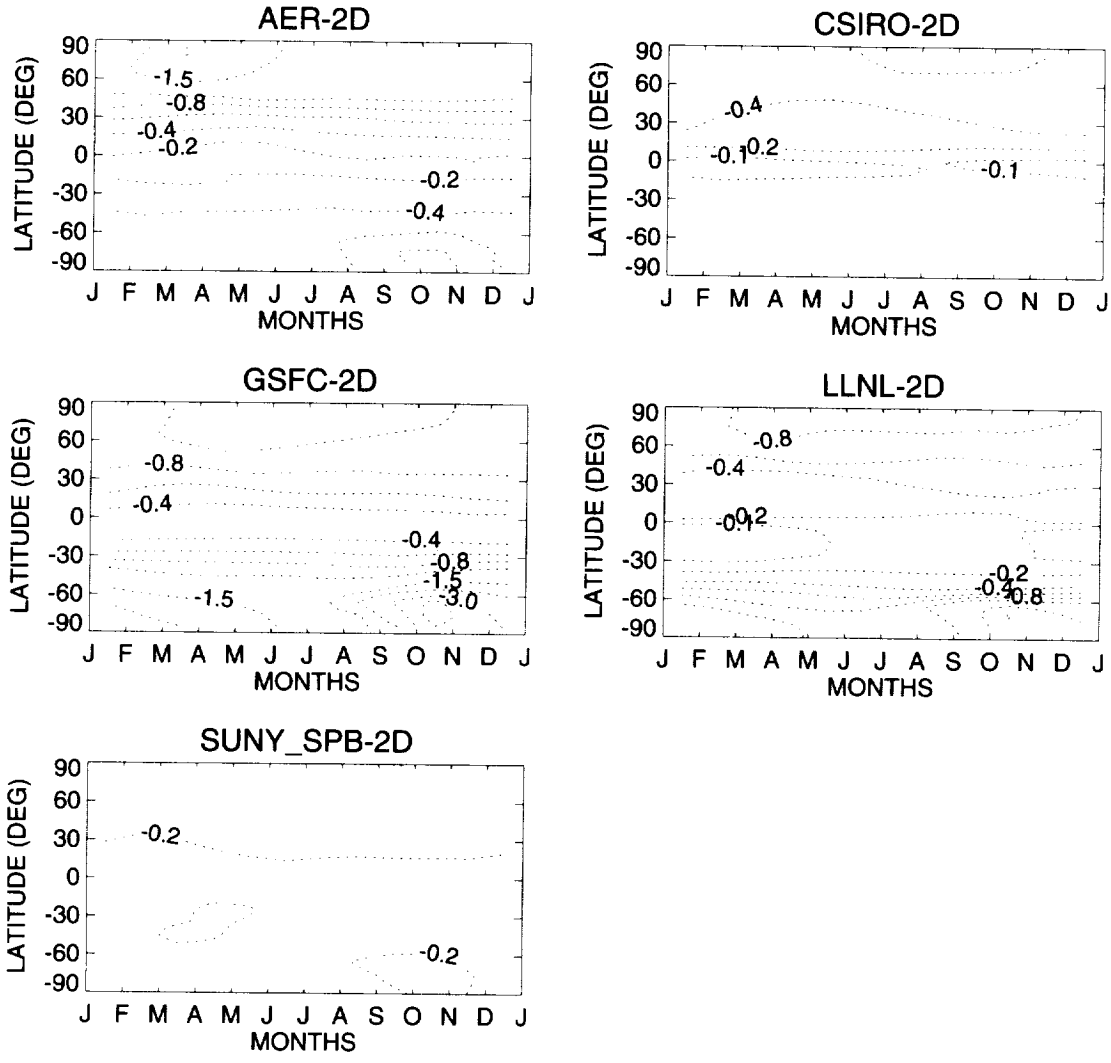

Figure 4-10b. Seasonal dependence of calculated O_3 change for scenario 9 (EI_{NO_x} = 5 g NO_2/kg fuel, 500 aircraft, 10% sulfur gas-to-particle conversion) relative to scenario 1 (subsonic only condition). Only 2-D models carried out calculations for this scenario.

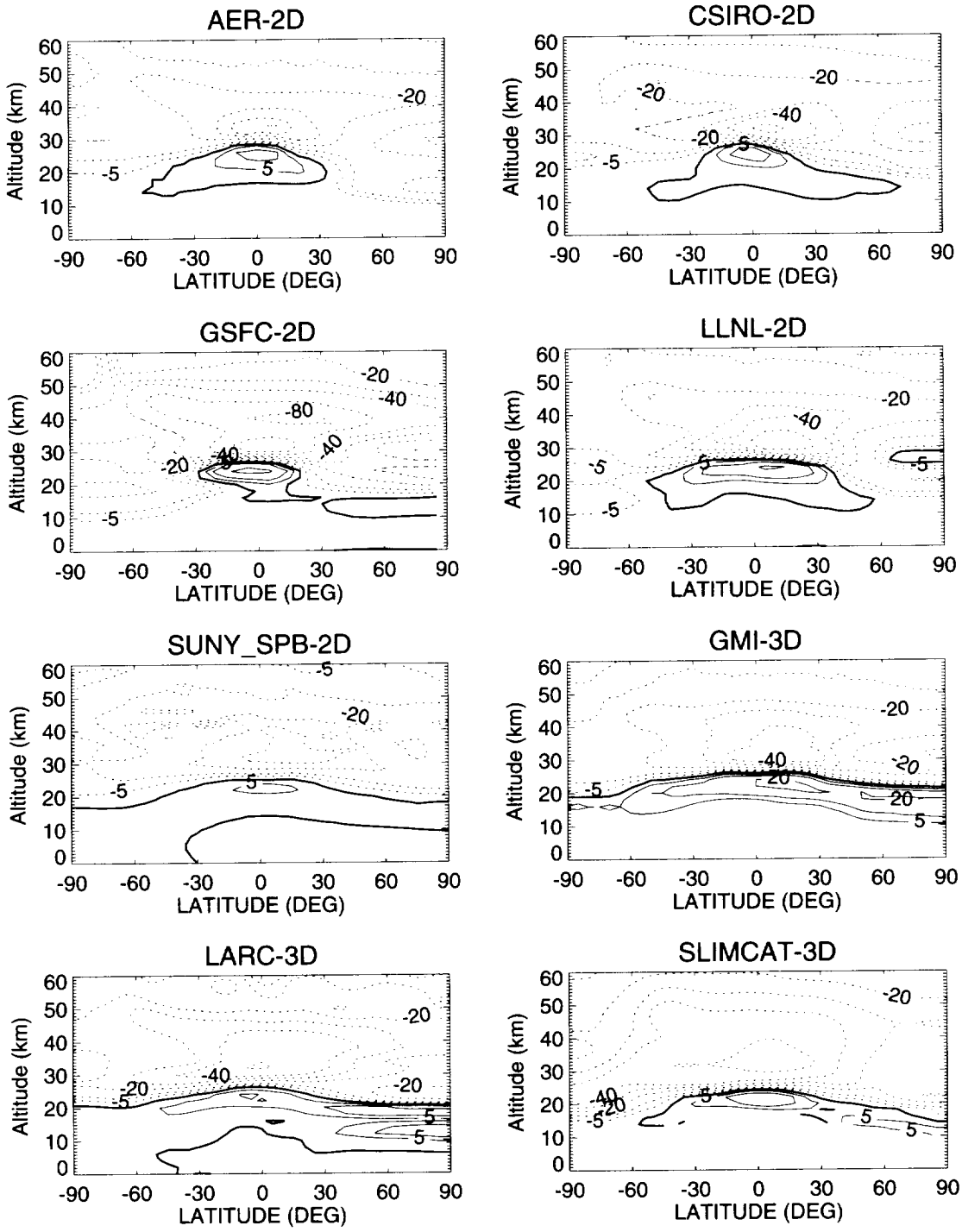

Figure 4-11. Calculated HSCT-induced change in ozone (ppbv) as a function of latitude and altitude. Results are shown for scenario 4 (EI_{NO_x} = 5g NO_2/kg fuel, 500 aircraft, no sulfur emission) relative to scenario 1 (subsonic only conditions). Calculations are shown for June 15 conditions.

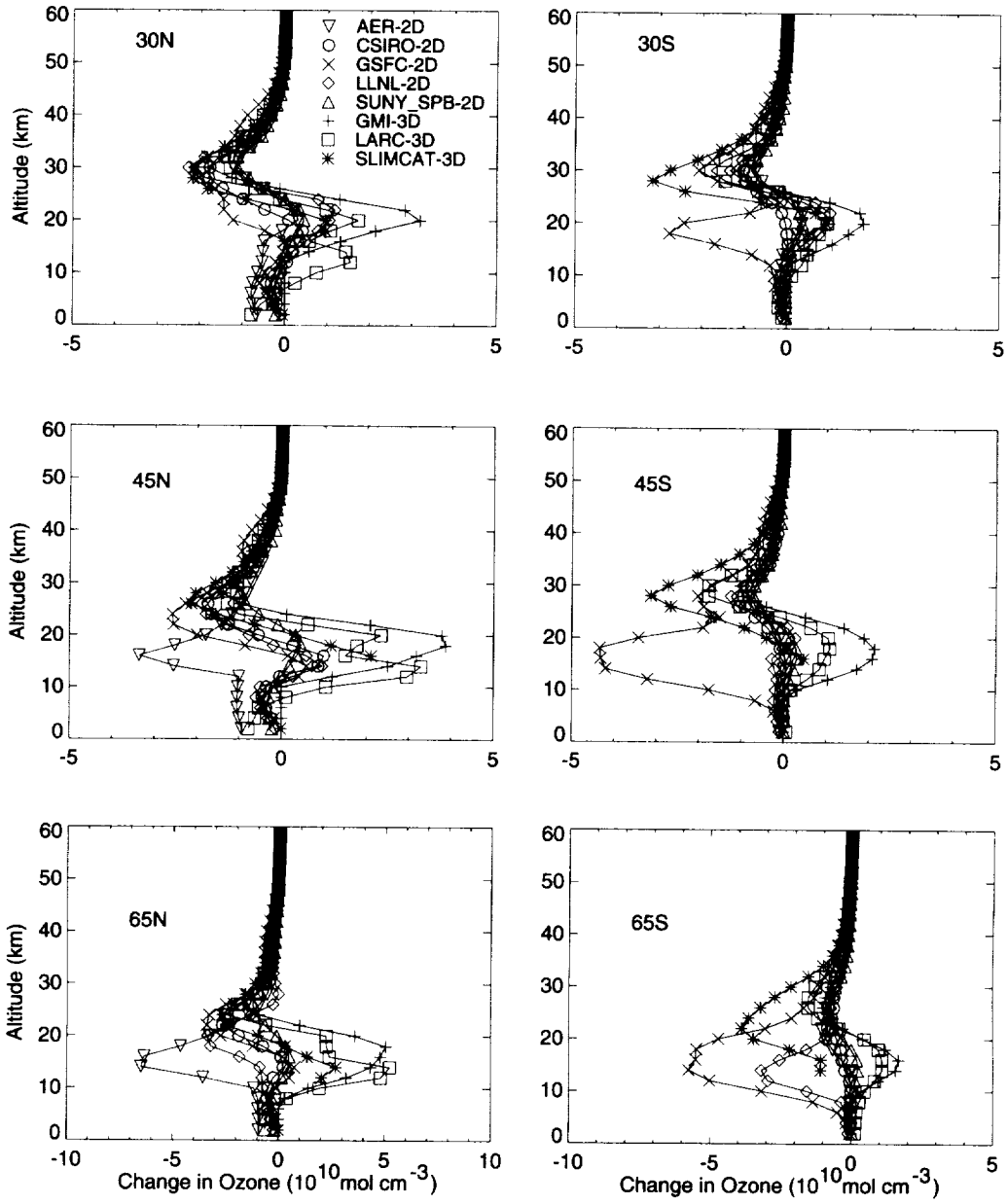

Figure 4-12a. Calculated HSCT-induced change in O_3 (10^{10} molecules/cm^3) as a function of altitude during June, for mid-latitudes in the Northern and Southern Hemispheres. Results are shown for scenario 4 (EI_{NO_x} = 5 g NO_2/kg fuel, 500 aircraft) relative to scenario 1 (subsonic only conditions) for all participating models. Note differing x-axis scales.

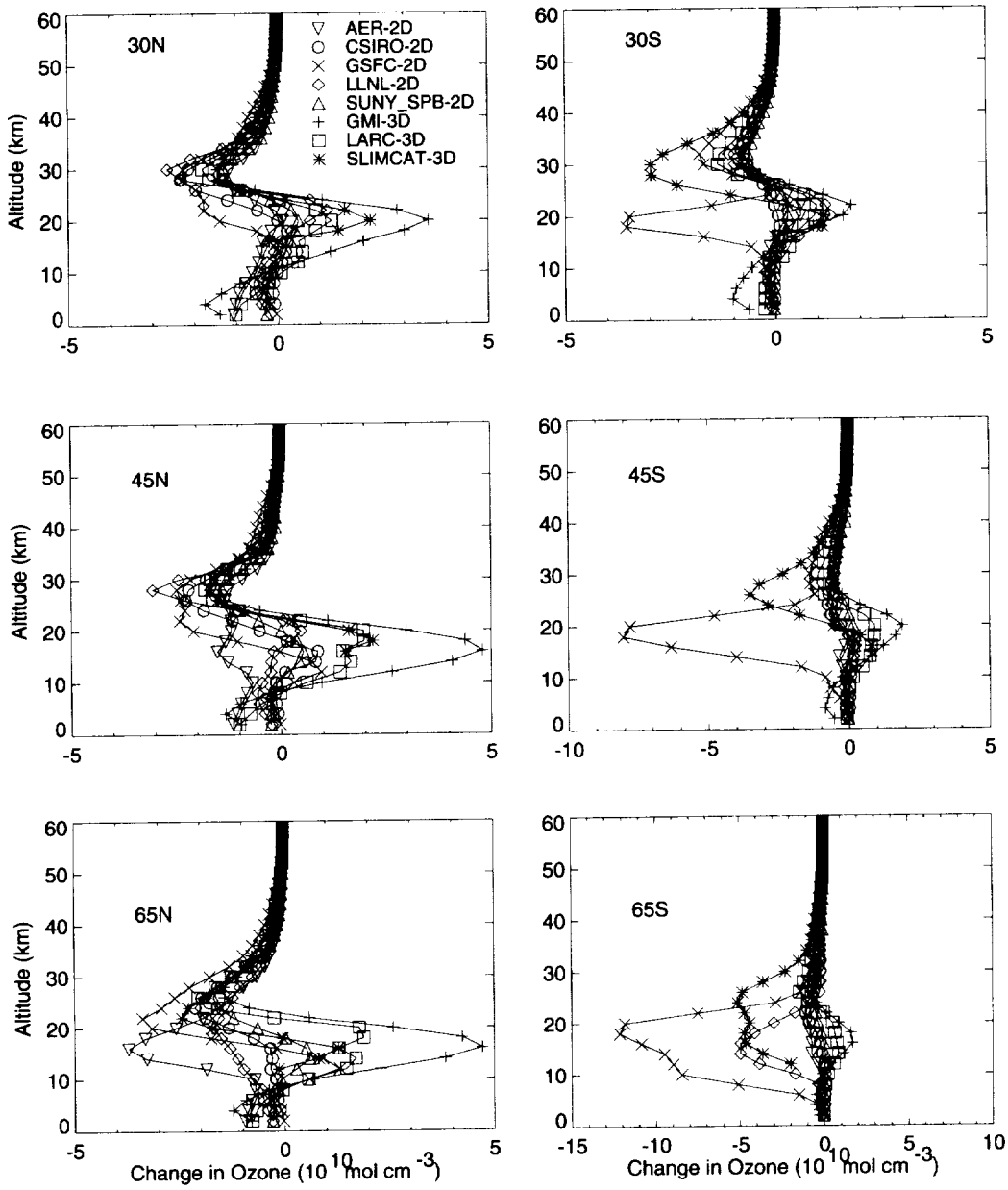

Figure 4-12b. Same as 4-12a, but for December conditions.

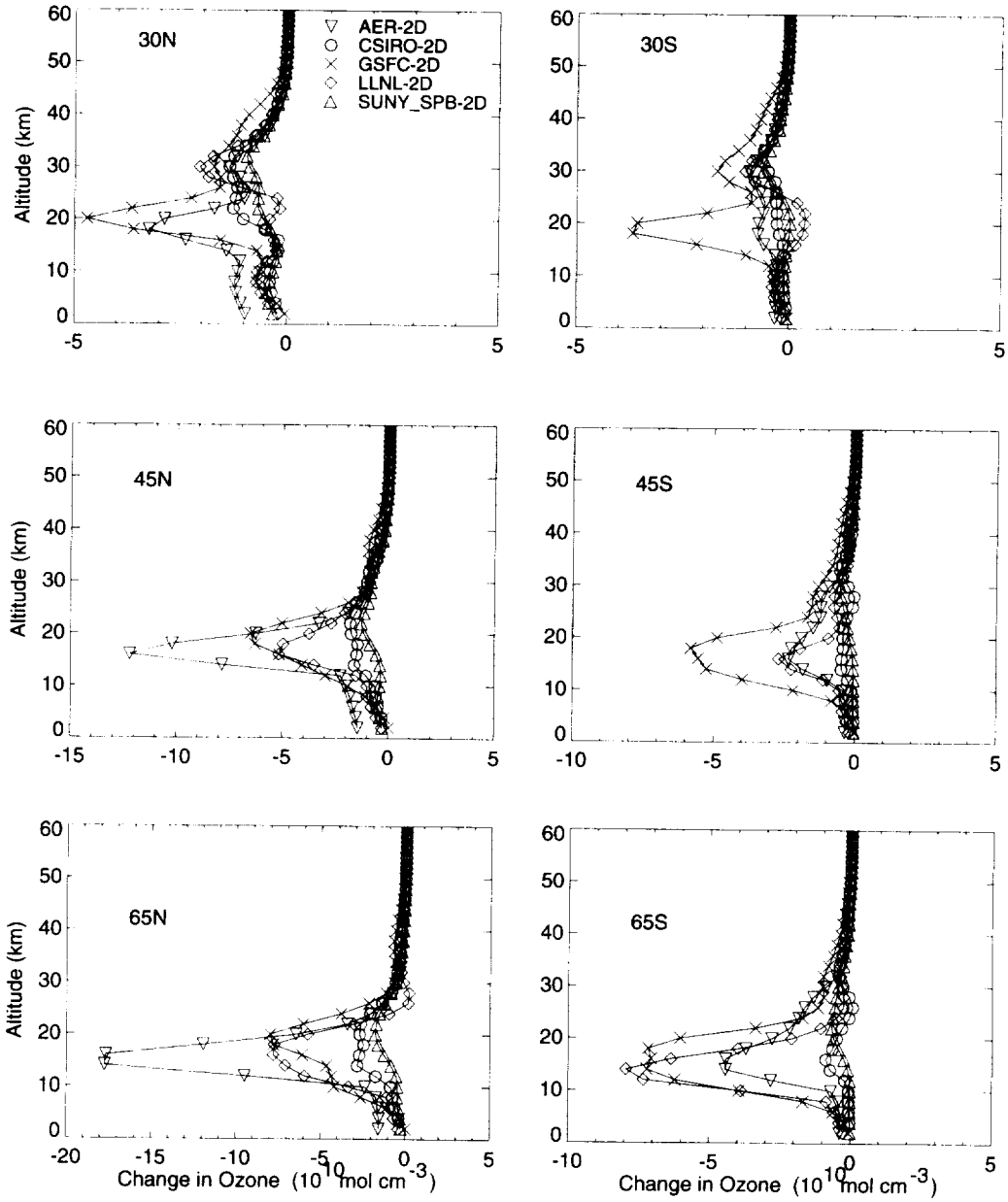

Figure 4-12c. Same as for 4-12a, but for scenario 9 (EI_{NOx} = 5 g NO_2/kg fuel, 500 aircraft, 10% sulfur gas-to-particle conversion) relative to scenario 1 (subsonic only conditions). Only 2-D models carried out calculations for this scenario. Note differing x-axis scales.

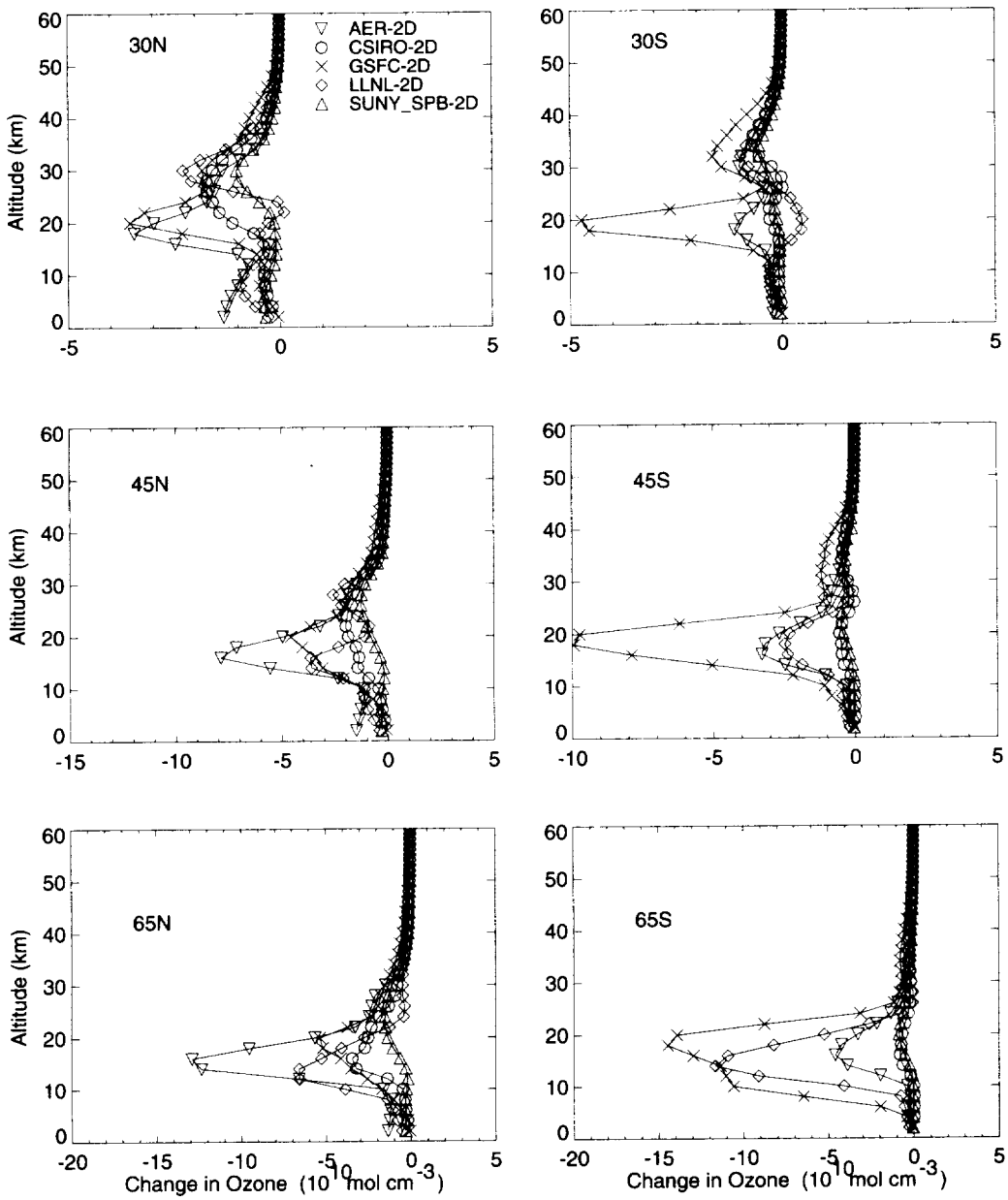

Figure 4-12d. Same as 4-12c, but for December conditions.

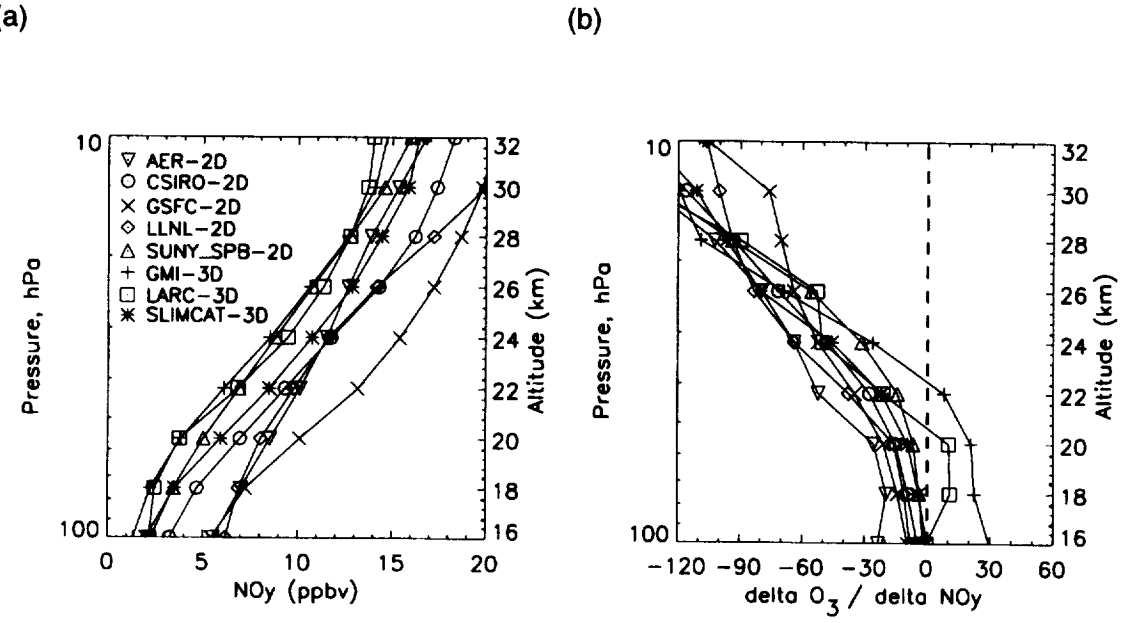

Figure 4-13. Profiles of model derived quantities at 45°N during June. Panel (a) shows the background NO_y abundance (ppbv) for each assessment model. Panel (b) shows the ratio of delta O_3 (ppbv) to delta NO_y (ppbv) for HSCT scenario 4 (EI_{NO_x} = 5 g NO_2/kg fuel, 500 aircraft) relative to scenario 1 (subsonic only condition). Delta NO_y is positive in all cases.

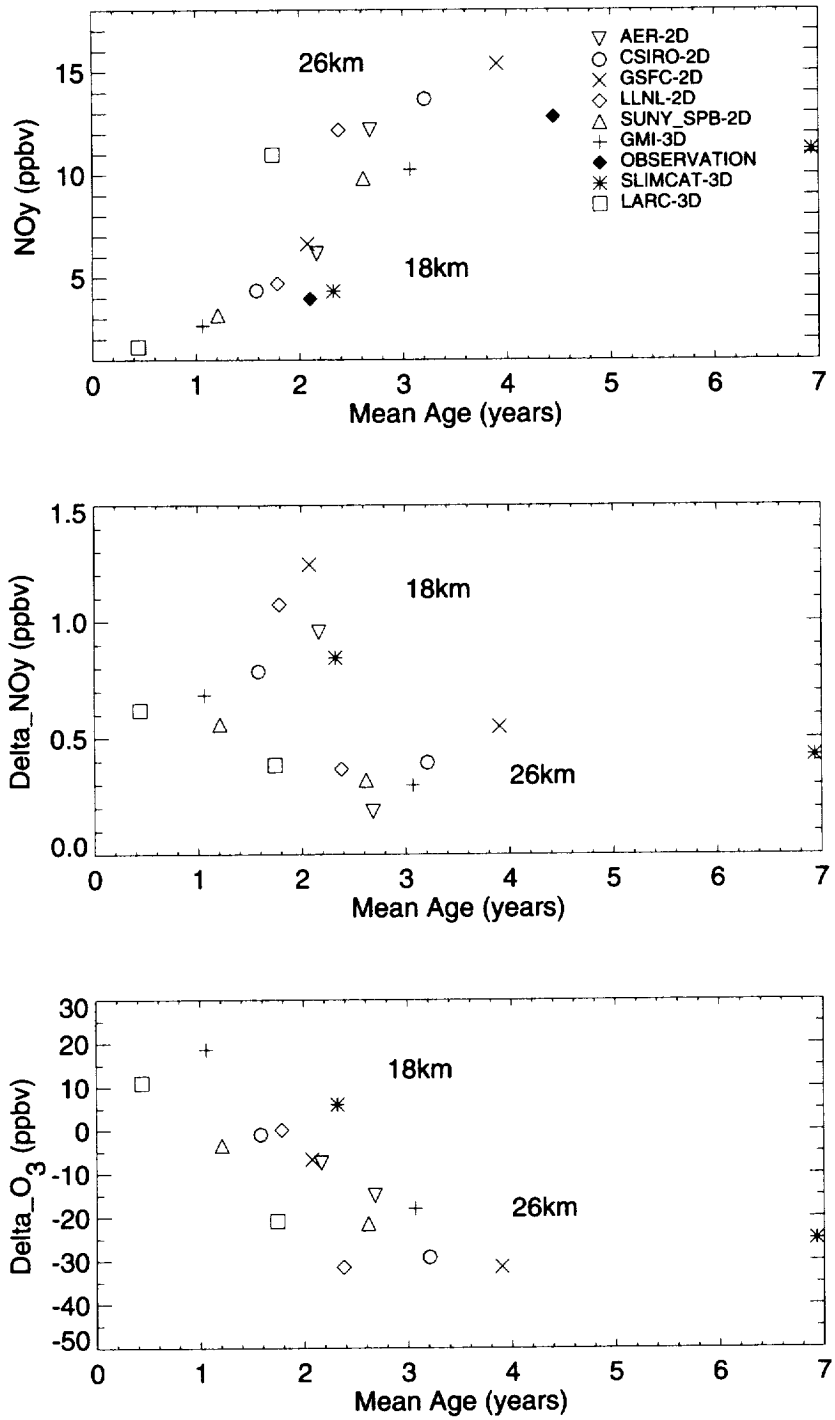

Figure 4-14. Scatter plots of different models for calculated atmospheric parameters versus calculated mean age of air at 18 and 26 km. Correlations against mean age are shown for: (a) background NO_y (ppbv); (b) accumulated HSCT NO_y (Delta NO_y; ppbv); and (c) local change in ozone (ppbv) due to HSCT perturbation (delta O_3). The observational points in (a) were obtained from analysis of ER-2 and OMS data [A. Andrews, personal communication]. The 18 km age comes from average mean age (from CO_2) from all ER-2 flights near 40°N. The 26 km age is obtained from the OMS flight at 35°N.

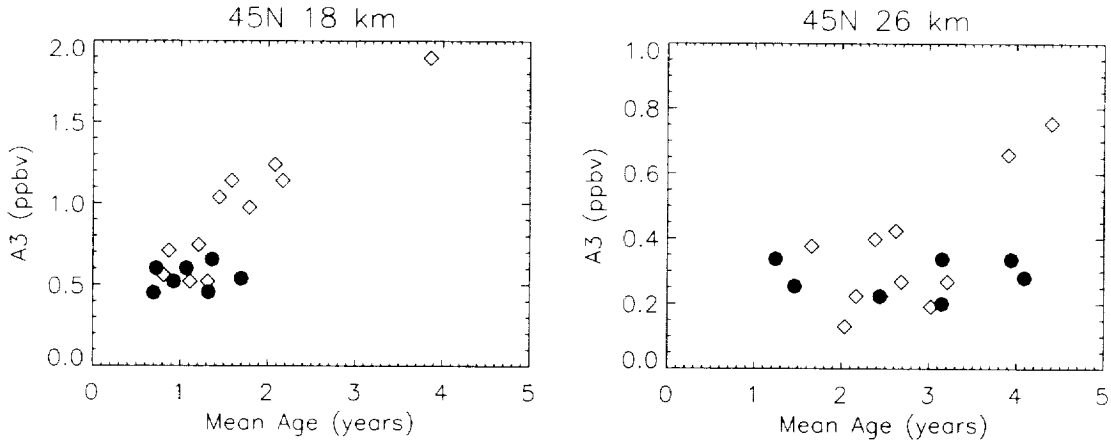

Figure 4-15. Scatter plots of the accumulations calculated in the M&M II A3 experiment vs. calculated age, at 45°N and 18 km (panel a) and 26 km (panel b). The open symbols correspond to 2-D models, and the filled symbols are obtained from 3-D models. A3 is an HSCT tracer scalable to the water perturbation. All models participating in M&M II are plotted, including some which did not participate in the AESA assessment.

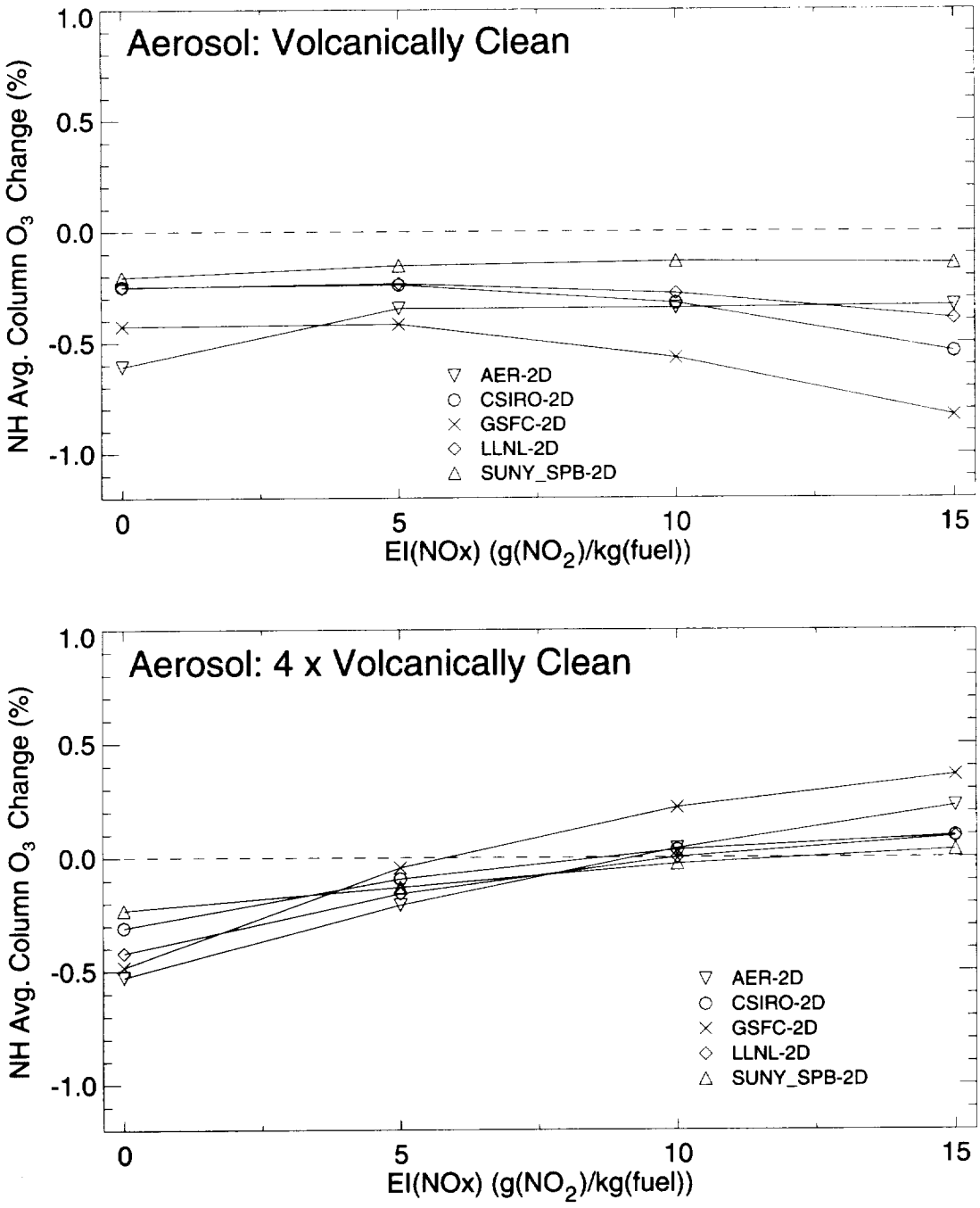

Figure 4-16. Predicted change in the NH averaged column ozone (%) as a function of EI_{NO_x} for a fleet of 500 HSCTs. The top panel shows results for a volcanically-clean background aerosol loading, while the bottom panel shows the case where background aerosol has been enhanced by a factor of 4 due to volcanic activity. These calculations assume no sulfur emission from the HSCT.

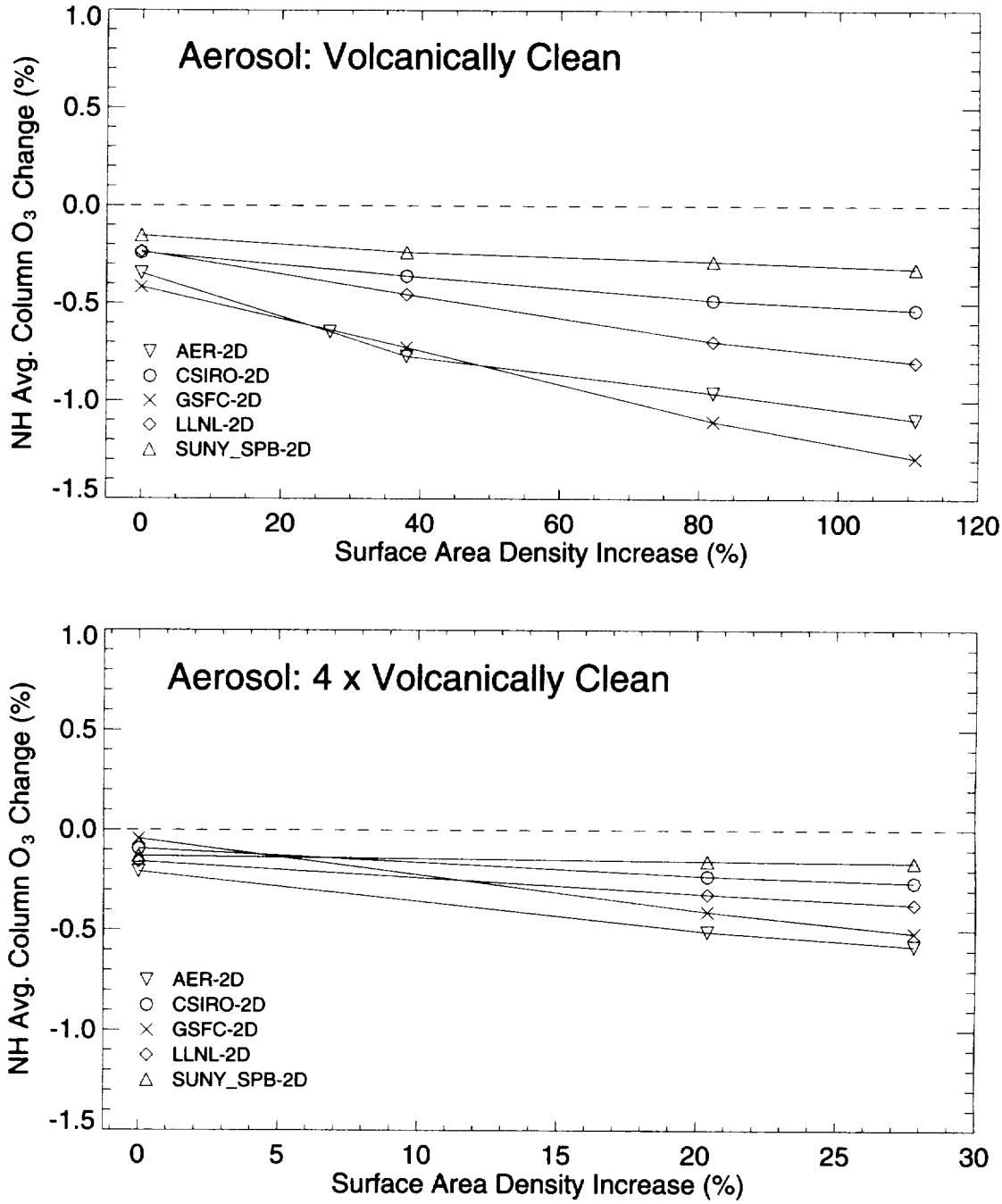

Figure 4-17. Predicted change in the NH averaged column ozone (%) as a function of percentage increase in SAD in the 14 to 21 km, 35°-90°N region (see text for details). The top panel shows the model results for increases in SAD relative to a volcanically clean atmosphere. The bottom panel shows model results relative to background SAD enhanced by a factor of 4 due to simulated volcanic activity. All scenarios used in this figure assume an EI_{NO_x} = 5 g NO_2/kg fuel, 500 aircraft fleet.

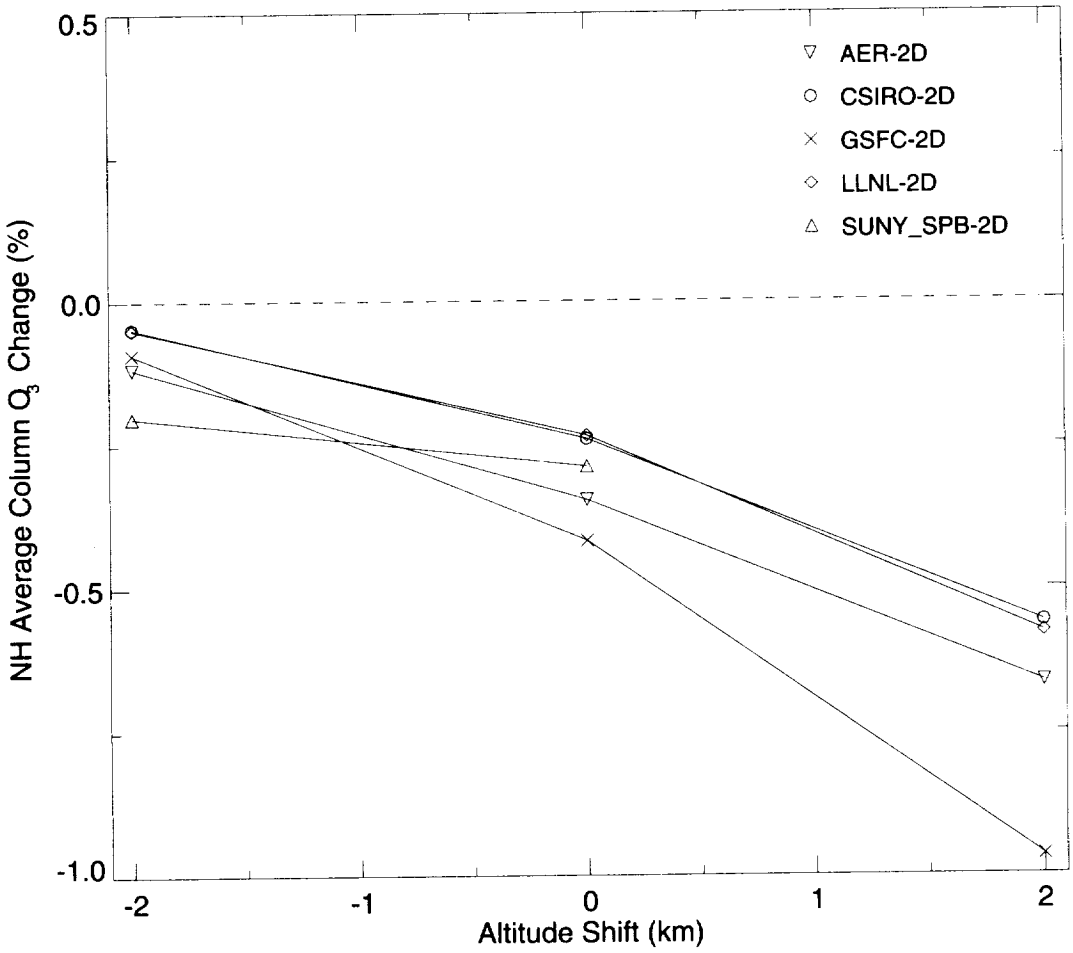

Figure 4-18. Sensitivity of predicted ozone change to HSCT altitude displacement from the nominal cruising altitude of the standard TCA scenario.

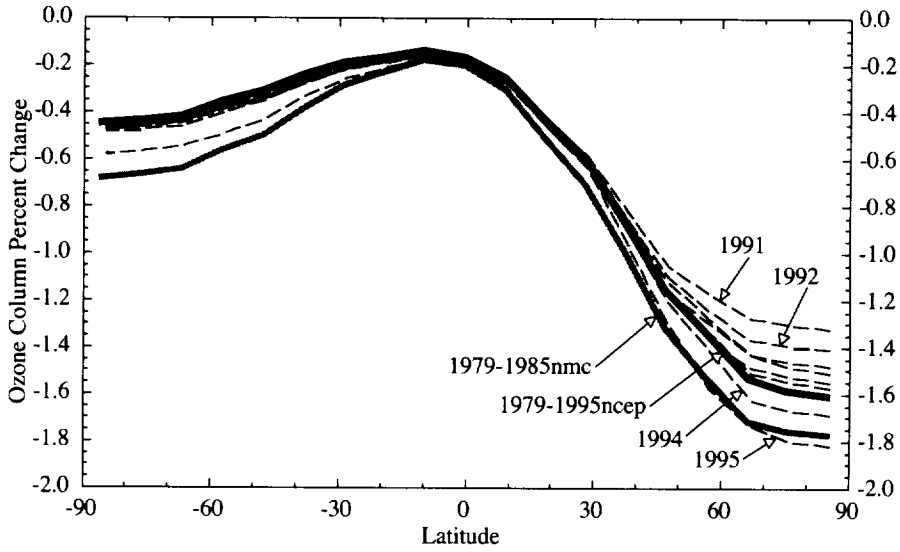

Figure 4-19. Sensitivity of predicted change in column ozone to adopted temperature temporal and spatial distributions. Predicted change in annual average column ozone (%) is calculated by the AER 2-D model (EI_{NO_x} = 5 g NO_2/kg fuel, 500 aircraft fleet). Results are shown using a time-dependent calculation between 1988 and 1995, where the temperatures for each year were adopted from the NCEP climatology. For comparison, calculations are also shown for the 1979 to 1985 NMC and 1979 to 1995 NCEP climatological averages. Calculation includes the impact of additional surface area density from a 50% sulfur gas-to-particle conversion assumption. The stratospheric circulation in the model does not change from year to year.

5. SYNTHESIS AND DISCUSSION OF UNCERTAINTIES

5.1 Framework for Scientific Estimation of Effects of HSCTs on the Atmosphere

In this chapter, we synthesize the findings from the chapters on Fundamental Physics and Chemistry, Emissions, and Modeling into assessments of the most probable change in stratospheric ozone due to HSCTs, the uncertainty range in calculating that impact, and the sensitivity of the HSCT impact to varying assumptions about emissions and the future atmosphere. Numerical estimates based on model calculations and our assessment of confidence in the numbers are given. The progress, concerns, and issues behind these assessments are summarized in the discussion.

The chapter is divided into three sections. The Framework introduces the scope of the HSCT prediction problem, provides the historical context of the HSCT assessment, and discusses the improvements of our predictions since the previous 1995 assessment and concerns for the current assessment. The second section provides both our current best estimate of the HSCT impact, and the uncertainties associated with that estimate. The final section discusses the future pathway for improvements to current estimates of HSCT impacts. All three sections are focussed on the overall assessment problem, the evolutionary nature of our advancing science, and the impact of this knowledge advancement on our predictive capabilities.

5.1.1 INTRODUCTION

Prediction of ozone change accurate to the 1% level or less, typical of the predicted HSCT-produced change, is difficult. Errors in the predictions accrue in three stages: (1) simulation of the current atmosphere, (2) prediction of the state of the future atmosphere, and (3) prediction of the HSCT perturbation on the future atmosphere. Simulating ozone is particularly difficult because the ozone distribution depends on both transport and chemistry in a complex interaction over a wide range of time and spatial scales. For example, ozone loss in the stratosphere depends on the mix of reactive chemicals, temperature, and sunlight. The reactive species distributions depend in turn on the mix of source and reservoir gases (e.g., CFCs, halons, etc., [see Chapter 2]) potentially including HSCT emissions, aerosol content, temperature, sunlight, and interactions with other reactive species including ozone. The source and reservoir gas distributions depend strongly on transport and reactions with radical species, as does ozone itself. Aerosol amounts depend on volcanic emissions, source gas reactions, transport, and particle microphysics. These linkages make prediction of ozone changes extremely challenging.

Predicting the future atmosphere requires accurate forecasting of both meteorological climate conditions and chemical composition. Future climate and chemistry are coupled in a complex way and they depend on factors external to this assessment, e.g., population growth, pollution control, or natural variations. We rely on climate [IPCC, 1996] and ozone trend [WMO, 1999] assessments for these inputs. In some cases, we test the uncertainty in inputs with HSCT sensitivity tests over a range of input conditions. Obviously our ability to cover possible futures is limited. Finally, predicting the HSCT exhaust perturbation requires accurately calculating its transport, accumulation, and interaction with the background atmosphere.

The HSCT assessment is based on current theoretical and observational information using the best modeling and analysis tools available. These models have evolved to simulate ozone and its underlying chemical distributions with an ever-increasing degree of accuracy. We have identified aspects of the models, however, which are not accurate in comparison to data and which are expected to be significant in calculating the HSCT perturbation. In some of these areas we do not yet know how to correct the model deficiencies nor quantitatively how the errors will influence the HSCT calculation. The models do many things well and they have improved tremendously over the course of stratospheric ozone assessments. Our understanding and confidence in simulating and predicting ozone have increased markedly, but the models are not indisputably accurate at the level of the HSCT ozone change. Our challenge, then, is to assess how adequately current tools and knowledge can be applied to the HSCT perturbation problem. The result must be useful for guiding technological and policy decision making.

5.1.2 HISTORICAL PERSPECTIVE

Familiarity with the history of stratospheric ozone assessment is valuable to interpreting the HSCT assessment. Extensive research on understanding stratospheric ozone was initiated by the Climate Impact Assessment Program (CIAP) in the early 1970s. The research efforts were summarized in a series of international scientific assessments, the first in 1974 for a hypothetical fleet of SSTs [CIAP, 1975]. Since CIAP we have known that the injection of H_2O and NO_x from the exhaust of supersonic aircraft flying in the stratosphere poses a risk to the ozone layer. The quantitative evaluation of ozone depletion from proposed supersonic fleets has, however, varied since the end of CIAP in 1974 as we continue to learn more about the stratosphere and improve our predictive capability.

During the late 1970s, research attention turned to CFC-induced ozone depletion. A wide-ranging research program in atmospheric measurements, laboratory experiments, and computational modeling of stratospheric ozone was developed by NASA's Upper Atmosphere Research Program (UARP) in response to the Clean Air Act, which requires a periodic report from NASA on the ozone layer. Together with other national and international programs, assessments of perturbations have followed every few years since that time, leading to a unique international treaty (Montreal Protocol) to protect the stratosphere from CFCs [WMO, 1986, 1989, 1992, 1995, 1999]. The Atmospheric Effects of Stratospheric Aircraft (AESA) project was organized in 1989 under the NASA High-Speed Research Program. AESA was built upon this assessment foundation and has teamed with UARP and related programs in driving many of the advances in our understanding of stratospheric ozone.

Several events took place during this time that changed prevailing concepts of the processes which control stratospheric ozone. These conceptual changes led to changes in the numerical models and variations in ozone perturbation calculations over the years. The Antarctic ozone hole was discovered in 1985, and a year later the importance of particles in chemical reactions (i.e., heterogeneous chemistry) was recognized with the role of PSCs in forming the Antarctic ozone hole. This polar chlorine-catalyzed ozone depletion was well outside the range of then-current models. By the early 1990s, the importance of the heterogeneous reaction of N_2O_5 on the stratospheric sulfate particles was established. With inclusion of stratospheric sulfate-layer chemistry, the calculated ozone sensitivity to NO_x from HSCTs was diminished while sensitivity

to H_2O and sulfate particles increased. Throughout this time, stratospheric observations were becoming more available both from global satellite data sets and intensive aircraft missions (i.e., the NASA ER-2 campaigns), sponsored in part by AESA. The improved observations have continued to refine our understanding of stratospheric ozone processes, but it must be acknowledged that aspects of observed ozone trends and volcanic perturbations could not be modeled accurately [WMO, 1999]. Figure 5-1 illustrates that the predicted HSCT perturbation is of relatively small magnitude in comparison to observed polar ozone trends and interannual variability over this period.

Numerical models have evolved in completeness and sophistication thanks to expanded computer power and scientific development efforts. The first CIAP assessments used mainly 1-D (vertical) models. Until recently, models used to assess ozone depletion were primarily 2-D, i.e., the longitudinal dimension was averaged and temporal variability was limited to monthly averages. Now 3-D models explicitly simulate constituent transport and diurnally time dependent processes for several HSCT scenarios. The Models and Measurements workshops (I and II) changed traditional assessment model intercomparisons to model-data comparisons with a standard set of atmospheric measurements. The development of the GMI by AEAP has allowed for the first modular comparison of stratospheric ozone models. This, combined with new measurements of a wider range of tracers, has led to new bounds on the uncertainty of the buildup of HSCT exhaust in the stratosphere. In this assessment we have, for the first time, estimated an uncertainty for transport and used measurements to constrain the range of modeled exhaust accumulation.

The historical perspective shows that tremendous progress has been made in the science of assessing perturbations to stratospheric ozone. This progress enables us to make predictions with greater confidence than was possible in the past. On the other hand, history records important perturbations that were not accurately forecast based on the past state of the art. Thus, we must be cautious in assessing the uncertainty of current predictions for HSCT impacts.

5.1.3 Progress Since the Last Assessment

Major progress has been made in ozone assessment science since the previous HSCT assessment [Stolarski *et al.*, 1995]. Progress has been led by new atmospheric observations and numerical model development. Observations pave the way for improved understanding and simulation of transport, chemistry, and emission processes. Model development is producing models that are more soundly based in physical principals with fewer restrictive assumptions.

Observations of long-lived tracers, studies using analyzed meteorological fields and idealized models, and theoretical advances have improved understanding and quantification of several key components of transport necessary to predicting the distribution of HSCT exhaust. Observations provide new diagnostics for testing model transport and highlight specific areas for improvement.

- *In situ* measurements of chemical tracers have been obtained within the previously data-sparse tropics. In particular, the time scale for mixing into the tropics, and the vertical diffusion and ascent rates within the tropics have been estimated. These are key pathways

for dispersal of HSCT exhaust into the upper stratosphere where chemical sensitivity to NO_x is high.

- Measurements of CO_2, SF_6, and HF over a range of latitude and altitude have enabled mean ages of air in the stratosphere to be determined. Mean age depends on the integrated effect of the different stratospheric transport processes, in particular meridional circulation, quasi-horizontal mixing in the stratosphere, and transport across the tropopause. Age of air is a directly measured diagnostic that is related to stratospheric residence time and hence to the potential accumulation of HSCT exhaust in the stratosphere.

- The quantification of tropical transport processes and mean age provide stringent tests of the transport within numerical models. Comparisons between observations and models have identified specific differences in the models used in this assessment. The identification of specific problems is valuable for assessing the uncertainty in the ozone perturbation and in developing more accurate models.

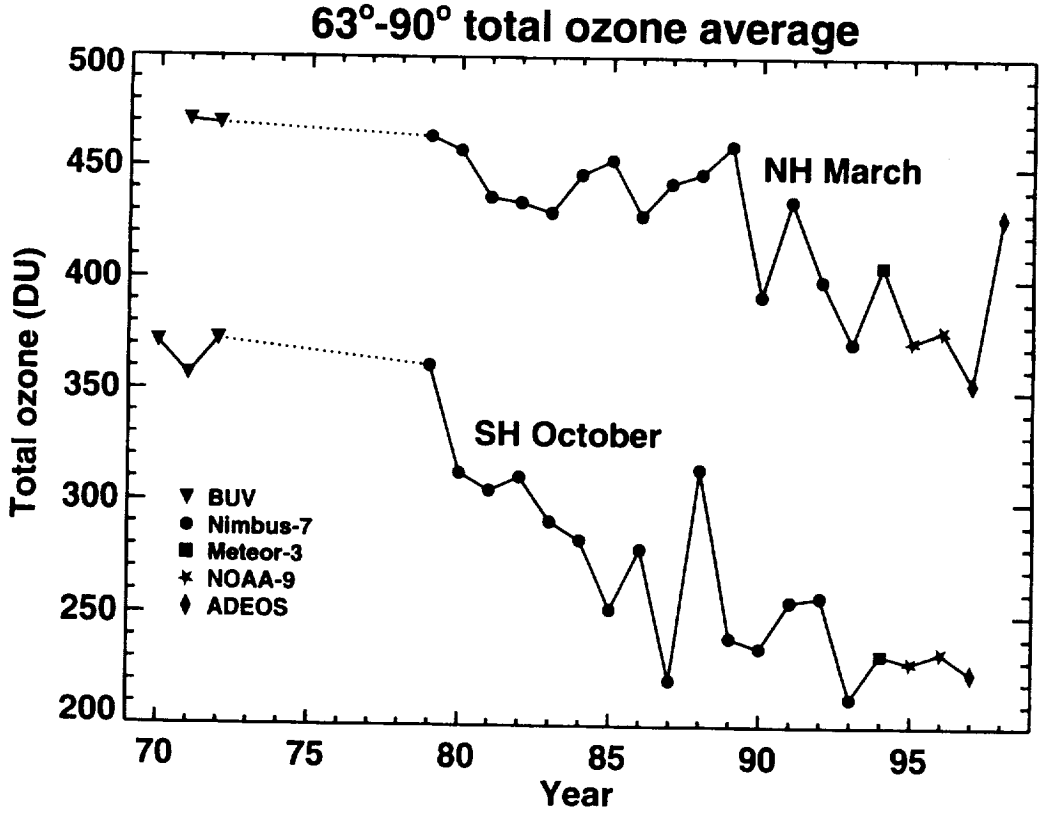

Figure 5-1. Time series of average springtime polar ozone from 1970 to present. Total ozone data from a succession of satellite instruments are averaged poleward of 63° for March in the NH and October in the SH (adapted from Newman *et al.* [1997]).

Progress in understanding of HSCT-related chemical reaction rates has come about largely through observational activities to obtain data on chemicals not previously measured and more accurate data over a more comprehensive range of conditions. The importance of this progress cannot be overstated. This is the best method we have to decrease the probability of significant missing reactions or unknown species that would invalidate our HSCT calculations.

- Direct simultaneous *in situ* measurements of the major radical species involved in chemical loss of ozone were made over extensive regions of the stratosphere, including some (NO_2, $ClONO_2$) for the first time (Sections 2.4.2 to 2.4.4). The wide range of conditions sampled, including the first in summer polar regions, allows us to quantitatively evaluate our established chemical mechanisms and the mechanistic response of the chemical system to the HSCT perturbation.

- Atmospheric observations of key species have been placed in a model framework capable of assimilating diverse data to diagnose the accuracy of computed photochemical rates. Comparisons for reactive species demonstrated considerable improvement in partitioning free radicals and stable components of NO_y, Cl_y, and HO_x in the models.

- Laboratory measurements provided improved quantification of several processes and reactions important to the HSCT calculations such as $BrONO_2$ hydrolysis and the physical chemistry of stratospheric ternary solutions (Sections 2.4.3 and 2.4.5).

Progress in this assessment has also come in confirming the importance of the emission and near-wake production of small sulfate particles by HSCTs. The possibility of emission of numerous aerosol particles and the global sensitivity of ozone to this emission was raised in the previous assessment. New direct measurements for existing aircraft and continued comparison with plume-wake models and idealized calculations has reduced our uncertainty in applying current knowledge to the proposed future fleet emission.

- Formation of volatile ultra-fine aerosol particles has been detected in exhaust plumes from all aircraft sampled. The number of particles is a strong function of the fuel sulfur content. Altitude chamber measurements of a military engine and measurements in the plumes of aircraft indicate that sulfur emissions at the engine exit plane are primarily SO_2. The measurements support earlier inferences of a composition of H_2SO_4/H_2O for the volatile particles formed in the plume (Section 3.6.2). Model simulation of particle formation and growth shows dependence on fuel sulfur content and the fraction of fuel sulfur oxidized to SO_3 in the engine.

- Soot emissions from current aircraft engines are highly variable, but are roughly two orders of magnitude lower in number emission index than are volatile aerosols measured in the plume. Based on combustor rig measurements, projected soot emissions from the LPP combustor concept for the HSCT are expected to be significantly lower than emissions from current engines.

- Limited measurements of gaseous constituents, including HO_x and NO_x, emitted from current aircraft are consistent with expected emissions and plume models of gas-phase chemical and dispersion processes (with the exception of sulfuric acid aerosol precursors as discussed in Section 3.5).

Major progress in model development parallels the progress made via new atmospheric observations. Most notable is the application of 3-D atmospheric models to the HSCT assessment problem. Three-dimensional models incorporate a more physically realistic representation of the atmosphere than 2-D models. For example, 3-D models can explicitly simulate 3-D mixing processes and longitudinal variations in temperatures and PSCs, whereas these have to be parameterized in 2-D models. Correct representation of these processes is crucial to predicting HSCT impacts. In addition, 2-D models have been improved and all of the models have been systematically evaluated in comparison to data.

- A modular 3-D model for chemistry and transport has been developed, and 3-D simulations of the chemical perturbation due to HCST have been used for the first time in this assessment. This provides answers to questions about the possible effects of zonally averaging 3-D processes in HSCT simulations from 2-D models.

- The modular design of the GMI 3-D model has enabled the sensitivity to the different components within the model (e.g., the numerical transport algorithm and the source of the wind and temperature fields) to be examined. Objective criteria for performance have been applied. Thus we can probe differences among models in their response to the HSCT perturbation and begin to weigh their results.

- Two-dimensional models have incorporated more complete process representations including those for aircraft aerosol exhaust, PSCs, heterogeneous reaction rates, and wave-driven mixing. This gives us more confidence in our physical representation of the stratospheric system.

- A major model-measurement comparison and model intercomparison (M&M II) has been conducted by AESA and the NASA Atmospheric Chemistry Modeling and Analysis Program (ACMAP). Model evaluation is essential to assess uncertainties in the ozone assessment. All models in this assessment have been tested in comparison to a standard set of performance benchmarks for photolysis and chemical kinetics solvers.

5.1.4 Areas of Concern for This Assessment

Several areas of concern for the reliability of the assessment calculations have been identified. The nature of these issues ranges from known model deficiencies, to uncertainty in predicting the future state of the atmosphere, to areas of expected high sensitivity to changes in NO_x, H_2O, or aerosol. These issues are often coupled and their impact on the HSCT calculation is difficult to access quantitatively. Known model deficiencies occur in representations of transport, chemistry, and aerosol emissions. Many unknowns are involved in predicting the future atmosphere. The possibility of unknown and unmodeled processes influencing the HSCT calculations is discussed in Section 5.2.

Transport

Concern about transport arises from simulations of the current atmosphere. Transport is largely responsible for the model distributions of tracers and ozone. To the extent that these do not match reality, the HSCT perturbation will be superimposed on an incorrect background atmosphere. Moreover, the transported distribution of the aircraft exhaust may not be correct.

- Model simulations display distinct differences in comparison to observational transport diagnostics. Models generally have too rapid mixing into the tropics, too much vertical diffusion within the tropics, and ages that are too young. The fact that models underestimate age in most regions suggests that the actual accumulation of HSCT exhaust might be underestimated in the models.

- Models differ in their simulation of key tracers such as NO_y, N_2O, and Cl_y. Although tracers and age are correlated among models, some models overestimate NO_y while some underestimate it, presenting an inconsistency with the age diagnostic. The result is that there is no clear choice among models for which to weigh most heavily in the HSCT perturbation. Three-dimensional models are expected to perform better in this regard, but their development is not yet mature enough to use them exclusively.

- The remedies for some of the problems with model transport identified in this assessment are currently unknown. In particular, it is not known how to correct the models so that they have realistic mean age and NO_y distributions.

- There is a large variation among models in the simulated amount and spatial distribution of the HSCT exhaust. These differences are broadly correlated with variations in the ozone impact. Since we do not currently know how to constrain the simulations of the accumulation of aircraft emissions, this variation translates to a relatively large uncertainty in the HSCT impact.

Aerosol Emissions

Concern about the amount of sulfate aerosol that will be produced in HSCT exhaust has emerged as a major uncertainty in the assessment. Model tests show that particle exhaust nearly doubles the calculated HSCT ozone loss for 500 aircraft relative to H_2O and NO_x emission alone. Yet, we are unable to confidently predict the number and mass of particles that will be produced by an HSCT. The uncertainty is compounded by concerns for transport of exhaust discussed above as well as representation of the natural particle sources and microphysical processes.

- The mechanism for gas-phase sulfur oxidation through the hot sections of an aircraft engine is not well understood. Measurements of particles in the plumes of existing engines vary widely and standard plume models underestimate their abundance. Without a solid theoretical mechanism for sulfur oxidation and particle formation, we cannot accurately predict what the HSCT engine will produce.

- Mechanisms for formation of volatile, H_2SO_4/H_2O aerosols have been proposed but direct measurements at the engine exit plane of the assumed aerosol precursors (SO_3 and molecular ions) are not available to test them. Since the plume aerosol models use these assumed concentrations as initial conditions, conclusions from these models are still uncertain and it is difficult to extrapolate to the HSCT conditions.

Polar Processes

The assessment of HSCT impacts in polar regions is difficult for several reasons. The heterogeneous processes that take place in the cold temperatures of polar winter are highly non-linear in their dependence on aircraft emitted species, NO_y, H_2O, and particles. This is a highly sensitive regime because of PSC processes. This sensitivity combines with model transport difficulty in the region and lack of a solid fundamental theory for calculating microphysical processes to produce large uncertainty in predicting effects of HSCTs locally and globally, for both the current and future atmosphere.

- Seasonal ozone loss at polar latitudes results from heterogeneous chlorine reactions on the surface of PSCs, which are composed of H_2O, HNO_3, and sulfuric acid–all species that will be increased by HSCT emissions. As a result of a combination of non-linear reaction processes, phase change transitions, and exponential dependence on the particle size distribution, the ozone loss can be highly leveraged by relatively small changes in condensibles at temperatures near those commonly observed in the polar stratosphere (Section 2.4.5). This raises the possibility that synergistic effects may occur among the emitted species increasing the likelihood of severe ozone depletion in the NH polar region.

- Fundamental questions about the microphysics and composition of PSCs limit our ability to parameterize key processes such as sedimentation and heterogeneous chlorine activation, which control winter/spring polar ozone loss. The representation of these processes in assessment models is highly simplified and very model-dependent. We are currently unable to satisfactorily reproduce observed ozone loss such as depicted in Figure 5-1.

- The 2-D models used in the assessment do not properly isolate the winter polar vortex air mass. Lack of isolation of the vortex may lead to too much of the exhaust being transported into the vortex and too much of the processed air being transported out of the vortex. In this case, the model would tend to overestimate the HSCT impact at high latitudes. Problems with the representation of wintertime polar transport (formation of polar vortices and transport across the edges of the vortices) lead to uncertainties in the simulated HSCT perturbations to H_2O, NO_x, aerosol, and ozone within the lower stratospheric polar vortices.

- Strong local effects at high latitudes are possible and the impact may be felt at mid-latitudes. Model column ozone losses due to HSCTs are largest at high latitudes in almost all cases. For some models the maximum HSCT ozone loss occurs in polar winter/spring, but the difference among models is large lending little confidence to the quantitative estimates. In general, model global column ozone losses increase slightly when PSC processes are included in the perturbation calculations (Section 4.4.3.4).

Gas-Phase Chemistry

Gas-phase chemistry concern arises in one case from discrepancies between models and recent observations; this is a recognized problem whose solution has not appeared in time to be incorporated into this report. In another case, a potential concern is raised because of a heightened sensitivity to the vertical distribution of ozone change.

- Models partition too small a fraction of NO_y to NO_x, which will tend to cause an underestimation of HSCT impacts. Underestimation of the NO_x:NO_y ratio in the summer polar region raises concerns about errors in the chemical rates and missing chemistry. Some of these concerns appear to be resolved by recent laboratory measurements but these have not yet been included in the assessment models.

- The total column ozone changes due to HSCTs are strongly affected by compensation, where increases below about 20 km cancel decreases above. A small relative error in one or the other region could produce a large error in the difference. We are concerned whether the compensation point (crossover from NO_x-poor to NO_x-rich) is correct, since it is near the lower boundary of the stratosphere where the small scale processes responsible for transport are difficult to model.

Future Atmosphere Structure and Composition

Proper calculation of HSCT impacts requires that the atmosphere, onto which the aircraft perturbation is superimposed, be accurately described in the models. Concerns for predicting the future atmospheric state are related to the meteorology, trace gas abundances, and aerosol amounts. All of the assessment model calculations are keyed to present-day meteorology with the exception of several sensitivity runs discussed in Chapter 4. Source gas predictions and aerosol sensitivity are also tested over a limited range of possibilities. None of our model sensitivity tests shows unexpected major differences from the base calculations (Section 5.2.2), but if the future atmosphere differs substantially from that in our simulations, then the predictions of the HSCT impact will be different.

- Greenhouse gases are increasing in the atmosphere, and this will almost certainly modify stratospheric meteorology. Increasing amounts of greenhouse gases in the atmosphere tend to produce cooler temperatures in the stratosphere. In addition, wave driven mixing and transport may be different than the present. As discussed above, polar regions are most sensitive to such changes, which could influence chlorine-catalyzed ozone loss. The observed ozone decline in the Arctic from 1990 to 1997 (Figure 5-1) amplified concerns about the sensitivity of ozone loss to colder temperatures. HSCT exhaust gases incorporated into a colder, more persistent polar vortex that is near threshold temperatures for formation of PSCs could promote additional particle sedimentation, amplifying denitrification and vortex ozone loss.

- Future source gas concentrations (CH_4, Cl_y, Br_y, N_2O, H_2O) could differ from our projections. For example, future methane changes are uncertain. Methane is a source of H_2O in the stratosphere. In addition, stratospheric H_2O may change due to climatological changes in

tropopause temperatures, which control the H_2O source from the troposphere. Errors in predicting the future amount of H_2O will lead to incorrect estimations of HO_x-catalyzed ozone loss and water vapor available for particle formation and growth. Once again, the polar regions are particularly sensitive.

- Volcanic eruptions can dramatically increase aerosol surface area for periods of years. We test the interaction of HSCT aerosol with volcanic aerosol based on measurements from past eruptions, but the distribution and chemistry of future volcanic material is unpredictable. In general the impact of major volcanoes, such as Mt. Pinatubo, would overwhelm any impact from HSCTs. Models consistently predict a smaller HSCT impact on ozone when the background aerosol concentrations are large.

- Measurements of chemical responses *in situ* have been tested and have given us confidence that the chemical mechanisms represented in models are nearly complete for current-day conditions. We must realize that the chemical responses will be somewhat different in the modified future atmosphere and that the mechanisms have not been tested under those conditions.

5.2 Estimating the Impacts of HSCTs

In this section we estimate the central value for the HSCT ozone impact, the uncertainty range in predicting that impact, and the range of variation in the impact under a variety of input assumptions regarding HSCT technology and the future state of the atmosphere. We emphasize calculated changes in NH mean total column ozone. These estimates are intended to provide guidance for decisions on the development of the HSCT fleet for both environmental policy and aeronautical technology. The primary tool for deriving these estimates is the set of CTMs. The central value, uncertainty range, and sensitivity estimates represent a combination of model output, evaluation of model performance, and expert opinion. There is no unique statistical method for determining the values and ranges or combining the various components of uncertainty. These are our best estimates.

One of the most difficult problems in evaluating the HSCT impact is to assess the possibility that the actual impact will be significantly outside our current estimated range. In other words, what is the risk of making a serious mistake in predicting the impact? Our modeling tools are closely scrutinized, but they are not perfect. They have known systematic problems, as discussed above, which infer that processes may be missing from our current knowledge base. History shows examples. On the other hand, progress in stratospheric science has produced much better information to reduce the risk. For example, the HSCT is a very different problem than CFCs at a very different place in assessment history. We have stated the uncertainty range below to limit the risk of a "surprise" to be as small as possible, while still providing useful bounds on the problem.

5.2.1 ESTIMATED CHANGE IN STRATOSPHERIC O_3

Analysis of fundamental processes (Chapter 2) and subsequent comparison of model results to atmospheric measurements (Chapter 4) identified two observational diagnostics of primary importance in evaluating model performance and estimating a central value for the model HSCT predictions. These diagnostics are the age of air and the background amount of NO_y calculated in the model lower stratosphere. These two diagnostics focus the problem on how much of the exhaust accumulates in the lower stratosphere and what is the chemical state of the atmosphere upon which the HSCT perturbation is imposed. Other diagnostics, such as background water and inorganic chlorine, appear to have less leverage on the problem.

Calculated model exhaust accumulations are correlated with the model's age of air. However, the relationship between accumulations and age of air across 2-D models is different from that across 3-D models, with 2-D models predicting higher accumulations for a given age of air. Thus we cannot directly infer a value for the exhaust accumulation for a given age of air, but we assume that the best estimate lies between the values calculated by 2-D and 3-D models whose age of air best approximates observations (GSFC 2-D, Monash1 3-D). For NO_y, the models used in this assessment produce a wide range of concentrations in the lower stratosphere, with values ranging from about a factor of two smaller to a factor of two larger than those derived from ER-2 observations (Section 4.6).

Taking into account the above comparisons, we select results from a model that: (a) calculates NO_y in good agreement with observations, and (b) whose calculated accumulation is within the range spanned by 3-D models and 2-D models with age of air closest to observations. The CSIRO model best fulfills both criteria, and thus we choose the value of -0.4% for mean Northern Hemispheric ozone loss, in the case of 500 aircraft, EI_{NO_x} = 5 with 10% of the fuel sulfur converted to small particles in the wake (Scenario 9, Table 4-3).

The mean central-value ozone change is comprised of changes that vary widely in season, latitude, and altitude. The magnitude of the local changes also varies between models. All models show the maximum exhaust accumulation in the vicinity of the HSCT source region in the lower stratosphere in all seasons, but the amount of accumulation and dispersion through the stratosphere varies by a factor of two or more (Section 4.4.3.2). The induced ozone change is the sum of an ozone increase at lower stratospheric/upper tropospheric altitudes plus a decrease generally at and above the HSCT flight altitude. The balance between increase and loss is different for different models and depends strongly on latitude but less so on season. The result is that all models show their largest amount of column ozone loss at high latitudes, although some occur in the Northern Hemisphere and others in the South. Those with maximum losses in the SH occur in association with enhancing the springtime Antarctic ozone "hole." The seasonal maximum change in the North is not consistent among the models, with some predicting a springtime maximum decrease and others a maximum in the summer or fall. These variations are connected to the models' sensitivity to cold polar processes and PSCs. All models predict a minimum HSCT impact on column ozone in the tropics. The effect of HSCT sulfate aerosol emissions in the models is to increase the ozone loss rates in the lower stratosphere thus increasing the net loss in column ozone.

5.2.2 UNCERTAINTY RANGE IN O_3 IMPACT

In this section, we derive estimates for how the eventual HSCT impact may vary relative to the central estimated value. We discuss two sources of variance in the impact. The first is potential error in our modeling of processes that would result in a different impact than the central estimate discussed above. The second is differences in the model inputs to which the O_3 impact is sensitive. The latter includes engineering sensitivity tests for HSCT design parameters.

Process Modeling Uncertainty

In order to obtain the best description of that part of the uncertainty that we can presently represent in models, we individually examine the links in the chain we use to calculate ozone perturbations. The emphasis is on the uncertainty in the calculations of HSCT impact on both total column ozone and on the distribution of ozone concentrations. Some parts of this chain are better understood and quantified than others. We can qualitatively classify the confidence in these estimates using a similar scheme to the paradigm put forward by Mahlman [1997] to describe the understanding of climate change. Processes and phenomena are divided into the following categories:

1) Well understood and demonstrated by measurements;

2) Highly likely to be correct but not demonstrated by measurements; and

3) Uncertain and difficult to quantify.

We can devise probability estimates that apply, with diminishing confidence, in categories 1-3. We must also acknowledge the possibility that the eventual reality may lie outside our model estimates because the models may be based on incorrect assumptions or lack currently unknown processes. We have made our best attempt to assure that "surprise" error is small but we are not able to estimate the probability. Specific areas of concern are discussed above.

The key steps following the emission of pollutants from a fleet of HSCTs are:

1) Emissions to the atmosphere – What is emitted and how is it deposited in the atmosphere? How much fuel will be burned and where? How much NO_x is emitted per kilogram of fuel? How many particles of what size and composition will be emitted or formed in the exhaust plume?

2) Transport of emissions – Where will they go? How much will build up in various regions of the atmosphere?

    a) Will emissions be primarily confined to mid-latitude lower stratosphere where it is emitted?

    b) How much of the emissions will be transported to equatorial region and then upward where NO_x is a more effective catalyst?

c) How much of the emissions will be transported to polar regions where polar stratospheric cloud chemistry is occurring?

d) How rapidly will the emissions be transported down into the lowermost stratosphere and upper troposphere where they will be lost?

3) Representation of the atmosphere in which the aircraft will fly – How well can we represent the background atmosphere against which the HSCT perturbation is superimposed? This is a question of both how well we simulate the current atmosphere and how well we can forecast future conditions.

4) Chemical effect of emissions – How much will emissions from HSCTs increase or decrease the ozone loss rate? How different are chemical sensitivities in the model from those in the atmosphere, due to incorrect background atmosphere in the model? How will the particles emitted by HSCTs affect the surface area and reactivity of stratospheric aerosol?

5) Effects in polar regions – How will emissions interact chemically with existing polar composition? How much will condensibles (H_2O, HNO_3, sulfur) and emitted aerosols change the particle and polar stratospheric cloud amounts and chemical properties in the polar regions? What will be the impact under cooler conditions possibly forced by greenhouse gas changes?

6) Transport and distribution of the HSCT ozone perturbation – How will the chemical perturbation be moved around by atmospheric transport?

Confidence ratings (1 to 3 above) and estimates for the uncertainty in ozone impact that arises from the uncertainty in each of these processes are given in Table 5-1. The confidence categorization is based on our ability to simulate the current atmosphere as determined by model and measurement comparisons. It reflects our subjective evaluation of the degree to which we can quantitatively estimate the uncertainty in the HSCT ozone impact from that process. The numerical uncertainties in the ozone impact are estimated based on a combination of numerical tests, comparison with measurements, and theoretical expectations. The method of arriving at each number is discussed following the tables. The purpose of these estimates is to support the overall estimate for the uncertainty in the HSCT ozone impact and to demonstrate where the major uncertainties lie.

We use the uncertainties from Table 5-1 to estimate the uncertainty range about the central value estimated for the HSCT ozone impact. Recognizing that no statistical method is known for combining these quantities, we derived the overall range estimate by taking the root sum of squares of the individual terms. We estimate that the HSCT ozone impact is likely to fall in the range of -2.5 to +0.5% for the central test scenario. We also note that the maximum seasonal and latitudinal ozone changes will be greater than the hemispheric annual mean.

Table 5-1. Process uncertainties.

Process	Confidence Category	Uncertainty of ΔO_3
Exhaust Emission		
Aerosols	3	-1 to 0.1%
Transport		
Long-term circulation and exhaust accumulation	2 to 3	±1.0%
Background Atmosphere		
Halogens	1 to 2	<0.1%
NO_y	2	±0.3%
H_2O	1 to 2	±0.2%
Chemical Impact		
NO_x/NO_y	2 to 3	-1 to 0.1%
Reaction kinetics	1 to 2	±1.0%
Heterogeneous processes	2 to 3	±0.5%

- **Central value, -0.4%**
- **Actual response likely to fall in range, -2.5 to +0.5%**
- **Latitudinal and seasonal changes will be larger than hemispheric annual mean**

Central value base case is 500 aircraft in year 2015, EI_{NO_x} = 5 g/kg, 10% fuel sulfur conversion to aerosol particles (NH, annual average column ozone change).

Response of Ozone Impact to Varying Input Parameters

Variations of the HSCT ozone impact to varying input parameters are given in Table 5-2. The uncertainty in input parameters is evaluated via sensitivity tests using different scenarios in the model calculations. Responses to variations in the HSCT engineering parameters as well as the meteorology and chemical composition are explored. The method for obtaining these estimates follows the table and the sensitivities are summarized in Section 5.2.3.

Table 5-2. Ozone impact sensitivity.

Parameter	Parameter change relative to base case	ΔO_3 relative to base
Exhaust Emission		
Fuel consumption	to 1000 aircraft	-0.3%
Sulfur content	to 0	+0.3%
	to 0 with 4 x background	+0.1%
EI_{NOx}	to 10 g/kg	-0.1%
Altitude	2 km below base case	+0.2%
	2 km above base case	-0.4%
Future Atmosphere		
Halogens	3 to 2 ppb	-0.1%
H_2O	base case -2 ppm	-0.1%
	base case +2 ppm	+0.1%
Aerosol	background to 4 x background	+0.1%
Temperature	Warm to cold	+0.1 to -0.1%

Notes on Table 5-1 Process Uncertainties:

Exhaust Emission, Aerosols: Emission process uncertainty is dominated by exhaust particle production. Critical parameters are fuel sulfur content, the physics of formation for exhaust aerosols (Section 3.6), and their interaction with ambient stratospheric aerosols. The uncertainty for ΔO_3 is derived from model sensitivity tests (Section 4.4.3.5). Most likely future fuel will have non-zero sulfur content; hence, we use 10% conversion as our most likely scenario.

Transport, Long-Term Circulation and Exhaust Accumulation: There is at least a factor of 2 difference among model-derived HSCT changes to NO_y and H_2O. Most models are suspected to underestimate those changes (Sections 2.3.7, 4.4.3.2, Figure 4-13). In addition, key model tracer distributions differ from observations, giving erroneous background upon which HSCT changes are superposed (Sections 4.3.3). Because of the variations between models and the lack of a unique way to evaluate them, we estimate a 1% uncertainty in HSCT ozone impact from model transport processes. We do not have a clear way to estimate the asymmetry of this uncertainty about the central value.

Background Atmosphere, Halogens: Cl_y is defined by recent data within ±10%; Br_y is known to better than 20%. Models agree to about that same precision (M&M II). The change in ozone from HSCTs is not very sensitive to halogens (Section 4.4.3.8), although actual ozone levels are very sensitive to halogens [WMO, 1999].

NO_y: The models vary by ±30% due mostly to transport differences (Figures 4-2 and 4-4). The effect on the HSCT ozone perturbation could be positive or negative. Most models are biased towards low NO_y, likely giving an underestimate of O_3 loss (Section 4.3.3).

H_2O: H_2O is known to ±20% from observations. For a volcanically clean atmosphere and no fuel sulfur, aircraft water causes a -0.6 to -0.2% modeled ozone change (Table 4-3, scenario 3).

Chemical Impact, NO_x/NO_y: Models appear to have a bias towards NO_x - NO_y ratios about 30% lower than observed. This bias underestimates ozone reduction by HSCTs because the models depict that stratosphere as NO_x poor (Section 2.4.3.3).

Reaction Kinetics: Random propagation of errors in chemical kinetic rates, based on uncertainty in laboratory measurements, leads to an uncertainty in calculated ΔO_3 of about 1% [Stolarski *et al.*, 1995].

Heterogeneous Processes: The representation of these highly non-linear processes in assessment models is primitive and very model-dependent. Strong local effects at high latitudes are possible and these impacts may influence the predictions globally (Sections 2.4.5 and 4.4.3.4). We note that the central value chosen from the CSIRO model was calculated without a PSC representation.

Notes on Table 5-2 Parameter Sensitivities:

The parameter sensitivities are based on perturbations to our base case estimate of the HSCT ozone change. For example, doubling the fleet size to 1000 aircraft from the base case of 500 aircraft leads to an additional 0.3% ozone loss in the NH. We have primarily used the CSIRO model to estimate these parametric ozone changes because of the quality of the background NO_y distribution in the model with respect to observations

Exhaust Emission, Fuel Consumption: For a volcanically clean atmosphere with no particle emissions, the doubling of fleet size to 1000 aircraft approximately doubles the ozone loss (Table 4-3, scenarios 4 and 6). Most of the additional ozone loss is a result of increased emission of water (cf., scenarios 4, 5, and 6).

Fuel Sulfur Content: The production of particles is controlled, at least partially, by sulfur in the fuel (Section 3.6.2). Assuming no particle production, as might be expected for removing sulfur from the fuel, would diminish ozone loss by 0.3% for a volcanically clean atmosphere (Table 4-3, scenarios 4 and 9) and 0.1% for a background enhanced by a factor of 4 (Table 4-4, linearly interpolating between scenarios 26 and 29 to 10% conversion).

EI_{NO_x}: Doubling the EI from 5 to 10 increases ozone loss by an additional 0.1% in the NH with no sulfur particle emission (Table 4-3, scenarios 4 and 5).

Altitude: A downward shift of the reference cruise altitude (TCA, Section 3.7) by 2 km reduces the ozone loss from about -0.2% to nearly zero, while a 2 km upward shift increases the loss to about -0.6% for the case without particle emission (Figure 4-17).

Future Atmospheres, Halogens: The halogen loading of the stratosphere should continue to decrease over the next few decades, which will increase ambient ozone. Differences in HSCT-

produced ozone loss under Cl_y loading of 2 ppb (scenario 6) and 3 ppb (scenario 27) suggest that the Cl_y conditions are not a major factor in HSCT ozone loss.

H_2O: Changes of water vapor concentrations affect the distribution of ozone losses. Using the AER model, an increase of 2 ppm of water entering the stratosphere reduces mid-latitude losses causing a 0.1% average reduction of NH loss. A decrease of 2 ppm increases mid-latitude losses, but substantially reduces northern polar spring ozone loss. See Section 4.4.3.8.

Aerosol: The aerosol background could be 1 to 4 times the present global values, depending on volcanic activity. The presence of volcanic aerosol decreases sensitivity to aircraft-produced particles and NO_x (Section 4.4.3.5).

Temperature: To explore the effect of greenhouse gases cooling the future stratosphere, we have calculated the range of HSCT ozone loss in the AER model using temperature variations from the last 2 decades. Under cold conditions (e.g., 1995) polar losses are -0.5% larger than for warm conditions (e.g., 1991). The sensitivity at mid-latitudes is less (see Figure 4-19).

5.2.3 SUMMARY OF O_3 IMPACTS

The HSCT impacts on stratospheric ozone from Tables 5-1 and 5-2 are summarized here to help guide possible policy and technological decisions regarding the HSCT fleet. Based on the assessment of model results, our central estimate of the annual mean response of NH total column ozone (during volcanically quiescent periods) for a fleet of 500 HSCTs operating at Mach 2.4 with an $EI_{NO_x} = 5$ is -0.4%. Combining estimates of the uncertainty in chemical and transport processes with model sensitivity tests (Table 5-1) we conclude that the mean column ozone response will likely be in the range of -2.5 to +0.5%. These estimates are acknowledged to be expert opinion since we do not have a fully rigorous, quantitative method for evaluating and combining the component uncertainties. Larger peak ozone changes are expected on regional and seasonal scales.

Each of the HSCT emissions of H_2O, NO_x, and sulfur contribute significantly to the calculated response, with H_2O being the single largest contributor. Aircraft emissions of soot and metals are not included in the assessment calculations since their roles in ozone chemistry are expected to be negligible. The predicted ozone change depends on the aircraft design parameters: fleet size (or fuel use), the EI_{NO_x}, flight altitude, and sulfate aerosol production in the engine plume.

The calculated ozone loss is approximately proportional to fleet size (or fuel use) from 500 to 1000 aircraft for the cases without sulfur particle emission. This sensitivity occurs primarily through the amount of water emission and secondarily through NO_x. It is consistent among all models. The ozone response is not uniformly dependent on NO_x EI. The EI sensitivity is small and model-dependent for EI_{NO_x} from 0 to 10 for 500 aircraft. Only at larger EI_{NO_x} or larger fleet size does ozone loss increase distinctly in all models. For enhanced background aerosol amounts, higher EI_{NO_x} is inversely related to ozone loss.

Production of sulfate aerosol particles also makes a significant contribution to the calculated ozone impact. Including aerosol production nearly doubles the ozone impact relative to NO_x and

H_2O emissions only. However, the sensitivity with respect to fuel sulfur is notably uncertain because the connection between aerosol generation, fuel sulfur levels, and engine technology is not well understood.

Calculated ozone change is quite sensitive to the flight altitude. Specifically, a 2 km decrease in flight altitude results in an approximate 50% decrease in calculated ozone loss. The atmospheric residence time of the exhaust is decreased and the chemical sensitivity is less. This relative conclusion is consistent among all the models.

The ozone response also depends on the state of the future atmosphere, especially on global temperature and levels of background gases and particles. The calculated ozone loss for a fleet of HSCTs increases if future background levels of chlorine, water vapor, or sulfate are less than the ones we have assumed. The ozone response to changing global temperature is more difficult to predict but could be substantial if a temperature decrease promotes the occurrence of non-linear gas-particle processes such as denitrification. In that case, the possible routing of HSCT traffic through the arctic polar region would be an important consideration relative to ozone response.

5.2.4 HSCT Climate Impacts

The forcing of climate attributable to an HSCT fleet has been calculated (Section 4.5). The most prominent climate-related perturbations are to stratospheric H_2O, global CO_2, and stratospheric O_3. The impacts of sulfate aerosol and soot are negligible in comparison. The net result is a surface warming in 2050, which is small relative to that expected from other anthropogenic sources. The perturbation of water vapor in the stratosphere produces the dominant HSCT climate forcing. The total radiative forcing from 1000 HSCTs is calculated to be +0.1 W m^{-2} in 2050. This number can be compared to a total anthropogenic forcing of +3.8 W m^{-2} and an estimated +0.2 W m^{-2} from the projected subsonic fleet, although large uncertainties are attached to these numbers. The HSCT number is a concern because its radiative forcing is disproportionately large compared to HSCT fuel use (about 1%) and equivalent to about 50% of the forcing from the entire projected subsonic fleet. Climate forcing is sensitive to HSCT emissions because the H_2O accumulation is localized in the lower stratosphere.

The uncertainty in the HSCT climate forcing is estimated to be about a factor of 3. This is due to uncertainty in the exhaust accumulation and uncertainty in the temperature adjustment to a non-uniform perturbation of radiatively active gas in the stratosphere. For example, a calculation in a full global climate model produced a surface warming of about 0.06°C, which is only half of that expected from a uniform radiative forcing of the HSCT magnitude. Compensating changes in humidity and clouds in the upper troposphere partially offset surface warming.

The large uncertainties in the HSCT climate impact calculations make it difficult to assess how seriously to consider this concern in making decisions about the potential fleet. Clearly we need to refine these estimates and reduce the level of uncertainty. The climate response calculation can be no better than the estimates of HSCT constituent change, so resolving uncertainty in exhaust transport and distribution applies here as well as to the ozone problem. In addition, methods for generating radiative forcing in models need to be established for emissions that are

not uniformly distributed horizontally and vertically. Finally, the link between radiative forcing and surface temperature response needs to be established for inhomogeneous distributions. Then we will be able to assess the seriousness of the HSCT climate impact. Note also that concerns raised previously about changes in the composition and climate of the future atmosphere apply as well to the HSCT climate impact calculations.

5.3 The Path Forward

The findings of this assessment lead us to several conclusions about how to most effectively resolve the HSCT impact problem to a greater degree of certainty. The path follows areas of major uncertainty and high sensitivity, where progress can be expected.

The first point of attack is to improve assessment confidence through better physical representation of transport in numerical models. We seek improved model transport simulations of the current atmosphere to attain better age-of-air and tracer distributions. The approach is to continue 3-D model development and test model formulations and sensitivities in comparison to data. This should include continued investigation of atmospheric physical processes with a broad range of tools in varying dimensionality. The effort must include specific comparison with data for model transport into/from polar regions.

Coupled with improved diagnosis of transport for the current atmosphere, we need to reduce assessment uncertainty due to differing predicted HSCT exhaust distributions among the models. The recommended approach here is to measure tracers with sources in various regions of the stratosphere to test model predictions of exhaust transport and accumulation. Specifically, cosmogenic radionuclides and their abundance ratios are tracers whose source and sink regions are similar to HSCT exhaust gases.

For emissions, we need to understand the mechanism for production of particle precursors in current engines, subsequent production of particles in exhaust plumes, and their dependence on fuel sulfur, well enough to predict HSCT emissions. Because the largest uncertainty remains in the mechanism and magnitude of sulfur oxidation in the engine, we need direct measurements at the exhaust plane of SO_3, SO_2, OH, and chemi-ions over a range of operating conditions for an engine whose operational characteristics are approximately representative of the expected HSCT engine at cruise conditions. These can then be used to test models of engine chemistry to verify our understanding of the processes controlling sulfur oxidation.

In the chemistry area, we need to continue quantitatively testing local photochemical processes and exploring regions of the atmosphere where confidence in our understanding is not high. Two problems merit specific attention. We need a better fundamental parameterization of polar microphysical processes, one that is not strongly model-dependent and has been extensively compared to data. This will come about through targeted measurements in winter polar regions, process model development, incorporation into global models, and comparison with data. The second chemical activity is to explore the impact of recent laboratory kinetics measurements for NO_x/NO_y on data comparisons and global HSCT calculations. In addition to these specific areas, new chemical observations and laboratory measurements in all areas must continually be related

to model simulations to further reduce the risk of being influenced by unknown or missing processes.

Finally, we need to better constrain the potential climate impacts of HSCTs. Reducing the uncertainty in the exhaust accumulation will address one side of the climate uncertainty. We also need to establish methodology to calculate radiative forcing and temperature response to forcing from non-uniform or layered gases. Along with this, we should pursue to a more reliable description of future meteorology and composition.

APPENDICES

APPENDIX A

REFERENCES

Abbatt, J. P. D., Interactions of HBr, HCl, and HOBr with supercooled sulfuric acid solutions of stratospheric composition, *J. Geophys. Res., 100* (D7), 14009-14017, 1995.

Albritton, D. L., W. H. Brune, A. R. Douglass, F. L. Dryer, M. K. W. Ko, C. E. Kolb, R. C. Miake-Lye, M. J. Prather, A. R. Ravishankara, R. B. Rood, R. S. Stolarski, R. T. Watson, and D. J. Wuebbles, *The Atmospheric Effects of Stratospheric Aircraft: Interim Assessment Report of the NASA High-Speed Research Program*, NASA Reference Publication 1333, 1993.

Anderson, B. E., W. R. Cofer, D. R. Bagwell, K. E. Brunke, J. W. Barrick, C. H. Hudgins, and G. D. Nowicki, Airborne observations of aircraft aerosol emissions, I: Total and nonvolatile particle emission indices, *Geophys. Res. Lett., 25*, 1689-1692, 1998a.

Anderson, B. E., W. R. Cofer, D. R. Bagwell, K. E. Brunke, J. W. Barrick, C. H. Hudgins, and G. D. Nowicki, Airborne observations of aircraft aerosol emissions, II: Factors controlling volatile particle production, *Geophys. Res. Lett., 25*, 1693-1696, 1998b.

Anderson, B. E., R. W. Cofer III, and D. S. McDougal, *Air Force F-16 Aircraft Engine Aerosol Emissions Under Cruise Altitude Conditions,* NASA/TM-1999-209102, March, 1999.

Anderson, D. E., R. DeMajistre, S. A. Lloyd, and P. K. Swaminathan, Impact of aerosols and clouds on the troposphere and stratosphere radiation field with application to twilight photochemistry at 20 km, *J. Geophys. Res., 100,* 7135-7145, 1995.

Anderson, M. R., R. C. Miake-Lye, R. C. Brown, and C. E. Kolb, Calculation of exhaust plume structure and emissions of the ER 2 aircraft in the stratosphere, *J. Geophys. Res., 101*, 4025-4032, 1996a.

Anderson, M. R., R. C. Miake-Lye, R. C. Brown, and C. E. Kolb, Numerical modeling of reacting engine plumes and aircraft wake interactions, AIAA paper 96-0948, 1996b.

Andrews, A. E., K. A. Boering, B. C. Daube, S. C. Wofsy, E. J. Hinsta, E. M. Weinstock, and T. P. Bui, Empirical age spectra for the lower tropical stratosphere from *in situ* observations of CO_2: Implications for stratospheric transport, *J. Geophys. Res.*, in press, 1999.

Andrews, D. G., J. R. Holton, and C. B. Leovy, *Middle Atmosphere Dynamics*, xi, 489 pp., Academic Press, Orlando, 1987.

Appenzeller, C., H. C. Davies, and W. A. Norton, Fragmentation of stratospheric intrusions, *J. Geophys. Res., 101* (D1), 1435-1456, 1996a.

Appenzeller, C., J. R. Holton, and K. H. Rosenlof, Seasonal variation of mass transport across the tropopause, *J. Geophys. Res., 101* (D10), 15071-15078, 1996b.

Appleman, H., The formation of exhaust condensation trails by jet aircraft, *Bull. Am. Meteorol. Soc.*, *34*, 14-20, 1953.

Arnold, F., T. Stilp, R. Busen, and U. Schumann, Jet engine exhaust chemi-ion measurements: Implications for gaseous SO_3 and H_2SO_4, *Atmos. Environ.*, 32, 3073-3077, 1998.

Avallone, L. M., and M. J. Prather, Photochemical evolution of ozone in the lower tropical stratosphere, *J. Geophys. Res.*, *101* (D1), 1457-1461, 1996.

Avallone, L. M., D. W. Toohey, S. M. Schauffler, W. H. Pollock, L. E. Heidt, and E. L. Atlas, *In situ* measurements of BrO during AASE II, *Geophys. Res. Lett.*, *22* (7), 831-834, 1995.

Barnes, R. J., M. Lock, J. Coleman, and A. Sinha, Observation of a new absorption of HOBr and its atmospheric implications, *J. Phys. Chem.*, *100* (2), 453-457, 1996.

Battle, M., M. Bender, T. Sowers, P. Tans, J. Butler, J. Elkins, J. Ellis, T. Conway, N. Zhang, P. Lang, and A. Clark, Histories of atmospheric gases from the firn at south pole, *Nature*, *383* (6597), 231-235, 1996.

Baughcum, S. L., *Aircraft Emission Deposited in the Stratosphere and Within the Arctic Polar Vortex*, NASA CR-4714, 1996.

Baughcum, S. L., and S. C. Henderson, *Aircraft Emission Inventories Projected in Year 2015 for a High Speed Civil Transport (HSCT) Universal Airline Network,* NASA CR-4659, 1995.

Baughcum, S. L., and S. C. Henderson, *Aircraft Emission Scenarios Projected in Year 2015 for the NASA Technology Concept Aircraft (TCA) High Speed Civil Transport,* NASA CR-1998-207635, 1998.

Baughcum, S. L., S. C. Henderson, P. S. Hertel, D. R. Maggiora, and C. A. Oncina, *Stratospheric Emissions Effects Database Development,* NASA CR-4592, 1994.

Baughcum, S. L., S. C. Henderson, T. G. Tritz, and D. C. Pinkett, *Scheduled Civil Aircraft Emission Inventories for 1992: Database Development and Analysis,* NASA CR-4700, 1996.

Baughcum, S. L., S. C. Henderson, and D. J. Sutkus, *Scheduled Civil Aircraft Emission Inventories Projected for 2015: Database Development and Analysis,* NASA CR-1998-207638, 1998.

Baumgardner, D., R. C. Miake-Lye, M. R. Anderson, and R. C. Brown, An evaluation of temperature, water vapor and vertical velocity structure of an aircraft contrail, *J. Geophys. Res.*, *103*, 8727-8736, 1998.

Bekki, S., On the possible role of aircraft-generated soot in the middle latitude ozone depletion, *J. Geophys. Res.*, *102* (D9), 10751-10758, 1997.

Bischof, W., R. Borchers, P. Fabian, and B. C. Krüger, Increased concentration and vertical distribution of carbon dioxide in the stratosphere, *Nature*, *316*, 708-710, 1985.

Blake, D. F., and K. Kato, Latitudinal distribution of black carbon soot in the upper troposphere and lower stratosphere, *J. Geophys. Res.*, *100* (D4), 7195-7202, 1995.

Boering, K. A., AC files, (balloon category) included in *Photochemistry of Ozone Loss in the Arctic Region in Summer* (CD-ROM NASA/UARP-008), S. Gaines (ed.), NASA Ames Research Center, Moffett Field, CA, 1998.

Boering, K. A., S. C. Wofsy, B. C. Daube, H. R. Schneider, M. Loewenstein, J. R. Podolske, and I. J. Conway, Stratospheric mean ages and transport rates from observations of carbon dioxide and nitrous oxide, *Science, 274* (5291), 1340-1343, 1996.

Bonne, G. P., R. M. Stimpfle, R. C. Cohen, P. B. Voss, K. K. Perkins, J. G. Anderson, R. J. Salawitch, J. W. Elkins, G. S. Dutton, K. W. Jucks, G. C. Toon, and B. Sen, An examination of the inorganic chlorine budget in the lower stratosphere, submitted to *J. Geophys. Res.*, 1999.

Borrmann, S., S. Solomon, J. E. Dye, D. Baumgardner, K. K. Kelly, and K. R. Chan, Heterogeneous reactions on stratospheric background aerosols, volcanic sulfuric acid droplets, and type I PSCs: Effects of temperature fluctuations and differences in particle phase, *J. Geophys. Res., 102*, 3639-3648, 1997.

Boville, B. A., Middle atmosphere version of the CCM2 (MACCM2): Annual cycle and interannual variability, *J. Geophys. Res., 100,* 9017-9039, 1995.

Brock, C. A., P. Hamill, J. C. Wilson, H. H. Jonsson, and K. R. Chan, Particle formation in the upper tropical troposphere: A source of nuclei for the stratospheric aerosol, *Science, 270* (5242), 1650-1653, 1995.

Brown, R. C., R. C. Miake-Lye, M. R. Anderson, C. E. Kolb, and T. J. Resch, Aerosol dynamics in near-field aircraft plumes, *J. Geophys. Res., 101,* 22939-22953, 1996a.

Brown, R. C., M. R. Anderson, R. C. Miake-Lye, C. E. Kolb, A. A. Sorokin, and Y. Y. Buriko, Aircraft exhaust sulfur emissions, *Geophys. Res. Lett., 23*, 3603-3606, 1996b.

Brown, S. S., R. K. Talukdar, and A. Ravishankara, Rate constants for the reaction $OH + NO_2 + M \rightarrow HNO_3$ under atmospheric conditions, *Chem. Phys. Lett.*, 299, 277-284, 1999.

Burkholder, J. B., A. R. Ravishankara, and S. Solomon, UV/visible and IR absorption cross sections of $BrONO_2$, *J. Geophys. Res., 100* (D8), 16793-16800, 1995.

Butler, J. H., S. A. Montzka, A. D. Clarke, J. M. Lobert, and J. W. Elkins, Growth and distribution of halons in the atmosphere, *J. Geophys. Res., 103* (D1), 1503-1511, 1998.

Butler, J. H., M. Battle, M. Bender, S. A. Montzka, A. D. Clarke, E. S. Saltzman, C. Sucher, J. Severinghaus, and J. W. Elkins, A Twentieth century record of atmospheric halocarbons in polar firn air, submitted to *Nature*, 1999.

Carslaw, K. S., B. P. Luo, S. L. Clegg, T. Peter, P. Brimblecombe, and P. J. Crutzen, Stratospheric aerosol growth and HNO_3 gas phase depletion from coupled HNO_3 and water uptake by liquid particles, *Geophys. Res. Lett., 21* (23), 2479-2482, 1994.

Carslaw, K. S., B. Luo, and Th. Peter, An analytic expression for the composition of aqueous HNO_3-H_2SO_4 stratospheric aerosols including gas-phase removal of HNO_3, *Geophys. Res. Lett., 22*, 1877-1880, 1995.

Carslaw, K. S., T. Peter, and S. L. Clegg, Modeling the composition of liquid stratospheric aerosols, *Rev. Geophys., 35* (2), 125-154, 1997.

Chang, A. Y., R. J. Salawitch, H. A. Michelsen, M. R. Gunson, M. C. Abrams, R. Zander, C. P. Rinsland, J. W. Elkins, G. S. Dutton, C. M. Volk, C. R. Webster, R. D. May, D. W. Fahey, R. S. Gao, M. Loewenstein, J. R. Podolske, R. M. Stimpfle, D. W. Kohn, M. H. Proffitt, J. J. Margitan, K. R. Chan, M. M. Abbas, A. Goldman, F. W. Irion, G. L. Manney, M. J. Newchurch, and G. P. Stiller, A comparison of measurements from ATMOS and instruments aboard the ER-2 aircraft: Halogenated gases, *Geophys. Res. Lett., 23* (17), 2393-2396, 1996a.

Chang, A. Y., R. J. Salawitch, H. A. Michelsen, M. R. Gunson, M. C. Abrams, R. Zander, C. P. Rinsland, M. Loewenstein, J. R. Podolske, M. H. Proffitt, J. J. Margitan, D. W. Fahey, R. S. Gao, K. K. Kelly, J. W. Elkins, C. R. Webster, R. D. May, K. R. Chan, M. M. Abbas, A. Goldman, F. W. Irion, G. L. Manney, M. J. Newchurch, and G. P. Stiller, A comparison of measurements from ATMOS and instruments aboard the ER-2 aircraft: Tracers of atmospheric transport, *Geophys. Res. Lett., 23* (17), 2389-2392, 1996b.

Chatfield, R. B., and P. J. Crutzen, Sulfur dioxide in remote oceanic air: Cloud transport of reactive precursors, *J. Geophys. Res., 89* (D5), 7111-32, 1984.

Chen, P., Isentropic cross-tropopause mass exchange in the extratropics, *J. Geophys. Res., 100,* 16661-16673, 1995.

Chen, Y., S. M. Kreidenweis, L. M. McInnes, D. C. Rogers, and P. J. DeMott, Single particle analyses of ice nucleating aerosols in the upper troposphere and lower stratosphere, *Geophys. Res. Lett., 25,* 1391-1394, 1998.

Chin, M., and D. D. Davis, A reanalysis of carbonyl sulfide as a source of stratospheric background sulfur aerosol, *J. Geophys. Res., 100* (D5), 8993-9005, 1995.

Chipperfield, M. P., Multiannual simulations with a three-dimensional chemical transport model, *J. Geophys. Res., 104,* 1781-1805, 1999.

Chughtai, A. R., M. E. Brooks, and D. M. Smith, Effect of metal oxides and black carbon (soot) on $SO_2/O_2/H_2O$ reactions systems, *Aerosol Sci. Technol., 19,* 121-132, 1993.

Chughtai, A. R., M. E. Brooks, and D. M. Smith, Hydration of black carbon, *J. Geophys. Res., 101,* 19505-19514, 1996.

CIAP Monograph 2, *Propulsion Effluents in the Stratosphere,* Climate Impact Assessment Program, DOT-TST-75-52, U.S. Department of Transportation, Washington, DC, 1975.

Clancy, R. T., D. W. Rusch, R. J. Thomas, M. Allen, and R. S. Eckman, Model ozone photochemistry on the basis of Solar Mesospheric Explorers mesospheric observations, *J. Geophys. Res., 92,* 3067-3080, 1987.

Cohen, R. C., P. O. Wennberg, R. M. Stimpfle, J. Koplow, J. G. Anderson, D. W. Fahey, E. L. Woodbridge, E. R. Keim, R. Gao, M. H. Proffitt, M. Loewenstein, and K. R. Chan, Are models of catalytic removal of O_3 by HO_x accurate? Constraints from *in situ* measurements of the OH to HO_2 ratio, *Geophys. Res. Lett., 21* (23), 2539-2542, 1994.

Considine, D. B., A. R. Douglass, and C. H. Jackman, Effects of a polar stratospheric cloud parameterization on ozone depletion due to stratospheric aircraft in a two-dimensional model, *J. Geophys. Res., 99,* 18879-18894, 1994.

Coy, L., E. R. Nash, and P. A. Newman, Meteorology of the polar vortex: March 1997, *Geophys. Res. Lett., 24,* 2693-2696, 1997.

Crutzen, P. J., J.-U. Gross, C. Brühl, R. Müller, and J. M. Russell III, A reevaluation of the O_3 budget with HALOE UARS data: No evidence for the O_3 deficit, *Science, 268,* 705-708, 1995.

Curtius, J., B. Sierau, F. Arnold, R. Baumann, R. Busen, P. Schulte, and U. Schumann, First direct sulfuric acid detection in the exhaust plume of a jet aircraft in flight, *Geophys. Res. Lett., 25,* 923-926, 1998.

Dahlberg, S. P., and K. P. Bowman, Climatology of large-scale isentropic mixing in the Arctic winter stratosphere from analyzed winds, *J. Geophys. Res., 99* (D10), 20585-20599, 1994.

Dameris, M., V. Grewe, and B. Steil, Assessment of the future development of the ozone layer, *Geophys. Res. Lett., 25,* 3579-3582, 1998.

Daniel, J. S., S. M. Schauffler, W. H. Pollock, S. Solomon, A. Weaver, L. E. Heidt, R. R. Garcia, E. L. Atlas, and J. F. Vedder, On the age of stratospheric air and inorganic chlorine and bromine release, *J. Geophys. Res., 101* (D11), 16757-16770, 1996.

Danilin, M. Y., and J. C. McConnell, Heterogeneous reactions in a stratospheric box model: A sensitivity study, *J. Geophys. Res., 99* (D12), 25681-25696, 1994.

Danilin, M. Y., J. M. Rodriguez, M. K. W. Ko, D. K. Weisenstein, R. C. Brown, R. C. Miake-Lye, and M. R. Anderson, Aerosol particle evolution in an aircraft wake: Implications for the high-speed civil transport fleet impact on ozone, *J. Geophys. Res., 102,* 21453-21463, 1997.

De Rudder, A., N. Larsen, X. Tie, G. P. Brasseur, and C. Granier, Model study of polar stratospheric clouds and their effect on stratospheric ozone, 1. Model description, *J. Geophys. Res., 101,* 12567-12574, 1996.

Del Negro, L. A., D. W. Fahey, S. G. Donnelly, R. S. Gao, E. R. Keim, R. C. Wamsley, E. L. Woodbridge, J. E. Dye, D. Baumgardner, B. W. Gandrud, J. C. Wilson, H. H. Jonsson, M. Loewenstein, J. R. Podolske, C. R. Webster, R. D. May, D. R. Worsnop, A. Tabazadeh, M. A. Tolbert, K. K. Kelly, and K. R. Chan, Evaluating the role of NAT, NAD, and liquid $H_2SO_4/H_2O/HNO_3$ solutions in Antarctic polar stratospheric cloud aerosol: Observations and implications, *J. Geophys. Res., 102* (D11), 13255-82, 1997.

DeMore, W. B., S. P. Sander, D. M. Golden, R. F. Hampson, M. J. Kurylo, C. J. Howard, A. R. Ravishankara, C. E. Kolb, and M. J. Molina, *Chemical Kinetics and Photochemical Data for use in Stratospheric Modeling,* JPL Publication 94-26, 1994.

DeMore, W. B., S. P. Sander, D. M. Golden, R. F. Hampson, M. J. Kurylo, C. J. Howard, A. R. Ravishankara, C. E. Kolb, and M. J. Molina, *Chemical Kinetics and Photochemical Data for use in Stratospheric Modeling,* JPL Publication 97-4, 1997.

Dessler, A. E., E. M. Weinstock, E. J. Hintsa, J. G. Anderson, C. R. Webster, R. D. May, J. W. Elkins, and G. S. Dutton, An examination of the total hydrogen budget of the lower stratosphere, *Geophys. Res. Lett.*, *21* (23), 2563-2566, 1994.

Dessler, A. E., E. J. Hintsa, E. M. Weinstock, J. G. Anderson, and K. R. Chan, Mechanisms controlling water vapor in the lower stratosphere: 'A tale of two stratospheres', *J. Geophys. Res.*, *100* (D11), 23167-23172, 1995.

Dessler, A. E., S. R. Kawa, A. R. Douglass, D. B. Considine, J. B. Kumer, A. E. Roche, J. L. Mergenthaler, J. W. Waters, J. M. Russell III, and J. C. Gille, A test of the partitioning between ClO and $ClONO_2$ using simultaneous UARS measurements of ClO, NO_2, and $ClONO_2$, *J. Geophys. Res.*, *101* (D7), 12515-12521, 1996a.

Dessler, A. E., S. R. Kawa, D. B. Considine, J. W. Waters, L. Froidevaux, and J. B. Kumer, UARS measurements of ClO and NO_2 at 40 km and 46 km and implications for the model 'ozone deficit', *Geophys. Res. Lett.*, *23*, 339-342, 1996b.

Dessler, A. E., D. B. Considine, J. E. Rosenfield, S. R. Kawa, A. R. Douglass, and J. M. Russell III, Lower stratospheric chlorine partitioning during the decay of the Mt. Pinatubo aerosol cloud, *Geophys. Res. Lett.*, *24* (13), 1623-1626, 1997.

Dibb, J. E., L. D. Meeker, R. C. Finkel, J. R. Southon, M. W. Caffee, and L. A. Barrie, Estimation of stratospheric input to the Arctic troposphere ^{7}Be and ^{10}Be in aerosols at Alert, Canada, *J. Geophys. Res.*, *99* (D6), 12855-12864, 1994.

Dlugokencky, E. J., K. A. Masarie, P. M. Lang, and P. P. Tans, Continuing decline in the growth rate of the atmospheric methane burden, *Nature*, *393* (6684), 447-450, 1998.

Donahue, N. M., M. K. Dubey, R. Mohrschladt, K. L. Demerjian, and J. G. Anderson, High-pressure flow study of the reactions OH + NO_x to $HONO_x$: Errors in the falloff region, *J. Geophys. Res.*, *102* (D5), 6159-6168, 1997.

Dopplick, T. G., Radiative heating of the global atmosphere: Corrigendum, *J. Atmos., Sci.*, *36*, 1812-1817, 1979.

Douglass, A. R., R. B. Rood, S. R. Kawa, and D. J. Allen, A three-dimensional simulation of the evolution of the middle latitude winter ozone in the middle stratosphere, *J. Geophys. Res.*, *102*, 19217-19232, 1997.

Douglass, A. R., M. P. Prather, T. M. Hall, S. E. Strahan, P. J. Rasch, L. C. Sparing, L. Coy, and J. M. Rodriguez, Choosing meteorological input for the global modeling initiative assessment of high speed aircraft, submitted to *J. Geophys. Res.*, 1999.

Dransfield, T. J., K. K. Perkins, N. M. Donahue, J. G. Anderson, M. M. Sprengnether, and K. L. Demerjian, Temperature and pressure dependent kinetics of the gas-phase reaction of the hydroxyl radical with nitrogen dioxide, *Geophys. Res. Lett.*, *26*, 687-690, 1999.

Dubey, M. K., G. P. Smith, W. S. Hartley, D. E. Kinnison, and P. S. Connell, Rate parameter uncertainty effects in assessing stratospheric ozone depletion by supersonic aviation, *Geophys. Res. Lett.*, *24*, 2737, 1997.

Dunkerton, T., and D. O'Sullivan, Mixing zone in tropical stratosphere above 10 mb, *Geophys. Res. Lett., 23*, 2497-2500, 1996.

Dürbeck, T., and T. Gerz, Dispersion of aircraft exhausts in the free atmosphere, *J. Geophys. Res., 101*, 26007-26015, 1996.

Durlak, S. K., Investigation of aerosol formation and sulfur speciation in subsonic jet aircraft engines, Ph.D. Dissertation, University of Cincinnati, Ohio, 1997.

Eckman, E. C., W. L. Grose, R. E. Turner, W. T. Blackshear, and J. M. Russell III, Stratospheric trace constituents simulated by a three-dimensional general circulation model: Comparison with UARS data, *J. Geophys. Res. 100* (D7), 13951-13966, 1995.

Elkins, J. W., D. W. Fahey, J. M. Gilligan, G. S. Dutton, T. J. Baring, C. M. Volk, R. E. Dunn, R. C. Myers, S. A. Montzka, P. R. Wamsley, A. H. Hayden, J. H. Butler, T. M. Thompson, T. H. Swanson, E. J. Dlugokencky, P. C. Novelli, D. F. Hurst, J. M. Lobert, S. J. Ciciora, R. J. McLaughlin, T. L. Thompson, R. H. Winkler, P. J. Fraser, L. P. Steele, and M. P. Lucarelli, Airborne gas chromatograph for *in situ* measurements of long-lived species in the upper troposphere and lower stratosphere, *Geophys. Res. Lett., 23* (4), 347-350, 1996.

Eluszkiewicz, J., and M. Allen, A global analysis of ozone deficit in the upper stratosphere and lower mesosphere, *J. Geophys. Res., 98,* 1069-1082, 1993.

Eluszkiewicz, J., D. Crisp, R. Zurek, L. Elson, E. Fishbein, L. Froidevaux, J. Waters, R. G. Grainger, A. Lambert, R. Harwood, and G. Peckham, Residual circulation in the stratosphere and lower mesosphere as diagnosed from Microwave Limb Sounder data, *J. Atmos. Sci., 53* (2), 217-240, 1996.

Elrod, M. J., R. F. Meads, J. B. Lipson, J. V. Seeley, and M. J. Molina, Temperature dependence of the rate constant for the HO_2 + BrO reaction, *J. Phys. Chem., 100* (14), 5808-5812, 1996.

Engel A., U. Schmidt, and D. McKenna, Stratospheric trends of CFC-12 over the past two decades: Recent observational evidence of declining growth rates, *Geophys. Res. Lett., 25* (17), 3319-3322, 1998.

Fabian, P., and B. Kärcher, The impact of aviation upon the atmosphere: An assessment of present knowledge, uncertainties and research needs, *Phys. Chem. Earth, 22,* 503-598, 1997.

Fahey, D. W., D. M. Murphy, K. K. Kelly, M. K. W. Ko, M. H. Proffitt, C. S. Eubank, G. V. Ferry, M. Loewenstein, and K. R. Chan, Measurements of nitric oxide and total reactive odd-nitrogen in the Arctic stratosphere: Observations and chemical implications, *J. Geophys. Res., 94,* 16665-16681, 1989.

Fahey, D. W., S. R. Kawa, E. L. Woodbridge, P. Tin, J. C. Wilson, H. H. Jonsson, J. E. Dye, D. Baumgardner, S. Borrmann, D. W. Toohey, L. M. Avallone, M. H. Proffitt, J. Margitan, M. Loewenstein, J. R. Podolske, R. J. Salawitch, S. C. Wofsy, M. K. W. Ko, D. E. Anderson, M. R. Schoeberl, and K. R. Chan, *In situ* measurements constraining the role of sulphate aerosols in mid-latitude ozone depletion, *Nature, 363* (6429), 509-514, 1993.

Fahey, D. W., E. R. Keim, K. A. Boering, C. A. Brock, J. C. Wilson, H. H. Jonsson, S. Anthony, T. F. Hanisco, P. O. Wennberg. R. C. Miake-Lye, R. J. Salawitch, N. Louisnard, E. L. Woodbridge, R. S. Gao, S. G. Donnelly, R. C. Wamsley, L. A. Del Negro, S. Solomon, B. C. Danube, S. C. Wofsy, C. R. Webster, R. D. May, K. K. Kelly, M. Loewenstein, J. R. Podolske, and K. R. Chan, Emission measurements of the Concorde supersonic aircraft in the lower stratosphere, *Science, 270,* 70-74, 1995a.

Fahey, D. W., E. R. Keim, E. L. Woodbridge, R. S. Gao, K. A. Boering, B. C. Daube, S. C. Wofsy, R. P. Lohmann, E. J. Hintsa, A. E. Dessler, C. R. Webster, R. D. May, C. A. Brock, J. C. Wilson, R. C. Miake-Lye, R. C. Brown, J. M. Rodriguez, M. Loewenstein, M. H. Proffitt, R. M. Stimpfle, S. W. Bowen, and K. R. Chan, *In situ* observations in aircraft exhaust plumes in the lower stratosphere at midlatitudes, *J. Geophys. Res., 100,* 3065-3074, 1995b.

Fahey, D. W., S. G. Donnelly, E. R. Keim, R. S. Gao, R. C. Wamsley, L. A. Del Negro, E. L. Woodbridge, M. H. Proffitt, K. H. Rosenlof, D. K. Weisenstein, C. J. Scott, C. Nevison, S. Solomon, and K. R. Chan, *In situ* observation of NO_y, and the NO_y/O_3 in the lower stratosphere, *Geophys. Res. Lett., 23,* 1653-1656, 1996.

Fendel, W., D. Matter, H. Burtscher, and A. Schmidtott, Interaction between carbon or iron aerosol particles and ozone, *Atmos. Environ., 29* (9), 967-973, 1995.

Fenter, F. F., and M. J. Rossi, Heterogeneous kinetics of HONO on H_2SO_4 solutions and on ice: Activation of HCl, *J. Phys. Chem.*, 100, 13765-13775, 1996.

Fish, D. J., S. R. Aliwell, and R. L. Jones, Mid-latitude observations of the seasonal variation of BrO, 2: Interpretation and modeling study, *Geophys. Res. Lett., 24* (10), 1199-202, 1997.

Frenzel, A., and F. Arnold, Sulfuric acid cluster ion formation by jet engines: Implications for sulfuric acid formation and nucleation, in *DLR-Mitt. 94-06, Deutsche Forschungsanstalt f. Luft-u. Raumfahrt*, Köln, Germany, 106-112, 1994.

Friedl, R. R., S. L. Baughcum, B. E. Anderson, J. Hallett, K.-N. Liou, P. J. Rasch, D. H. Rind, K. Sassen, H. B. Singh, L. R. Williams, and D. J. Wuebbles, *Atmospheric Effects of Subsonic Aircraft: Interim Assessment Report of the Advanced Subsonic Technology Program,* NASA Reference Publication 1400, 1997.

Fusco, F. C., and M. L. Salby, Interannual variations in total ozone and their relationship to variation of planetary wave activity, *J. Clim.,* in press, 1999.

Gaines, S. (ed.), *Airborne Southern Hemisphere Ozone Experiment/Measurements for Assessing the Effects of Stratospheric Aircraft* [CD-ROM NASA/UARP-005], NASA Ames Research Center, Moffett Field, CA, 1995.

Gaines, S. (ed.), *Photochemistry of Ozone Loss in the Arctic Region in Summer* [CD-ROM NASA/UARP-008], NASA Ames Research Center, Moffett Field, CA, 1998.

Gaines, S. and S. Hipskind (eds.), *Stratospheric Tracers of Atmospheric Transport* [CD-ROM NASA/UARP-006], NASA Ames Research Center, Moffett Field, CA, 1997.

Gao, R. S., D. W. Fahey, R. J. Salawitch, S. A. Lloyd, D. E. Anderson, R. DeMajistre, C. T. McElroy, E. L. Woodbridge, R. C. Wamsley, S. G. Donnelly, L. A. Del Negro, M. H. Proffitt, R. M. Stimpfle, D. W. Kohn, S. R. Kawa, L. R. Lait, M. Loewenstein, J. R. Podolske, E. R. Keim, J. E. Dye, J. C. Wilson, and K. R. Chan, Partitioning of the reactive nitrogen reservoir in the lower stratosphere of the Southern Hemisphere: Observations and modeling, *J. Geophys. Res., 102* (D3), 3935-3949, 1997.

Gao, R. S., D. W. Fahey, L. A. Del Negro, S. G. Donnelly, E. R. Keim, J. A. Neuman, L. Teverovskaia, P. O. Wennberg, T. F. Hanisco, E. J. Lanzendorf, M. H. Proffitt, J. J. Margitan, J. C. Wilson, J. W. Elkins, R. M. Stimpfle, R. C. Cohen, C. T. McElroy, T. P. Bui, R. J. Salawitch, S. Brown, A. R. Ravishankara, R. Portmann, M. K. W. Ko, D. K. Weisenstein, and P. A. Newman, A comparison of observations and model simulations of the NO_x/NO_y ratio in the lower stratosphere, *Geophys. Res. Lett., 26,* 1153-1156, 1999.

Garcia, R. R., and S. Solomon, A numerical model of the zonally averaged dynamical and chemical structure of the middle atmosphere, *J. Geophys. Res., 88,* 1379-1400, 1983.

Garcia, R. R., Parameterization of planetary wave breaking in the middle stratosphere, *J. Atmos., Sci., 48,* 1405-1419, 1991.

Garnier, F. S. Brunet, and L. Jacquin, Modelling exhaust plume mixing in the near field of an aircraft, *Ann. Geophys., 15,* 1468-1477, 1997.

Gettelman, A., The lifetime of aircraft emission in the stratosphere, *Geophys. Res. Lett., 25,* 2129-2132, 1998.

Gettelman, A., J. Holton, and K. H. Rosenlof, Mass fluxes of O_3, CH_4, N_2O and CF_2l_2 in the lower stratosphere calculated from observational data, *J. Geophys. Res., 102,* 19149-14159, 1997.

Granier, C., and G. Brasseur, Ozone and other trace gases in the Arctic and Antarctic regions: Three-dimensional model simulations, *J. Geophys. Res., 96,* 2995-3011, 1991.

Grecu, J. C., M. Lowenstein, and J. R. Podolske, Correlations of nitrous oxide with ozone and reactive nitrogen species in the lower stratosphere, *EOS Trans., AGU, 77,* Fall meeting Supplement, F104, 1996.

Hadaller, O. J., and A. M. Momenthy, *The Characteristics of Future Fuels*, Boeing publication D6-54940, 1989.

Hadaller, O. J., and A. M. Momenthy, Characteristics of Future Aviation Fuels, Chapter 10 in *Transportation and Global Climate Change*, D. L. Greene and D. J. Santini (eds.), American Council for an Energy-Efficient Economy, Washington, DC, 1993.

Hagen, D. E., P. D. Whitefield, and H. Schlager, Particle emissions in the exhaust plume from commercial jet aircraft under cruise conditions, *J. Geophys. Res., 101,* 19551-19557, 1996.

Hagen, D., P. Whitefield, J. Paladino, M. Trueblood, and H. Lilenfeld, Particulate sizing and emission indices for a jet engine exhaust sampled at cruise, *Geophys. Res. Lett.*, 25, 1681-1684, 1998.

Hall, T. M., and R. A. Plumb, Age as a diagnostic of stratospheric transport, *J. Geophys. Res., 99* (D1), 1059-1070, 1994.

Hall, T. M., and D. Waugh, Tracer transport in the tropical stratosphere due to vertical diffusion and horizontal mixing, *Geophys. Res. Lett., 24* (11), 1383-1386, 1997a.

Hall, T. M., and D. W. Waugh, Timescales for the stratospheric circulation derived from tracers, *J. Geophys. Res., 102* (D7), 8991-9001, 1997b.

Hall, T. M., D. W. Waugh, K. A. Boering, and R. A. Plumb, Evaluation of transport in stratospheric models, *J. Geophys. Res.*, in press, 1999.

Hanisco, T. F., P. O. Wennberg, R. C. Cohen, J. G. Anderson, D. W. Fahey, E. R. Keim, R. S. Gao, R. C. Wamsley, S. G. Donnelly, L. A. Del Negro, R. J. Salawitch, K. K. Kelly, and M. H. Proffitt, The role of HO_x in super- and subsonic aircraft exhaust plumes, *Geophys. Res. Lett.*, 24, 65-68, 1997.

Hansen, J., R. Ruedy, M. Sato, and R. Reynolds, Global surface air temperature in 1995: Return to pre-Pinatubo level, *Geophys. Res. Lett., 23,* 1665-1668, 1996.

Hanson, D. R., Reaction of N_2O_5 with H_2O on bulk liquids and on particles and the effect of dissolved HNO_3, *Geophys. Res. Lett., 24* (9), 1087-1090, 1997.

Hanson, D. R., and E. R. Lovejoy, The reaction of $ClONO_2$ with submicrometer sulfuric acid aerosol, *Science, 267* (5202), 1326-1328, 1995.

Hanson, D. R., and K. Mauersberger, Laboratory studies of the nitric acid trihydrate: Implications for the south polar stratosphere, *Geophys. Res. Lett., 15,* 855-858, 1988.

Hanson, D. R., and A. R. Ravishankara, Reactive uptake of $ClONO_2$ onto sulfuric acid due to reaction with HCl and H_2O, *J. Phys. Chem., 98,* 5728-5735, 1993.

Hanson, D. R., A. R. Ravishankara, and S. Solomon, Heterogeneous reactions in sulfuric acid aerosols: A framework for model calculations, *J. Geophys. Res., 99* (D2), 3615-3629, 1994.

Hanson, D. R., A. R. Ravishankara, and E. R. Lovejoy, Reaction of $BrONO_2$ with H_2O on submicron sulfuric acid aerosol and the implications for the lower stratosphere, *J. Geophys. Res., 101* (D4), 9063-9069, 1996.

Harder, H., C. Camy-Peyret, F. Ferlemann, R. Fitzenberger, T. Hawat, H. Osterkamp, M. Schneider, D. Perner, U. Platt, P. Vradelis, and K. Pfeilsticker, Stratospheric BrO profiles measured at different latitudes and seasons: Atmospheric observations, *Geophys. Res. Lett., 25* (20), 3843-3846, 1998.

Harnisch, J., R. Borchers, P. Fabian, and M. Maiss, Tropospheric trends for CF_4 and C_2F_6 since 1982 derived from SF_6 dated stratospheric air, *Geophys. Res. Lett., 23* (10), 1099-1102, 1996.

Hathaway, P., S. Gaines, and S. Hipskind (eds.), *Stratospheric Photochemistry, Aerosols and Dynamics Expedition* [CD-ROM NASA/HSRP-001], NASA Ames Research Center, Moffett Field, CA, 1994.

Haynes, P. H., C. J. Marks. M. E. McIntyre, T. G. Shepherd, and K. P. Shione, On the 'downward control' of extratropical diabatic circulations by eddy-induced mean zonal forces, *J. Atmos. Sci., 48,* 651-678, 1991.

Herman, R. L., D. C. Scott, C. R. Webster, R. D. May, E. J. Moyer, R. J. Salawitch, Y. L. Yung, G. C. Toon, B. Sen, J. J. Margitan, K. H. Rosenlof, H. A. Michelsen, and J. W. Elkins, Tropical entrainment time scales inferred from stratospheric N_2O and CH_4 observations, *Geophys. Res. Lett., 25,* 2781-2784, 1998.

Hess, P. G., and J. R. Holton, The origin of temporal variance in long-lived trace constituents in the summer stratosphere, *J. Atmos. Sci., 42,* 1455-1463, 1985.

Hintsa, E., K. A. Boering, E. M. Weinstock, J. G. Anderson, B. L. Gary, L. Pfister, B. C. Daube, S. C. Wofsy, M. Loewenstein, J. R. Podolske, J. J. Margitan, and T. P. Bui, Troposphere-to-stratosphere transport in the lowermost stratosphere from measurements of H_2O, CO_2 N_2O and O_3, *Geophys. Res. Lett., 25,* 2655-2658, 1998.

Hitchman, M. H., M. McKay, and C. R. Trepte, A climatology of stratospheric aerosol, *J. Geophys. Res., 99,* 20689-20700, 1994.

Hofmann, D. J., Increase in the stratospheric background sulfuric acid aerosol mass in the past 10 years, *Science, 248* (4958), 996-1000, 1990.

Holmes, K. J., and J. H. Ellis, Potential environmental impacts of future halocarbon emissions, *Env. Sci. Tech., 30,* 348A-355A, 1996.

Holton, J. R., P. H. Haynes, M. E. McIntyre, A. R. Douglass, R. B. Rood, and L. Pfister, Stratosphere-troposphere exchange, *Rev. Geophys., 33* (4), 403-439, 1995.

Hood, L. L, J. P. McCormick, and K. Labtizke, An investigation of dynamical contributions to midlatitude ozone trends during winter, *J. Geophys. Res., 102,* 13079-13093, 1997.

Howard, R. P., J. C. Wormhoudt, and P. D. Whitefield, *Experimental Characterization of Gas Turbine Emissions at Simulated Flight Altitude Conditions*, AEDC-TR-96-3, 1996.

Hu, J. H., and J. P. D. Abbatt, Reaction probabilities for N_2O_5 hydrolysis on sulfuric acid and ammonium sulfate aerosols at room temperature, *J. Phys. Chem., 101* (5), 871-878, 1997.

Hurst, D. F., G. S. Dutton, P. A. Romashkin, P. R. Wamsley, F. L. Moore, J. W. Elkins, E. J. Hintsa, E. M. Weinstock, C. R. Webster, R. D. May, R. L. Herman, E. J. Moyer, and D. C. Scott, Closure of the total hydrogen budget of the northern extratropical lower stratosphere, *J. Geophys. Res.,* 104, 8191-8200, 1999.

IPCC, Climate Change 1995, *The Science of Climate Change, Contribution of Working Group I to the Second Assessment Report of the Intergovernmental Panel on Climate Change*, J. T. Houghton, L. G. M. Filho, B. A. Callander, N. Harris, A. Kattenberg, and K. Maskell (eds.), Cambridge University Press, Cambridge, UK, 1996.

Jackman, C. H., A. R. Douglass, K. F. Brueske, and S. A. Klein, The influence of dynamics on two-dimensional model results: Simulations of ^{14}C and stratospheric NO_x injections, *J. Geophys. Res., 96,* 22559-22572, 1991.

Jackman, C. H., E. L. Fleming, S. Chandra, D. B. Considine, and J. E. Rosenfield, Past, present, and future modeled ozone trends with comparisons to observed trends, *J. Geophys. Res.*, *101*, 28753-28767, 1996.

Jacobson, M. A., Computation of global photochemistry with SMVGEARII, *Atmos. Environ*, *29A*, 2541-2546, 1995.

Jaeglé, L., Y. L. Yung, G. C. Toon, B. Sen, and J. F. Blavier, Balloon observations of organic and inorganic chlorine in the stratosphere: The role of $HClO_4$ production on sulfate aerosols, *Geophys. Res. Lett., 23* (14), 1749-1752, 1996.

Jaeglé, L., C. R. Webster, R. D. May, D. C. Scott, R. M. Stimpfle, D. W. Kohn, P. O. Wennberg, T. F. Hanisco, R. C. Cohen, M. H. Proffitt, K. K. Kelly, J. Elkins, D. Baumgardner, J. E. Dye, J. C. Wilson, R. F. Pueschel, K. R. Chan, R. J. Salawitch, A. F. Tuck, S. J. Hovde, and Y. L. Yung, Evolution and stoichiometry of heterogeneous processing in the Antarctic stratosphere, *J. Geophys. Res., 102* (D11), 13235-13253, 1997.

Johnston, H. S., Reduction of stratospheric ozone by nitrogen oxide catalysts from supersonic transport exhaust, *Science, 173,* 517-522, 1971.

Johnston, H. S, Evaluation of excess carbon 14 and strontium 90 data for suitability to test two-dimensional stratospheric models. *J. Geophys. Res., 94,* 18485-18493, 1989.

Jonsson, H. H., J. C. Wilson, C. A. Brock, J. E. Dye, G. V. Ferry, and K. R. Chan, Evolution of the stratospheric aerosol in the Northern Hemisphere following the June 1991 volcanic eruption of Mount Pinatubo - role of tropospheric-stratospheric exchange and transport, *J. Geophys. Res., 101* (D1), 1553-1570, 1996.

Jost, H., M. Loewenstein, L. Pfister, J. J. Margitan, A. Y. Chang, R. J. Salawitch, and H. A. Michelsen, Laminae in the tropical middle stratosphere: Origin and age estimation, *Geophys. Res. Lett., 23,* 4337-4340, 1998.

Jucks, K. W., D. G. Johnson, K. V. Chance, W. A. Traub, R. J. Salawitch, and R. A. Stachnik, Ozone production and loss rate measurements in the middle stratosphere, *J. Geophys. Res., 101* (D22), 28785-28792, 1996.

Kalnay, E., *et al.,* The NCEP/NCAR 40-year reanalysis project, *Bull. Am. Meteorol. Soc., 77,* 437-471, 1996.

Kärcher, B., Aircraft-generated aerosols and visible contrails, *Geophys. Res. Lett., 23,* 1933-1936, 1996.

Kärcher, B., and D. W. Fahey, The role of sulfur emission in volatile particle formation in jet aircraft exhaust plumes, *Geophys. Res. Lett., 24,* 389-392, 1997.

Kärcher, B., and S. Meilinger, Perturbation of the aerosol layer by aviation-produced aerosols: A parameterization of plume processes, *Geophys. Res. Lett., 25,* 4465-4468, 1998.

Kärcher, B., M. M. Hirschberg, and P. Fabian, Small-scale evolution of aircraft exhaust species at cruising altitudes, *J. Geophys. Res., 101,* 15169-15190, 1996.

Kärcher, B., F. Yu, F. P. Schröder, and R. P. Turco, Ultrafine aerosol particles in aircraft plumes: Analysis of growth mechanisms, *Geophys. Res. Lett., 25,* 2793-2796, 1998a.

Kärcher, B., R. Busen, A. Petzold, F. P. Schröder, U. Schumann, and E. J. Jensen, Physicochemistry of aircraft generated liquid aerosols, soot and ice particles, II: Comparison with observations and sensitivity studies, *J. Geophys. Res., 103* (D14), 17129-17147, 1998b.

Kasten, F., Falling speed of aerosol particles, *J. Appl. Met., 7*, 944-947, 1968.

Kattenberg, A., *et al.*, Climate Models - Projections of Future Climate, Chapter 6 in Radiative Forcing of Climate Change, in *Climate Change 1995, The Science of Climate Change, Intergovernmental Panel on Climate Change,* J. T. Houghton, L. G. M. Filho, B. A. Callander, N. Harris, A. Kattenberg, and K. Maskell (eds.), Cambridge University Press, pp. 285-357, 1996.

Kawa, S. R., P. A. Newman, L. R. Lait, M. R. Schoeberl, R. M. Stimpfle, D. W. Kohn, C. R. Webster, R. D. May, D. Baumgardner, J. E. Dye, J. C. Wilson, K. R. Chan, and M. Loewenstein, Activation of chlorine in sulfate aerosol as inferred from aircraft observations, *J. Geophys. Res., 102* (D3), 3921-3933, 1997.

Keim, E. R., D. W. Fahey, L. A. Del Negro, E. L. Woodbridge, R. S. Gao, P. O. Wennberg, R. C. Cohen, R. M. Stimpfle, K. K. Kelly, E. J. Hintsa, J. C. Wilson, H. H. Jonsson, J. E. Dye, D. Baumgardner, S. R. Kawa, R. J. Salawitch, M. H. Proffitt, M. Loewenstein, J. R. Podolske, and K. R. Chan, Observations of large reductions in the NO/NO_y ratio near the mid-latitude tropopause and the role of heterogeneous chemistry, *Geophys. Res. Lett., 23* (22), 3223-3226, 1996.

Keim, E. R., M. Loewenstein, J. R. Podolske, D. W. Fahey, R. S. Gao, E. L. Woodbridge, R. C. Wamsley, S. G. Donnelly, L. A. Del Negro, C. D. Nevison, S. Solomon, K. H. Rosenlof, C. J. Scott, M. K. W. Ko, D. Weisenstein, and K. R. Chan, Measurements of the NO_y-N_2O correlation in the lower stratosphere: Latitudinal and seasonal changes and model comparisons, *J. Geophys. Res., 102* (D11), 13193-13212, 1997.

Kinnison, D. E., H. S. Johnston, and D. J. Wuebbles, Model study of atmospheric transport using carbon 14 and strontium 90 as inert tracers, *J. Geophys. Res., 99,* 20647-20664, 1994.

Ko, M. K. W., K. K. Tung, D. Weisenstein, and N. D. Sze, A zonal mean model of stratospheric tracer transport in isentropic coordinates: Numerical simulations for nitrous oxide and nitric acid, *J. Geophys. Res., 90*, 2313-2329, 1985.

Koch, D., and D. Rind, Beryllium 10/beryllium 7 as a tracer of stratospheric transport, *J. Geophys. Res., 103* (D4), 3907-3917, 1998.

Koike, M., Y. Kondo, W. A. Matthews, P. V. Johnston, and K. Yamazaki, Decrease of stratospheric NO_2 at 44 degrees N caused by Pinatubo volcanic aerosols, *Geophys. Res. Lett., 20* (18), 1975-1978, 1993.

Kondo, Y., U. Schmidt, T. Sugita, P. Aimedieu, M. Koike, H. Ziereis, and Y. Iwasaka, Total reactive nitrogen, N_2O, and ozone in the winter Arctic stratosphere, *Geophys. Res. Lett., 21* (13), 1247-1250, 1994.

Kondo, Y., U. Schmidt, T. Sugita, A. Engel, M. Koike, P. Aimedieu, M. R. Gunson, and J. Rodriguez, NO_y correlation with N_2O and CH_4 in the midlatitude stratosphere, *Geophys. Res. Lett., 23* (17), 2369-2372, 1996.

Krueger, A. J., L. S. Walter, P. K. Bhartia, C. C. Schnetzler, N. A. Krotkov, I. Sprod, and G. J. S. Bluth, Volcanic sulfur dioxide measurements from the total ozone mapping spectrometer instruments, *J. Geophys. Res., 100* (D7), 14057-14076, 1995.

Lamarque, J. F., and P. G. Hess, Cross-tropopause mass exchange and potential vorticity budget in a simulated tropopause folding, *J. Atmos. Sci., 51,* 2246-2269, 1994.

Landau, Z. H., M. Metwally, R. Van Alstyne, and C. A. Ward, *Jet Aircraft Engine Exhaust Emissions Database Development -- Year 1990 and 2015 Scenarios,* NASA CR-4613, 1994.

Larichev, M., F. Maguin, G. Lebras, and G. Poulet, Kinetics and mechanism of the BrO+HO_2 reaction, *J. Phys. Chem., 99* (43), 15911-15918, 1995.

Lary, D. J., M. P. Chipperfield, R. Toumi, and T. Lenton, Heterogeneous atmospheric bromine chemistry, *J. Geophys. Res., 101* (D1), 1489-1504, 1996.

Lary, D. J., A. M. Lee, R. Toumi, M. J. Newchurch, M. Pirre, and J. B. Renard, Carbon aerosols and atmospheric photochemistry, *J. Geophys. Res., 102* (D3), 3671-3682, 1997.

Le Texier, H., S. Solomon, and R. R. Garcia, The role of molecular hydrogen and methane oxidation in the water vapour budget of the stratosphere, *Q. J. R. Meteorol. Soc., 114* (480), 281-295, 1988.

Lewellen, D. C., and W. S. Lewellen, Large-eddy simulation of the vortex-pair breakup in aircraft wakes, *AIAA J., 34,* 2337-2345, 1996.

Li, Z. J., R. R. Friedl, and S. P. Sander, Kinetics of the HO_2 + BrO reaction over the temperature range 233-348 K, *J. Chem. Soc. Faraday Trans., 93* (16), 2683-2691, 1997.

Lin, S. J., and R. B. Rood, Multidimensional flux form semi-Lagrangian transport schemes, *Mon. Weather Rev., 24,* 2046-2970, 1996.

Lipson, J. B., M. J. Elrod, T. W. Beiderhase, L. T. Molina, and M. J. Molina, Temperature dependence of the rate constant and branching ratio for the OH + ClO reaction, *J. Chem. Soc. Faraday Trans., 93* (16), 2665-2673, 1997.

Lukachko, S. P., I. A. Waitz, R. C. Miake-Lye, R. C. Brown, and M. R. Anderson, Production of sulfate aerosol precursors in the turbine and exhaust nozzle of an aircraft engine, *J. Geophys. Res.*, 103, 16159-16174, 1998.

Mahlman, J. D., and W. J. Moxim, Tracer simulation using a global general circulation model: Results from a midlatitude instantaneous source experiment, *J. Atmos., Sci., 35,* 1340-1374, 1978.

Mahlman, J. D., Uncertainties in projections of human-caused climate warming, *Science, 278,* 1416-1417, 1997.

Marti, J. J., and K. Mauersberger, Laboratory simulations of PSC particle formation, *Geophys. Res. Lett., 20,* 359-362, 1993.

McCormick, M. P., L. W. Thomason, and C. R. Trepte, Atmospheric effects of the Mt Pinatubo eruption, *Nature, 373* (6513), 399-404, 1995.

McElroy, M. B., and R. J. Salawitch, Changing composition of the global stratosphere, *Science, 243,* 763-770, 1989.

McPeters, R. D., S. M. Hollandsworth, L. E. Flynn, J. R. Herman, and C. J. Seftor, Long-term ozone trends derived from the 16-year combined Nimbus 7/Meteor 3 TOMS Version 7 record, *Geophys. Res. Lett., 23,* 3699-3702, 1996.

Metwally, M., Jet *Aircraft Engine Emissions Database Development--1992 Military, Charter, and Nonscheduled Traffic,* NASA CR-4684, 1995.

Metwally, M., *High Speed Civil Transport Forecast: Simulated Airlines Scenarios for Mach 1.6, Mach 2.0, and Mach 2.4 Configurations for Year 2015,* NASA CR-4719, 1996.

Miake-Lye, R. C., M. Martinez-Sanchez, R. C. Brown, and C. E. Kolb, Plume and wake dynamics, mixing, and chemistry behind an HSCT aircraft, *J. Aircraft, 30,* 467-470, 1993.

Miake-Lye, R. C., B. E. Anderson, W. R. Cofer, H. A. Wallio, G. D. Nowicki, J. O. Ballenthin, D. E. Hunton, W. B. Knighton, T. M. Miller, J. V. Seeley, and A. A. Viggiano, SO_x oxidation and volatile aerosol in aircraft exhaust plumes depend on fuel sulfur content, *Geophys. Res. Lett., 25,* 1677-1680, 1998.

Michelsen, H. A., R. J. Salawitch, M. R. Gunson, C. Aellig, N. Kampfer, M. M. Abbas, M. C. Abrams, T. L. Brown, A. Y. Chang, A. Goldman, F. W. Irion, M. J. Newchurch, C. P. Rinsland, G. P. Stiller, and R. Zander, Stratospheric chlorine partitioning: Constraints from shuttle-borne measurements of [HCl], [$ClNO_3$], and [ClO], *Geophys. Res. Lett., 23* (17), 2361-2364, 1996.

Michelsen, H. A., *et al.,* Stratospheric ozone loss enhanced by aerosol reactions at temperatures above 200K, paper presented at the 1997 Conference on the Atmospheric Effects of Aviation, Virginia Beach, Virginia, 1997.

Mills, M. J., A. O. Langford, T. J. Oleary, K. Arpag, H. L. Miller, M. H. Proffitt, R. W. Sanders, and S. Solomon, On the relationship between stratospheric aerosols and nitrogen dioxide, *Geophys. Res. Lett., 20* (12), 1187-1190, 1993.

Minschwaner, K., A. E. Dessler, J. W. Elkins, C. M. Volk, D. W. Fahey, M. Loewenstein, J. R. Podolske, A. E. Roche, and K. R. Chan, Bulk properties of isentropic mixing into the tropics in the lower stratosphere, *J. Geophys. Res., 101* (D5), 9433-9439, 1996.

Molina, M., and F. S. Rowland, Stratospheric sink for chlorofluoromethanes: Chlorine atom catalyzed destruction of ozone, *Nature, 249,* 810, 1974.

Montzka, S. A., J. H. Butler, R. C. Myers, T. M. Thompson, T. H. Swanson, A. D. Clarke, L. T. Lock, and J. W. Elkins, Decline in the tropospheric abundance of halogen from halocarbons: Implications for stratospheric ozone depletion, *Science, 272* (5266), 1318-1322, 1996.

Mortlock, A. M., and R. Van Alstyne, *Military, Charter, Unreported Domestic Traffic and General Aviation: 1976, 1984, 1992, and 2015 Emission Scenarios,* NASA CR-1998-207639, 1998.

Mote, P. W., K. H. Rosenlof, J. R. Holton, R. S. Harwood, and J. W. Waters, Seasonal variations of water vapor in the tropical lower stratosphere, *Geophys. Res. Lett., 22* (9), 1093-1096, 1995.

Mote, P. W., K. H. Rosenlof, M. E. McIntyre, E. S. Carr, J. C. Gille, J. R. Holton, J. S. Kinnersley, H. C. Pumphrey, J. M. Russell III, and J. W. Waters, An atmospheric tape recorder: The imprint of tropical tropopause temperatures on stratospheric water vapor, *J. Geophys. Res., 101* (D2), 3989-4006, 1996.

Mote, P. W., T. J. Dunkerton, M. E. McIntyre, E. A. Ray, P. H. Haynes, and J. M. Russell III, Vertical velocity, vertical diffusion, and dilution by midlatitude air in the tropical lower stratosphere, *J. Geophys. Res., 103,* 8651-8666, 1998.

Murphy, D. M., D. W. Fahey, M. H. Proffitt, S. C. Liu, K. R. Chan, C. S. Eubank, S. R. Kawa, and K. K. Kelly, Reactive nitrogen and its correlation with ozone in the lower stratosphere and upper troposphere, *J. Geophys. Res., 98,* 8751-8773, 1993.

Murphy, D. M., and A. R. Ravishankara, Temperature averages and rates of stratospheric reactions, *Geophys. Res. Lett., 21,* 2471-2474, 1994.

Murphy, D. M., and D. S. Thomson, Laser ionization mass spectroscopy of single aerosol particles, *Aerosol Sci. and Tech., 22,* 237-249, 1995.

Murphy, D. M., D. S. Thomson, and M. J. Mahoney, *In situ* measurements of organics, meteoritic material, mercury, and other elements in aerosols at 5 to 19 kilometers, *Science, 282,* 1664-1669, 1998.

Nakazawa, T., K. Miyashita, S. Aoki, and M. Tanaka, Temporal and spatial variations of upper tropospheric and lower stratospheric carbon dioxide, *Tellus, 43B,* 106-117, 1991.

Nakazawa, T., T. Machida, S. Sugawara, S. Murayama, S. Morimoto, G. Hashida, H. Honda, and T. Itoh, Measurements of the stratospheric carbon dioxide concentration over Japan using a balloon-borne cryogenic sampler, *Geophys. Res. Lett., 22* (10), 1229-1232, 1995.

Nash, E. R., P. A. Newman, J. E. Rosenfield, and M. R. Schoeberl, An objective determination of the polar vortex using Ertel's potential vorticity, *J. Geophys. Res., 101* (D5), 9471-9478, 1996.

Natarajan, M., and L. B. Callis, Stratospheric photochemical studies with Atmospheric Trace Molecule Spectroscopy (ATMOS) measurements, *J. Geophys. Res., 96,* 9361-9370, 1991.

National Research Council, *U.S. Supersonic Commercial Aircraft: Assessing NASA's High Speed Research Program,* National Academy Press, Washington, 1997.

Nedoluha, G. E., D. E. Siskind, J. T. Bacmeister, R. M. Bevilacqua, and J. M. Russell III, Changes in upper stratospheric CH_4 and NO_2 as measured by HALOE and implication for changes in transport, *Geophys. Res. Lett., 25,* 987-990, 1998.

Nevison, C., and E. Holland, A reexamination of the impact of anthropogenically fixed nitrogen on atmospheric N_2O and the stratospheric O_3 layer, *J. Geophys. Res., 102* (D21), 25519-25536, 1997.

Nevison, C. D., S. Solomon, R. R. Garcia, D. W. Fahey, E. R. Keim, M. Loewenstein, J. R. Podolske, R. S. Gao, R. C. Wamsley, S. G. Donnelly, and L. A. Del Negro, Influence of Antarctic denitrification on two-dimensional model NO_y/N_2O correlations in the lower stratosphere, *J. Geophys. Res., 102* (D11), 13183-13192, 1997.

Newchurch, M. J., M. Allen, M. R. Gunson, R. J. Salawitch, G. B. Collins, K. H. Huston, M. M. Abbas, M. C. Abrams, A. Y. Chang, D. W. Fahey, R. S. Gao, F. W. Irion, M. Loewenstein, G. L. Manney, H. A. Michelsen, J. R. Podolske, C. P. Rinsland, and R. Zander, Stratospheric NO and NO_2 abundances from ATMOS solar-occultation measurements, *Geophys. Res. Lett., 23* (17), 2373-2376, 1996.

Newman, P. A., M. R. Schoeberl, and R. A. Plumb, Horizontal mixing coefficients for two-dimensional chemical models calculated from National Meteorological Center data, *J. Geophys. Res., 91*, 7919-7924, 1986.

Newman, P. A., J. F. Gleason, R. D. McPeters, and R. S. Stolarski, Anomalously low ozone over the Arctic, *Geophys. Res. Lett., 24 (22),* 2689-2692, 1997.

Osterman, G. B., R. J. Salawitch, B. Sen, G. C. Toon, R. A. Stachnik, H. M. Pickett, J. J. Margitan, J.-F. Blavier, and D. B. Peterson, Balloon-borne measurements of stratospheric radicals and their precursors: Implications for the production and loss of ozone, *Geophys. Res. Lett., 24,* 1107-1110, 1997.

Pan, L., S. Solomon, W. Randel, J. F. Lamarque, P. Hess, J. Gille, E. W. Chiou, and M. P. McCormick, Hemispheric asymmetries and seasonal variations of the lowermost stratospheric water vapor and ozone derived from SAGE II data, *J. Geophys. Res., 102* (D23), 28177-28184, 1997.

Park, J. H., M. K. W. Ko, R. A. Plumb, C. H. Jackman, J. A. Kaye, and K. H. Sage (eds.), *Report of the Models and Measurements Workshop II,* NASA Reference Publication, National Aeronautics and Space Administration, Washington, DC, in press, 1999.

Patra, P. K., S. Lal, B. H. Subbaraya, C. H. Jackman, and P. Rajaratnam, Observed vertical profile of sulfur hexafluoride (SF_6) and its atmospheric applications, *J. Geophys. Res., 102* (D7), 8855-8859, 1997.

Peter, T., Microphysics and heterogeneous chemistry of polar stratospheric clouds, *Ann. Rev. Phys. Chem., 48,* 785-822, 1997.

Peter, T., C. Brühl, and P. J. Crutzen, Increases in PSC formation probability caused by high-flying aircraft, *Geophys. Res. Lett., 18,* 1465-1468, 1991.

Peters, D., and D. W. Waugh, Influence of barotropic shear on the poleward advection of upper-tropospheric air, *J. Atmos. Sci., 53* (21), 3013-3031, 1996.

Petzold, A., and F. P. Schröder, Jet engine exhaust aerosol characterization, *Aerosol Sci. Technol., 28,* 62-76, 1998.

Pitari, G., L. Ricciardulli, and G. Visconti, High-speed civil transport impact: Role of sulfate, nitric acid trihydrate, and ice aerosols studied with a two-dimensional model including aerosol physics, *J. Geophys. Res., 98,* 23141-23164, 1993.

Pitchford, M., J. G. Hudson, and J. Hallett, Size and critical supersaturation for condensation of jet engine exhaust particles, *J. Geophys. Res., 96,* 20787-20793, 1991.

Plumb, R. A., and J. D. Mahlman, The zonally averaged transport characteristics of the GFDL general circulation/tracer model, *J. Atmos. Sci., 44,* 298-327, 1987.

Plumb, R. A., and M. K. W. Ko, Interrelationships between mixing ratios of long lived stratospheric constituents, *J. Geophys. Res., 99* (D9), 10145-10156, 1992.

Pollock, W. H., L. E. Heidt, R. A. Lueb, J. F. Vedder, M. J. Mills, and S. Solomon, On the age of stratospheric air and ozone depletion potentials in polar regions, *J. Geophys. Res., 97* (D12), 12993-12999, 1992.

Poole, L. R., and M. C. Pitts, Polar stratospheric cloud climatology based on Stratospheric Aerosol Measurement II observation from 1978 to 1989, *J. Geophys. Res., 99,* 13083-13089, 1994.

Portmann, R. W., S. Solomon, R. R. Garcia, L. W. Thomason, L. R. Poole, and M. P. McCormick, Role of aerosol variations in anthropogenic ozone depletion in the polar regions, *J. Geophys. Res., 101*, 22991-23006, 1996.

Prather, M. J., and E. E. Remsberg (eds.), *The Atmospheric Effects of Stratospheric Aircraft: Report of the 1992 Models and Measurements Workshop,* NASA Reference Publication 1292, NASA, Washington, DC, 1993.

Prather, M., M. McElroy, S. Wofsy, G. Russell, and D. Rind, Chemistry of the global troposphere: Fluorocarbons as tracers of air motion, *J. Geophys. Res., 92* (D6), 6579-6613, 1987.

Pueschel, R. F., K. A. Boering, S. Verma, S. D. Howard, G. V. Ferry, J. Goodman, D. A. Allen, and P. Hamill, Soot aerosol in the lower stratosphere: Pole-to-pole variability and contributions by aircraft, *J. Geophys. Res., 102* (D11), 13113-13118, 1997.

Pueschel, R. F., S. Verma, G. V. Ferry, S. D. Howard, S. Vay, S. A. Kinne, J. Goodman, and A. W. Strawa, Sulfuric acid and soot particle formation in aircraft exhaust, *Geophys. Res. Lett., 25*, 1685-1688, 1998.

Raisbeck, G. M., F. Yiou, M. Fruneau, J. M. Loiseaux, M. Lieuvin, and J. C. Ravel, Cosmogenic $^{10}Be/^{7}Be$ as a probe of atmospheric transport processes, *Geophys. Res. Lett., 8* (9), 1015-1018, 1981.

Ramaroson, R., Modélisation locale à une et trois dimensions des processus photochimiques de l'atmosphère moyenne, Thèse de l'UNIVERSITE Paris VI, 6 juillet, (PhD thesis: Local, one and three dimensional modeling of chemical processes in the middle atmosphere), 1989.

Ramaroson, R., M. Pirre, and D. Cariolle, A box model for on-line computations of diurnal variations in multi-dimensional models: Application to the one-dimensional case, *Ann. Geophys., 10*, 416-428, 1992.

Randel, W. J., and R. R. Garcia, Application of a planetary wave breaking parameterization to stratospheric circulation statistics, *J. Atmos., Sci., 51*, 1157-1168, 1994.

Randel, W. J., F. Wu, J. M. Russell, A. Roche, and J. W. Waters, Seasonal cycles and QBO variations in stratospheric CH_4 and H_2O observed in UARS HALOE data, *J. Atmos. Sci., 55,* 163-184, 1998.

Randenyia, L. K., P. F. Vohralik, I. C. Plumb, and K. R. Ryan, Heterogeneous $BrONO_2$ Hydrolysis: Effect on NO_2 columns and ozone at high latitudes in summer, *J. Geophys. Res.*, *102* (D13), 23543-23557, 1997.

Rasch, P. J, X. Tie, B. A. Boville, and D. L. Williamson, A three-dimensional transport model for the middle atmosphere, *J. Geophys. Res., 99,* 999-1017, 1994.

Rattigan, O. V., D. J. Lary, R. L. Jones, and R. A. Cox, UV-visible absorption cross sections of gaseous Br_2O and HObr, *J. Geophys. Res., 101* (D17), 23021-23033, 1996.

Reeves, J. M., J. C. Wilson, C. A. Brock, D. W. Gesler, B. G. Lafleur, L. W. Thomason, and H. H. Jonsson, Comparison of aerosol extinction and surface area from ER-2 and SAGE II measurements, poster presented at AGU meeting, San Francisco, Fall 1998.

Rind, D., and P. Lonergan, Modeled impacts of stratospheric ozone and water vapor perturbations with implications for high-speed civil transport aircraft, *J. Geophys. Res., 100,* 7381-7396, 1995.

Rind, D., R. Suozzo, N. K. Balachandran, and M. J. Prather, Climate change and the middle atmosphere, I: The doubled CO_2 climate, *J. Atmos. Sci., 47,* 475-494, 1990.

Rind, D., D. Shindell, P. Lonergan,. and N. K. Balachandran, Climate change and the middle atmosphere, Part III: The doubled CO_2 climate revisited, *J. Clim., 11,* 876-894, 1998.

Robinson, G. N., D. R. Worsnop, J. T. Jayne, C. E. Kolb, and P. Davidovits, Heterogeneous uptake of $ClONO_2$ and N_2O_5 by sulfuric acid solutions, *J. Geophys. Res., 102* (D3), 3583-3601, 1997.

Roche, A. E., J. B. Kumer, and J. L. Mergenthaler, CLAES observations of $ClONO_2$ and HNO_3 in the Antarctic stratosphere, between June 15 and September 17, 1992, *Geophys. Res. Lett., 20,* 1223-1226, 1993.

Roche, A. E., J. B. Kumer, R. W. Nightingale, J. L. Mergenthaler, G. A. Ely, P. L. Bailey, S. T. Massie, J. C. Gille, D. P. Edwards, M. R. Gunson, M. C. Abrams, G. C. Toon, C. R. Webster, W. A. Traub, K. W. Jucks, D. G. Johnson, D. G. Murcray, F. H. Murcray, A. Goldman, and E. C. Zipf, Validation of CH_4 and N_2O measurements by the cryogenic limb array etalon spectrometer instrument on the Upper Atmosphere Research Satellite, *J. Geophys. Res., 101* (D6), 9679-9710, 1996.

Rodriguez, J. M., R.-L. Shia, M. K. W. Ko, C. W. Heisey, D. K. Weisenstein, R. C. Miake-Lye, and C. E. Kolb, Subsidence of aircraft engine exhaust in the stratosphere: Implications for calculated ozone depletions, *Geophys. Res. Lett., 21,* 69-72, 1994.

Rogaski, C. A., D. M. Golden, and L. R. Williams, Reactive uptake and hydration experiments on amorphous carbon treated with NO_2, SO_2, O_3, HNO_3, and H_2SO_4, *Geophys. Res. Lett., 24* (4), 381-384, 1997.

Rosenlof, K. H., Seasonal cycle of the residual mean meridional circulation in the stratosphere, *J. Geophys. Res., 100* (D3), 5173-5191, 1995.

Rosenlof, K. H., A. F. Tuck, K. K. Kelly, J. M. Russell, and H. P. McCormick, Hemispheric asymmetries in water vapor and inferences about transport in the lower stratosphere, *J. Geophys. Res., 102* (D11), 13213-13234, 1997.

Russell, J. M., III, L. Mingzhao, R. J. Cicerone, and L. E. Deaver, Satellite confirmation of the dominance of chlorofluorocarbons in the global stratospheric chlorine budget, *Nature, 379* (6565), 526-529, 1996.

Salawitch, R. J., S. C. Wofsy, P. O. Wennberg, R. C. Cohen, J. G. Anderson, D. W. Fahey, R. S. Gao, E. R. Keim, E. L. Woodbridge, R. M. Stimpfle, J. P. Koplow, D. W. Kohn, C. R. Webster, R. D. May, L. Pfister, E. W. Gottlieb, H. A. Michelsen, G. K. Yue, J. C. Wilson, C. A. Brock, H. H. Jonsson, J. E. Dye, D. Baumgardner, M. H. Proffitt, M. Loewenstein, J. R. Podolske, J. W. Elkins, G. S. Dutton, E. J. Hintsa, A. E. Dessler, E. M. Weinstock, K. K. Kelly, K. A. Boering, B. C. Daube, K. R. Chan, and S. W. Bowen, The distribution of hydrogen, nitrogen, and chlorine radicals in the lower stratosphere: Implications for changes in O_3 due to emission of NO_y from supersonic aircraft, *Geophys. Res. Lett., 21* (23), 2547-2550, 1994a.

Salawitch, R. J., S. C. Wofsy, P. O. Wennberg, R. C. Cohen, J. G. Anderson, D. W. Fahey, R. S. Gao, E. R. Keim, E. L. Woodbridge, R. M. Stimpfle, J. P. Koplow, D. W. Kohn, C. R. Webster, R. D. May, L. Pfister, E. W. Gottlieb, H. A. Michelsen, G. K. Yue, M. J. Prather, J. C. Wilson, C. A. Brock, H. H. Jonsson, J. E. Dye, D. Baumgardner, M. H. Proffitt, M. Loewenstein, J. R. Podolske, J. W. Elkins, G. S. Dutton, E. J. Hintsa, A. E. Dessler, E. M. Weinstock, K. K. Kelly, K. A. Boering, B. C. Daube, K. R. Chan, and S. W. Bowen, The diurnal variation of hydrogen, nitrogen, and chlorine radicals: Implications for the heterogeneous hydrolysis of HNO_4, *Geophys. Res. Lett., 21* (23), 2551-2554, 1994b.

Santer, B. D., *et al.,* Detection of Climate Change and Attribution of Causes, Chapter 8 in *Climate Change 1995, The Science of Climate Change, Intergovernmental Panel on Climate Change,* J. T. Houghton, L. G. M. Filho, B. A. Callander, N. Harris, A. Kattenberg, and K. Maskell (eds.), Cambridge University Press, pp. 406-443, 1996.

Schauffler, S. M., E. L. Atlas, F. Flocke, R. A. Lueb, V. Stroud, and W. Travnicek, Measurements of bromine containing organic compounds at the tropical tropopause, *Geophys. Res. Lett., 25* (3), 317-320, 1998.

Schmidt, U., and A. Khedim, *In situ* measurements of carbon dioxide in the winter Arctic vortex and at midlatitudes: An indicator of the 'age' of stratospheric air, *Geophys. Res. Lett., 18* (4), 763-766, 1991.

Schröder, F. P., B. Kärcher, A. Petzold, R. Baumann, R. Busen, C. Hoell, and U. Schumann, Ultrafine aerosol particles in aircraft plumes: *In situ* observations, *Geophys. Res. Lett., 25,* 2789-2792, 1998.

Schoeberl, M. R., and D. F. Strobel, The response of the zonally averaged circulation to stratospheric ozone reductions. *J. Atmos. Sci., 35,* 1751-1757, 1978.

Schoeberl, M. R., A. E. Roche, J. M. Russell III, D. Ortland, P. B. Hays, and J. W. Waters, An estimation of the dynamical isolation of the tropical lower stratosphere using UARS wind and trace gas observations of the quasi-biennial oscillation, *Geophys. Res. Lett., 24* (1), 53-56, 1997.

Schoeberl, M. R., C. H. Jackman, and J. E. Rosenfield, A lagrangian estimate of aircraft effluent lifetime, *J. Geophys. Res., 103,* 10817-10825, 1998.

Schulte, P., H. Schlager, H. Ziereis, U. Schumann, S. L. Baughcum, and F. Deidewig, NO_x emission indices of subsonic long-range jet aircraft at cruise altitude: *In situ* measurements and predictions, *J. Geophys. Res., 102*, 21431-21442, 1997.

Schumann, U., P. Konopka, R. Baumann, R. Busen, T. Gerz, H. Schlager, P. Schulte, and H. Volkert, Estimate of diffusion parameters of aircraft exhaust plumes near the tropopause from nitric oxide and turbulence measurements, *J. Geophys. Res., 100,* 14147-14162, 1995.

Sen, B., G. C. Toon, G. B. Osterman, J. F. Blavier, J. J. Margitan, R. J. Salawitch, and G. K. Yue, Measurements of reactive nitrogen in the stratosphere, *J. Geophys. Res., 103* (D3), 3571-3585, 1998.

Sheridan, P. J., C. A. Brock, and J. C. Wilson, Aerosol particles in the upper troposphere and lower stratosphere: Elemental composition and morphology of individual particles in northern midlatitudes, *Geophys. Res. Lett., 21* (23), 2587-2590, 1994.

Shia, R.-L., M. K. W. Ko, M. Zhou, and V. R. Kotamarthi, Cross tropopause transport of excess ^{14}C in a two-dimensional model, *J. Geophys. Res., 98*, 18599-18606, 1993.

Shia, R.-L., M. K. W. Ko, D. K. Weisenstein, C. Scott, and J. Rodriguez, Transport between the tropical and midlatitude lower stratosphere: Implication for ozone response to HSCT emissions, *J. Geophys. Res., 103 (D19),* 25435-25446, 1998.

Shindell, D. T., D. Rind, and P. Lonergan, Increased polar stratospheric ozone losses and delayed eventual recovery owing to increasing greenhouse-gas concentrations, *Nature, 392,* 589-592, 1998.

Shindell, D., D. Rind, and P. Lonergan, Increased polar stratospheric ozone losses and delayed eventual recovery owing to increasing greenhouse-gas concentrations, *Nature, 392,* 589-592, 1998.

Shorter, J. H., C. E. Kolb, P. M. Crill, R. A. Kerwin, R. W. Talbot, M. E. Hines, and R. C. Harriss, Rapid degradation of atmospheric methyl bromide in soils (ozone depletion implications), *Nature, 377* (6551), 717-719, 1995.

Slusser, J. R., D. J. Fish, E. K. Strong, R. L. Jones, H. K. Roscoe, and A. Sarkissian, Five years of NO_2 vertical column measurements at Faraday (65°S): Evidence for the hydrolysis of $BrONO_2$ on Pinatubo aerosols, *J. Geophys. Res., 102* (D11), 12987-12993, 1997.

Slusser, J., X. Liu, K. Stamnes, G. Shaw, R. Smith, R. Storvold, F. Murcray, A. Lee, and P. Good, High-latitude stratospheric NO_2 and HNO_3 over Fairbanks (65°N) 1992-1994, *J. Geophys. Res., 103* (D1), 1549-1554, 1998.

Smith, D. M., and A. R. Chughtai, Spectroscopic study of the nature and reactivity of black carbon, *Trends in Appl. Spectroscopy, 1,* 325-366, 1993.

Smyshlyaen, S. P., V. Dvortsov, M. A. Geller, and V. A. Yudin, A two-dimensional model with input parameters from a GCM: Ozone sensitivity to different formulations for the longitude temperature variation, *J. Geophys. Res., 103,* 28373-28387, 1998.

Solomon, S., J. T. Kiehl, R. R. Garcia, and W. Grose, Tracer transport by diabatic circulation deduced form satellite observations, *J. Atmos. Sci., 43,* 1603-1617, 1986.

Solomon, S., R. W. Portmann, R. R. Garcia, W. Randel, F. Wu, R. Nagatani, J. Gleason, L. Thomason, L. R. Poole, and M. P. McCormick, Ozone depletion at mid-latitudes: Coupling of volcanic aerosols and temperature variability to anthropogenic chlorine, *Geophys. Res. Lett., 25* (11), 1871-1874, 1998.

Sparling, L. C., and M. R. Schoeberl, Mixing entropy analysis of dispersal of aircraft emissions in the lower stratosphere, *J. Geophys. Res., 100* (D8), 16805-16812, 1995.

Sparling, L. C., M. R. Schoeberl, A. R. Douglass, C. J. Weaver, P. A. Newman, and L. R. Lait, Trajectory modeling of emissions from lower stratospheric aircraft, *J. Geophys. Res., 100* (D1), 1427-1438, 1995.

Spicer, C. W., M. W. Holdren, D. L. Smith, D. P. Hughes, and M. D. Smith, Chemical composition from aircraft turbine engines, *J. Eng. Gas Turbines Power, 114,* 111-117, 1992.

Spicer, C. W., M. W. Holdren, R. M. Riggin, and T. F. Lyon, Chemical composition and photochemical reactivity of exhaust from aircraft turbine engines, *Ann. Geophys, 12,* 944-955, 1994.

Steele, H. M., and P. Hamill, Effects of temperature and humidity on the growth and optical properties of sulfuric acid-water droplets in the stratosphere, *J. Aerosol Sci., 12,* 517-528, 1981.

Stephens, S., J. M. Rossi, and D. M. Golden, The heterogeneous reaction of ozone on carbonaceous surfaces, *Int. J. Chem. Kin., 18,* 1133-1149, 1986.

Stimpfle, R. M., J. P. Koplow, R. C. Cohen, D. W. Kohn, P. O. Wennberg, D. M. Judah, D. W. Toohey, L. M. Avallone, J. G. Anderson, R. J. Salawitch, E. L. Woodbridge, C. R. Webster, R. D. May, M. H. Proffitt, K. Aiken, J. Margitan, M. Loewenstein, J. R. Podolske, L. Pfister, and K. R. Chan, The response of ClO radical concentrations to variations in NO_2 radical concentrations in the lower stratosphere, *Geophys. Res. Lett., 21* (23), 2543-2546, 1994.

Stimpfle, R., R. C. Cohen, G. P. Bonne, P. B. Voss, K. K. Perkins, L. C. Koch, J. G. Anderson, R. J. Salawitch, S. A. Lloyd, R. S. Gao, L. A. Del Negro, E. R. Keim, and T. P. Bui, The coupling of $ClONO_2$, ClO and NO_2 in the lower stratosphere from *in situ* observations using the NASA ER-2 aircraft, *J. Geophys. Res.,* in press, 1999.

Stolarski, R. S., S. L. Baughcum, W. H. Brune, A. R. Douglass, D. W. Fahey, R. R. Friedl, S. C. Liu, R. A. Plumb, L. R. Poole, H. L. Wesoky, and D. R. Worsnop, *1995 Scientific Assessment of the Atmospheric Effect of Stratospheric Aircraft,* NASA Reference Publication 1381, Washington, DC, 1995.

Stothers, R. B., Major optical depth perturbations to the stratosphere from volcanic eruptions: Pyrheliometric period, 1881-1960, *J. Geophys. Res., 101* (D2), 3901-3920, 1996.

Strahan, S. E., M. Loewenstein, and J. R. Podolske, Climatology and small-scale structure of lower stratospheric N_2O based on *in situ* observations, *J. Geophys. Res., 104,* 2195-2208, 1999.

Summers, M. E., R. R. Conway, D. E. Siskind, M. H. Stevens, D. Offermann, M. Riese, P. Preusse, D. F. Strobel, and J. M. Russell III, Implications of satellite OH observations for middle atmospheric H_2O and ozone, *Science, 277,* 1967-1970, 1997.

Sykes, R. I., and D. S. Henn, Representation of velocity gradient effects in a Gaussian puff model, *J. Appl. Meteorol., 34,* 2715-2723, 1995.

Tabazadeh, A., and R. P. Turco, A model for heterogeneous chemical processes on the surfaces of ice and nitric acid trihydrate particles, *J. Geophys. Res., 98,* 12727-12740, 1993.

Tabazedeh, A., O. B. Toon, and B. J. Jensen, Formation and implications of ice particle nucleation in the stratosphere, *Geophys. Res. Lett., 24,* 2007-2010, 1997.

Thlibi, J., and J. C. Petit, A study of the NO_y/soot interaction in the temperature range 303-1223 K, in *Impact of Emissions from Aircraft and Spacecraft upon the Atmosphere: Proceedings of an International Scientific Colloquium,* Koln, Germany, April 18-20, 1994, U. Schumann and D. Wurzel (eds.), 152-157, 1994.

Thomason, L. W., L. R. Poole, and T. Deshler, A global climatology of stratospheric aerosol surface area density deduced from Stratospheric Aerosol and Gas Experiment II measurements: 1984-1994, *J. Geophys. Res., 102* (D7), 8967-8976, 1997.

Tie, X., Potential impact on stratospheric ozone due to emission of hydrocarbons from high-altitude aircraft, *Tellus, 46B,* 286-293, 1994.

Tuck, A. F., T. Davies, S. J. Hovde, M. Noguer-Alba, D. W. Fahey, S. R. Kawa, K. K. Kelly, D. M. Murphy, M. H. Proffitt, J. J. Margitan, M. Loewenstein, J. R. Podolske, S. E. Strahan, and K. R. Chan, Polar stratospheric cloud processed air and potential vorticity in the northern hemisphere lower stratosphere at mid-latitudes during winter, *J. Geophys. Res., 97* (D8), 7883-7904, 1992.

Tuck, A. F., D. Baumgardner, K. R. Chan, J. E. Dye, J. W. Elkins, S. J. Hovde, K. K. Kelly, M. Loewenstein, J. J. Margitan, R. D. May, J. R. Podolske, M. H. Proffitt, K. H. Rosenlof, W. L. Smith, C. R. Webster, and J. C. Wilson, The Brewer-Dobson circulation in the light of high altitude *in situ* aircraft observations, *Q. J. R. Meteorol. Soc., 123* (537), 1-69, 1997.

Tung, K. K., On the two-dimensional transport of stratospheric trace gases in isentropic coordinates, *J. Atmos., Sci., 39,* 2330-2355, 1982.

Turco, R. P., and F. Yu, Aerosol invariance in expanding coagulating plumes, *Geophys. Res. Lett., 24,* 1223-1226, 1997.

Turco, R. P., O. B. Toon, P. Hamill, and R. C. Whitten, Effects of meteoritic debris on stratospheric aerosols and gases, *J. Geophys. Res., 86,* 1113-1128, 1981.

Twohy, C. H., and B. W. Gandrud, Electron microscope analysis of residual particles from aircraft contrails, *Geophys. Res. Lett.*, 25, 1359-1362, 1998.

U.S. Standard Atmosphere, M. Dubin, A. Hall, and K. S. W. Champion (eds.), U.S. Government Printing Office, Washington, DC, 1976.

Vaughan, G., and C. Timmis, Transport of near-tropopause air into the lower midlatitude stratosphere, *Q. J. R. Meteorol. Soc., 124,* 1559-1578, 1997.

Vohralik, P. F., L. K. Randeniya, I. C. Plumb, and K. R. Ryan, Use of correlations between long-lived atmospheric species in assessment studies, *J. Geophys. Res., 103,* 3611-3627, 1998.

Volk, C. M., J. W. Elkins, D. W. Fahey, R. J. Salawitch, G. S. Dutton, J. M. Gilligan, M. H. Proffitt, M. Loewenstein, J. R. Podolske, K. Minschwaner, J. J. Margitan, and K. R. Chan, Quantifying transport between the tropical and mid-latitude lower stratosphere, *Science, 272* (5269), 1763-1768, 1996.

Wamsley, P. R., J. W. Elkins, D. W. Fahey, G. S. Dutton, C. M. Volk, R. C. Myers, S. A. Montzka, J. H. Butler, A. D. Clarke, P. J. Fraser, L. P. Steele, M. P. Lucarelli, E. L. Atlas, S. M. Schauffler, D. R. Blake, F. S. Rowland, W. T. Sturges, J. M. Lee, S. A. Penkett, A. Engel, R. M. Stimpfle, K. R. Chan, D. K. Weisenstein, M. K. W. Ko, and R. J. Salawitch, Distribution of halon-1211 in the upper troposphere and lower stratosphere and the 1994 total bromine budget, *J. Geophys. Res., 103* (D1), 1513-1526, 1998.

Wauben, W. M. F., R. Bintanja, P. F. J. van Velthoven, and H. Kelder, On the magnitude of transport out of the Antarctic polar vortex, *J. Geophys. Res., 102* (D1), 1229-1238, 1997.

Waugh, D. W., Seasonal variation of isentropic transport out of the tropical stratosphere, *J. Geophys. Res., 101* (D2), 4007-4023, 1996.

Waugh, D. W., R. A. Plumb, R. J. Atkinson, M. R. Schoeberl, L. R. Lait, P. A. Newman, M. Loewenstein, D. W. Toohey, L. M. Avallone, C. R. Webster, and R. D. May, Transport out of the lower stratospheric Arctic vortex by Rossby wave breaking, *J. Geophys. Res.*, 99, 1071-1088, 1994.

Waugh, D. W., T. M. Hall, W. J. Randel, P. J. Rasch, B. A. Boville, K. A. Boering, S. C. Wofsy, B. C. Daube, J. W. Elkins, D. W. Fahey, G. S. Dutton, C. M. Volk, and P. F. Vohralik, Three-dimensional simulations of long-lived tracers using winds from MACCM2, *J. Geophys. Res., 102* (D17), 21493-21513, 1997.

Weaver, C. J. A. R. Douglass, and R. B. Rood, Tracer transport for realistic aircraft emission scenarios calculated using a three-dimensional model, *J. Geophys. Res., 100,* 5203-5214, 1995.

Webster, C. R., R. D. May, L. Jaeglé, H. Hu, S. P. Sander, M. R. Gunson, G. C. Toon, J. M. Russell III, R. M. Stimpfle, J. P. Koplow, R. J. Salawitch, and H. A. Michelsen, Hydrochloric acid and the chlorine budget of the lower stratosphere, *Geophys. Res. Lett., 21,* 2575-2578, 1994.

Webster, C. R., R. D. May, H. A. Michelsen, D. C. Scott, J. C. Wilson, H. H. Jonsson, C. A. Brock, J. E. Dye, D. Baumgardner, R. M. Stimpfle, J. P. Koplow, J. J. Margitan, M. H. Proffitt, L. Jaeglé, R. L. Herman, H. Hu, G. J. Flesch, and M. Loewenstein, Evolution of HCl concentrations in the lower stratosphere from 1991 to 1996 following the eruption of Mt. Pinatubo, *Geophys. Res. Lett., 25* (7), 995-998, 1998.

Weinstock, E. M., E. J. Hintsa, A. E. Dessler, and J. G. Anderson, Measurements of water vapor in the tropical lower stratosphere during the CEPEX campaign: Results and interpretation, *Geophys. Res. Lett., 22* (23), 3231-3234, 1995.

Weinstock, E., E. Hintsa, J. G. Anderson, A. E. Andrews, R. Herman, R. May, C. Webster, and P. Bui, Evaluation of the seasonal cycle of water vapor in the stratosphere derived from tropical tropopause temperatures using a CO photochemical clock, submitted to *J. Geophys. Res.*, 1999.

Weisenstein, D. K., M. K. W. Ko, N. D. Sze, and J. M. Rodriguez, Potential impact of SO_2 emissions from stratospheric aircraft on ozone, *Geophys. Res., Lett., 23,* 161-164, 1996.

Weisenstein, D. K., G. K. Yue, M. K. W. Ko, N. D. Sze, J. M. Rodriguez, and C. J. Scott, A two-dimensional model of sulfur species and aerosols, *J. Geophys. Res., 102* (D11), 13019-13035, 1997.

Weisenstein, D. K., M. K. W. Ko, I. G. Dyominov, G. Pitari, L. Ricciardulli, G. Visconti, and S. Bekki, The effects of sulfur emissions from HSCT aircraft: A 2-D model intercomparison, *J. Geophys. Res., 103,* 1527-1547, 1998.

Wennberg, P. O., R. C. Cohen, R. M. Stimpfle, J. P. Koplow, J. G. Anderson, R. J. Salawitch, D. W. Fahey, E. L. Woodbridge, E. R. Keim, R. S. Gao, C. R. Webster, R. D. May, D. W. Toohey, L. M. Avallone, M. H. Proffitt, M. Loewenstein, J. R. Podolske, K. R. Chan, and S. C. Wofsy, The removal of lower stratospheric O_3 by free radical catalysis: *In situ* measurements of OH, HO_2, NO, NO_2, ClO, and BrO, *Science, 266,* 398-404, 1994.

Wennberg, P. O., R. J. Salawitch, D. J. Donaldson, T. F. Hanisco, E. J. Lanzendorf, K. K. Perkins, S. A. Lloyd, V. Vaida, R. S. Gao, E. J. Hintsa, R. C. Cohen, W. H. Swartz, T. L. Kusterer, and D. E. Anderson, Twilight observations suggest unknown sources of HO_x, *Geophys. Res. Lett.,* in press, 1999.

Wey, C. C., C. Wey, D. J. Dicki, K. H. Loos, D. E. Noss, D. E. Hagen, P. D. Whitefield, M. B. Trueblood, M. E. Wilson, D. Olson, J. O. Ballenthin, T. M. Miller, A. A. Viggiano, J. Wormhoudt, T. Berkoff, and R. C. Miake-Lye, *Engine Gaseous, Aerosol Precursor and Particulate at Simulated Flight Altitude Conditions*, NASA/TM-1998-208509, ARL-TR-1804, 1998.

Wilhite, A. W., and R. J. Shaw, HSCT research picks up speed, *Aerospace America*, 24-41, August, 1997.

Wilson, J. C., D. W. Gesler, C. A. Brock, P. J. Sheridan, and B. E. Anderson, Analysis of particles emitted by C-30 and F-16 aircraft and collected in SNIF III, *Presented at the 1998 Conference on the Atmospheric Effects of Aviation, 27 April - 1 May 1998*, Virginia Beach, VA, 1998.

WMO, *Atmospheric Ozone 1985, Assessment of our Understanding of the Processes Controlling its Present Distribution and Change,* World Meteorological Organization Global Ozone Research and Monitoring Project-Report No. 16, 1986.

WMO, *Report of the International Ozone Trends Panel 1988,* World Meteorological Organization Global Ozone Research and Monitoring Project-Report No. 18, 1989.

WMO, *Scientific Assessment of Ozone Depletion: 1991,* World Meteorological Organization Global Ozone Research and Monitoring Project-Report No. 25, 1992.

WMO, *Scientific Assessment of Ozone Depletion: 1994,* World Meteorological Organization Global Ozone Research and Monitoring Project-Report No. 37, 1995.

WMO, *Scientific Assessment of Ozone Depletion: 1998,* World Meteorological Organization Global Ozone Research and Monitoring Project-Report No. 44, 1999.

Yang, H., and K. K. Tung, Cross-isentropic stratosphere-troposphere exchange of mass and water vapor, *J. Geophys. Res., 101* (D5), 9413-9423, 1996.

Yokelson, R. J., J. B. Burkholder, R. W. Fox, and A. R. Ravishankara, Photodissociation of ClONO2, 2. Time-resolved absorption studies of product quantum yields, *J. Phys. Chem., 101* (36), 6667-6678, 1997.

Yu, F., and R. P. Turco, The role of ions in the formation and evolution of particles in aircraft plumes, *Geophys. Res. Lett., 24,* 1927-1930, 1997.

Yu, F., and R. P. Turco, The formation and evolution of aerosols in stratospheric aircraft plumes: Numerical simulations and comparisons with observations, *J. Geophys. Res.*, 103, 25915-25934, 1998.

Yu, F., R. P. Turco, B. Kärcher, and F. P. Schröder, On the mechanisms controlling the formation and properties of volatile particles in aircraft wakes, *Geophys. Res. Lett.*, 25, 3839-3842, 1998.

Yudin, V. A., S. P. Smyshlyaev, M. A. Geller, and V. L. Dvortsov, Transport diagnostics of GCMs and implications for 2-D chemistry-transport model of troposphere and stratosphere, submitted to *J. Atmos. Sci.*, 1999.

Yvon-Lewis, S. A., and J. H. Butler, The potential effect of oceanic biological degradation on the lifetime of atmospheric CH_3Br, *Geophys. Res. Lett., 24* (10), 1227-1230, 1997.

Zander, R., E. Mahieu, M. R. Gunson, M. C. Abrams, A. Y. Chang, M. Abbas, C. Aellig, A. Engel, A. Goldman, F. W. Irion, N. Kampfer, H. A. Michelsen, M. J. Newchurch, C. P. Rinsland, R. J. Salawitch, G. P. Stiller, and G. C. Toon, The 1994 northern midlatitude budget of stratospheric chlorine derived from ATMOS/ATLAS-3 observations, *Geophys. Res. Lett., 23* (17), 2357-2360, 1996.

Zhang, R., M.-T. Leu, and L. F. Keyser, Heterogeneous chemistry of HONO on liquid sulfuric acid: a new mechanism of chlorine activation on stratospheric sulfate aerosols, *J. Phys. Chem., 100,* 339-345, 1995.

APPENDIX B

AUTHORS, CONTRIBUTORS, AND REVIEWERS

Assessment Chair

S. Randolph Kawa	NASA Goddard Space Flight Center

Lead Authors

James G. Anderson	Harvard University
Steven L. Baughcum	Boeing Company
Charles A. Brock	University of Denver
William H. Brune	Pennsylvania State University
Ronald C. Cohen	University of California, Berkeley
Douglas E. Kinnison	National Center for Atmospheric Research (formerly affiliated with Lawrence Livermore National Laboratory)
Paul A. Newman	NASA Goddard Space Flight Center
Jose M. Rodriguez	University of Miami
Richard S. Stolarski	NASA Goddard Space Flight Center
Darryn Waugh	Johns Hopkins University
Steven C. Wofsy	Harvard University

Contributors and Reviewers

Donald E. Anderson	The Johns Hopkins University Applied Physics Laboratory/NASA Goddard Space Flight Center
Kristie A. Boering	University of California, Berkeley
Lisa Chang	US Environmental Protection Agency
Martyn Chipperfield	University of Leeds
Med Colket	United Technologies Research Center/Pratt & Whitney
David Considine	University of Maryland
Robert Cuthbertson	Boeing Commercial Airplane Group
Willard J. Dodds	General Electric Aircraft Engines
Anne R. Douglass	NASA Goddard Space Flight Center
James W. Elkins	NOAA Climate Monitoring and Diagnostics Laboratory
David W. Fahey	NOAA Aeronomy Laboratory
Randall R. Friedl	Jet Propulsion Laboratory
Marvin A. Geller	State University of New York, Stony Brook
William L. Grose	NASA Langley Research Center
Tom F. Hanisco	Harvard University
James R. Holton	University of Washington
Charles H. Jackman	NASA Goddard Space Flight Center

Harold S. Johnston	University of California, Berkeley
Bernd Kärcher	DLR Institute for Atmospheric Physics
Jack A. Kaye	NASA Headquarters
Malcolm K. W. Ko	Atmospheric and Environmental Research, Inc.
Charles E. Kolb	Aerodyne Research, Inc.
Michael J. Kurylo	National Institute of Standards and Technology/NASA Headquarters
Richard J. Lawrence	NASA Goddard Space Flight Center
Richard C. Miake-Lye	Aerodyne Research, Inc.
Mario J. Molina	Massachusetts Institute of Technology
Alan K. Mortlock	Boeing Company
Joyce E. Penner	University of Michigan
Michael J. Prather	University of California, Irvine
David H. Rind	NASA Goddard Institute for Space Studies
Helen Rogers	University of Cambridge
Richard B. Rood	NASA Goddard Space Flight Center
Douglas Rotman	Lawrence Livermore National Laboratory
Keith R. Ryan	Commonwealth Scientific and Industrial Research Organization (CSIRO)
Ulrich Schumann	DLR Institute for Atmospheric Physics
Sergei Smyshlyaev	State University of New York, Stony Brook
Saadat A. Syed	Pratt & Whitney
Darin W. Toohey	University of Colorado, Boulder
Peter Vohralik	Commonwealth Scientific and Industrial Research Organization (CSIRO)
Debra Weisenstein	Atmospheric and Environmental Research, Inc.
Howard L. Wesoky	Federal Aviation Administration
Allen H. Whitehead	NASA Langley Research Center

Contributing Editors

Rose M. Kendall	Computer Sciences Corporation
Kathy A. Wolfe	Computer Sciences Corporation

APPENDIX C

ACRONYMS AND ABBREVIATIONS

1-D	one-dimensional
2-D	two-dimensional
3-D	three-dimensional
AA	annual average
AASE II	Airborne Arctic Stratospheric Expedition II
ACMAP	Atmospheric Chemistry Modeling and Analysis Program
AEAP	Atmospheric Effects of Aviation Project
AER	Atmospheric and Environmental Research, Inc.
AESA	Atmospheric Effects of Stratospheric Aircraft
ASHOE	Airborne Southern Hemisphere Ozone Expedition
ATLAS	Airborne Tunable Laser Absorption System
ATMOS	Atmospheric Trace Molecule Spectroscopy
ATTAS	Advanced Technology Testing Aircraft System
CFCs	chlorofluorocarbons
CIAP	Climatic Impact Assessment Program
CLAES	Cryogenic Limb Array Etalon Spectrometer
CSIRO	Commonwealth Scientific and Industrial Research Organization, Australia
CTMs	chemical transport models
DAO	Data Assimilation Office
DAS	Direct Access System
EI	emission index
EP	Eliassen-Palm
FSC	fuel sulfur content
GCMs	general circulation models
GISS	Goddard Institute for Space Studies
GMI	Global Modeling Initiative
GSFC	Goddard Space Flight Center
HALOE	Halogen Occultation Experiment
HCFCs	hydrochlorofluorocarbons
HG	horizontal gradients
HSCT	high speed civil transport
HSR	High Speed Research

IPCC	Intergovernmental Panel on Climate Change
IR	infrared
ISCCP	International Satellite Cloud Climatology Project
JPL	Jet Propulsion Laboratory
LaRC	Langley Research Center
LBS	liquid binary sulfate
LLNL	Lawrence Livermore National Laboratory
LPP	lean premixed prevaporized
MACCM2	Middle Atmosphere Community Climate Model version 2
MAESA	Measurements for Assessing the Effects for Stratospheric Aircraft
M&M II	Models and Measurements II
NAC	northern annual cycle
NASA	National Aeronautics and Space Administration
NAT	nitric acid trihydrate
NCAR	National Center for Atmospheric Research
NCEP	National Centers for Environmental Protection
NH	Northern Hemisphere
nm	nanometers
NMC	National Meteorological Center
OMS	Observations of the Middle Stratosphere
ONERA	Office National d'Etudes et Recherches Aerospatiales
POLARIS	Photochemistry of Ozone Loss in the Arctic Region in Summer
PSCs	polar stratospheric clouds
PSS	Photostationary State
ppbv	parts per billion by volume
ppmm	parts per million by mass
ppmv	parts per million by volume
pptv	parts per trillion by volume
PV	potential vorticity
QBO	Quasi-Biennial Oscillation
RF	radiative forcing
RQL	rich burn, quick quench, lean burn
SAC	southern annual cycle
SAD	surface area density
SAGE	Stratospheric Aerosol and Gas Experiment
SH	Southern Hemisphere

SOLVE	SAGE III Ozone Loss and Validation Experiment
SOM	Second-Order Moments
SPADE	Stratospheric Photochemistry, Aerosols and Dynamics Expedition
SST	supersonic transport
STRAT	Stratospheric Tracers of Atmospheric Transport
STS	supercooled ternary sulfate
SUCCESS	SUbsonic aircraft: Contrail and Cloud Effects Special Study
SULFUR 5	SULFUR series of airborne experiments, coordinated by the German agency, the Deutsches Zentrum für Luft- und Raumfahrt (DLR), focused on understanding the influence of fuel sulfur content on subsonic aircraft emissions
SUNY	State University of New York
TAC	tropical annual cycle
TCA	Technology Concept Airplane
TEM	transformed Eulerian-mean
TOMS	Total Ozone Mapping Spectrometer
UARP	Upper Atmosphere Research Program
UARS	Upper Atmosphere Research Satellite
UCI	University of California, Irvine
UKMO	United Kingdom Meteorological Office
UV	ultraviolet
VG	vertical gradients
WMO	World Meteorological Organization

APPENDIX D

CHEMICAL NOMENCLATURE AND FORMULAE

Br	bromine atom
BrO	bromine monoxide
$BrONO_2$	bromine nitrate
BrO_x	bromine oxides
Br_y	inorganic bromine
CF_4	perfluoromethane
CH_3Br	methyl bromide
CH_3Cl	methyl chloride
CH_4	methane
Cl	atomic chlorine
Cl_y	inorganic chlorine
ClO_x	chlorine oxides
$ClONO_2$	chlorine nitrate
CO_2	carbon dioxide
H	atomic hydrogen
HO_x	hydrogen oxides
HOBr	hypobromous acid
HONO	nitrous acid
H_2	molecular hydrogen
H_2O	water
H_2SO_4	sulfuric acid
HCl	hydrogen chloride
HF	hydrogen fluoride (hydrofluoric acid)
HNO_3	nitric acid
N_2O	nitrous oxide
N_2O_5	dinitrogen pentoxide
NO	nitric oxide
NO_2	nitrogen dioxide
NO_x	nitrogen oxides ($NO + NO_2$)
NO_y	odd nitrogen ($= NO + NO_2 + HNO_3 + 2N_20_5 + ClONO_2 + HO_2NO_2$ + PAN + ...)
O^1D	atomic oxygen (first excited state)
O_2	molecular oxygen
O_3	ozone
OCS	carbonyl sulfide

OH	hydroxyl radical
S	atomic sulfur
SF_6	sulfur hexafluoride
SO_2	sulfur dioxide
SO_x	sulfur oxides

APPENDIX E

DESCRIPTION OF THE CHEMISTRY SOLVER BENCHMARK

Chemistry solver benchmark differences among the assessment model results reported here and in the 1995 AESA Assessment [Stolarski *et al.*, 1995] arise from combinations of differences in the model components of transport, radiation, and photochemistry calculations. A variety of photochemistry solution techniques have been chosen by the 2-D and 3-D assessment model groups, with consideration of chemical kinetic theory and practice, numerical accuracy, and computational speed. In the same manner as the photolysis benchmark [Stolarski *et al.*, 1995], a chemistry solver benchmark calculation is presented here which attempts to isolate some aspects of the contribution of the chemistry solution techniques to the differences among model results.

This chemistry solver benchmark was defined using a Gear-type integration code with a consensus set of chemical species and reactions common to the majority of the stratospheric assessment models, using rate coefficients from JPL 94-26 [DeMore *et al.*, 1994]. The error control of the Gear integration technique and its ability to deal with stiffness in the differential equations allows it to be considered an accurate solution, to within the specified error limits and the approximation used of recalculating photolysis parameters only every 15 minutes. The chemical mechanism was integrated in a diurnal manner with fixed values for O_3, CH_4, H_2O, CO, H_2, and fixed family totals of inorganic NO_y, Cl_y, and Br_y. The integration was continued until diurnally averaged production and loss terms for all variable species were balanced to better than about 1 part per hundred thousand, representing the equilibrium partitioning of the members of the various families. Portions of the photochemical solution modules used in the HSCT perturbation calculations by the 2-D and 3-D models were then applied to the given mechanism, kinetic and photolysis rate parameters, with the fixed species and family concentrations taken as initial conditions.

Three cases or regions were chosen to represent situations in which different processes dominate ozone loss: (A) 40 km / 2.7 hPa, 65°N, April 11, with fixed species and families measured or inferred from the ATMOS measurements outside the polar vortex between April 8 and 14, 1993; (B) 20 km / 67 hPa, 38°N, May 11 with concentrations from the SPADE aircraft campaign diurnal flights in 1993; and (C) 20 km / 64 hPa, 59°N, November 4 with concentrations from the ASHOE/MAESA aircraft mission northern survey flight in 1994.

In Table E-1, the benchmark diurnally averaged mole fractions are shown for all the chemical species in region B, along with the respective numerical solvers comparison results, expressed as differences in percent from the benchmark values. Results for regions A and C are consistent with region B. The shaded cells highlight important stratospheric odd-oxygen loss controlling species.

Careful interpretation of these results is necessary. Each of the eight contributing models uses a different approach to treating the diurnal cycle in an assessment calculation. CSIRO and LLNL, which calculate diurnal averaging coefficients periodically through the model year by application of solvers essentially similar to the benchmark solver (i.e., implicit solver), produce results from their diurnal average calculations, which are closely consistent with the benchmark. Here, LLNL and CSIRO use the benchmark results directly to define their diurnal averaging coefficients. This chemistry benchmark test, for these models, is essentially restricted to identifying mechanism implementation errors and diurnal averaging assumptions. AER uses an irregular 17-time step representation of diurnal behavior, while GSFC's technique depends on daytime averages of process rates and species concentrations and analytic treatment of day/night effects. For these models, the benchmark represents a somewhat more complete test of their assessment calculation technique. The differences from the benchmark reflect for AER the effects of their choice of diurnal time step. The differences are reduced substantially when the diurnal time step is cut by an order of magnitude (the model slows accordingly), but a sensitivity test calculation with shorter time steps for an HSCT perturbation shows little change in the result. Similarly for GSFC, the differences reflect the accuracy of the analytical representations of daytime/nighttime radical behavior and production and loss processes, which have been chosen to achieve a desired computational efficiency. Similar statements can be made for the LaRC, Office National d'Etudes et Recherches Aerospatiales (ONERA) (GMI solver), SUNY-SPB, and SLIMCAT chemical solution approaches.

In addition, the benchmark mechanism results have been compared to the solver module in the Photostationary State (PSS) model used by Salawitch and coworkers [e.g., Salawitch *et al.*, 1994a, b] in their studies of aircraft observations (Note: the photolysis rate parameters used in the benchmark were provided by Salawitch). Diurnal average radical concentrations are almost uniformly consistent to within 1% between the benchmark result and PSS solver results with a closely similar mechanism. This begins to provide a connection of the predictive 2-D and 3-D models to the data now available to evaluate their accuracy. This is discussed more fully elsewhere in this report.

Table E-1. The change in diurnal average species abundances (%) are shown for Region B (20 km, 38°N, May) of the chemistry solver benchmark. Shaded regions highlight chemical species that are important in stratospheric odd-oxygen balance.

SPECIES	MOLE FRACTION	AER 2-D	CSIRO 2-D	GMI ONERA 3-D	GSFC 2-D	LaRC 3-D	LLNL 2-D	SLIMCAT 3-D	SUNY-SPB 2-D
O	3.25 (-13)	-2.0	-0.2	1.1	-0.8	3.4	0.0	-0.4	-0.2
O^1D	2.97 (-19)	-0.0	-0.1	1.1	-0.9	-0.1	0.0	-0.8	-0.1
O_3	1.43 (-6)	0.0	0.0	0.0	0.0	0.0	0.0	0.0	0.0
NO	1.72 (-10)	-1.6	-0.2	0.6	10.7	-0.3	-0.0	-0.0	0.4
NO_2	**3.65 (-10)**	**0.2**	**0.1**	**0.0**	**-0.5**	**0.0**	**-0.0**	**-0.0**	**0.6**
NO_3	5.81 (-13)	-1.6	-0.8	-2.7	-25.1	0.7	0.0	1.1	-1.4
N_2O_5	2.16 (-11)	-2.5	-0.0	-1.0	-13.7	2.2	0.0	0.8	-0.6
HNO_3	4.15 (-9)	-0.0	-0.0	-0.0	-0.6	0.1	0.0	0.0	-0.1
HO_2NO_2	7.53 (-11)	1.1	-0.0	-0.1	6.0	-1.9	-0.0	-0.8	0.1
H_2O	4.86 (-6)	0.0	0.0	0.0	0.0	-0.0	0.0	0.0	-0.0
H	2.21 (-20)	-0.9	-0.4	0.6	-14.1	-0.7	0.0	-1.8	-0.5
OH	**3.12 (-13)**	**-0.5**	**-0.1**	**0.5**	**-14.4**	**-0.3**	**0.0**	**-1.8**	**-0.2**
HO_2	**1.75 (-12)**	**-0.4**	**-0.0**	**0.6**	**-8.6**	**1.0**	**0.0**	**-1.2**	**-0.5**
H_2O_2	1.00 (-11)	-0.9	-0.1	-0.0	-35.7	4.5	0.0	-0.7	-0.9
H_2	5.25 (-7)	0.0	0.0	0.0	0.0	0.0	0.0	NA	0.0
CH_4	1.46 (-6)	0.0	0.0	0.0	0.0	0.0	0.0	0.0	0.0
CH_3	2.58 (-21)	-1.1	-0.4	0.6	-12.6	-0.5	NA	-1.6	-0.5
CH_3O	3.92 (-18)	-1.1	-0.4	0.5	-12.6	-0.5	NA	-1.6	-0.5
CH_3O_2	1.73 (-13)	2.0	-0.0	-0.1	-12.3	2.0	0.0	-10.1	-1.0
CH_3OOH	2.28 (-12)	-1.2	-0.1	0.0	-32.9	-45.1	0.0	-54.2	-1.1
HCO	1.53 (-22)	-0.7	-0.5	0.6	-15.1	-0.1	NA	-1.5	-0.6
CH_2O	1.42 (-11)	1.9	0.0	0.1	-8.4	-6.2	0.0	-46.4	-0.1
CO	1.40 (-8)	0.0	0.0	0.0	0.0	0.0	0.0	0.0	0.0
Cl	6.17 (-15)	-1.0	-0.2	0.5	-12.8	-0.2	0.0	-1.3	-0.3
Cl2	1.57 (-14)	-3.4	0.0	4.0	0.0	29.7	0.0	NA	-0.9
ClO	**9.58 (-12)**	**-1.0**	**-0.1**	**0.8**	**-11.3**	**0.9**	**0.0**	**-0.8**	**-0.7**
ClOO	1.91 (-16)	-0.6	0.0	0.4	NA	0.1	NA	NA	-0.1
OClO	1.52 (-14)	1.3	0.2	9.1	NA	-32.5	0.0	-19.3	-13.8
Cl_2O_2	2.05 (-14)	-0.1	0.0	1.2	-22.2	-1.6	0.0	-5.9	-1.3
HCl	9.76 (-10)	-0.3	0.0	0.0	1.2	-0.2	-0.0	0.0	0.0
HOCl	3.45 (-12)	8.3	0.0	0.6	-26.9	-29.7	0.0	-7.8	-0.9
$ClONO_2$	1.81 (-10)	1.5	-0.0	-0.1	-5.3	1.6	0.0	0.1	-0.1
Br	1.61 (-13)	-2.1	-0.1	0.8	-1.5	-1.8	0.0	0.4	0.0
BrCl	8.00 (-15)	-0.8	0.0	4.1	-7.9	-13.3	0.0	-2.3	-2.7
BrO	**2.69 (-12)**	**-3.0**	**-0.0**	**0.8**	**3.7**	**0.6**	**0.0**	**0.2**	**-0.1**
HBr	4.30 (-13)	-0.5	0.0	-0.0	-2.0	-36.2	0.0	-1.1	-0.0
HOBr	1.40 (-12)	5.6	0.0	1.0	9.2	-20.7	0.0	-5.3	-0.6
$BrONO_2$	6.44 (-12)	0.1	0.0	-0.6	-7.4	6.7	-0.0	1.1	0.2

APPENDIX F

DESCRIPTION OF PARTICIPATING MODELS (NON-GMI)

Model calculated responses of ozone to HSCT aircraft from seven numerical models of the stratosphere are presented in this chapter. These are five 2-D models and two 3-D models as listed in Table 4-1. The calculated ozone response depends on the amount of emitted materials calculated to remain in the lower stratosphere, how they are redistributed in the lower stratosphere, and how they affect ozone. We will discuss the transport and chemistry treatment of the models below with emphasis on the differences that may explain the different model predictions.

1. Transport Formulation

DOMAIN AND RESOLUTION

All 2-D models have the lower boundary at the ground and use log-pressure coordinate in the vertical with the equal resolution in the troposphere and the stratosphere. Key parameters for model grid and resolution are summarized in Table F-1. The LaRC 3-D spectral, chemical transport model [Eckman *et al.*, 1995] has horizontal resolution of ~5.5° x 5.5° (i.e., T16) for the calculations presented herein. However, winds and temperatures truncated from a higher resolution (T32) version of the LaRC spectral GCM were used for input to the CTM. Sigma coordinates are used in the vertical dimension with ten layers in the troposphere and 14 layers in the stratosphere. The vertical resolution is ~3 km in the stratosphere and decreases in the troposphere to less than 1 km near the surface. The SLIMCAT model has horizontal resolution of ~7.3° x 7.3° (i.e., T15). The winds and temperature are from the UKMO analysis generated at a resolution of 2.5° x 3.75°. The SLIMCAT model does not have a troposphere, the lower boundary is at 335 K potential temperature and the concentrations of the trace gases at the boundary are taken from a 2-D model. The model uses isentropic surfaces as vertical coordinates with 12 layers in the stratosphere with resolutions of about 2 km in the lower stratosphere and 6 km in the upper stratosphere.

All models (except SLIMCAT) use temperature lapse rates to define the location of the tropopause which changes with season and latitude. The LaRC 3-D model uses temperature calculated by a T32-version of the Langley spectral GCM. Four of the five 2-D models use temperature from climatology while the SUNY-SPB model uses temperature from the MACCM2 output. The troposphere in the 2-D models is distinguished from the stratosphere by assigning large values of K_{yy} (typically 1-1.5x10^6 m^2/sec) and K_{zz} (4-10 m^2/sec). Studies indicate that strat-trop exchange may be dominated by transport from the middle-world to the troposphere [Eluszkiewicz *et al.*, 1996]. In a 2-D model, this will manifest itself as eddy flux along

isentropic surfaces across the boundary [Shia *et al.*, 1993]. If this is true, the model calculated residence time of aircraft emissions in the lower stratosphere would be sensitive to the horizontal and vertical resolutions of the models that determine the location and seasonal variation of the tropopause.

TEMPERATURE AND TRANSPORT PARAMETERS

The results in this report are generated by the models in the CTM mode, i.e., results are obtained using pre-calculated temperature and transport fields. The temperature is used in the models to compute temperature dependent reaction rate constants, and, in some models, to predict the surface area of PSCs. In addition, the temperature is also used in computing the winds and eddy diffusion coefficients in the 2-D models. These are summarized in Tables F-2 and F-3. A more detailed description is given below.

Temperatures and wind fields for the LaRC 3-D model are taken from the LaRC GCM output. SLIMCAT uses wind from the United Kingdom Meteorological Office (UKMO) analysis for this study [Chipperfield, 1999]. The AER model uses the zonal mean temperature and statistics for zonal-asymmetry in temperature from the eight-year average (1979 to 1986) from NMC. It computes the vertical velocity as the ratio of the heating rate (based loosely on published results of Dopplick [1979]) to the temperature lapse rate (see e.g., Tung [1982] and reference cited). The vertical velocity field is integrated to obtain a stream function with adjustment made to the heating rate to assure mass conservation (see Ko *et al.* [1985] for a description of the procedure). Values for K_{yy} are assigned to simulate the tropical barrier [Shia *et al.*, 1998] guided by exchange time constant between mid-latitudes and the tropics derived from observations (see e.g., Minschwaner *et al.* [1996]; Volk *et al.* [1996]; Schoeberl *et al.* [1997]). Values chosen are 0.7-1.3 x 10^5 m^2/s for the tropics and 3-10 x 10^5 m^2/s elsewhere. Values of 0.1 m^2/sec are adopted for K_{zz} near the tropopause increasing with altitude to 1 m^2/sec. Values of K_{yz} are obtained by projecting the K_{yy} from isentropic surfaces to pressure surfaces.

The CSIRO model uses the zonal mean temperature from the eight-year average (1979 to 1986) from NMC. The heating rates (a combination of archived tropospheric and stratospheric values in the M&M report [Prather and Remsberg, 1993], calculated values in the mesosphere based on climatological ozone and temperature, and latent heat in the troposphere from Dopplick) are used along with the adopted climatological zonal-mean temperature field to compute the velocities from the zonal-mean energy equation (see Solomon *et al.* [1986]). K_{yy} values are calculated as the ratio of the Eliassen-Palm (E-P) flux divergence to the meridional gradient of potential vorticity where the E-P flux is determined diagnostically from the zonal-mean momentum equation using the calculated velocities and the zonal wind determined from the zonal-mean temperature (see Randeniya *et al.* [1997] for details). Values for K_{zz} in the stratosphere are taken to be 0.1 to 0.25 m^2/sec. Values of K_{yz} are obtained by projecting the K_{yy} from isentropic surfaces to pressure surfaces.

The GSFC and LLNL models use the seventeen-year average (1979 to 1995) from NCEP. Both models use the climatological 3-D temperature field to compute the zonal-mean winds and K_{yy} in a self-consistent way. The GSFC model (see Jackman *et al.* [1996]) uses observed ozone and temperature to compute the diabatic heating which is augmented by the latent heat to provide the

net heating in the energy equation. Mechanical forcing from planetary waves (calculated using the 3-D temperature database using six waves) and effects of gravity wave breaking provide the wave driving for the momentum equation. The stream function is obtained by solving an elliptic equation obtained by combining the zonal-mean momentum and energy equations (see e.g., Garcia and Solomon [1983]). The LLNL model solves the similar set of equations but employs different methods to compute the heating and the forcing from the 3-D temperature database using 2 planetary waves. Both models use the ratio of the E-P flux divergence and gradient of potential vorticity computed using the 3-D temperature database to calculate K_{yy} (see e.g., Garcia [1991]; Randel and Garcia [1994]), and use a gravity wave breaking parameterization to calculate K_{zz}. The K_{yz} is zero in both models.

It should be noted that K_{yy} calculated using observed temperature often have negative values (see e.g., Newman *et al.* [1986]). In those cases, the models reassign a minimum value, typically about 0.1×10^5 m^2/sec. CSIRO also assigns 0.1×10^5 m^2/sec whenever the zonal wind (derived from temperature data) is easterly. This model also resets values larger than 30×10^5 m^2/sec to the latter value.

The SUNY-SPB model derives a consistent set of zonally averaged transport parameters (residual circulation and diffusivity tensor) from MACCM2 using the extension of Plumb and Mahlman [1987] technique developed by Yudin *et al.* [1999]. Briefly, this was done by applying the flux-gradient relationship to the results of 3-D transport experiments with two artificial orthogonal tracers.

While no specific study has been performed to confirm this, it is reasonable to assume that each model has checked on their own that their velocities and numerical schemes are mass conserving. Judging from the minimum value chosen for K_{yy} in the models, one would assume that numerical diffusion should not be an issue.

Given the different methods used in deriving the transport parameters in the models, it is not surprising that there are large differences in the calculated distributions of the trace gases in the models. Large differences in model simulated distributions of chemically inert tracers such as sulfur hexafluoride point to transport differences as a major contributor. The community is trying to identify a climatological database for zonal-mean distributions of trace gases that can be used to diagnose the transport parameters.

2. Chemistry Treatment

GAS-PHASE CHEMISTRY

The kinetic reaction rate constants are from JPL-97 [DeMore *et al.*, 1997]. CSIRO and SLIMCAT assume a 5% yield of HCl from OH + ClO. The 3-D models use the temperature from the GCM (LaRC) or analysis (SLIMCAT) to compute the reaction rates at each model grid-point. The rate constants are computed using the zonal mean temperature in the CSIRO and GSFC models. The AER and LLNL models use rate constants weighted by the probability distribution of the zonal asymmetric temperature structure from climatology.

HETEROGENEOUS CHEMISTRY

The following six heterogeneous reactions were identified in JPL-97 as possible reactions on sulfate and/or PSC.

A. $N_2O_5 + H_2O$ (condensed) $\rightarrow 2HNO_3$
B. $ClONO_2 + H_2O$ (condensed) $\rightarrow HNO_3 + HOCl$
C. $BrONO_2 + H_2O$ (condensed) $\rightarrow HNO_3 + HOBr$
D. $ClONO_2 + HCl$ (condensed) $\rightarrow HNO_3 + Cl_2$
E. $HOCl + HCl$ (condensed) $\rightarrow Cl_2 + H_2O$
F. $HOBr + HCl$ (condensed) $\rightarrow BrCl + H_2O$

Most models assume that the rate constant is in the form $\gamma vA/4$, where γ is the sticking coefficient, v is the thermal velocity of the reactant, and A is the surface area of the sulfate or PSC.

REACTIONS ON SULFATE AEROSOLS

For reactions on sulfate, AER, GSFC, LLNL, SUNY-SPB and SLIMCAT include all six reactions. CSIRO include the first 3, while LaRC includes only the first two. All models use $\gamma = 0.1$ for reaction A. There are slight variations in the temperature dependence of γ for the other reactions on sulfate particles. Previous analyses [Murphy and Ravishankara, 1994; Borrmann *et al.*, 1997; Michelson *et al.*, 1997] have shown that the γ for some of the reactions are very sensitive to temperature. Ignoring the zonal asymmetry in temperature by using the zonal mean temperature in calculations may underestimate the ozone impact from HSCT [Weisenstein *et al.*, 1998]. Since the sulfate surface area is specified in the calculations, the temperature dependence comes from γ and v. The AER, LLNL, and SUNY-SPB models use the 3-D temperature distribution to calculate a weighted γv. CSIRO and GSFC use zonal mean temperature.

The model calculated ozone responses to HSCT would depend on the sulfate surface area density (SAD) in the atmosphere. In this study, all models except SLIMCAT use in the background atmosphere the SAD from WMO [1992] corresponding to the clean background with no volcanic influence. The SLIMCAT model treat sulfate as advected tracers initialized each month by 2-D model calculations. Sulfur in the fuel will result in SO_2 emission from the engine, with the potential to perturb the SAD. The change in SAD depends on whether the emitted SO_2 is converted in the plume to sulfate particles [Weisenstein *et al.*, 1996; Danilin *et al.*, 1997]. The results in this study use SAD changes calculated from the AER sulfate model [Weisenstein *et al.*, 1997] with different assumptions on conversions in the plume. The changes in SAD from the AER model were found to be in general agreements with other model results [Weisenstein *et al.*, 1998].

REACTIONS ON COLD SULFATE AEROSOL AND/OR PSC ACTIVATED BY CONDENSATION OF HNO_3 AND H_2O

The reaction rate constant for reactions on PSCs are also in the form of $\gamma vA/4$, where A is the surface areas for Type 1 PSC (assumed to be NAT) or Type 2 PSC (assumed to be "ice") or ternary sulfate particles. The CSIRO model does not include any reaction on PSC. GSFC and AER treat all six reactions as surface reactions on ice and reactions A, B, D, and E on NAT using the sticking coefficient as stated in JPL-97. The GSFC model adjusts the rates for reactions B, D, and E to account for the dependence of these reaction rate constants on relative humidity, as suggested by Tabazadeh and Turco [1993] and Hanson and Ravishankara [1993]. Both models compute the PSC surface area following the approach of Considine *et al.* [1994]. AER assumes local thermodynamical equilibrium between gas and condensed phases for HNO_3 and H_2O with no supersaturation requirement. If the temperature is colder that the critical temperature for NAT, but warmer than the critical temperature for ice, the excess gas-phase HNO_3 and H_2O (enough to form the tri-hydrates) will be put into NAT particles with 0.5 micron radius and bulk density of 1.6 gm/cm^3. For temperature colder than the critical temperature of ice, it is assumed that some of the NAT that is formed previously will be coated by ice. After the excess gas-phase HNO_3 and some of the excess H_2O is put into 0.5 micron NAT particles, the left-over excess H_2O is used to cover some of the NAT particles to form 7 micron radius Type 2 PSC (considered as "ice" as far as assigning γ is concerned) with a bulk density of 0.93 gm/cm^3. As a result, both Type 1 and Type 2 PSCs are present in this case. GSFC adopts supersaturation ratios of 10 for NAT and 1.4 for ice in their calculations, effectively reducing the nucleation temperatures (i.e. the temperature threshold for particle formation) by 3 K and 2 K for Type 1 and Type 2 PSC, respectively. In the GSFC model, NAT is assumed to have a bulk density of 1.6 gm/cm^3, log normal size distribution with a mode radius of 1 micron and standard deviation of 1.8. The corresponding parameters for Type 2 PSC are 1.0 gm/cm^3, 10 micron radius and 1.8. Both AER and GSFC transport solid HNO_3 and solid H_2O separately with sedimentation velocities at each time step. The GSFC model takes temperature asymmetry into account when calculating surface area. The AER model uses the temperature asymmetry to calculate a weighted product for γvA.

LLNL simulates polar processing of radicals by allowing the six reactions to occur on sulfate ternary droplets. The rates are obtained from various published literatures and have not been reviewed by JPL-97. A surface area density of 1 x 10^{-8} cm^2/cm^3 is imposed within 25° of the poles when PSC climatology of Poole and Pitts [1994] indicates a PSC frequency of occurrence exceeding 0.08. Dehydration and denitrification is represented globally (independent of the PSC surface area parameterization) by assuming that the partial pressure in excess of the saturation vapor pressure over ice (calculated using zonal mean temperature) are removed permanently with first order time constants of 1 day for H_2O and 0.5 days for HNO_3.

The SUNY-SPB model accounts for the effects of the six reactions on frozen sulfate particles as well as PSCs. When the temperature is cold, the surface area of the frozen sulfate is calculated according to Danilin and McConnell [1994]. The reaction rates for frozen sulfuric acid are calculated as defined by Hanson and Ravishankara [1993]. The reaction of N_2O_5 + HCl is assumed on PSCs. Calculations of Type 1 and Type 2 PSC surface areas are based on the Danilin and McConnell [1994] parameterizations. Type 1 PSC particles are assumed to be NAT

and are formed with a supersaturation ratio of 8, or overcooling of 3 K. Type 2 PSC starts to form with a supersaturation ratio of 1.4, or overcooling of 1.8K (need size and bulk density of PSCs to get surface areas). Sedimentation of NAT the PSC are included in the transport. A superposition of the first three wave numbers is used to compute the effective rate constant.

SLIMCAT treats the reactions A, B, D, E, and N_2O_5 + HCl on PSCs using a routine based on code by Ken Carslaw to calculate rates [Chipperfield, 1999]. PSC processing, represented by first-order (for those involving H_2O) and second-order (for those involving HCl) rate constants, is triggered by UKMO temperatures. Denitrification is triggered by the model temperature and simulated by assuming fall velocities for NAT and ice particles. LaRC is similar to SLIMCAT in their treatment of heterogeneous reactions on PSCs. Denitrification is triggered by the model temperature and simulated by adopting first order removal rate constants to transform gas-phase HNO_3 to solid phase HNO_3. Solid HNO_3 is turned back into gas-phase HNO_3 with a time constant of 1 day when the temperature is above 195 K.

The above discussion shows that PSC treatments in models have not converged and are different among the models. For example, chlorine activation rate on PSC in the LaRC model does not respond to changes in concentrations HNO_3 and H_2O due to aircraft emissions.

As mentioned above, the AER, GSFC, LLNL, and SUNY-SPB models use temperature probability distributions derived from temperature climatologies to account for temperature deviations away from the zonal mean value [Considine *et al.,* 1994]. It should be noted that another method of accomplishing this has been developed, although it is not used in any of the models involved in this assessment. The "temperature wave" approach [De Rudder *et al.,* 1996; Portmann *et al.,* 1996] involves modulating the model zonal mean temperature with a periodic variation intended to approximate the temperature fluctuations a circulating atmospheric parcel might experience as it moves around the globe. The amplitude of the modulation typically varies in space and time and is proportional to either calculated or observed planetary wave amplitudes. The period of the modulation is also a spatially and temporally varying quantity, similar to the circumnavigation time of an air parcel in the atmosphere. Thus, the model temperature at some gridpoint can vary dramatically on short time scales and be very far from the zonal mean temperature of the gridpoint. The SUNY-SPB model uses the wave formulation described in Smyshlyaev *et al.* [1998]. The latter publication also describes systematic differences between the temperature distribution and temperature wave approaches.

CHEMISTRY SOLVERS

Finally, we would like to comment on the chemistry solvers used in the 2-D models. Previous model intercomparison exercises have shown that solvers in most models calculate the same partitioning of the radicals under the same constraints (solar zenith angle, overhead ozone, and local concentrations of the long-lived species) when used as a box model. Since the 2-D models transport zonal-mean concentrations, the zonal-mean production and loss rates are needed in the mass-continuity equations for the long-lived species. Different techniques are used to obtain the zonal mean production and loss rates. These include integrating the diurnally varying concentrations of the radicals obtained by explicit time marching to obtain the zonal-mean rates; and using diurnally-averaged radical concentrations calculated from average solar zenith angles

corrected by pre-calculated correction factors. The different approaches are summarized in Table F-5.

3. Sources and Sinks for Some Species

Aircraft emissions include H_2O, oxides of nitrogen and oxidation products from sulfur in the fuel. We will discuss how these are treated in the models.

Most 2-D models assigned tropospheric concentration of H_2O based on relative humidity and temperature. The exception is GSFC, which uses a first order removal time constant to relax the calculated concentrations to a pre-assigned relative humidity in the troposphere. The concentration in the stratosphere is computed using appropriate sources (*in situ* oxidation from methane, transport from the troposphere, and aircraft emission along flight corridors) and sinks (removal by transport out of the stratosphere and photochemical removal) in the mass-continuity equation using an assigned boundary condition at the tropopause. The water distribution in the SUNY-SPB model is taken from MACCM2. The LaRC model uses a fixed background H_2O determined from climatology. Distributions of water emission from aircraft in these two models are solved as a separate species and added to the background in the calculations.

To simulate the concentration of NO_y (HNO_3 + NO_x) in the lower stratosphere, all models include *in situ* oxidation of N_2O, transport of NO_x produced by lightning in the tropical upper troposphere, and NO_x emission from aircraft along the flight corridors. To simulate the effect of lightning, the models assigned a production rate of NO in the tropical upper troposphere. The exact location and the total amount differ slightly from model to model. The AER, CSIRO, GSFC, SUNY-SPB, and LaRC model use a total of 2 MT (N)/yr uniformly (constant in molecules/cm^3/sec) distributed between 4 to 14 km in the tropics. The LLNL model uses a total of 5 MT (N)/yr. The distribution in LLNL is derived from the International Satellite Cloud Climatology Project (ISCCP) cloud database.

Most models use first order removal rate constants to simulate washout rate for soluble species, with time constants of 3 to 5 days at the ground, decreasing to 30 to 50 days at 10 km. The washout rate in GSFC is longer, ranging from 25 days to 100 days. Washout rate for SUNY-SPB. Wash out in the LaRC model follows the treatment of Mahlman and Moxim [1978]. It should be noted that different models pick different species for washout. Some models remove NO_y, some only HNO_3 while others include N_2O_5, HNO_4, and $ClONO_2$. These are summarized in Table F-4. With the efficient washout, surface sources of NO_x have little impact on stratospheric NO_y.

There are significant differences in the H_2O and NO_y distributions (both in the background and the perturbed atmosphere) simulated by the models. No observation databases have been identified as the benchmarks for the climatological mean for these species in the present day atmosphere. It remains unclear as to whether the differences among the models are due to transport differences or differences in treatment of the sources.

Table F-1. Model grid and resolution.

Model		Height, Coordinate	Model Top Boundary	Tropopause
2-D	latitude			
AER	10°	1.2 km log-pressure	60 km	Temperature gradient from climatology
CSIRO	5°	2 km log-pressure	80 km	Temperature gradient from climatology
GSFC	10°	2 km log-pressure	0.0024 hPa 90 km	Temperature gradient from climatology
LLNL	5°	1.5 km log-pressure	0.01 hPa 84 km	Temperature gradient from climatology
SUNY-SPB	5°	2 km log-pressure	0.027 hPa 74 km	Mixing coefficients derived from MACCM2
3-D	Lat x long			
LaRC	5° x 5.5°	100 hPa interval below 100 hPa; 3 km interval above 100 hPa	0.1 hPa 65 km	Temperature gradient from climatology
SLIMCAT	7.3° x 7.3°	Isentropic surfaces; 2 km in the lower stratosphere and 6 to 10 km in the upper stratosphere	2700 K surface; approx. 50 km	No troposphere

Table F-2. Temperature, winds and K_{yy} used in the models.

Model	Zonal Mean Temperature	Zonal Asymmetry in Temperature	Winds	K_{yy}
2-D Models				
AER	8 year average (1979 to 1986) monthly mean T from NMC	Zonal asymmetry based on statistics from the same period by Kalnay *et al.* [1996] used in chemistry calculation only	$w=Q/\Gamma$ Heating rate based loosely on Dopplick, adjusted to get mass-conservation	assigned values to match exchange time constant across the tropical barrier
CSIRO	8 year zonal and monthly mean T from NMC as archived in M&M	Zonal asymmetry not used	Iterative procedure to solve transformed Eulerian-mean (TEM) energy equation (include dT/dt term) [Solomon *et al.*, 1986]: heating rates taken from M&M augmented by latent heat, computed for mesosphere	computed from $\frac{\text{EP Flux}}{\text{gradient of PV}}$
GSFC	17 year (1979 to 1995) average from NCEP	17 year (1979 to 1995) average from NCEP, used in chemistry calculations and in determination of winds and K_{yy}	Solve stream function using Garcia and Solomon [1983]: heating rate from climatological T, O_3 and H_2O, EP flux from planetary wave from T (6 waves), gravity wave breaking, latent heat from Newell, include SAO	computed from $\frac{\text{EP Flux}}{\text{gradient of PV}}$
LLNL	Fleming [personal communication]	Fleming [personal communication], used in chemistry calculations and in determination of winds and K_{yy}	Solve stream function using Garcia and Solomon [1983]: heating rate from climatological T and model calculated trace gases, EP flux from planetary wave from T (2 waves), gravity wave breaking, Rayleigh friction	computed from $\frac{\text{EP Flux}}{\text{gradient of PV}}$
SUNY-SPB	MACCM2	Superposition of first three zonal wave numbers calculated from MACCM2 temperature	From MACCM2 winds	From MACCM2 winds using artificial orthogonal tracers
3-D Models				
LaRC	T32 GCM output	NA	NA	NA
SLIMCAT	UKMO analysis	NA	NA	NA

Table F-3. Values of eddy coefficients used in the models.

Model	K_{yy}, trop $10^5 m^2/sec$	K_{zz}, trop m^2/sec	K_{yy}, strat $10^5 m^2/sec$	K_{zz}, strat m^2/sec	K_{yz}, strat m^2/sec
AER	15	10	0.7-1.3 in tropics, 3-10 elsewhere	0.1-1	Projected, typical ±100
CSIRO	10	4	Calculated from EP-Flux and PV divergence; set to 0.1 when wind is easterly, always between 0.1-30	0.25 between 21 km - 42 km; 0.1 elsewhere	Projected, magnitude can be as large as 1000
GSFC	Calculated (6 waves), minimum value of 15	Ground: 50 at tropics, 25 at the poles; tropopause 1	Calculated (6 waves), minimum value 0.1	0.03 at tropopause to 0.3 at stratopause, computed in mesosphere	0
LLNL	10	4	Calculated (2 waves), minimum value 0.1	Calculated, with minimum value of 0.2	0
SUNY-SPB	Derived from MACCM2	Derived from MACCM2	Derived from MACCM2	Derived from MACCM2	Derived from MACCM2

Table F-4. Parameterization of rainout.

Model	Species	Time Constant
2-D Models		
AER	H_2O_2, CH_3OOH, CH_2O, HNO_3, HCl, HBr,CF_2O, C_2H_5OOH, CH_3COOH,FX	5 days at the surface, 40 days at 10 km
CSIRO	NO_y, Cl_y, Br_y, H_2O_2, CH_2O, CH_3COOH	ground: 3 days 10 km: 28 days, no washout within 3 km of tropopause
GSFC	H_2O_2, CH_3OOH, HNO_3, HO_2NO_2, HCl, HBr, HF, CClFO, and COF_2	25 days to 100 days
LLNL	N_2O_5, HNO_3, HNO4, H_2O_2, CH_2O, ClO, HCl, HOCl, $ClONO_2$, $BrONO_2$	3 days below 4 km, 50 days near the tropopause
SUNY-SPB	H_2O_2, CH_3OOH, CH_2O, HNO_3, HCl, HBr	5 days below 5 km, exponentially decreasing up to the tropopause
3-D Models		
LaRC	H_2O_2, HNO_4, HNO_3, HCl, HBr	Mahlman and Moxim [1978]
SLIMCAT	NA (no troposphere)	NA (no troposphere)

Table F-5. Solvers used in the models.

Model	Solve Continuity Equations for:	Radicals and P & L for Long-Lived Species	Time-Step
2-D Models			
AER	Source gases, HNO_3, NO_y, O_x, Cl_y, Br_y; solid HNO_3, solid H_2O	Calculated everyday using explicit time-marching of radical species, initial conditions from previous day after adjusting for changes in Cl_y, Br_y, and NO_y, use diurnally varying radical concentrations to compute 24-hour averaged P & L for long-lived species	No operator splitting, explicit time-stepping with 6 hour time-step, tendency due to advection calculated using Smolarkiewicz, use P and loss frequency for chemical tendency
CSIRO	Source gases, NO_y, O_x, Cl_y, Br_y	Family approach; 24-hour averaged zonal-mean P & L calculated using correction factors obtained from a 24-hour integration, saved every 10 days	Use operator splitting, use variable order Bott scheme with 6 hour time-step. Keep same P & L for 10 days
GSFC	Source gases, HNO_3, N_2O_5, $ClNO_3$, NO_z, O_x, Cl_z, Br_y, solid HNO_3, solid H_2O	Use time marching for night-species (HNO_3, NO_2, NO_3, N_2O_5, HOCl, HCl, ClO, $ClNO_3$, BrO, HOBR, and $BrNO_3$), use daytime averaged J-rates and dawn values of night-species to get day-averaged values of all species to get diurnal average P & L for family species, updated daily	Split operator, Lin and Rood scheme, 12 hour for advection, 3 hour for vertical diffusion, 24 hour for horizontal diffusion, and 24 hour for chemistry
LLNL	Individual, non-family approach	Use 24-hour averaged sun and diurnal factor to time march the species with 900 second - step. Diurnal factors are calculated for each chlorine loading and sulfate surface area. Chemical solution uses an implicit numerical solution approach (SMVGEARII).	Use split operator, use Smolarkiewicz with 2 hour time-step to do transport for 2 days, the time-march chemical species for 2 days
SUNY-SPB	All model species transported with correction at each time-step to conserve mass within families	Model time-step is 1 day. Diurnal averaged production and loss rates are used; updated every 15 days calculated using explicit diurnal calculation	Use split operator, use Prather second moment scheme for advection, alternative direction semi-implicit scheme for diffusion and chemistry, time-step is 1 day
3-D Models			
LaRC	Source gases, O_x, NO_y, HNO_3, Cl_y, N_2O_5, H_2O_2, HCl $ClONO_2$, solid HNO_3	Use 24-hour average J-rates to calculate photochemical equilibrium concentrations of the radicals at each 3-D grid every 30 minutes	Leap frog with 30 minute time-step
SLIMCAT	Sources gases, O_x, H_2O_2, NO_x, N_2O_5, HNO_3, HNO_4, NO_3, $ClNO_3$, Cl_x, HCl, HOCl, OClO, Br_X, $BrNO_3$, BrCl, HOBr, HBr	Explicit integration of full diurnal cycle with 20-minute time step and time-dependent photolysis rates	Semi-implicit symmetric method [Ramaroson *et al.*, 1992]

APPENDIX G

DESCRIPTION OF GLOBAL MODELING INITIATIVE MODELS

---

1. Description of Meteorological Fields, Advection Algorithm

The current transport shell for the GMI model adopts the Lin and Rood [1996] advection scheme, together with polar and mass-conservation filters used in the University of Irvine, California (UCI)/GISS model [Prather *et al.*, 1987]. The number of vertical levels is the same as those of the original met fields: 44 for MACCM2, 29 for DAO, and 28 for GISS-2'. Vertical resolutions in the lower stratosphere are about 0.8 km for DAO, 1.5 km for MACCM2, and 3 km for GISS. A horizontal resolution of 4 x 5 is adopted by interpolating (or degrading if necessary) the original fields.

The impact of using different transport shells on the same set of winds has been tested for the different fields used. Higher-order interpolation in the vertical direction for the Lin and Rood scheme allows a good reproduction of the NO_y accumulation from HSCTs (experiment A3 in M&M II), as shown in Figure 4-1, which compares results of this experiment run in the GMI and original UCI/GISS shells.

The current transport shell has been parallelized, allowing it to run in a suite of different platforms. This has been a crucial element in allowing multi-year assessment calculations with this model.

2. Description of Chemical Mechanism and Solvers

As prescribed in the scenario description for the HSRP assessment, the GMI models adopt the recommendations from NASA/JPL [DeMore, 1997]. In particular, no HCl branching for the ClO + OH reaction was adopted in the assessment calculations, although this branching was included [Lipson, 1997] in the present-day simulations which are compared to observations.

Three chemical solvers were considered:

a) The SMVGEARII solver [Jacobson, 1995]. This solver is very accurate, but it places heavy demands on computational time for multi-year calculations. The solver was incorporated into the GMI model to carry out benchmark calculations against which other solvers can be tested.

b) A semi-implicit symmetric scheme solver, provided by R. Ramaroson [1989] from ONERA in Paris.

c) An Euler backward-implicit scheme, provided by J. Lamarque at NCAR [Granier and Brasseur, 1991].

Both the ONERA and NCAR solvers provide sufficient computational efficiency to carry out multi-year calculations. They were tested by running eight months of the GMI model with full chemistry, with DAO winds and 1996 conditions. The differences in calculated ozone are less than 1% over most of the stratosphere, increasing to about 3% during the nighttime in the upper stratosphere. The NCAR solver also performed satisfactorily, although the percent differences were somewhat higher. A combination of accuracy and computational efficiency in the chosen platform directed the choice of the ONERA solver for the assessment calculations.

This version of the GMI 3-D model does not include chemical and physical processes necessary for troposphere aircraft assessments (e.g., lightning nitrogen oxide production), therefore, the sensitivity of ozone change to subsonic aircraft NO_x emissions in the 2015 base and HSCT perturbed fleets were removed. The model tropopause height was diagnosed in the NH when the ozone vertical profile change was less than 60 ppbv/km and 45 ppbv/km for the February-August and the September-January periods respectively. The opposite relationship was used in the SH (e.g., 60 ppbv/km for the September-January period). The above approach for deriving tropopause height was based on ozone sonde observations [Logan, personal communication]. Therefore, for all the figures contained within this assessment report, the tropospheric ozone abundance in both the base and perturbed scenarios was set to the base scenario abundance.

3. Description of PSC, Cold Sulfates

The GMI model includes a parameterization of PSCs that will respond to the increases in HNO_3 and H_2O produced by aircraft emissions. Both Type 1 and Type 2 PSCs are considered. The composition of the Type 1 PSCs can be set to either NAT or STS. For the HSCT assessment runs described below, an STS composition was chosen. The assumed Type 2 PSC composition is ice. The parameterization also accounts for PSC sedimentation, which can produce both denitrification and dehydration at the model poles.

The GMI PSC parameterization is designed to be economical so it does not represent the microphysical processes governing PSC behavior. However, it still provides a fairly realistic representation of the formation, growth, evaporation, and sedimentation of PSCs which will respond to aircraft emissions, a desirable feature in a model designed to assess the global effects of aircraft emissions.

The parameterization calculates surface area densities for Type 1 and Type 2 PSCs using model-calculated temperatures and HNO_3 concentrations, transported and background H_2O distributions, the ambient pressure, and an H_2SO_4 concentration which is inferred from the background liquid binary sulfate (LBS) aerosol distribution specified in the model calculation. The Type 1 PSC calculation can be set to assume either a NAT or a STS composition (it is currently set to STS). The assumed composition of the Type 2 PSCs is water ice. The vapor pressure measurements of Hanson and Mauersberger [1988] are used for NAT PSCs; the approach of Carslaw *et al.* [1995] is used for the STS composition; and Marti and Mauersberger

[1993] vapor pressures are used for ice aerosols. The code removes both H_2O and HNO_3 from gas to condensed phase when particles form. To calculate the amount of material removed from gas phase, the parameterization assumes that thermodynamic equilibrium holds. When ice PSCs form, the algorithm assumes that a coexisting NAT phase also forms and is part of the Type 2 PSC. This provides a mechanism for significant denitrification of the polar stratosphere due to rapid sedimentation of the large Type 2 PSCs. The user has the option of specifying a threshold supersaturation ratio for both NAT and ice aerosols which must be exceeded before any mass is removed from gas phase. Current values for these ratios correspond to a 3 K supercooling for NAT aerosols and a 2 K supercooling for ice aerosols, consistent with the estimates of Peter *et al.* [1991] and Tabazadeh *et al.* [1997].

In order to calculate the surface area density corresponding to a particular amount of condensed phase mass, the code assumes the condensed phase mass to obey a log normal particle size distribution. The user can specify either the total particle number density and the distribution width, or the particle median radius and the width, which then determines the conversion from condensed phase mass to surface area density. When the particle number density is held constant, condensation or evaporation processes result in the growth or shrinkage of existing particles rather than new particle nucleation. This is thought to be more physically realistic, and is currently the mode in which the parameterization operates.

The parameterization also transports vertically the condensed phase H_2O and HNO_3 to account for particle sedimentation. The condensed phase constituents are also subject to transport by the model wind fields. Fall velocities are calculated according to Kasten [1968] and corrected to account for the range of fall velocities in a log normally distributed ensemble of aerosol particles. Because the GMI model currently specifies the background distribution of H_2O in the stratosphere, a special strategy had to be developed to allow for dehydration resulting from particles sedimentation. This takes the form of a transported constituent named "dehyd" which is produced when dehydration occurs due to particle sedimentation and is lost when moistening of a region results from local evaporation of particles sedimenting from higher altitudes. Ambient H_2O concentrations are then the difference between the background H_2O and dehyd.

It should be stressed that this parameterization is not microphysical. A good microphysical representation of PSCs would be quite time consuming and so is not appropriate in a model designed for assessment calculations. In the GMI parameterization, the amount of H_2O and HNO_3 in condensed phase is determined by assuming that the system is in thermodynamic equilibrium so that equilibrium vapor pressure measurements can be used. The parameterization also saves time by simply assuming that the condensed phase material is distributed in particles obeying a user-specified log normal size distribution, rather than explicitly considering the microphysical processes which determine particle size distributions.

4. Look-up Table for Photolysis Rates

Photolysis rates are calculated in a table look-up method from the Goddard 3-D CTM [Douglass *et al.*, 1997]. Normalized radiative fluxes calculated from the model of Anderson *et al.* [1995] are tabulated as a function of wavelength, solar zenith angle, overhead ozone, and pressure. Temperature-dependent molecular cross sections and quantum yields along with the solar flux

are tabulated separately. In the CTM, fluxes and cross sections are interpolated to the appropriate values for each grid point and integrated over wavelength to produce the photolysis rates. This method compares well in photolysis benchmark comparisons [Stolarski *et al.,* 1995]. The calculations discussed here were done using a uniform global mean surface albedo of 0.3 and a cloud-free atmosphere. Cross sections and quantum yields are from DeMore *et al.* [1997].

5.1 GRADING OF THE GMI MODEL

Because the HSCT perturbation depends greatly on the model transport and build-up of exhaust, it is required that the model transport be subject to careful scrutiny. One of the challenges in development of the GMI 3-D assessment model is the development of criteria on which to base the choice of the meteorological data set to be used for the assessment calculations. The criteria are based on comparisons of models with observations, in a manner parallel to the M&M II report. There are some ways in which this "grading" is different from the M&M II exercise. (a) The criteria were chosen based exclusively on transport calculations, not only due to the scheduling requirements to start calculations at an appropriate time, but also to isolate as much as possible transport-related issues in the testing of the models. (b) The experimental criteria included tests emphasizing the lower stratosphere, which were not included in M&M II. (c) The GMI team agreed to a quantitative, but somewhat subjective, evaluation of each of the wind fields in order to achieve partial and overall "scores" for model performance [Douglass *et al.,* 1999]. This model scoring is harder to implement to the wider set of tests in M&M II, and thus it has not been agreed upon by the M&M II community.

This approach to development of an assessment model differs from previous evaluations of such models in several key respects.

1. Provides an Objective Means to Discriminate Between Models Based on the Model Representation of Physical Processes

Comparison of model results with observations has been a traditional part of the assessment process. These comparisons have been used to provide a sense of the overall validity of the model results, and a means to interpret physically the differences in perturbation estimates calculated by different models. However, as articulated by Jackman *et al.* [1991], for 2-D (zonally averaged) models, agreement with one data set does not imply agreement with other data sets which rely on different aspects of model transport. Furthermore, comparisons have been largely subjective, and while they may have been used to explain differences in the calculated perturbations, they have not been used to provide an estimate of overall model reliability.

Establishment of objective standards of model performance makes it possible to move beyond understanding model differences towards ranking the model results based on model representation of physical processes. Though described here for 3-D models, the approach is valid for 2-D models as well.

2. Establishes Context to Evaluate Future Model Improvements

As more is learned about the atmosphere and atmospheric processes, often through comparison of model and observations, models are improved. Application of the same objective standard to the improved model provides a measure of the improvement.

A set of six tests was agreed upon; these include the following:

1. Temperature
2a. Residual Circulation and Mixing - Mid to Upper Stratosphere
2b. Residual Circulation and Mixing - Lower Stratosphere
3. Tropical, Mid-Latitude Separation
4. Tropical Propagation of the Annual Cycle
5. Separation of the Upper Troposphere and Lower Stratosphere
6. Horizontal Propagation of the CO_2 Signal

Objective standards were set to provide a quantitative score for each model. Based on the performance of the models on these tests, MACCM2 winds and temperatures were chosen as the primary meteorological fields to be used in the 3-D assessment of the HSCT perturbation. It is important to note, however, that none of the models has received high scores on all of the tests. Furthermore, further comparison of model results with other measurements (such as NO_y and O_3) will further elucidate the model performance.

5.2 The Tests and Model Performance

The first of the six tests described here considers the model temperature field, since many model processes are dependent on temperature (notably gas phase photochemical reactions, heterogeneous reactions of aerosol and PSC surfaces, and formation of PSCs). The other five tests address various aspects of model transport. The tests and the criteria for successes described here are physically based but still somewhat arbitrary. We anticipate that there may be future improvements to the selection of tests or to the tests themselves.

Test 1. Temperature

A climatology was developed using 18 years of NCEP temperatures at 50 hPa. Each month, the difference was calculated between the model monthly mean and the NCEP monthly mean for 40°-50°N and 60°-70°N. These comparisons were restricted to 50 hPa and northern middle-to-high latitudes as this is where most of the HSCT aircraft are expected to fly. The differences are scored using the following formula:

$$\text{grade}_\theta = 1 - \frac{1}{12}\sum_{i=1}^{12}\frac{\left|T_{\theta,i}^{\text{MODEL}} - T_{\theta,i}^{\text{NCEP}}\right|}{2\sigma_{\theta,i}^{\text{NCEP}}}$$

where T is the monthly mean temperature, sigma is the standard deviation from the monthly mean, theta refers to the latitude band, and the subscript "i" refers to each of the 12 months.

Thus the grade is high when the model difference from NCEP, weighted by the standard deviation of the NCEP temperatures, is small. The scores for all three models are summarized in Table G-1. Not surprisingly, results from Goddard Earth Observing System Data Assimilation System (GEOS) look best, since this model utilizes assimilated data to constrain their calculations.

Test 2a. Residual Circulation and Mixing - Mid to Upper Stratosphere

N_2O observations made by the UARS CLAES [Roche *et al.*, 1993] at 31.2, 10, and 2.2 hPa were averaged binning all data at these UARS standard pressure levels within latitude bands centered at the equator, 45°N and 45°S latitude (nine points in all). The models were run for N_2O with a fixed boundary condition in the troposphere and a prescribed stratospheric loss, to reach a repeating annual cycle. All the models used the numerical transport scheme described by Lin and Rood [1996]. Model values were calculated binning all model output in the same latitude bands and for 5 km altitude centered approximately on the UARS pressure levels.

This test has six components: the annual average (AA); the horizontal gradients (HG); the vertical gradients (VG); the tropical annual cycle (TAC); the northern annual cycle (NAC); the southern annual cycle (SAC). The maximum score for each of the six components is 1. The overall score for this test is the average of the score for the six components.

For AA, HG, and VG, the values derived from the models must be within 20% of the values derived from the observations to receive a score of 1. If the difference is greater than 20%, the score is zero. The score given in Table G-2 is the average of the 9 separate scores for AA and the six separate scores for HG and VG. The annual cycle representations are tested by considering the differences between the monthly averages and the time means. Again, a difference of 20% or less is given a score of 1. The results given in Table G-2 are the averages of 36 comparisons (12 at each latitude, for each level).

MACCM2 is superior to GEOS-Direct Access System (DAS) and GISS-2', but none of the models cleanly captures the observed features. In particular, none of the models capture the observed annual cycle.

Test 2b. Residual Circulation and Mixing - Lower Stratosphere

This test compares model N_2O profiles with N_2O climatology created using data from the Airborne Tunable Laser Absorption System (ATLAS) instrument on board the NASA ER-2. The climatology is compiled from data from 126 flights between December 1988 and September 1997. Eleven mean profiles from the climatology covering three latitude ranges and four seasons are used for the comparisons with models. (No aircraft data are available for the SH during austral summer.) The latitude ranges of the profiles are 35°–50°S, 10°S–10°N, and 35°–55°N. The mid-latitude ranges are specifically chosen to exclude vortex air. The vertical range is 380 to 500 K.

This test uses model output from the N_2O simulations described above. Models are evaluated by their ability to reproduce these eleven mean profiles. Model means are calculated for the same

seasons, latitude ranges, and potential temperatures as the mean profiles. Because model vertical resolution is coarse compared to that of the aircraft measurements, aircraft data are binned using 20 K wide bins. This results in six vertical levels in each model profile that can be compared to observations. Model results are scaled so that their mixing ratio entering the tropical tropopause is equal to the observed 380 K mixing ratio in the tropics.

Altogether there are 62 locations for comparison of model and measurements. At each location, a model earns from 0 to 1 point, depending on how close the model mean and one standard deviation are to the climatological mean and one standard deviation.

The three wind data sets produce notably different N_2O distributions. Outside the tropics, no one data set could reasonably reproduce both the lower and upper half of any given profile. In general, MACCM2 did the best job of simulating profiles above 420 K, and GEOS-DAS did the best job at 420 K and below. All three models produced reasonable tropical profiles, but GISS tropical variability was roughly ten times greater than both the observations and the other models. In summary, no one model excelled at all latitudes, heights, and seasons examined. The model scores for this test are 0.63 (GEOS-DAS), 0.43 (GISS-2'), and 0.68 (MACCM2).

Test 3. Tropical Mid-Latitude Distinctness

The separation between the tropics and the middle latitudes is only partially captured by comparison of the modeled and observed mean horizontal gradients. Figure G-1 shows histograms of all the CLAES observations in latitude bands (10°S–45°N) at about 30 km. The distribution of the data is double peaked. The peak centered at 200 ppmv represents observations in the tropics; the peak centered at about 75 ppmv represents observations at the middle latitudes. These two regions can be considered chemically distinct in that two distributions are maintained, and there is little mixing between them. This is important to the HSCT assessment, in that a model with inappropriate transport between the tropics and mid-latitudes will not maintain an appropriate pollutant distribution. The test, then, is to determine if the models maintain distinct distributions for the middle latitudes and the tropics. Three seasons (summer, fall, and winter) are considered for each of the three models. The score for this test does not depend on the magnitude of the separation or on the relative sizes of the peaks. That aspect of the N_2O/CLAES comparison is part of the score in section b. A point is given when the histogram shows two separate air masses, and a zero if not. The combined score is normalized to a maximum of 1. The MACCM2 N_2O distributions always show two peaks, as do the CLAES distributions, and MACCM2 receives a score of 1. GISS-2' N_2O shows five panels with separate peaks, for a score of 0.62. GEOS-DAS N_2O shows three panels with separate peaks, for a score of 0.38.

Test 4. Tropical Propagation of the Annual Cycle

Transport in the tropical lower stratosphere is important to the HSCT evaluation in that this is the dominant pathway for air to reach the upper stratosphere, and aircraft exhaust, which reaches the upper stratosphere, will have a much longer stratospheric lifetime in a part of the atmosphere where reactions with the nitrogen oxides in aircraft exhaust are of major importance to the ozone balance. The vertical propagation of an annual cycle in a tracer mixing ratio stringently tests model transport in this region. The performance in this test of participating 2-D and non GMI

3-D models are described in Section 4.3.3, test 5. The results, as applied to the GMI models, are summarized here in Table G-3. Further details of the test and the performance of other models are given in Park *et al.* [1999] and Douglass *et al.* [1999].

Model and measurements show a simple exponential decay of amplitude and uniform phase speed. Thus, this test has two components: (1) comparisons of the average phase speed c from 16 to 24 km with the phase speed derived from observations; and (2) comparison of the amplitude attenuation factor R with the value derived from observations. R is defined to be Ha/lambda, where Ha is the scale height of the exponential decay and lambda is the wavelength of the cycle. The score is 2 if the model value falls within the uncertainty range from observations; the score is 1 if the model phase speed is within 50% of the upper or lower bound of the observational range. The combined score is the average of the two separate scores, weighted to have a maximum of 1.

Test 5. The CO_2 Cycle at Middle Latitudes

This test concerns transport in the lowermost stratosphere, and the possibility of substantial vertical mixing between the lowermost stratosphere and upper troposphere. Nakazawa *et al.* [1991], using data taken on commercial aircraft, report a CO_2 seasonal cycle in the upper troposphere (UT) near 60°N with a May maximum. The CO_2 seasonal cycle in the lower stratosphere (LS) has smaller amplitude with a September maximum. These observations indicate a strong barrier to upward motion at the high-latitude tropopause. The models are tested by identifying the model tropopause, and then comparing the seasonal cycle in CO_2 at the lowest stratospheric level with the seasonal cycle in CO_2 at the highest tropospheric level. A model is given a score of 1 if the difference in phase between the maximum of the lowest stratospheric level and the highest tropospheric levels is at least two months. All three models score 1 on this test.

Test 6. Horizontal Propagation of the CO_2 Signal

This analysis examines transport in the lower stratosphere but above the level of the tropical tropopause. Boering *et al.* [1996] and Strahan *et al.* [1999] have found an extratropical CO_2 seasonal cycle between 380 to 440 K that appears to be transported there from the tropics. Above 440 K, there is no clear seasonal cycle in the northern middle latitudes. The seasonal cycle is the residual circulation is accounted for by considering the CO_2 on constant N_2O surfaces. To pass the test, the model mid-latitude seasonal cycle amplitude at 460 K must be less than 20% of the tropical seasonal cycle amplitude just above the tropopause (380 K), and the model seasonal cycle at 420 K in mid-latitudes must be at least 20% of the tropical seasonal cycle at 380 K. The models receive a score of 0.5 for each condition passed. GEOS-DAS receives a score of 0.5; MACCM2 score is 1; GISS-2' lacks vertical resolution to apply this test meaningfully.

The second test considers the phase of this model seasonal cycle in mid-latitude relative to the phase in the tropics. Boering *et al.* [1996] and Strahan *et al.* [1999] show that the observed seasonal maximum in the mid-latitudes appears two weeks after it appears in the tropics. MACCM2 and GEOS-DAS both score 1 on this part of the test; again, GISS-2' lacks vertical

resolution to apply the test. The scores from both parts are combined; MACCM2 score is 1; GEOS-DAS is 0.75, and GISS-2' receives no grade.

5.3 Results and Choice of Meteorological Fields

The final scores are computed for the three models; these are given in Table G-4. Note that a perfect score on each test would result in a score of 6.

Based on the performance of the models on these tests, MACCM2 winds and temperatures were chosen as the primary meteorological fields to be used in the 3-D assessment of the HSCT perturbation. It is important to note, however, that none of the models has received high scores on all of the tests. These tests do provide a physical basis for evaluating model results and also for evaluating future model improvements and the importance of the improvements to the model response to perturbations.

Table G-1. Temperature scores.

Model	40-50°N	60-70°N	Average
GEOS	0.79	0.90	0.84
MACCM2	0.67	0.43	0.55
GISS-2'	0.46	0.49	0.48

Table G-2. Residual circulation and mixing – mid-to-upper stratosphere grade.

Component	GEOS-DAS	MACCM2	GISS-2'
AA	0.22	0.61	0.44
HG	0.0	0.33	0.08
VG	0.42	0.83	0.58
TAC	0.06	0.12	0.10
NAC	0.04	0.14	0.08
SAC	0.10	0.17	0.06
GRADE	0.14	0.37	0.22

Table G-3. Propagation of the annual cycle grade.

Model	Ha	C	R	Score (R)	Score (C)	Score
GEOS-DAS	9.02	0.95	0.29	1	0	0.25
MACCM2	4.61	0.48	0.31	1	1	0.50
GISS-2'	2.31	0.40	0.18	1	1	0.25

Table G-4. Results and choice of meteorological fields grade.

Test	GEOS-DAS	MACCM2	GISS-2'
1	0.84	0.55	0.48
2a	0.14	0.37	0.22
2b	0.63	0.68	0.43
3	0.38	1.0	0.63
4	0.25	0.50	0.25
5	1.0	1.0	1.0
6	0.75	1.0	no grade
Average	0.57	0.73	0.51

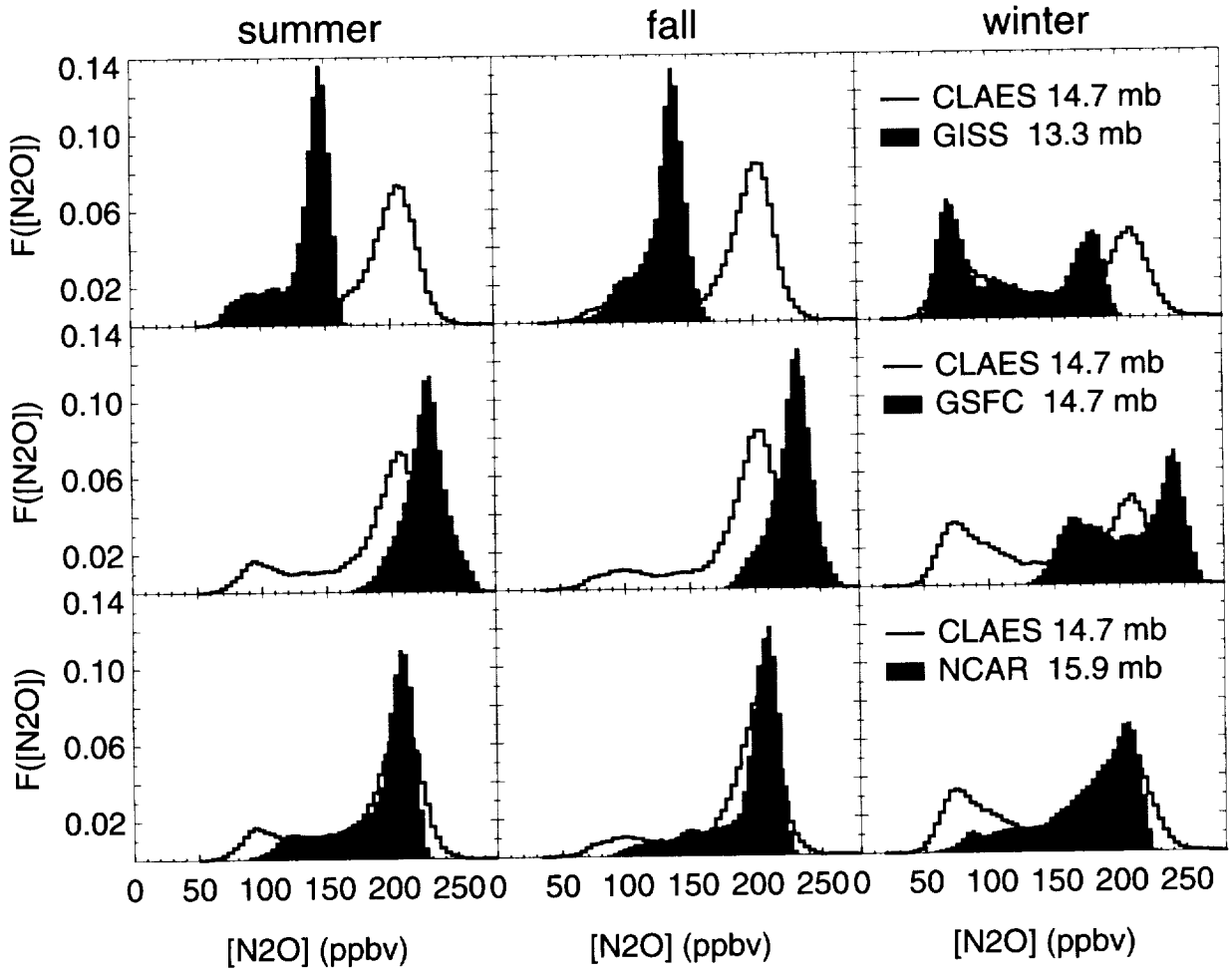

Figure G-1. Seasonal equal-area histograms of CLAES v.7 N_2O at vertical level 14.7 hPa for summer (June, July, August, 1992), fall (September, October, November, 1992), and winter (January, February, 1993). The shaded histograms are the model results, at vertical levels closest to the observations as indicated on the figure. Each row corresponds to a different model (top: GISS; middle: GEOS-DAS; bottom: MACCM2), and each column to a different season (left: summer; middle: fall; right: winter).

REPORT DOCUMENTATION PAGE

Form Approved
OMB No. 0704-0188

1. AGENCY USE ONLY *(Leave blank)*	2. REPORT DATE	3. REPORT TYPE AND DATES COVERED
	June 1999	Technical Paper

4. TITLE AND SUBTITLE
Assessment of the Effects of High-Speed Aircraft in the Stratosphere: 1998

5. FUNDING NUMBERS
401.0

6. AUTHOR(S)
S. Randolph Kawa, Assessment Chair

7. PERFORMING ORGANIZATION NAME(S) AND ADDRESS (ES)
Special Projects Office
Flight Projects Directorate
Goddard Space Flight Center
Greenbelt, Maryland 20771

8. PEFORMING ORGANIZATION REPORT NUMBER
99B00055

9. SPONSORING / MONITORING AGENCY NAME(S) AND ADDRESS (ES)
National Aeronautics and Space Administration
Washington, DC 20546-0001

10. SPONSORING / MONITORING AGENCY REPORT NUMBER
TP—1999–209237

11. SUPPLEMENTARY NOTES

12a. DISTRIBUTION / AVAILABILITY STATEMENT
Unclassified–Unlimited
Subject Category: 45
Report available from the NASA Center for AeroSpace Information,
7121 Standard Drive, Hanover, MD 21076-1320. (301) 621-0390.

12b. DISTRIBUTION CODE

13. ABSTRACT *(Maximum 200 words)*

This report assesses the potential atmospheric impacts of a proposed fleet of high-speed civil transport (HSCT) aircraft. The purpose of the report is to assess the effects of HSCT's on atmospheric composition and climate in order to provide a scientific basis for making technical, commercial, and environmental policy decisions regarding the HSCT fleet. The work summarized here was carried out as part of NASA's Atmospheric Effects of Aviation Project (a component of the High-Speed Research Program) as well as other NASA, U.S., and international research programs. The principal focus is on change in stratospheric ozone concentrations. The impact on climate change is also a concern. The report describes progress in understanding atmospheric processes, the current state of understanding of HSCT emissions, numerical model predictions of HSCT impacts, the principal uncertainties in atmospheric predictions, and the associated sensitivities in predicted effects of HSCT's.

14. SUBJECT TERMS
Ozone, stratosphere, high-speed civil transport, supersonic transport, climate, environmental assessment, aviation, aircraft.

15. NUMBER OF PAGES
150 + appendices

16. PRICE CODE

17. SECURITY CLASSIFICATION OF REPORT	18. SECURITY CLASSIFICATION OF THIS PAGE	19. SECURITY CLASSIFICATION OF ABSTRACT	20. LIMITATION OF ABSTRACT
Unclassified	Unclassified	Unclassified	UL